การประเมินอันตรายจากแผ่นดินไหวในประเทศไทย โดยวิธีความน่าจะเป็นและวิธีกำหนดค่า

นายสันติ ภัยหลบลี้

วิทยานิพนธ์นี้เป็นส่วนหนึ่งของการศึกษาตามหลักสูตรปริญญาวิทยาศาสตรดุษฎีบัณฑิต
สาขาวิชาธรณีวิทยา ภาควิชาธรณีวิทยา
คณะวิทยาศาสตร์ จุฬาลงกรณ์มหาวิทยาลัย
ปีการศึกษา 2552

SEISMIC HAZARD ASSESSMENT IN THAILAND USING PROBABILISTIC AND DETERMINISTIC METHODS

Mr. Santi Pailoplee

A Dissertation Submitted in Partial Fulfillment of the Requirements

for the Degree of Doctor of Philosophy Program in Geology

Department of Geology

Faculty of Science

Chulalongkorn University

Academic year 2009

Thesis Title	SEISMIC HAZARD ASSESSMENT IN THAILAND USING PROBABILISTIC AND DETERMINISTIC METHODS
By	Mr. Santi Pailoplee
Field of Study	Geology
Thesis Advisor	Associate Professor Punya Charusiri, Ph.D.
Thesis Co-Advisor	Yuichi Sugiyama, Ph.D.

Accepted by the Faculty of Science, Chulalongkorn University in Partial Fulfillment of the Requirements for the Doctoral Degree

..... Dean of the Faculty of Science

(Professor Supot Hannongbua, Dr.rer.nat.)

THESIS COMMITTEE

..... Chairman

(Associate Professor Visut Pisutha-arnond, Ph.D.)

..... Thesis Advisor

(Associate Professor Punya Charusiri, Ph.D.)

..... Thesis Co-Advisor

(Yuichi Sugiyama, Ph.D.)

..... Examiner

(Associate Professor Supot Teachavorasinskun, Ph.D.)

..... Examiner

(Thanop Thitimakorn, Ph.D.)

.....External Examiner

(Thanu Harnpattanapanich, Ph.D.)

..... External Examiner

(Prinya Putthapiban, Ph.D.)

สันติ ภัยหลบลี้ : การประเมินอันตรายจากแผ่นดินไหวในประเทศไทยโดยวิธีความน่าจะเป็นและวิธีกำหนดค่า. (SEISMIC HAZARD ASSESSMENT IN THAILAND USING PROBABILISTIC AND DETERMINISTIC METHODS) อ. ที่ปรึกษาวิทยานิพนธ์หลัก : รศ.ดร. ปัญญา จารุศิริ, อ. ที่ปรึกษาวิทยานิพนธ์ร่วม : Yuichi Sugiyama, Ph.D., 163 หน้า.

งานวิจัยนี้มุ่งเน้นประเมินอันตรายจากแผ่นดินไหวในประเทศไทยและพื้นที่ข้างเคียง โดยพิจารณาแหล่งกำเนิดแผ่นดินไหวจากการกระจายตัวของรอยเลื่อนมีพลังและเขตกำเนิดแผ่นดินไหวในพื้นที่ศึกษา พฤติกรรมของแต่ละแหล่งกำเนิดแผ่นดินไหวประเมินจากข้อมูลการสำรวจรอยเลื่อนมีพลัง ประมวลผลร่วมกับฐานข้อมูลแผ่นดินไหวที่ตรวจวัดได้จากเครื่องมือตรวจวัดในปัจจุบัน วิธีกำหนดค่าและวิธีความน่าจะเป็นได้ถูกประยุกต์ใช้ในการประเมินอันตรายจากแผ่นดินไหวนี้ จากผลประเมินพบว่า ในกรณีของวิธีกำหนดค่าประเทศไทยมีโอกาสได้รับผลกระทบด้านแรงสั่นสะเทือนแผ่นดินไหวประมาณ 0g-0.8g ในบริเวณภาคเหนือ ภาคตะวันตก และภาคใต้ของประเทศไทย ส่วนในกรณีวิธีความน่าจะเป็น แสดงการกระจายตัวของอันตรายจากแผ่นดินไหวคล้ายกับวิธีกำหนดค่าแต่ให้ค่าระดับอันตรายที่สูงกว่า เช่น กรณีในรอบ 50 ปี มีโอกาส 2% ที่แรงสั่นสะเทือนรุนแรงกว่า 1g และ 10% ที่แรงสั่นสะเทือนรุนแรงกว่า 0.5g ในประเทศไทย ในขณะที่ภาคตะวันตกของพม่าและหมู่เกาะนิโคบาร์ พบว่าแรงสั่นสะเทือนมีโอกาสสูงถึง 3g จาก 2% ในรอบ 50 ปี ทั้งนี้เป็นผลเนื่องมาจากอยู่ใกล้กับแนวการมุดตัวของแผ่นเปลือกโลก สุมาตรา-อันดามัน โดยสรุป ผลการวิเคราะห์อันตรายจากแผ่นดินไหวนี้แสดงค่าระดับอันตรายสูงกว่าที่เคยมีการนำเสนอไว้ในงานวิจัยเก่า แต่จากการเปรียบเทียบร่วมกับข้อมูลแรงสั่นสะเทือนจากแผ่นดินไหวที่รายงานไว้ในอดีต พบว่าระดับอันตรายจากแผ่นดินไหวจากการวิเคราะห์ครั้งนี้สอดคล้องและสามารถต้านทานแผ่นดินไหวที่อาจเกิดขึ้นได้ในอนาคต อย่างไรก็ตาม เพื่อให้การประเมินระดับอันตรายจากแผ่นดินไหวถูกต้องแม่นยำมากยิ่งขึ้น ในอนาคตควรมีการศึกษาเพิ่มเติมโดยละเอียดเกี่ยวกับรอยเลื่อนมีพลังและแบบจำลองการลดทอนแรงสั่นสะเทือนจากแผ่นดินไหวที่เหมาะสมกับพื้นที่ศึกษา

ภาควิชา .....ธรณีวิทยา ... ลายมือชื่อนิสิต .....สันติ ภัยหลบลี้.....

สาขาวิชา ...ธรณีวิทยา ... ลายมือชื่อ อ.ที่ปรึกษาวิทยานิพนธ์หลัก .....

ปีการศึกษา.2552 ..... ลายมือชื่อ อ.ที่ปรึกษาวิทยานิพนธ์ร่วม Yuichi Sugiyama

4873858023 : MAJOR GEOLOGY

KEYWORDS : SEISMIC HAZARD ASSESSMENT / ACTIVE FAULT / THAILAND

SANTI PAILOPLEE : SEISMIC HAZARD ASSESSMENT IN THAILAND USING PROBABILISTIC AND DETERMINISTIC METHODS. THESIS ADVISOR : ASSOC.PROF. PUNYA CHARUSIRI, Ph.D., THESIS CO-ADVISOR : YUICHI SUGIYAMA, Ph.D., 163 pp.

In this study, the seismic hazards (SHA) in Thailand are analyzed. Fifty-five active fault zones identified from remote-sensing and out of those twenty-one seismic source zones are recognized to be the earthquake sources. The earthquake potential parameters used for SHA are derived from both active fault and earthquake catalogues. The strong ground-motion attenuation models are selected by comparison of the application of several candidate models with strong ground-motion data recorded in Thailand. Both deterministic (DSHA) and probabilistic (PSHA) approaches are employed in this SHA. For Thailand, there are seismic hazards in areas dominated by active fault zones such as northern, western, and southern Thailand. The DSHA map reveals seismic hazard around 0g-0.8g. In PSHA, the PGA values for 50 year in these areas are around 0.5g and 1g for 10% and 2% probability of exceedance, respectively. For Myanmar and Nicobar Islands the PSHA up to 3g in case of 2% probability of exceedance in 50 year according to the Sumatra-Andaman Subduction Zone. Comparing with the previous works the SHA of this study are higher than those proposed previously. However, this SHA compatible with the past ground shaking reported in the literatures. The SHA presented here is an important step toward an accurate evaluation of seismic hazard in Thailand. Further work is needed to refine the analysis. More observations of ground motion in the region are needed and further paleo-seismological study should be encouraged.

Department : Geology Student's Signature SANTI PAILOPLEE

Field of Study : Geology Advisor's Signature

Academic Year : 2009 Co-Advisor's Signature Yuichi Sugiyama

ACKNOWLEDGEMENTS

This work is sponsored by the Royal Golden Jubilee PhD Scholarship, Thailand Research Fund (Code number PHD/0093/2549) through Mr. Santi Pailoplee. Great acknowledgement goes to my Advisor, Associate Professor Dr. Punya Charusiri, Department of Geology, Faculty of Science, Chulalongkorn University for his valuable supervision, encouragement. His inspiration on scientific thinking is greatly appreciated. I acknowledge to Dr. Yuichi Sugiyama, my co-advisor (Active Fault Research Center-AFRC, National Institute of Advanced Industrial Science and Technology-AIST, Japan) with sincere thanks for his advice on the seismic hazard analysis in advance.

Associate Professor Dr. Montri Choowong for his advises particularly his valuable consistent helpful and comment both technically and non-technically. Special recognition and thanks are to K. Satake, M. Yoshimi, and K. Yoshida for their critical reviews of the manuscript during preparation. All AFRC members are thanked for a thorough kindly support during my 1-year research live in Japan. Thanks go to Mr. Chitti Palasri and Mr. Rottana Laddachat for their computational helping; without his strength, I could not run my works.

It is not easy to mention all persons who have contributed to my research study. I, personally, have already expressed my gratitude to everyone that has direct and indirect assistance with this research. Finally, the knowledge that this research is concluded will be sufficient gratification to those I have omitted. I have to thanks my parents for their moral support and encouragement and Mrs. Teerarat Pailoplee who invariably help me directly and indirectly.

CONTENTS

Page

LIST OF TABLES

LIST OF FIGURES

Page

Page

Page

Page

Page

Page

Page

CHAPTER I
INTRODUCTION

1.1 Theme and Background

On 26th December 2004, tsunami triggered by the great Sumatra–Andaman earthquake hit coastal communities around the Indian Ocean and killed more than 283,100 people (USGS, 2005). Moreover, this Mw 9.0 earthquake (Martin, 2005) caused ground shaking in countries surrounding its source including Thailand (Figure 1.1). These devastations are unprecedented in terms of scale and social impact and has subsequently aroused a large number of researchers (e.g., Dewey et al., 2007; Geist et al., 2007; Hanson et al., 2007) to recognize the need for assessment of the natural hazard in this region particularly in tsunami and seismic (i.e. earthquake) hazards.

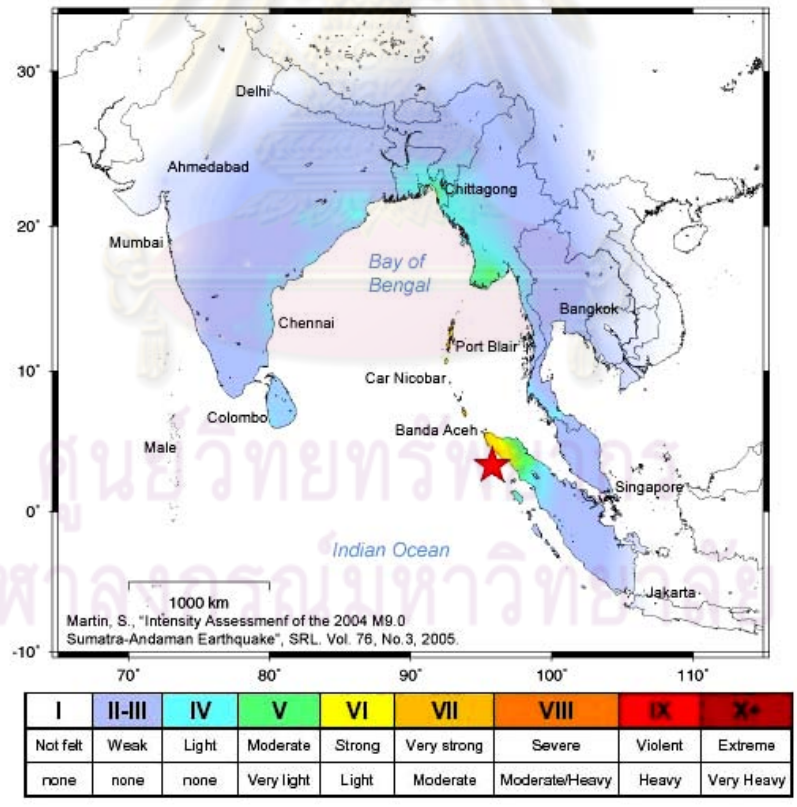

Figure 1.1. Map showing location of the Mw 9.0 Sumatra-Andaman shock (red star) and the area over which it was felt. Colored shades depict the maximum observed European Macro-seismic Scale intensity (Martin, 2005).

Up to the present, several methods of earthquake studies are developed. The final goal is an attempt to forecast the impending earthquakes in the long-term (years), intermediate-term (months-year), or even short-term (days-month) (Shebalin, 2006) (Table 1.1). Most methods inform approximately the time, location, or size of earthquakes that may occur in the future. However, this information doesn't solve exactly the critical impact of the earthquake to the public (e.g., ground shaking, liquefaction, landslide, and sink hole). Among these methods, "seismic hazard analysis (SHA)" is the unique one allowed to predict directly the possible ground shaking that may pose in individual areas when the earthquakes occur in the future anywhere and anytime (Cornell, 1968). Thus, this thesis research focuses mainly on the evaluation of earthquake ground shaking in Thailand and adjacent areas by using this SHA method.

Table 1.1. State of the art of the earthquake prediction (modified after Shebalin, 2006).

Method	Reference
A. Long-term (years)	
A1. Paleo-seismological study	McCalpin (1996); Pailoplee et al. (2009a)
A2. Historical study	McCue (2004); Stirling and Petersen (2006)
A3. Seismic hazard analysis	Kramer (1996); Pailoplee et al. (2009b)
A4. Global positioning system	Yagi et al. (2001); Fu and Sun (2006)
B. Intermediate-term (months-year)	
B1. b-value anomaly	Nuannin et al. (2004)
B2. Fractal dimension	Maryanto and Mulyana (2008)
B3. Artificial neural network	Bodri (2001); Alves (2006)
B4. Coulomb stress failure	Du and Sykes (2001); Bufe (2006)
C. Short-term (days-month)	
C1. Animal perception	Kirschvink (2000)
C2. Characteristic of cloud	Simons (2008)
C3. Ground water fluctuation	Oki and Hiraga (1988)
C4. Radon fluctuation	Zmazek et al. (2000)

1.2 Study Area

The area for the SHA is located between latitudes 5°N-21°N and longitudes 96°E-106°E and covers overall Thailand territory and some parts of the neighborhood countries. In practical, not only the earthquakes located within Thailand cause ground shaking to this region, but also the earthquakes in surrounding areas, such as Myanmar, Laos, Andaman-Nicobar Islands, or even Sumatra Island, can generate the earthquake ground shaking that propagates to Thailand. Empirically, Das et al. (2006) recommended that 300-km radius circle around the site of SHA interest should be investigated for the earthquake sources that may cause ground shaking to the site. This study, therefore, bounds the area where the earthquake source spreads out to the latitude 0°N-29°N and longitude 90°E-110°E (Figure 1.2).

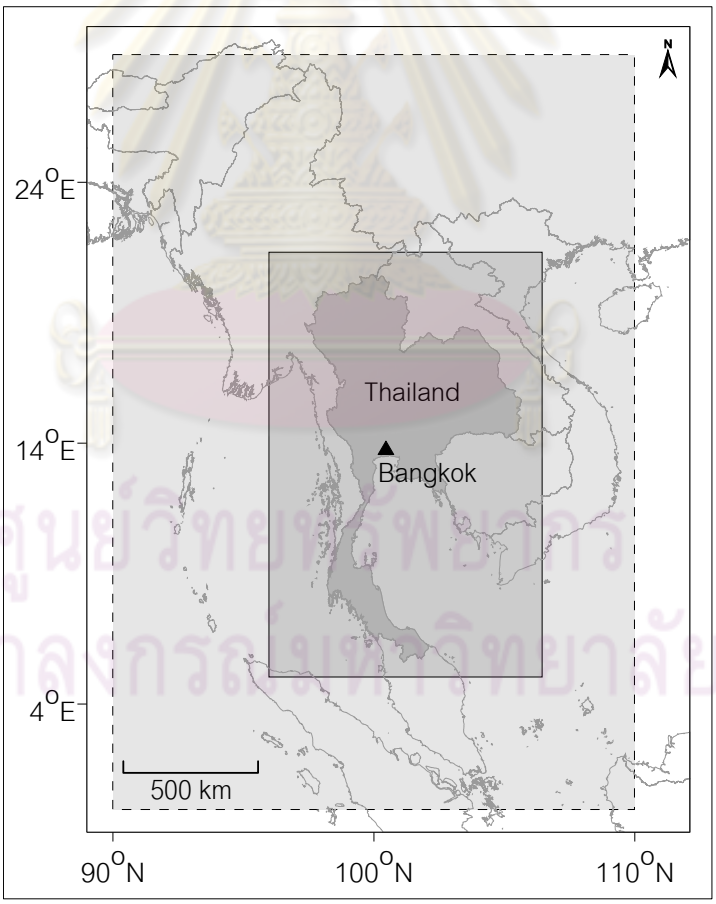

Figure 1.2. Map of Thailand and neighborhood countries showing the study area for SHA (inner box with solid line) and the area which the earthquake sources are investigated (outer box with dash line).

1.3 Literature Reviews

The previous seismic hazard investigation in the study area is reviewed. This information can guide about how to find out seismic sources and what kinds of specific equations and models are useful and suitable for this study. In this section, the outstanding previous works concerning with the seismic hazard analysis from global, regional and local scales are carefully investigated.

Giardini et al. (1999) complied the seismic hazard map in the global scale based on the Peak Ground Acceleration (PGA) (in unit m/sec^2). The map depicts the seismic hazard as 10% probability of exceedance in 50 years (Figure 1.3). The levels of ground shaking are determined in the rock site condition. The highest seismic hazard occur in the areas where have been, or are likely to be, the sites of major plate boundaries (Figure 1.3a). For Thailand, seismic hazard levels are around 0.8-1.6 m/sec^2 for northern and western parts whereas the rests are illustrated in 0–0.4 m/sec^2 (Figure 2b). The neighborhood countries are posed by the higher seismic hazard such as the central region of Myanmar (4-4.5 m/sec^2) and Sumatra Island of Indonesia (1.6-3.2 m/sec^2).

Recently, Petersen et al. (2004) evaluated the seismic hazard for the Sumatra Island, Indonesia with calculating in a probabilistic framework. Four regional seismic source zones were integrated with the inland active faults along the Sumatra Island in order to evaluate the potential of earthquake sources (Figure 1.4a). The strong ground-motion attenuation model proposed by Youngs et al. (1997) was modified for Sumatra-Andaman Subduction Zone earthquakes when compared with the strong ground-motion data occupied by the Global Digital Seismic Network (GDSN) in Malaysia and the Singapore Seismic Network (Figure 1.4b). For the shallow crustal earthquakes (i.e. earthquakes generated by inland active faults), the strong ground-motion attenuation model developed by Sadigh et al. (1997) was applied in this study. The seismic hazard maps reveal 2% and 10% probability of exceedance in 50 years for rock site condition.

Consequently, the seismic hazard maps (Figure 1.5) reveal that the ground motions across Sumatra range between about 6%g and 100%g for 10% probability of exceedance (g is the gravitational acceleration = 9.81 m/sec^2 as a result of 6%g and 100% is equal to 0.06g and 1g, respectively) and between about 10%g (i.e., 0.1g) up to

160%g (i.e., 1.6g) for 2% probability of exceedance. Moreover, they concluded that the largest earthquake contributor to seismic hazard is the Sumatra Fault Zone.

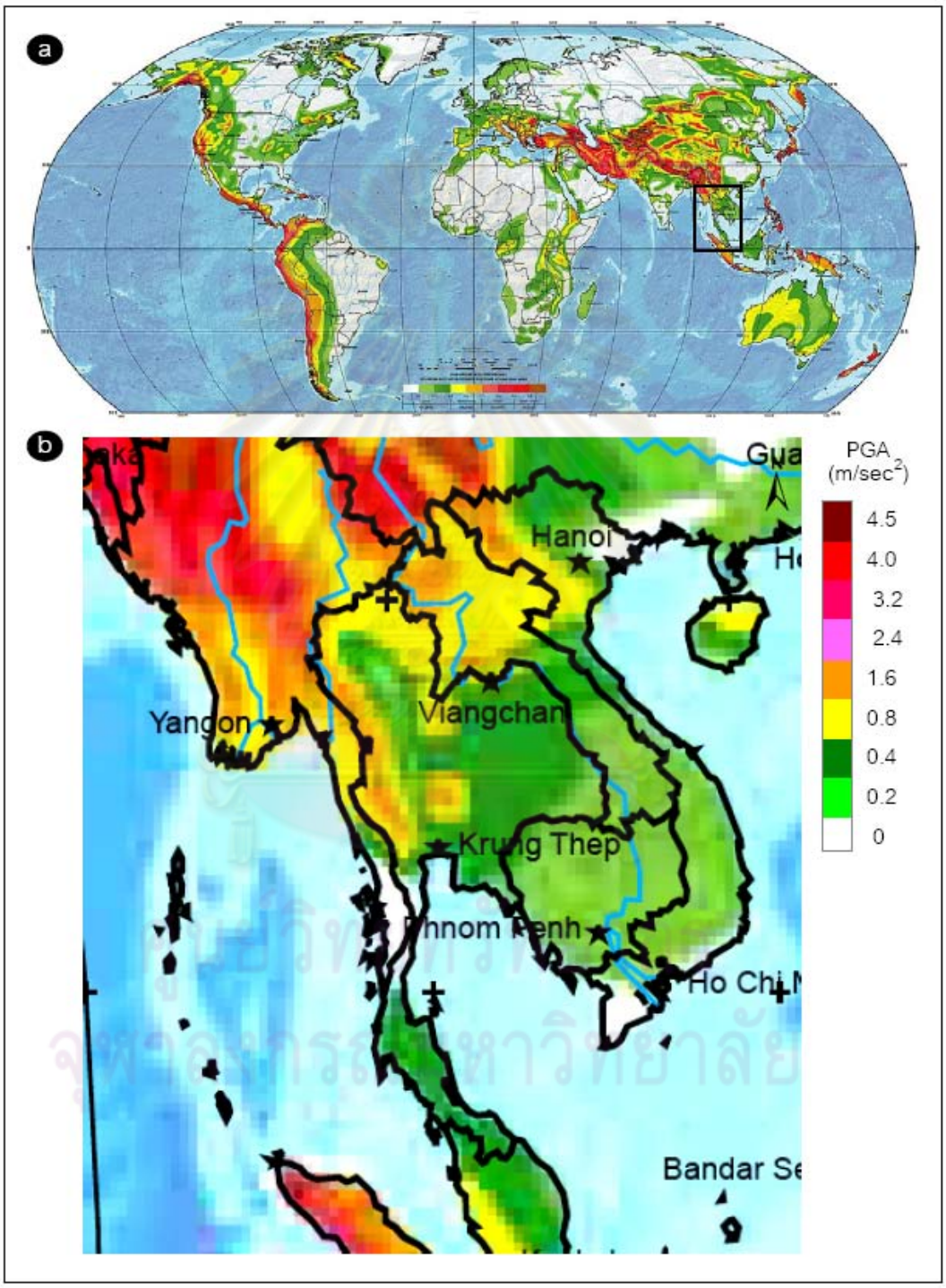

Figure 1.3. a) Global probabilistic seismic hazard map with a 10% probability of exceedance in 50 years (Giardini et al., 1999). Inserted box (in black) is Figure b. b) enlarged hazard map of Thailand and adjoining regions.

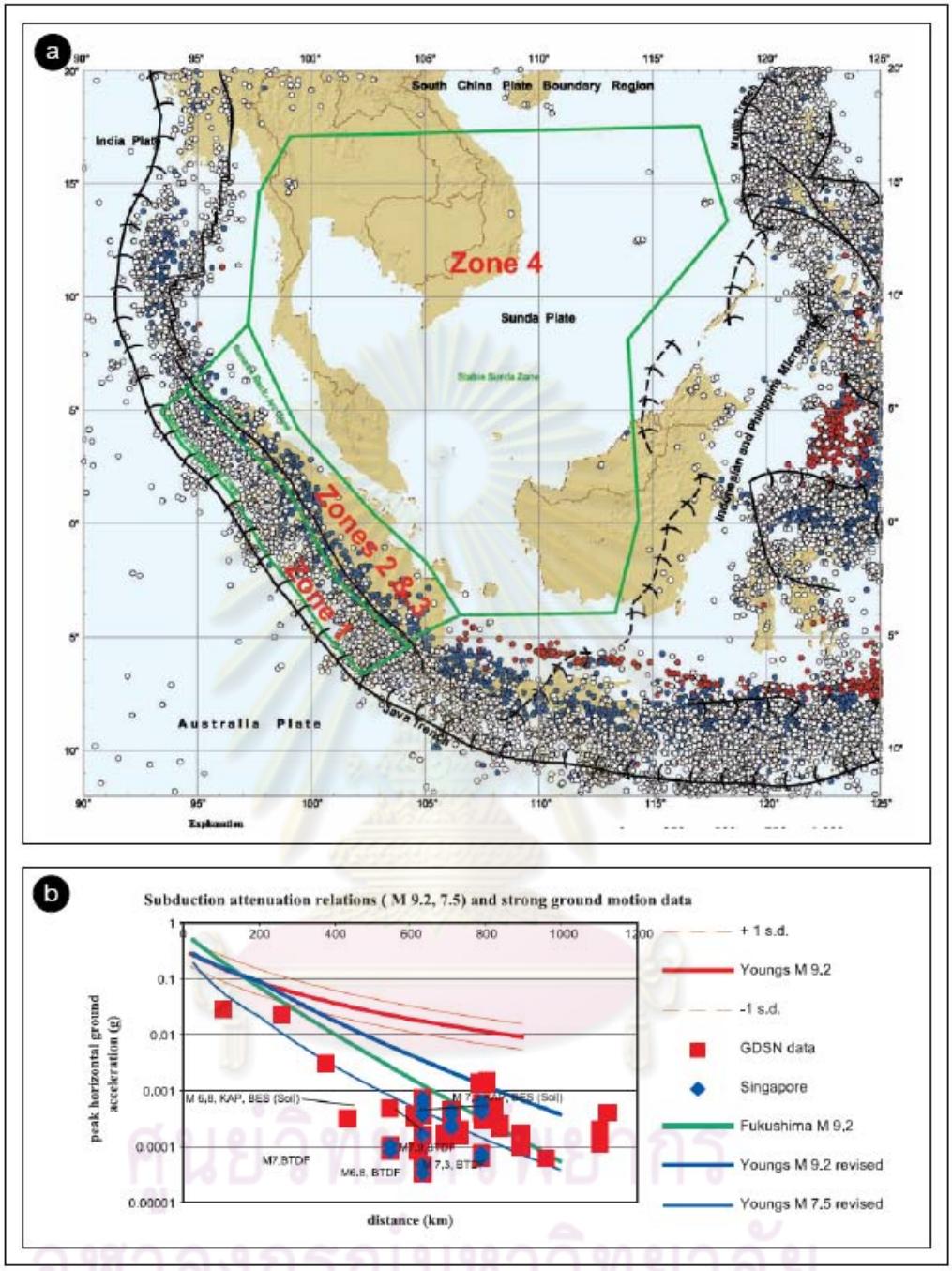

Figure 1.4. a) Map showing epicentral distribution (white, blue and red circles), seismic source zones (green polygons), and faults (black lines) used in Petersen et al. (2004); b) Plot showing ground acceleration (g) as a function of distance (km) from subduction zone attenuation relations and relevant data for large distances from the GDSN and Singapore seismic networks.

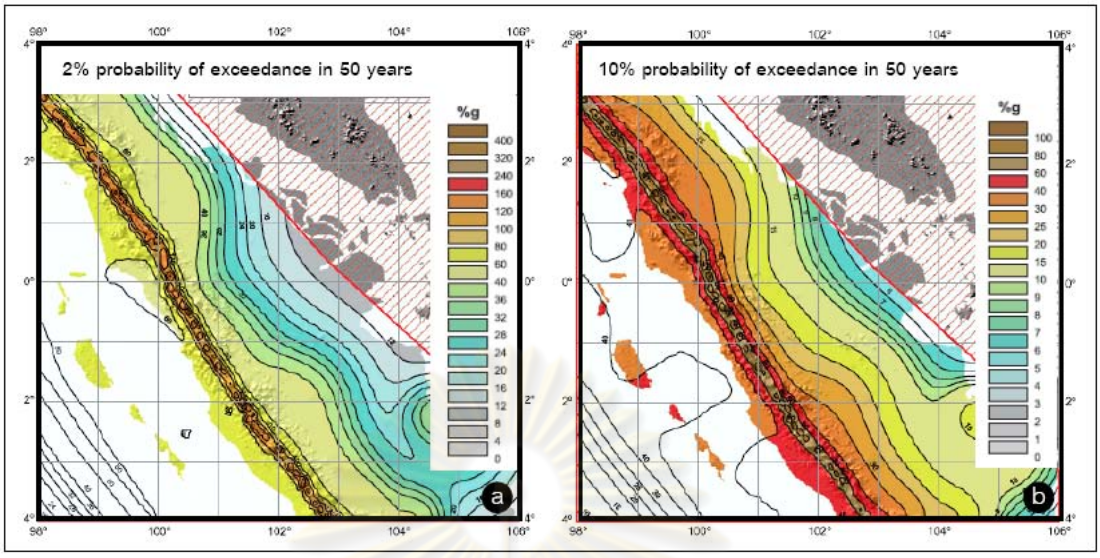

Figure 1.5. Map showing seismic hazard at a) 2% and b) 10% probability of exceedance in 50 years on rock site condition for Sumatra and the Malaysian peninsula (Petersen et al., 2004).

In Thailand region, there have been few recent seismic hazard analyses, Wanitchai and Lisantono (1996) is the pioneer who proposed the first seismic hazard map for Thailand in term of probability of exceedance. The analysis started with evaluation the earthquake potential from 11 seismic source zones proposed by Nutalaya et al. (1985) by using 80-year seismicity data (i.e. instrumental earthquake records) reported by Nutalaya et al. (1985) (Figure 1.6a). The strong ground-motion attenuation model proposed by Esteva and Villaverde (1973) was compromised to be the average ground-shaking attenuation characteristic in Thailand (the grey strip in Figure 1.6b) after comparing the models proposed for USA and Europe regions (Figure 1.6b). The PSHA was evaluated according to the well known Cornell's concept (Cornell, 1968). The obtained results are presented by a map showing contours of the expected PGA with a 10% chance of being exceeded in a 50 years. The map indicates the PGA in the range 0.08-0.25g in western and northern Thailand and the hazard decrease eastward and southward to 0 (Figure 1.7). The maximum hazard levels showed in this map are 0.45g which is located in Lao country, close to northern Thailand. Wanitchai and Lisantono (1996) also categorized the seismic hazard level in according to the U.S. Uniform Building Code (UBC) (Whittier, 1988). Northern and western Thailand are classified as

the moderate and moderately high seismic hazard zones equivalent to zone 2B and 3 respectively (Figure 1.7).

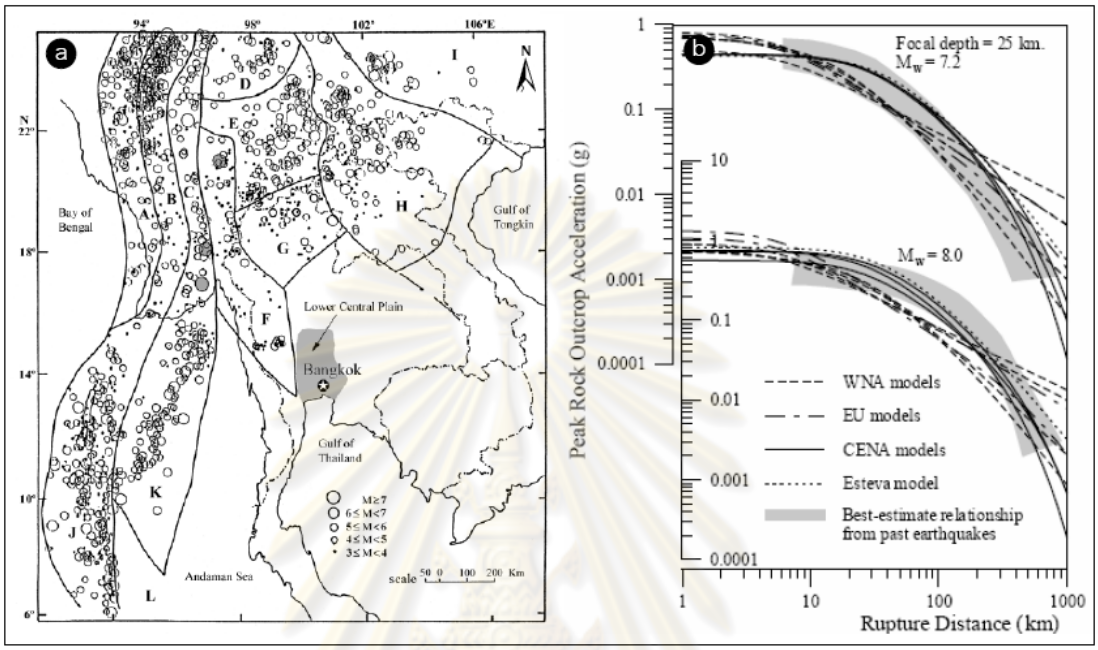

Figure 1.6. a) Twelve regional seismic source zones (zone A-L) in Thailand and adjacent areas and epicentral distributions of earthquakes recorded during 1910-2001 based on the work of Nutalaya et al. (1985); b) Graph showing the strong ground-motion attenuation relationships with the best estimate by Wanitchai and Lisantono (1996). The Esteva and Villaverde (1973)'s model is illustrated in the dot line.

After the seismic hazard map in Thailand, which analyzed numerically, was proposed by Wanitchai and Lisantono (1996), Department of Mineral Resources (DMR, 2005) proposed the other kind of seismic hazard map of Thailand in the geological point of view based on compilation of tectonic setting, active faults, and seismicity data. The proposed map categorized the seismic hazard in Thailand into 4 levels of the Modified Mercalli Intensity (MMI) scale (Figure 1.8). The map shows the highest seismic hazard in northern, western throughout southern part of Thailand (zones 2a and 2b). In contrast, the northeastern part and some of the central part of Thailand are classified to be the low seismic hazard region (zones 0 and 1).

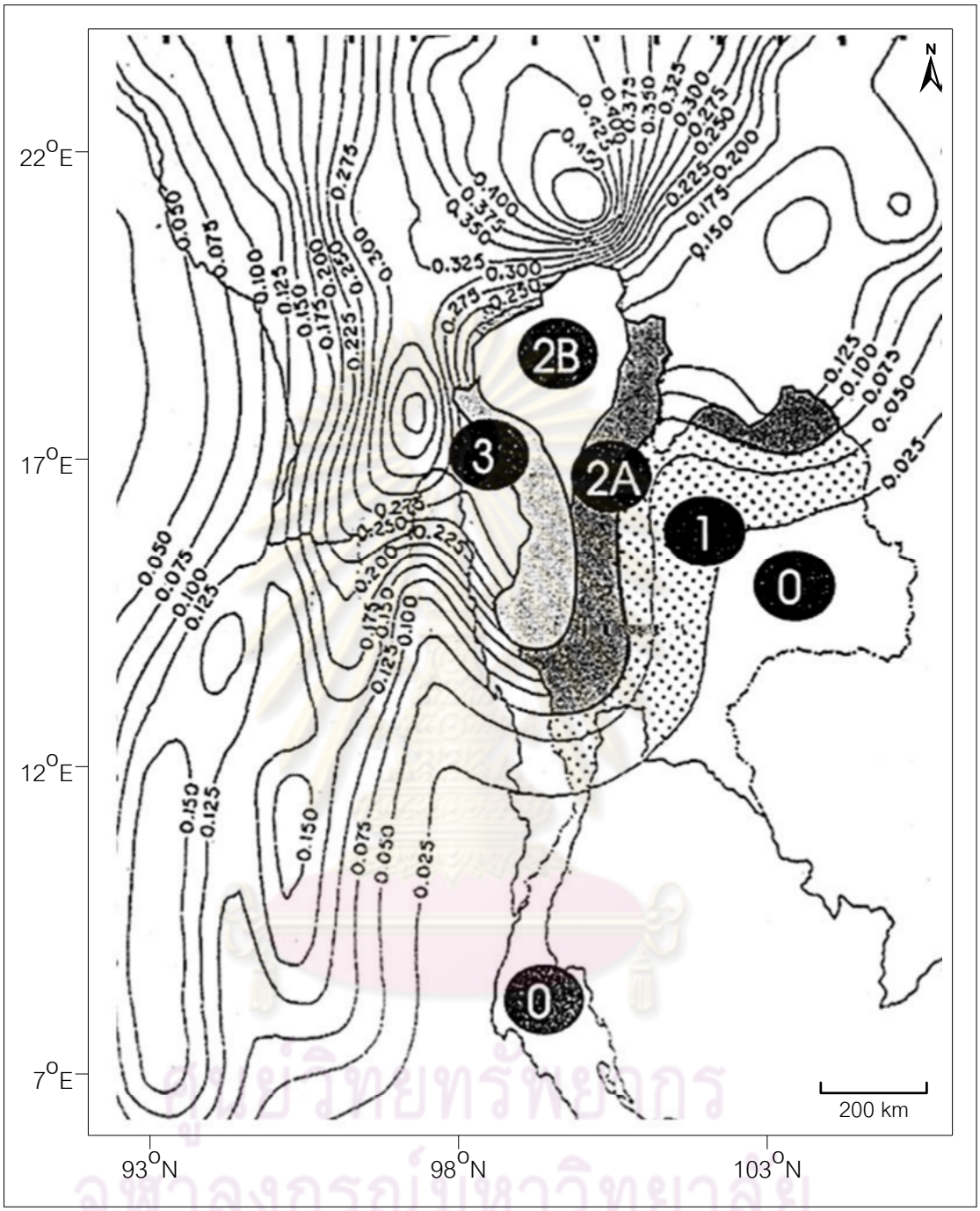

Figure 1.7. Map showing contours of the PGA with 10% chance of being exceeded in a 50 year, and seismic hazard zone for earthquake-resistant design based on the UBC code (Wanitchai and Lisantono, 1996). Note that southern peninsular Thailand was given as zone 0 in their report.

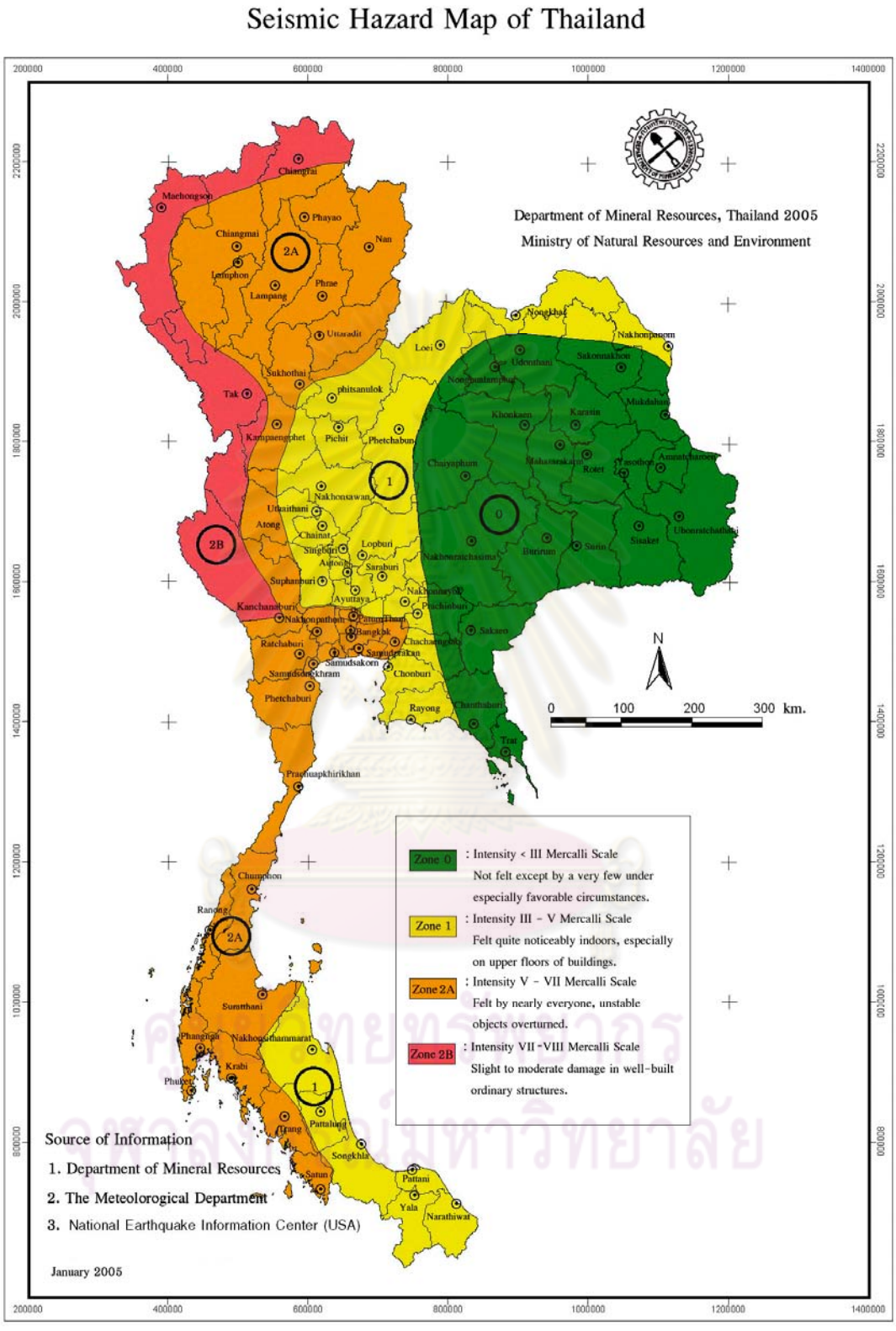

Figure 1.8. Seismic hazard map of Thailand showing in different colors represented difference seismic hazard levels in the scale of Modified Mercalli Intensity (MMI) (Department of Mineral Resources, 2005).

Subsequently, Palasri (2006) re-investigated the seismic hazard in Thailand and neighborhood areas in term of the probabilistic approach by using the more up-to-date instrumental earthquake records (A.D. 2003-2006) from the Thai Meteorological Department (TMD) and US Geological Survey (USGS). The new seismic source zones proposed by Charusiri et al. (2005) were applied to be the earthquake sources in this study (Figure 1.9a).

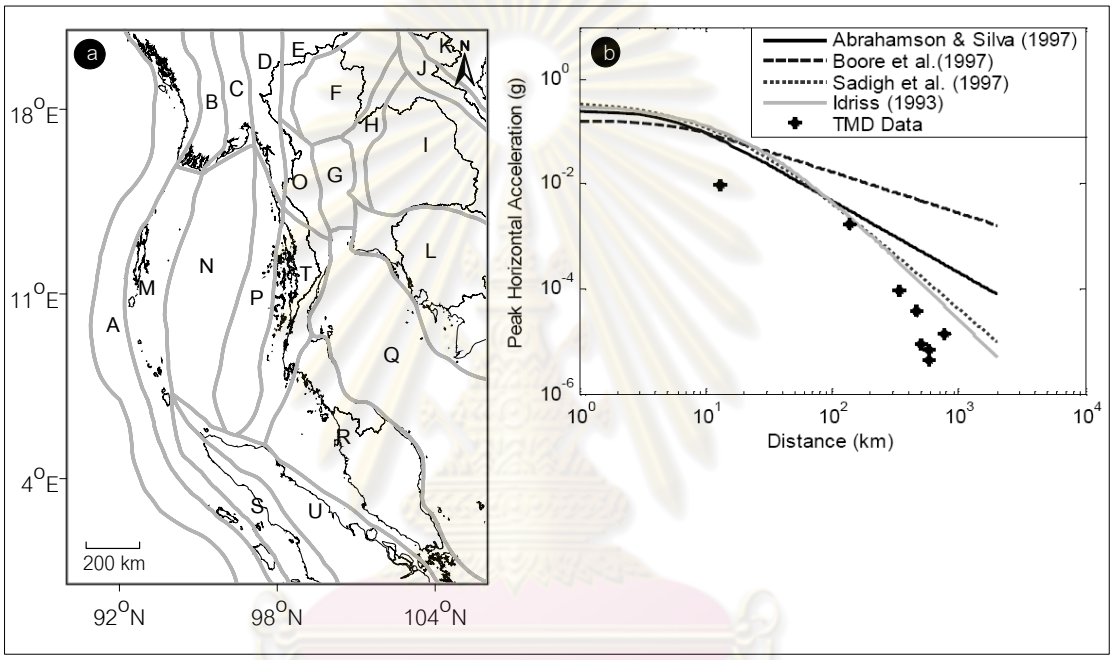

Figure 1.9. a) Twenty-one seismic source zones (zone A-U) in Thailand and adjacent areas based on the work of Charusiri et al. (2005). The capital letters are the zone code described in Table 4.1; b) Graphs showing relationship between the strong ground-motion attenuation relationships and strong ground-motion data observed by the Thai Meteorological Department (Palasri, 2006).

For strong ground-motion attenuation, Palasri (2006) followed the Petersen et al. (2004)'s model for the earthquakes occur along the Sumatra-Andaman region. For the shallow crustal earthquakes, Palasri (2006) proposed the new strong ground-motion attenuation which is different from that used in Wanitchai and Lisantono (1996)'s work. Palasri (2006) compared some of the strong ground-motion proposed previously for the

foreign regions with the strong-ground motion data which recorded by the Thai Meteorological Department (TMD)'s network. The single earthquake event which generated the ground motion is the Mw 5.1 earthquake which occurred in 13th December 2006 at Mae Rim district, Chiang Mai province, Thailand. The strong ground-motion attenuation model proposed by Sadigh et al. (1997) was selected to represent the attenuation characteristic of shallow crustal earthquakes in this region (Figure 1.9b). The map of 10% probability of exceedance in 50 years indicates the PGA around 0.2-0.3g in western and northern Thailand (Figure 1.10a). For 2% probability of exceedance (Figure 1.10b), the PGA increases up to twice from the 10% probability of exceedance for most areas.

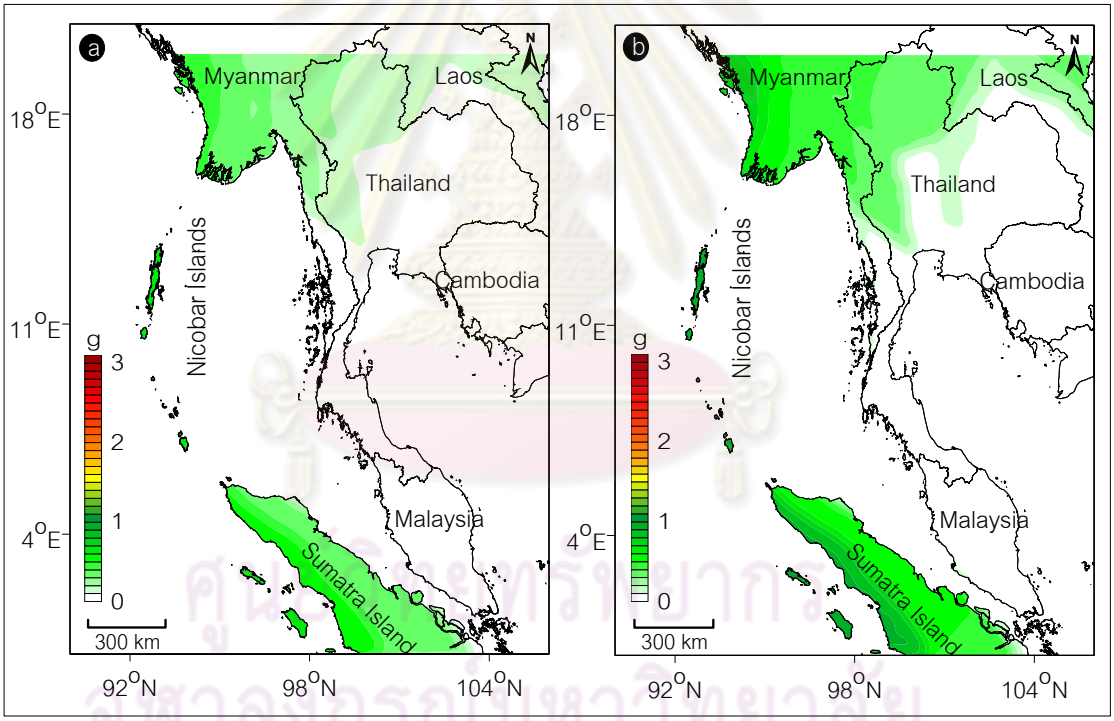

Figure 1.10. Probabilistic seismic hazard map of Thailand; a) 10% and b) 2% probability of exceedance in the 50-year return period (Palasri, 2006). Note that no hazard in southern peninsular Thailand.

Finally, Petersen et al. (2007) updated the Petersen et al. (2004)'s seismic hazard analysis model for Southeast Asia region by revising earthquake catalogs, developing new seismo-tectonic models, and implementing new fault data within and

close to Thailand (Figure 1.11). For 2% probabilities of exceedance in 50 years, the results reveal the seismic hazard level 10-20%g (0.1-0.2g) in regional Thailand territory (Figure 1.12b). The specific high hazard levels in Thailand are located in the western part at Three Pagoda Fault Zone and some area nearby the fault zones in northern Thailand. The hazard levels in the area nearby these fault zones are around 25-30%g (0.25-0.3g) whereas the seismic hazard levels analyzed along the Sagiang Fault, central Myanmar and Sumatra Fault, Sumatra Island reveals the ground shaking rise up to 110%g (1.1g). For 10% probability of exceedance in 50 years, the PGA decrease spatially to 50% compared with the map of 2% probability of exceedance in 50 years (Figure 1.12a).

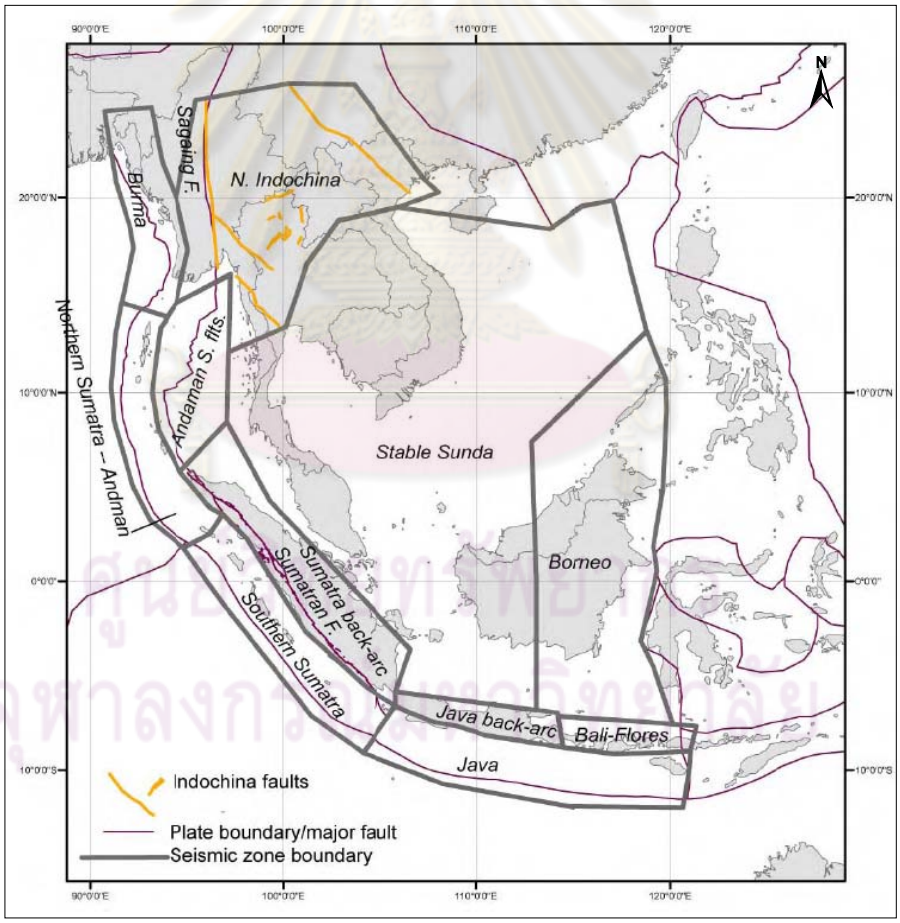

Figure 1.11. Map of seismic source zones (grey lines) including the active faults (yellow lines) and plate boundary/major faults (purple lines) that were considered for the seismic hazard analysis (Petersen et al., 2007).

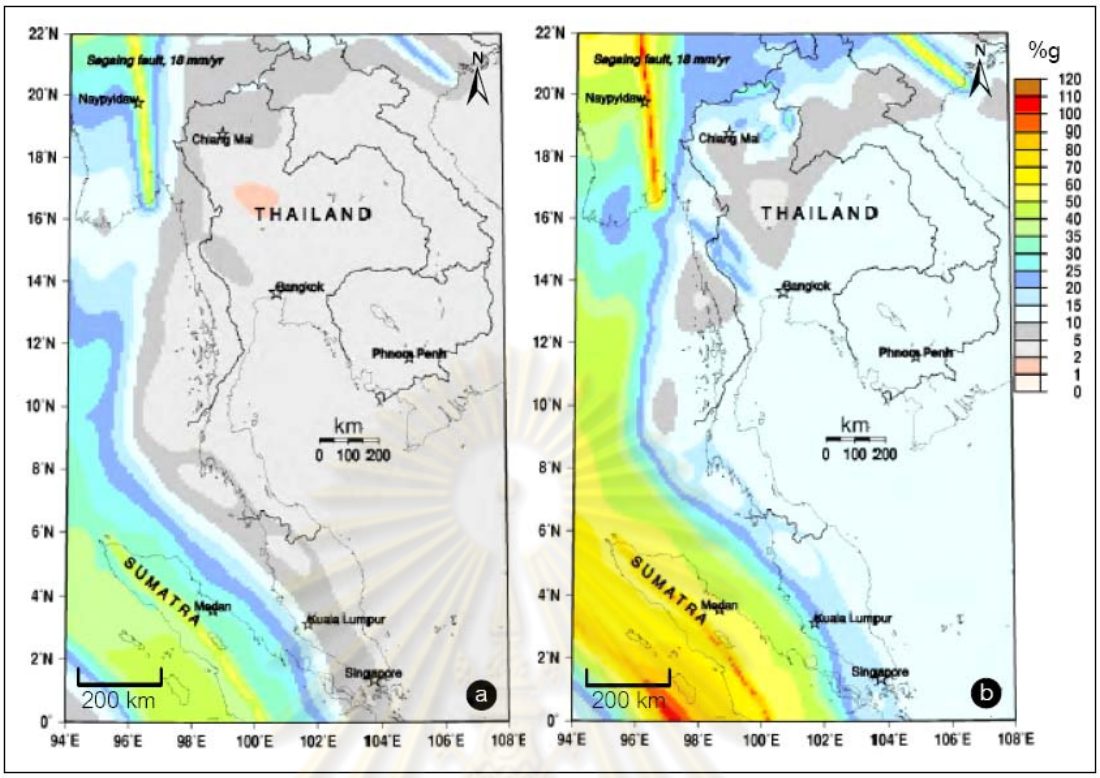

Figure 1.12. Probabilistic seismic hazard maps for mainland SE Asia showing the PGA with a) 10% and b) 2% probability of exceedance in 50-year return period for the rock site condition (Petersen et al., 2007).

1.4 Objectives

From the previous works described above, some of the assumptions and models are still suspect and not perfectly clear. For instance, two earlier workers (i.e. Wanitchai and Lisantono, 1996; Palasri, 2006) used the probabilistic approach to analyze the seismic hazard by using only the instrumental earthquake records to determine the potential of earthquake sources. Their results, however, may have limitations because of the short history of instrumental recording of earthquakes (i.e. 80 years in maximum). The time span covered by instrumental records is too short to represent the behavior of earthquake activity, in particular the large-size ones (Yeats et. al., 1996). Therefore, there is a need to redefine the SHA in Thailand and adjacent areas. More observations of earthquake sources and earthquake potentials are required and the strong ground-motion attenuation behaviors of the earthquakes are encouraged. The objectives show consecutively in detail as following:

- To investigate the paleo-seismology in some sites of interest;
- To compile the earthquake sources which cause ground shaking to the study area;
- To evaluate the earthquake potentials of individual sources from both geological (i.e. paleo-seismological) and seismological (i.e. instrumental) data;
- To refine the ground-motion attenuation models and select the appropriated models for the study area; and
- To evaluate the seismic hazard levels in the study area.

These complementary approaches can provide SHA results that are more up-to-date and more accurate than those currently available.

CHAPTER II
CONCEPT AND METHODOLOGY

2.1 Concept

Seismic Hazard Analysis (SHA) involves the quantitative estimation of earthquake ground shaking at a particular site (Kramer, 1996). By definition, "seismic hazard analysis" and "seismic risk analysis" are totally different. Seismic hazard describes phenomena and harm generated by earthquakes that can be evaluated from instrumental, historical, and geological observations, but seismic risk is the likelihood of human experiencing a specified level of seismic hazard in a given time exposure (see more details in Wang, 2006). High seismic hazard, therefore, does not necessarily mean high seismic risk. At present, the concept of SHA widely used nowadays (Kramer, 1996) can be divided into 2 concepts as shown below;

2.1.1 Deterministic seismic hazard analysis (DSHA)

DSHA developed by Costa et al. (1992, 1993) and subsequently applied to several regions of the world (e.g. Orozov-Stanishkova et al., 1996; Radulian et al., 1999; Alvarez et al., 1999; Panza et al., 1999; Aoudia et al., 2000). The DSHA aims at finding the maximum ground shaking as possible at a given site in which effects from the largest earthquake expected (also termed as Maximum Credible Earthquakes- $MCEs$) (Anderson et al., 2000). This assumption ensures that a structure can withstand the $MCEs$, it will automatically withstand all other (i.e. smaller) earthquakes as well. For this purpose, the methodology of DSHA is described in the following (see also Figure 2.1);

1. Identification and characterization of all earthquake sources, such as 1) point source (e.g. cluster of earthquake swarms in the volcanic eruption area), 2) line source (e.g. active fault lines), and 3) area source (e.g. seismic source zones which the epicentral earthquake distributions don't associated with specific faults) capable of producing significant ground motion in the study area. Source characterization includes definition of each earthquake source and the $MCEs$ (step 1 in Figure 2.1).

2. Evaluation of the source-to-site distances for individual earthquake source. In DSHA, the shortest distance between the earthquake source and the site of interest is selected (step 2 in Figure 2.1).
3. Selection of the controlling earthquake (i.e. the earthquake that is expected to produce the strongest level of ground shaking or ground motion) at the site. This selection is made by comparing the levels of $MCEs$ as identify in step 1 assumed to occur at the shortest distance as identified in step 2. Its characteristics are usually described by the empirical strong ground-motion attenuation model which represents the decreasing ground shaking level when the source-to-site distance is increase (step 3 in Figure 2.1).
4. Definition of the seismic hazard at the site of interest evaluated by DSHA approach is made in terms of the ground shaking produced at the site by the controlling earthquake (step 4 in Figure 2.1). Peak ground acceleration (PGA), is commonly used to characterize the level of ground shaking.

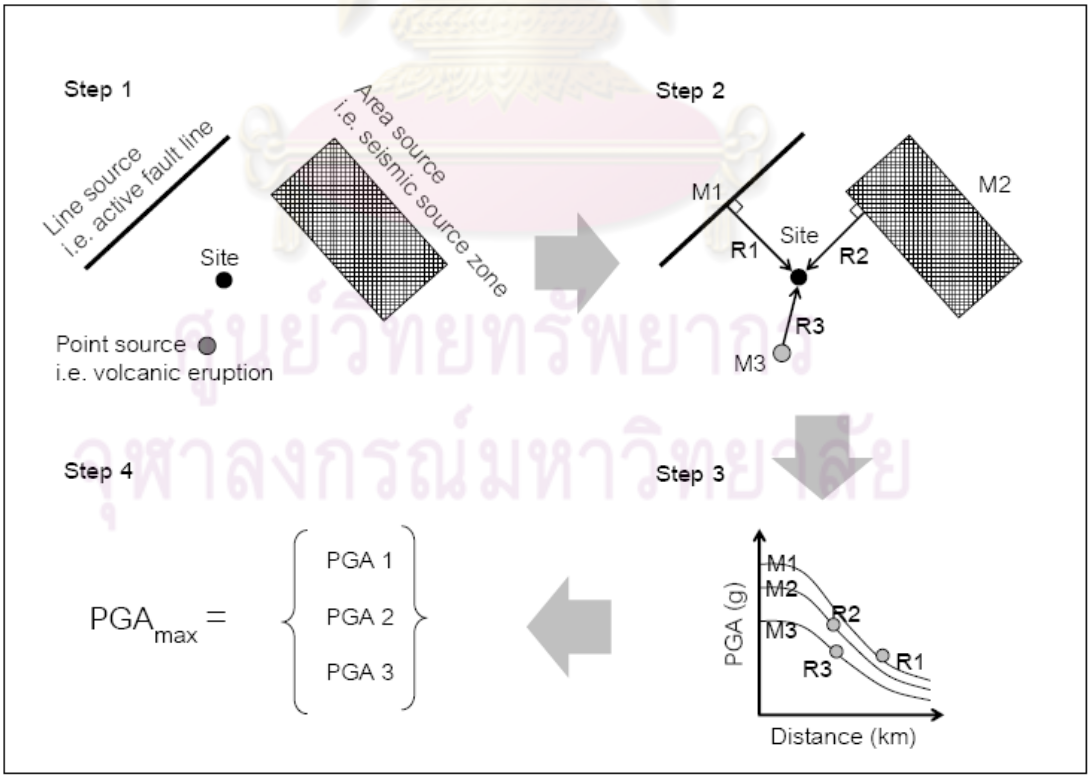

Figure 2.1. Four steps of a deterministic seismic hazard analysis (Kramer, 1996).

2.1.2 Probabilistic seismic hazard analysis (PSHA)

A PSHA is an evaluation of the ground shaking that will be exceeded at a specified annual frequency or probability (Cornell, 1968). The inputs to a PSHA are the same as those used in DSHA plus the assessment of the frequency of earthquake occurrences and the probability of the possible source-to-site distance. The following steps are taken in a PSHA which is somewhat similar to a deterministic analysis (see also Figure 2.2);

1. The first step, identification and characterization of earthquake sources, is identical to the first step of the DSHA, except that the probability distribution of potential rupture locations within the earthquake source must also be characterized. In most cases, uniform probability distributions are assigned to individual source zones, implying that earthquakes are equally likely to occur at any point within the earthquake source. These distributions are then combined with the source geometry to obtain the corresponding probability distribution of the source-to-site distance (step 1 in Figure 2.2).
2. Next, the temporal distribution of earthquake occurrences must be characterized. The earthquake frequency-magnitude relationship is used to characterize the earthquake potential of individual earthquake source (step 2 in Figure 2.2).
3. The ground motion produced at the site by an earthquake of any possible size occurring at any possible point in each source zone must be determined with the use of the empirical strong ground motion attenuation model as used in DSHA. Furthermore, the uncertainty (1 standard deviation, $1\,SD$) in the attenuation model is also considered in the PSHA (step 3 in Figure 2.2).
4. Finally, the uncertainties in earthquake location, earthquake size, and ground motion parameter prediction are combined to obtain the probability that the ground shaking level will be exceeded during a particular PGA (step 4 in Figure 2.2).

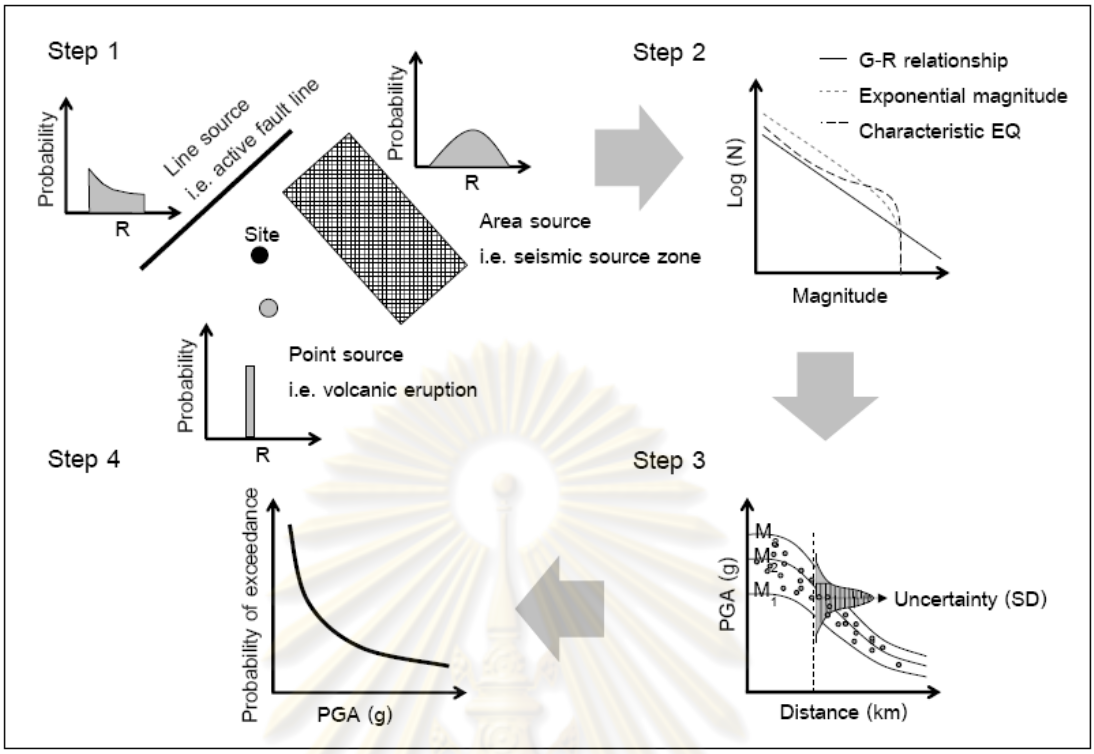

Figure 2.2. Four steps of a probabilistic seismic hazard analysis (Kramer, 1996).

2.2 Methodology

For both DSHA and PSHA in this research, the required input data and models that are recognized are the characteristics of the earthquake sources and the ground-shaking attenuation. In earthquake source, the location, geometry, including the nature of earthquake occurrence in individual sources has to be clarified. For instance, some sources generated frequently the small- to medium-size earthquakes whereas the others released only the large-size ones in the long return period. Moreover, in individual areas, the regional tectonic and geologic settings are varied. This difference causes the specific characteristics of the ground shaking attenuation when the seismic wave propagates through the medium. All of these understandings are necessary for this SHA. The details are described consecutively as shown below (see also Figure 2.3).

2.2.1 Paleo-seismological investigation

This procedure focuses on geological investigations (i.e. paleo-seismology) according to the method proposed by McCalpin (1996) (step 1 in Figure 2.3). A site of interest is selected for paleo-seismological investigation. The results are described in

stratigraphy associated with faulting. Simultaneous Thermoluminescence and AMS-radiocarbon dating are determined to constrain the dates of paleo-seismological results such as sip rates of the paleo-earthquakes.

Moreover, all possible active faults that may affect the study area are complied. The active fault lines proposed in the previous published maps and documents are re-interpreted by using enhanced remote sensing data. The paleo-seismological parameters for SHA are carefully summarized from the previous publications.

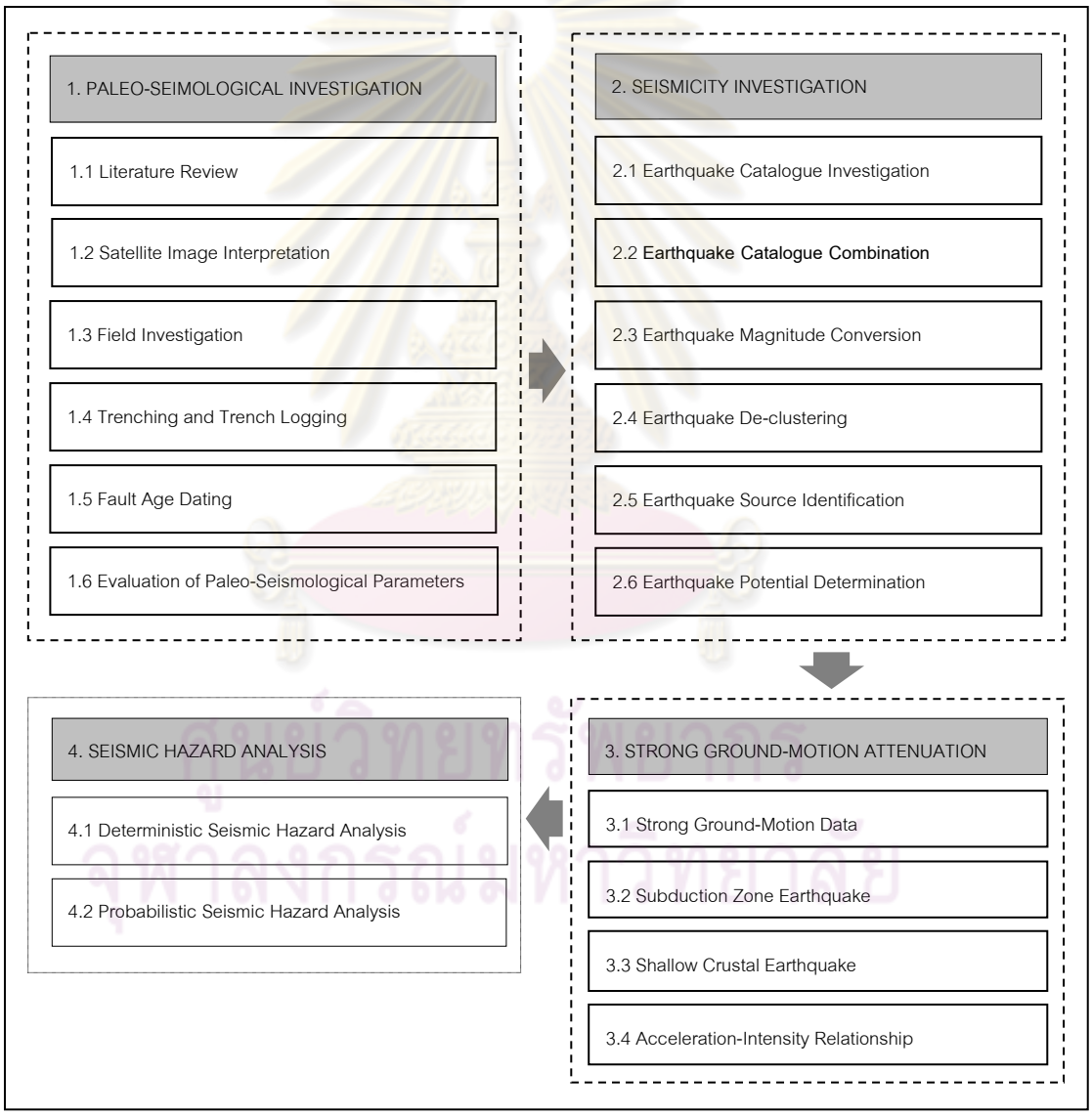

Figure 2.3. Simplified flow chart showing the methodology applied in this study.

2.2.2 Seismicity investigation

To determine the earthquake source potentials, not only the paleo-seismological data but also the seismicity data which reported in the earthquake catalogues, are required. Beside the paleo-seismological data which represent the long-recurrence and large-size earthquake, the seismicity data are always useful for understanding the short-recurrence of the small- to medium-size earthquakes. In the past, the obtained original earthquake catalogues has been recorded non-systematically in practice, those data are, therefore, un-reliable and not available for evaluation of earthquake source potential. As a result, before evaluation of earthquake source potential, the obtained earthquake catalogue must be improved. In this SHA, the improved methodology following Caceres and Kulhanek (2000) are applied as shown in step 2 in Figure 2.3 and described in more detail in chapter IV.

2.2.3 Strong ground-motion attenuation

As well as earthquake source described in two previous procedures, strong ground-motion attenuation models are essential for SHA. Thus this procedure focuses mainly on the investigation of the strong ground-motion attenuation models which represent the ground motion characteristic in the study area (step 3 in Figure 2.3). Different attenuation models for subduction earthquake and shallow crustal earthquake are carefully considered by using the strong ground-motion data occupied the TMD.

2.2.4 Seismic hazard analysis

In this procedure, the data and models obtained from the previous procedures are integrated to calculate the seismic hazard. According to lacking data of the soft soil related with ground shaking amplification, this seismic hazard is, therefore, investigated in the rock site condition. Both DSHA and PSHA scenario are applied in this study in order to use the advantages of both approaches (step 4 in Figure 2.3). For the time-independent DSHA, the worst-case of possible ground shaking is mapped in each area. Meanwhile different ground shaking levels depending on the specific time span of interest are mapped in PSHA. In individual time periods, PSHA maps are described, additionally, in 2 well known formats:

1. Map showing the ground shaking (in g unit) in individual % probability of exceedance and
2. Map showing the probability (in % unit) of ground shaking that is equal or larger than each ground shaking in the Modified Mercalli Intensity (MMI).

The former format is useful for engineering to decide the earthquake-resistant coefficient in the infrastructure construction whereas the latter is convenient in public announcement and also provides useful information for other purposes, such as estimation of earthquake insurance premiums and site-specific evaluation of seismic hazards.

CHAPTER III
PALEO-SEISMOLOGICAL INVESTIGATION

At present, it is accepted worldwide that paleo-seismological information is essential for evaluating the potential of earthquake source in SHA (Atakan et al., 2001; Gurpinar, 2005). This information obtained from active fault study can bridge the gap between instrumental and pre-instrumental data because active fault investigation can identify the large earthquakes which cannot be recorded in the instrumental or even historical time span. The accuracy of the paleo-seismological studies depends largely on the reliability of the scientific dating which constrains not only ages of faulting but also rates of fault slips and earthquake recurrences. This chapter provides a perspective on paleo-seismological investigations which fulfill the analysis in SHA. The detailed description is shown consecutively below (see also step 1 in Figure 2.3);

3.1 Literature Review

Even though no obvious surface-faulting earthquakes have been well documented in Thailand or nationhood area, wide spread evidence of Holocene surface deformation, however, has been recognized by Bott et al. (1997) and Fenton et al., (1997). The only surface rupture by faulting was reported by Nutalaya et al. (1985) after the large earthquake in 22 April 1983. From past two decades, some of the earthquake fault maps were proposed in this area.

The pioneer work is that of Chuaviroj (1991) who proposed the major fault zones in Thailand based on field and satellite image investigations. Totally, 13 fault zones are proposed (Figure 3.1); Pattani (PT), Klang (KL), Klong Marui (KM), Chiang Saen (CS) or Mae Chan, Mae Ping (MP), Mae Sariang (MS), Mae Tha (MT), Nam Pard (NP) or Uttaradit, Petchabun (PT), Phrae (PR), Ranong (RN), Sri Sawat (SS), and Three Pagoda (TP) Fault Zones.

Thereafter, Hinthong (1995) re-compiled the fault zones in Thailand based on satellite image interpretation, field investigation, historical and seismicity data. Some dates of earthquake faulting obtained from Thermoluminescence (TL) dating were also proposed to constrain the potential of fault activities. Finally, 22 fault zones in Thailand

were categorized in 4 classes; 1) potentially active, 2) historically and seismologically active, 3) neotectonically active and 4) tentatively active classes (Figure 3.2).

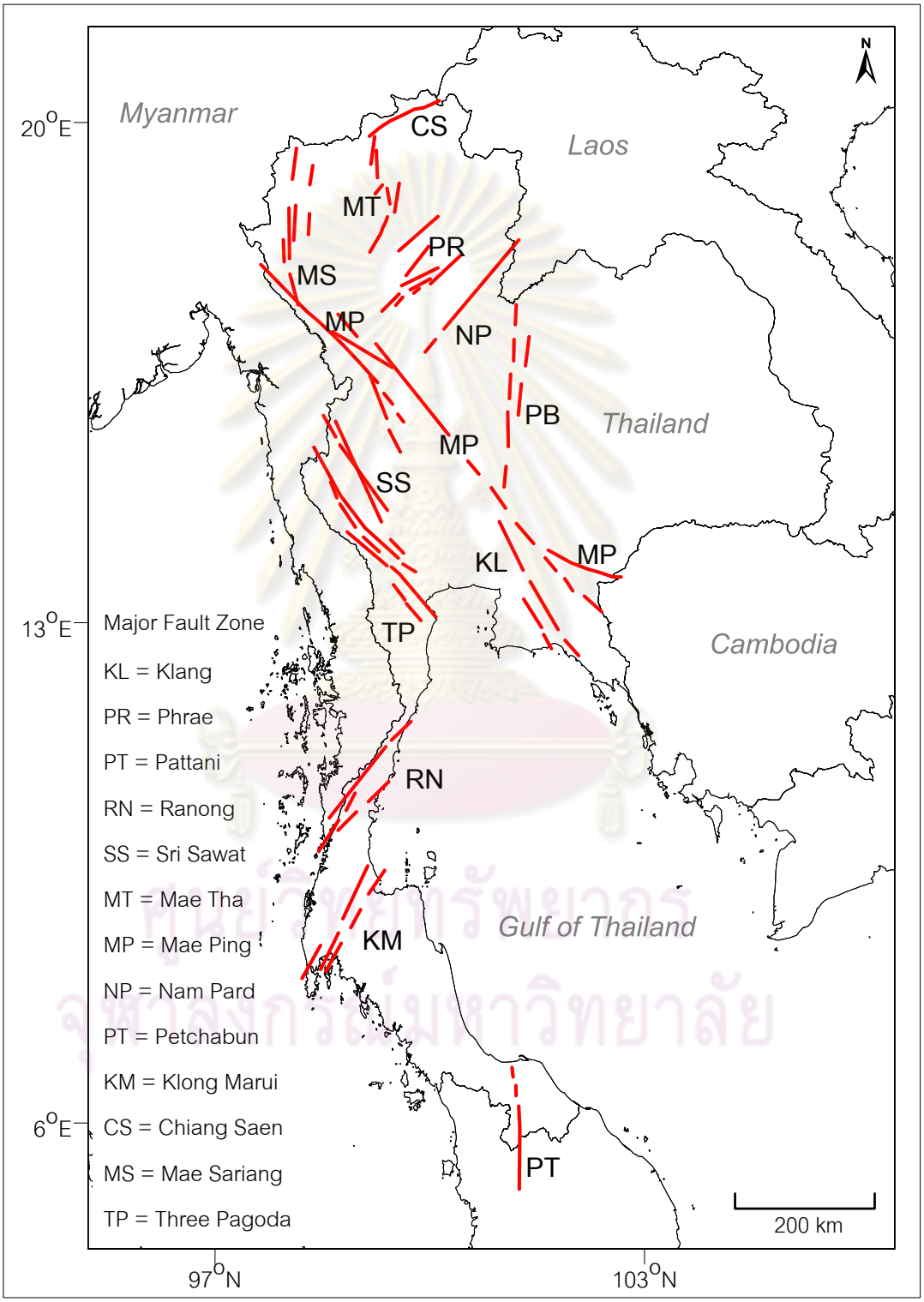

Figure 3.1. Map showing the major fault zones in Thailand (Chuaviroj, 1991).

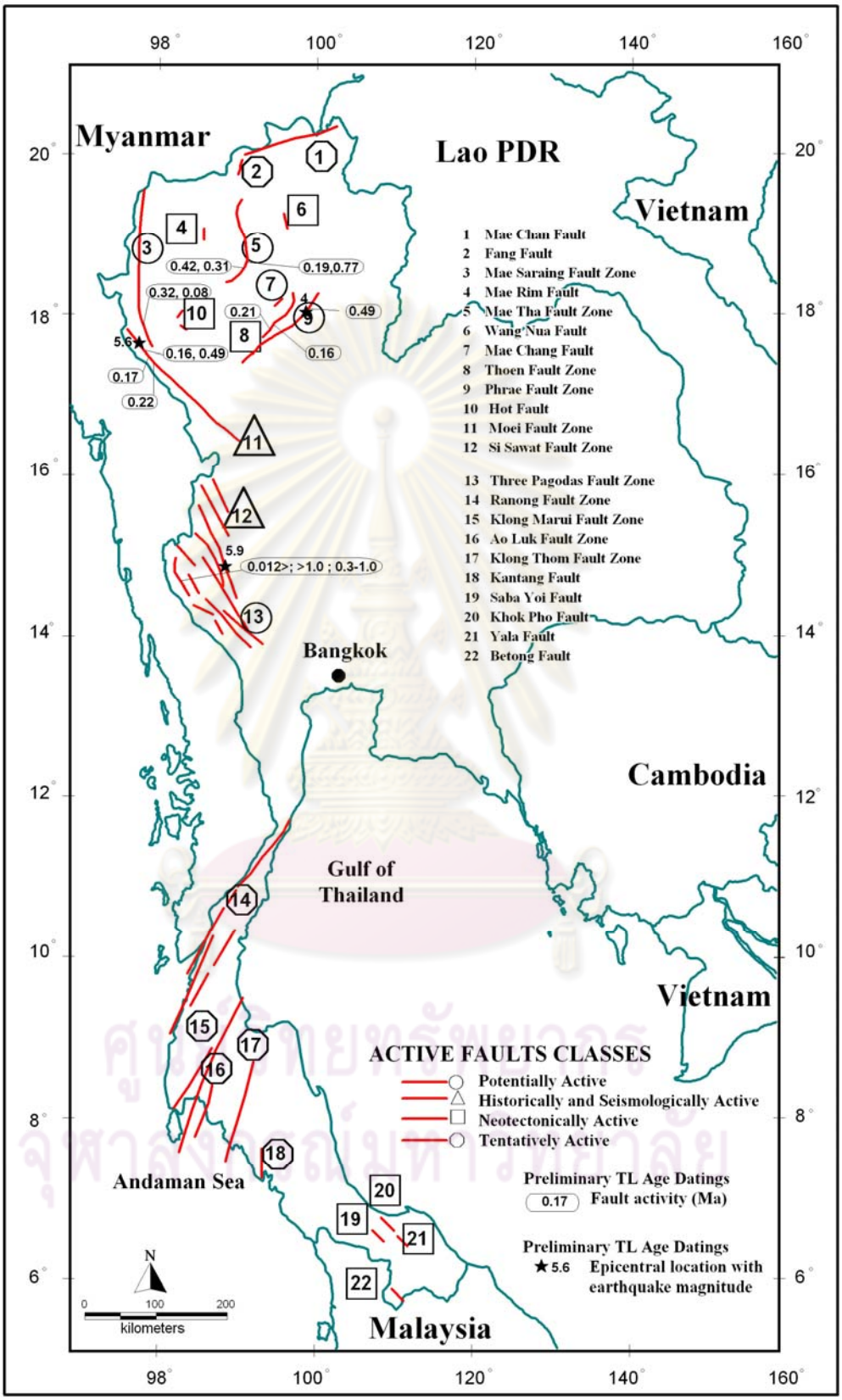

Figure 3.2. Map showing 22 active faults and their classes in Thailand (Hinthong, 1995).

In comparison with Chuaviroj (1991), the NW-SE Mae Ping Fault Zone was restricted in only the north-western Thailand and renamed it as “Moei Fault Zone” (Figure 3.2). The Phrae Fault Zone of Chuaviroj (1991) was separated to be Phrae Fault bounded the Phrae basin and Thoen Fault located along the eastern part of the Lampang basin. Some fault zones were newly proposed such as Hot, Mae Rim, Wang Nua, and Fang Fault Zones whereas the Klang, Nam Pard, and Petchabun Fault Zones of Chuaviroj (1991) were omitted in Hingthong (1991)’s fault map.

Then, Charusiri et al. (2001) published the map of seismically active belts (SAB) including active fault zones in Thailand. They classified the fault zone into 3 groups based mainly on the plenty TL dates of fault activities; active, potentially active, and 3) tentatively active. Three new fault zones were proposed in this map; The Pua and Payao Faults in the north and the Tha Kheak Fault in the northeast. Note that, the Mae Hong Son Fault Zone in this map and the Mae Sariang Fault Zone proposed previously is identical (Figure 3.3).

At present, the most up-to-date active fault map in Thailand was proposed by the Department of Mineral Resources (DMR, 2006). The map was contributed by knowledge integration of all updated relevant data. Moreover in many fault zones, detailed paleo-seismological studies were partly clarified following the empirical McCalpin (1996)’s methodology. Finally, DMR (2006) delineated 15 active fault zones in Thailand as shown in Figure 3.4 including Mae Chan, Phayao, Mae Ing, Mae Tha, Mae Hong Son, Mae Yom, Pua, Thoen, Uttaradit, Moei, Tha Kheak, Sri Sawat, Three Pagoda, Ranong, and Klong Marui Fault Zones.

Beside the active fault in Thailand, the faults located outside Thailand are also recognized in this SHA. From investigation, the almost active fault zones were reported abundantly in central Myanmar, Laos–southern China border, northern Vietnam and on Sumatra Island, Indonesia. The major active fault zone in Myanmar is the strike-slip Sagiang Fault Zone (Bertrand and Rangin, 2003). This fault zone traverses the central part of Myanmar from north to south. Although a morpho-tectonic representation of this feature cannot be identified in the Andaman Sea, the present-day seismicity shows that the inland Sagiang Fault Zone extends southward into the Andaman Sea and joins with

the clearly defined Sumatra Fault Zone on Sumatra Island (Petersen et al., 2004). In addition for eastern Myanmar, Nutalaya et al. (1985) proposed 3 fault zones, such as Papun, Panlouang, and Tong Gyi Fault Zones (Figure 3.5). These fault zones spread in northwest-southeast direction from the Sagiang Fault Zone and extend to northern and western Thailand.

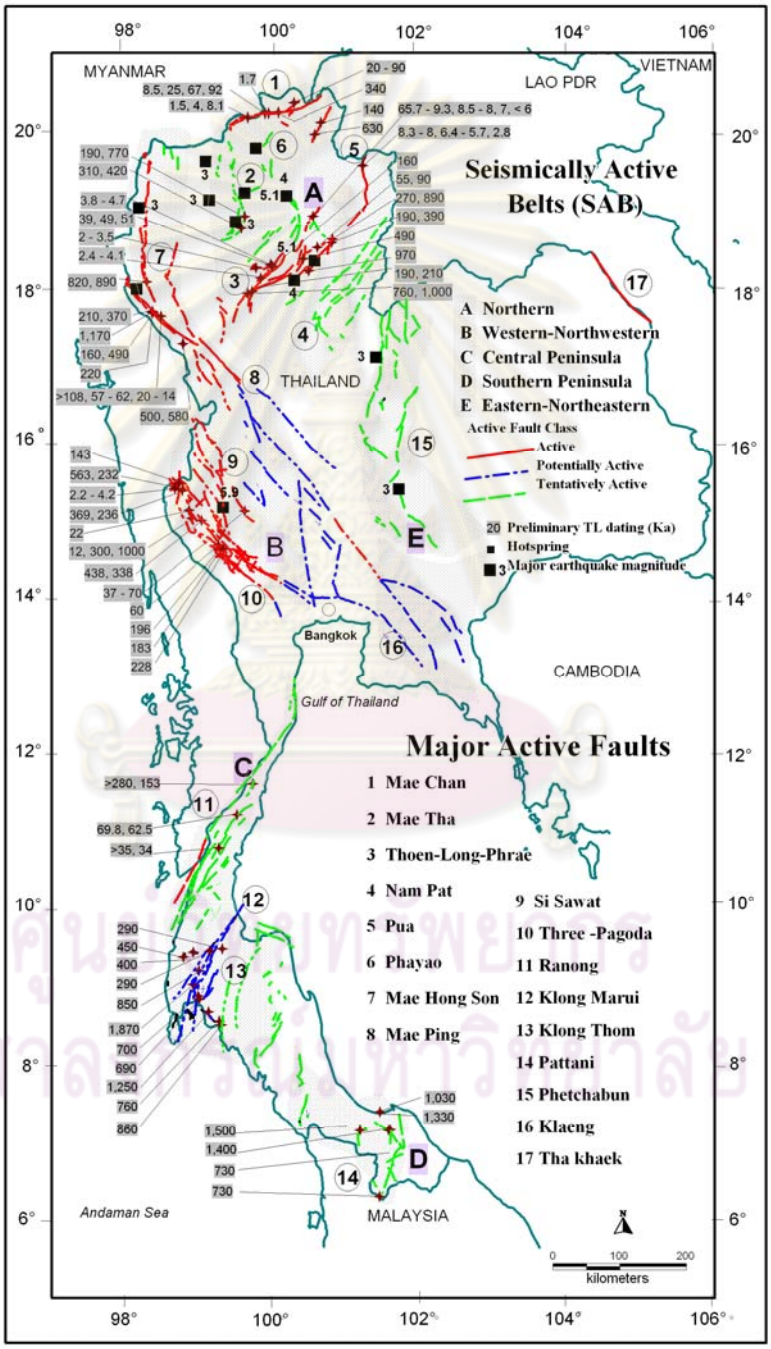

Figure 3.3. Seismically active belts map showing major active faults in Thailand with Thermoluminescence (TL) dates of individual faults (Charusiri et al., 2001).

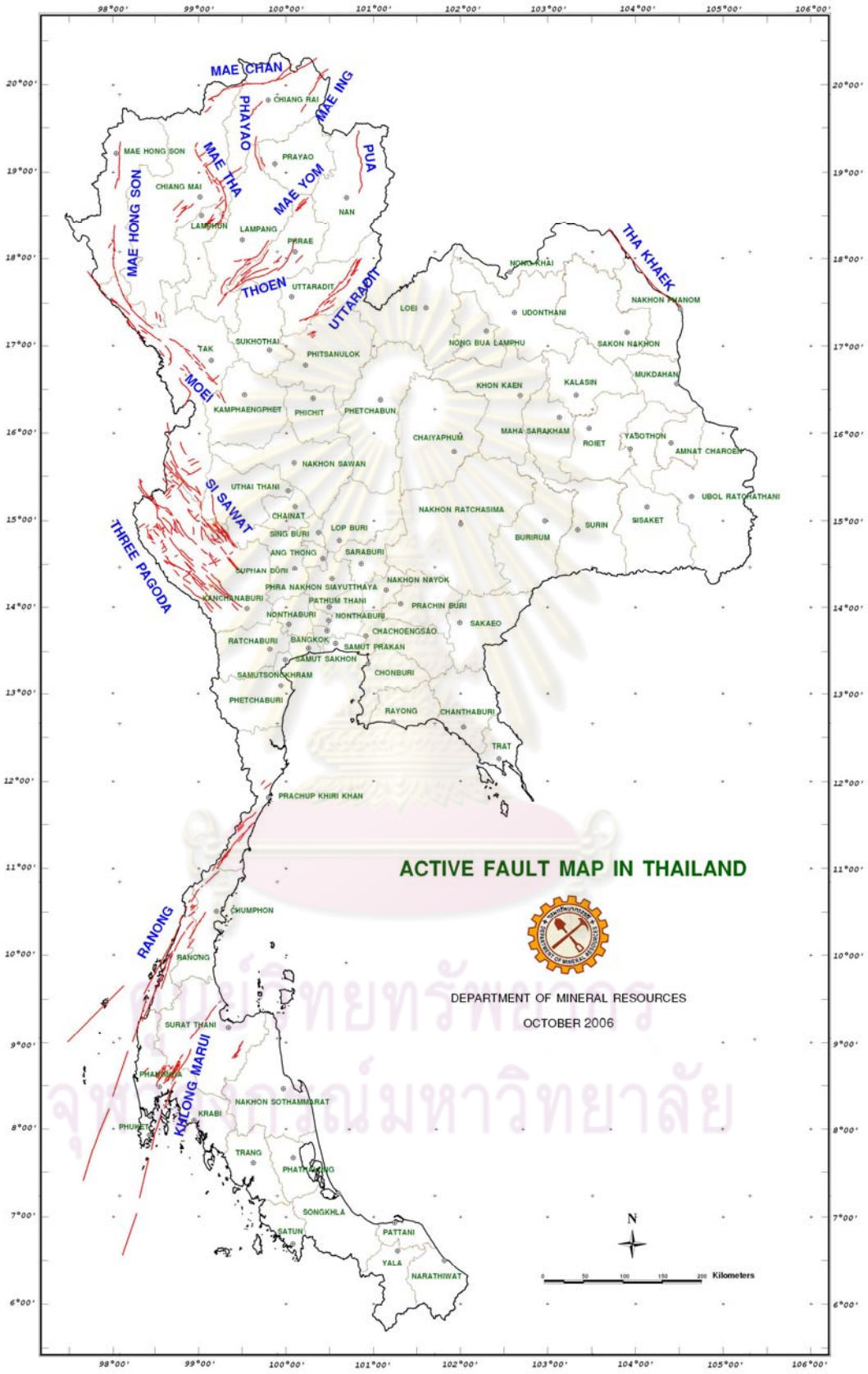

Figure 3.4. Active fault map of Thailand (Department of Mineral Resources, 2006).

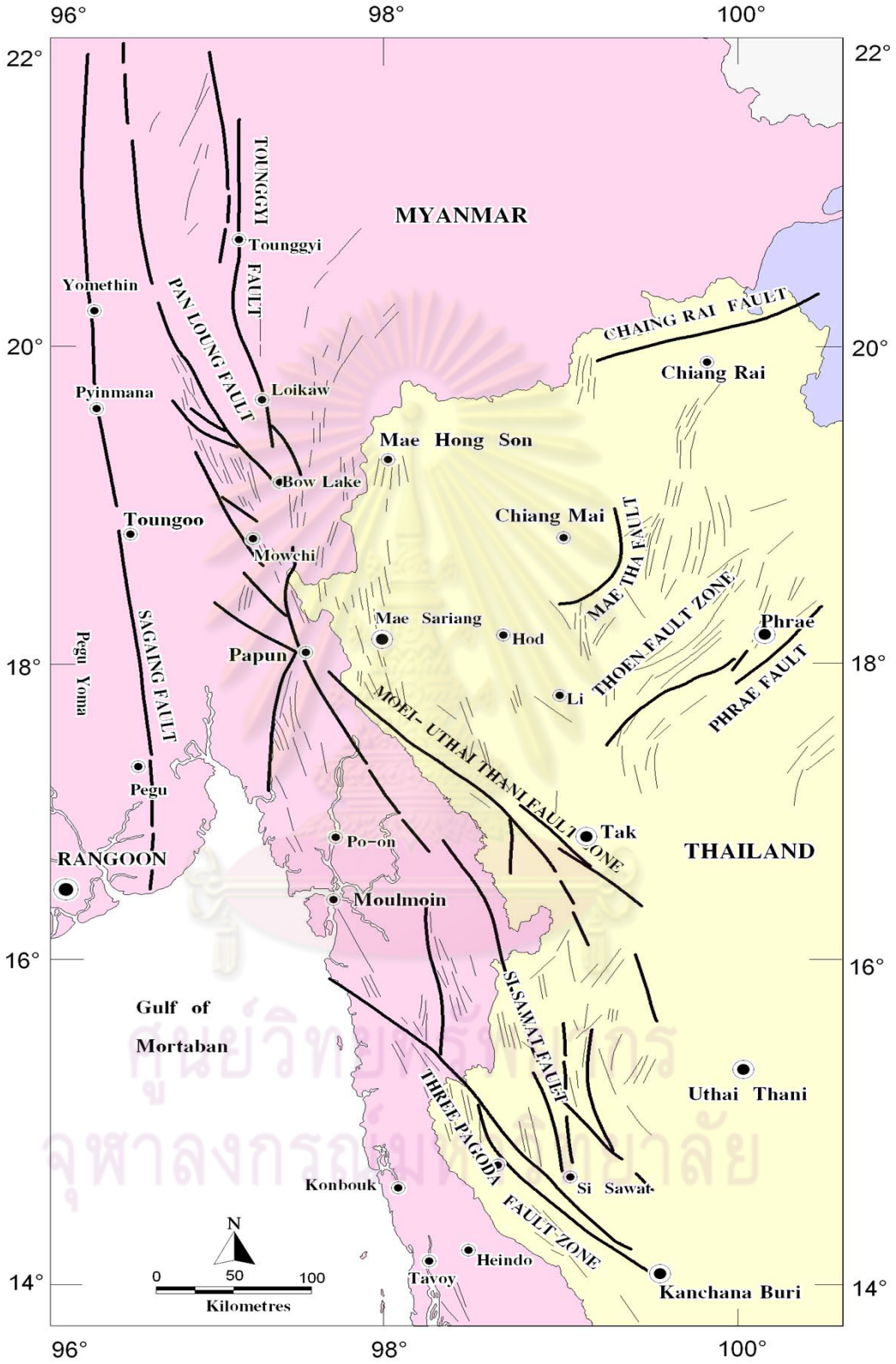

Figure 3.5. Map showing the distribution of faults in eastern Myanmar including western and northwestern Thailand regions (Nutalaya et al., 1985).

In the Laos – southern China border, there are a large number of fault and shear zones caused by the collision of the Indian and Eurasian tectonic plates (Polachan et al., 1991; Charusiri et al., 2007). These include the Chong Shan shear zone (Akciz et al., 2008), Gaoligong Shan shear zone (Akciz et al., 2008), Dein Bein Fu Fault Zone (Zuchiewicz et al., 2004), Hsenwi–Nanting Fault Zone (Lacassin et al., 1998), and Linchang Fault Zone (Lacassin et al., 1998). The present-day earthquake records reveal that these complex zones have generated contemporaneous seismic activity.

In northern Vietnam, the longest fault zone is the Red River Fault Zone (Duong and Feigl, 1999). Some other obvious fault zones have been reported in this region, such as Cao Bang – Tien Yen (Cuong et al., 2006), Dong Trieu (Charusiri et al., 2002), Song Ca (Takemoto et al., 2005), Song Chay (Cuong and Zuchiewichz, 2001), and Song Da and Song Ma (Phoung, 1991) Fault Zones. All of these fault zones have a NW–SE orientation and mainly follow the regional deformational structure. Present-day earthquake records from this area show that several medium to large-scale earthquakes are commonly associated with these fault zones.

3.2 Satellite Image Interpretation

The remote-sensing data are complied and analyzed in this study to infer the active faults in Thailand and nearby areas. The purpose is to define lines of morpho-tectonic evidence on the earth surface, such as fault scarps, triangular facets, shutter ridges and offset streams etc. (Figure 3.6). The next step is to re-locate, re-shape, and re-group the active fault zones reported in the previous studies and to find out new active fault zones. The names and regional locations of individual fault zones are cited mostly from previous publications as reviewed above.

Several remote sensing data have been applied for the current investigation. The joint interpretation of Digital Elevation Model (DEM) and different satellite images (i.e., MODIS, LANDSAT, and IKONOS) are analyzed for identifying the possible active faults in individual fault zones (Figures 3.7-3.10).

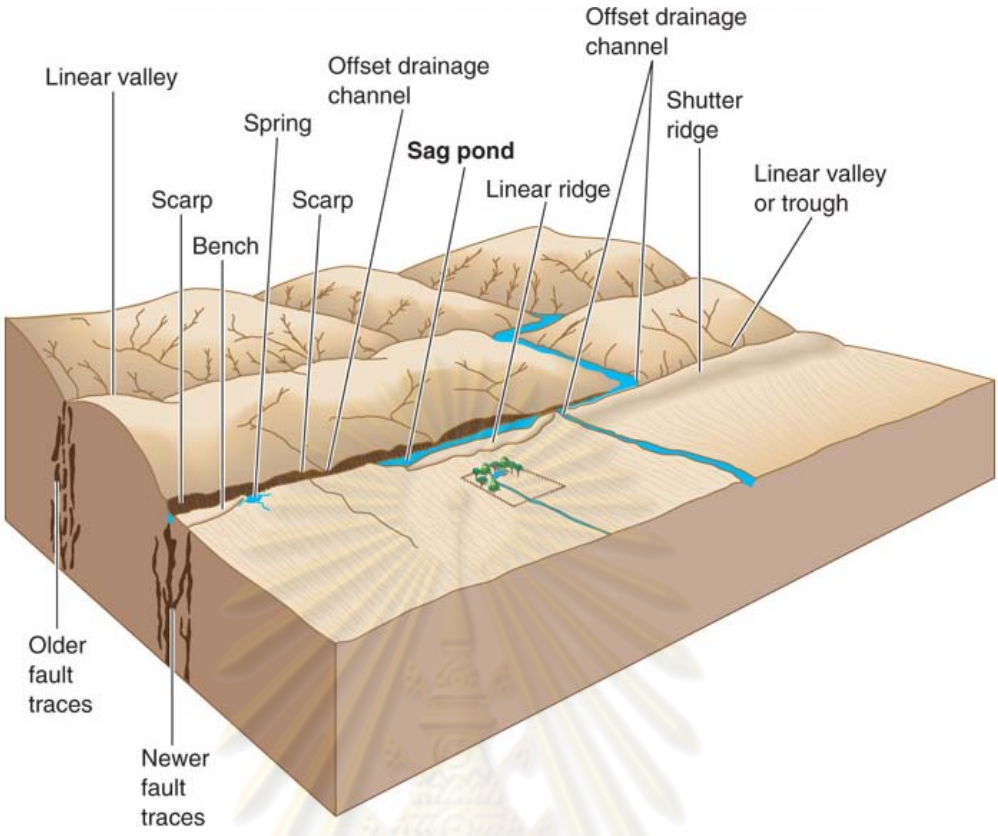

Figure 3.6. Characteristics of morpho-tectonic landforms associated with active faulting (McCalpin, 1996).

DEM with the resolution of 90 x 90 m was applied for tracing lineaments and fault segments in the regional scale (Figure 3.7) whereas satellite images of different types can support the morpho-tectonic evidence associated with surface faulting in more detail. For instance, MODIS image illustrates clearly the fault scarp in the Mae Tha and Mae Kuang Fault Zones (Figures 3.8). LANSAT image is successful to identify the series of triangular facets showing the normal faulting in the Pua Fault Zone (Figure 3.9). In addition, IKONOS image with the resolution of 1x1 m constrains geometry of the outstanding surface rupture along the Sagiang Fault Zone, central Myanmar (Figure 3.10). Both of DEM and various satellite images, in this study, are interpreted by adjusting and fitting together in individual fault segments to take the most precise fault lines. As a result, totally 55 candidates of active fault zones are proposed to represent the earthquake sources in this SHA (Figure 3.11, see also Table 4.1 in chapter IV).

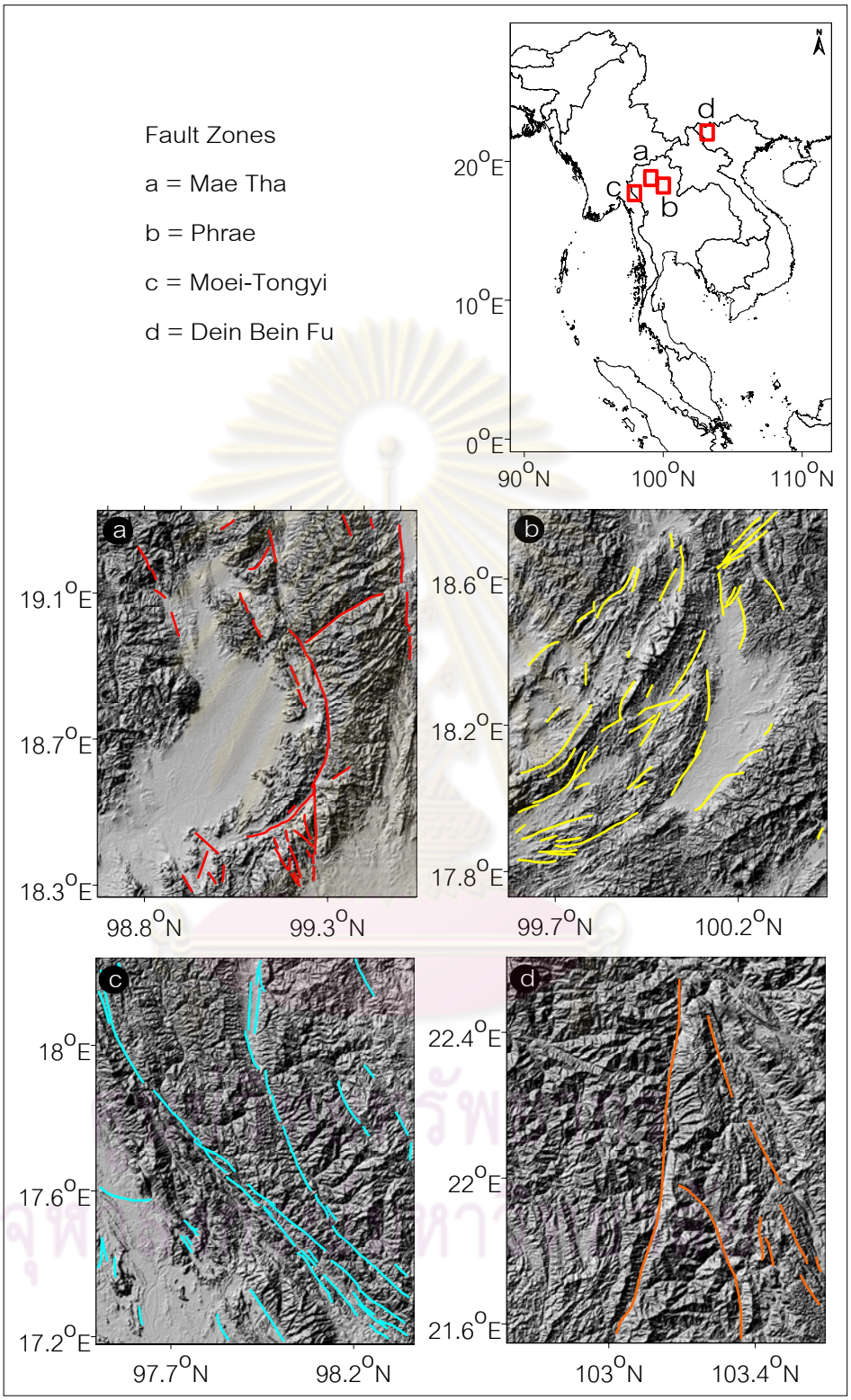

Figure 3.7. Map showing the possible active fault interpreted from the Digital Elevation Model (DEM). a) Mae Tha fault zone; b) Lampang-Thoen and Phrae fault zones; c) Moei-Tongyi and Mae Hong Sorn fault zones; and d) Dein Bein Fu fault zone, respectively.

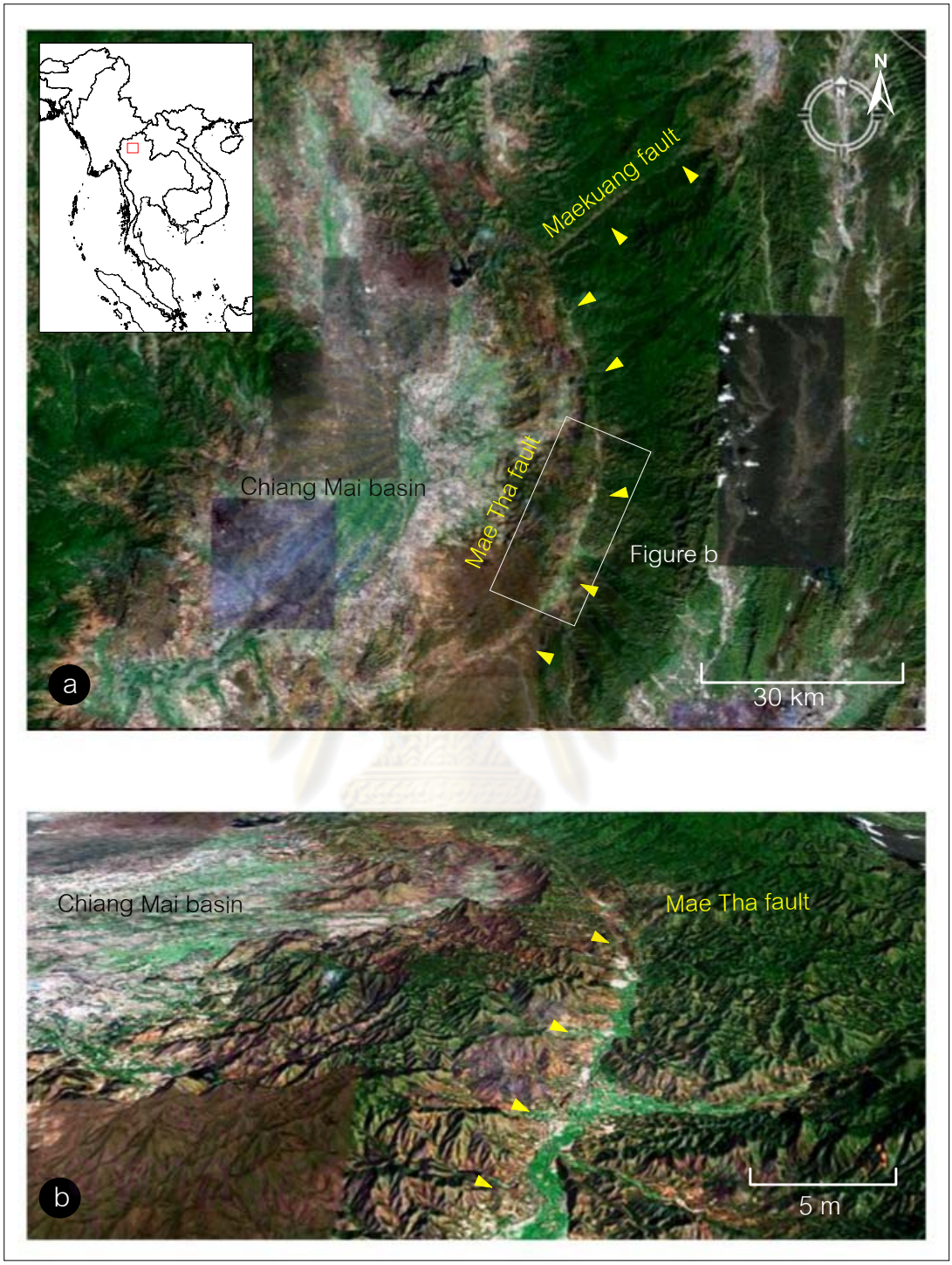

Figure 3.8. a) Map showing the Mae Tha and Mae Kuang Faults (point by yellow arrows) traced from MODIS satellite image, and b) closed up 3-D view of the Mae Tha fault showing the fault scarps along the southern part of the Mae Tha fault.

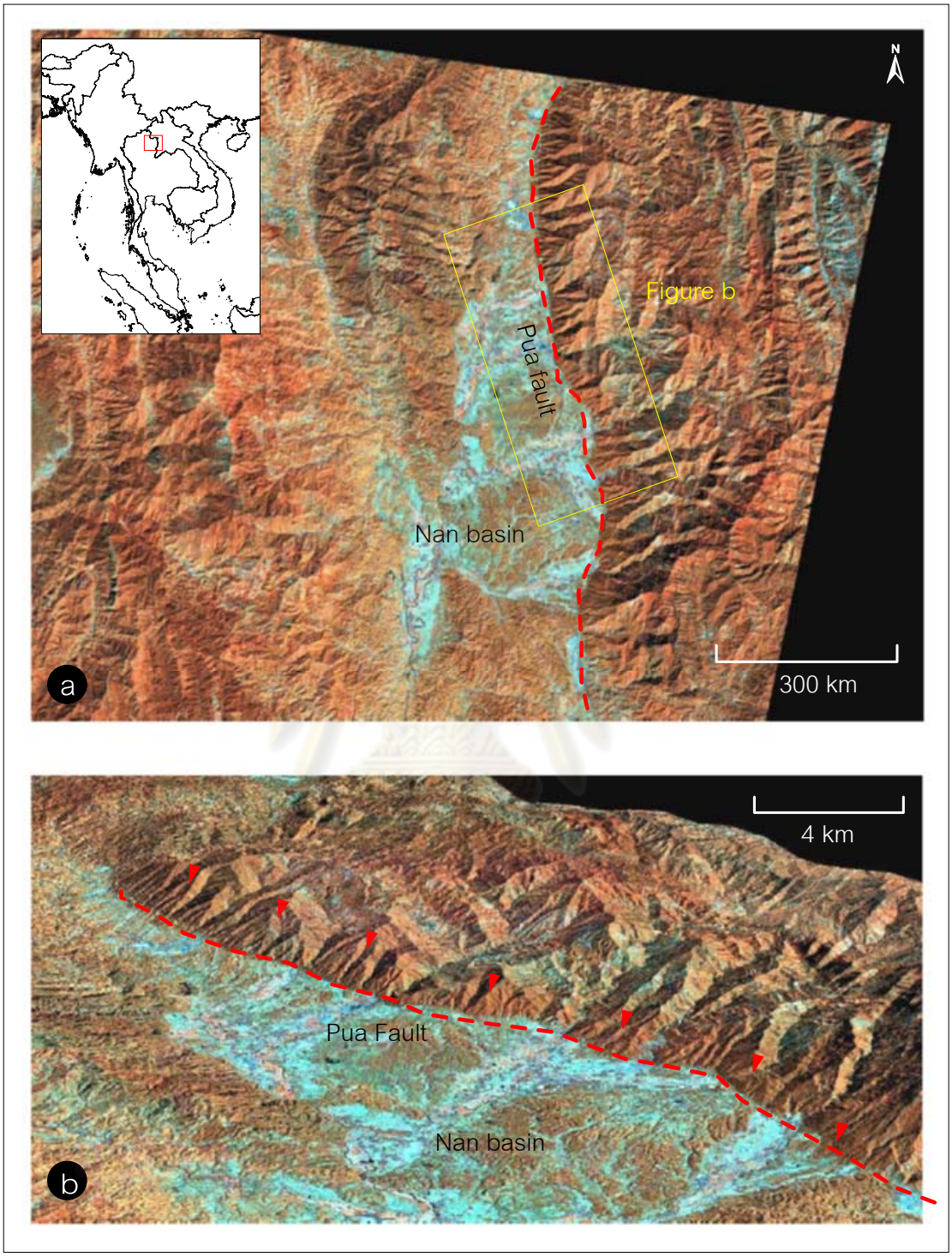

Figure 3.9. a) Map showing the Pua Fault (red dash line) interpreted from LANSAT satellite image, and b) closed up 3-D view of the Pua Fault showing obviously the series of triangular facets (shown by red arrows).

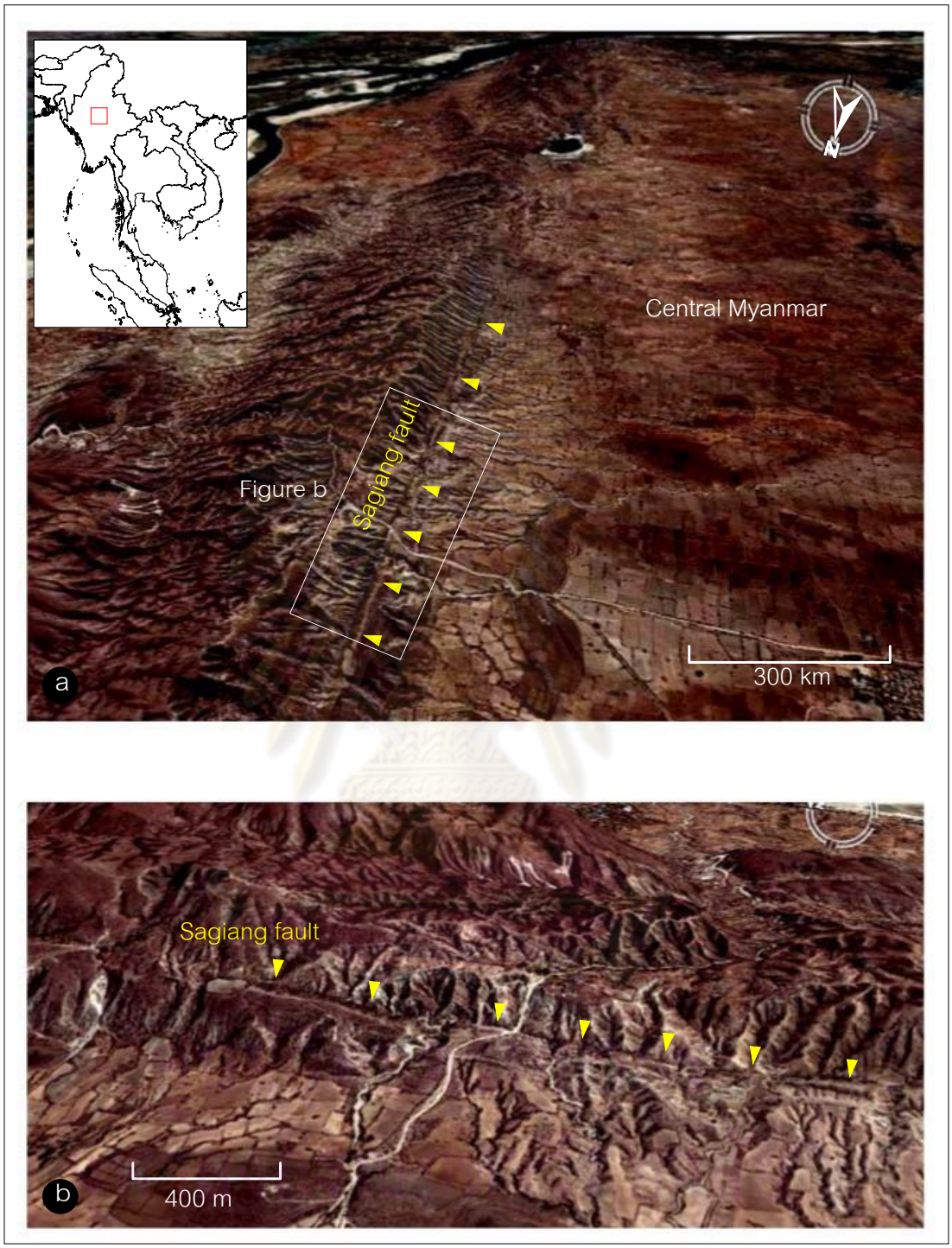

Figure 3.10. a) Map showing the Sagiang Fault (indicated by yellow arrows) traced from IKONOS image, and b) closed up 3-D view of the Sagiang fault showing the obvious surface rupturing along the Sagiang fault.

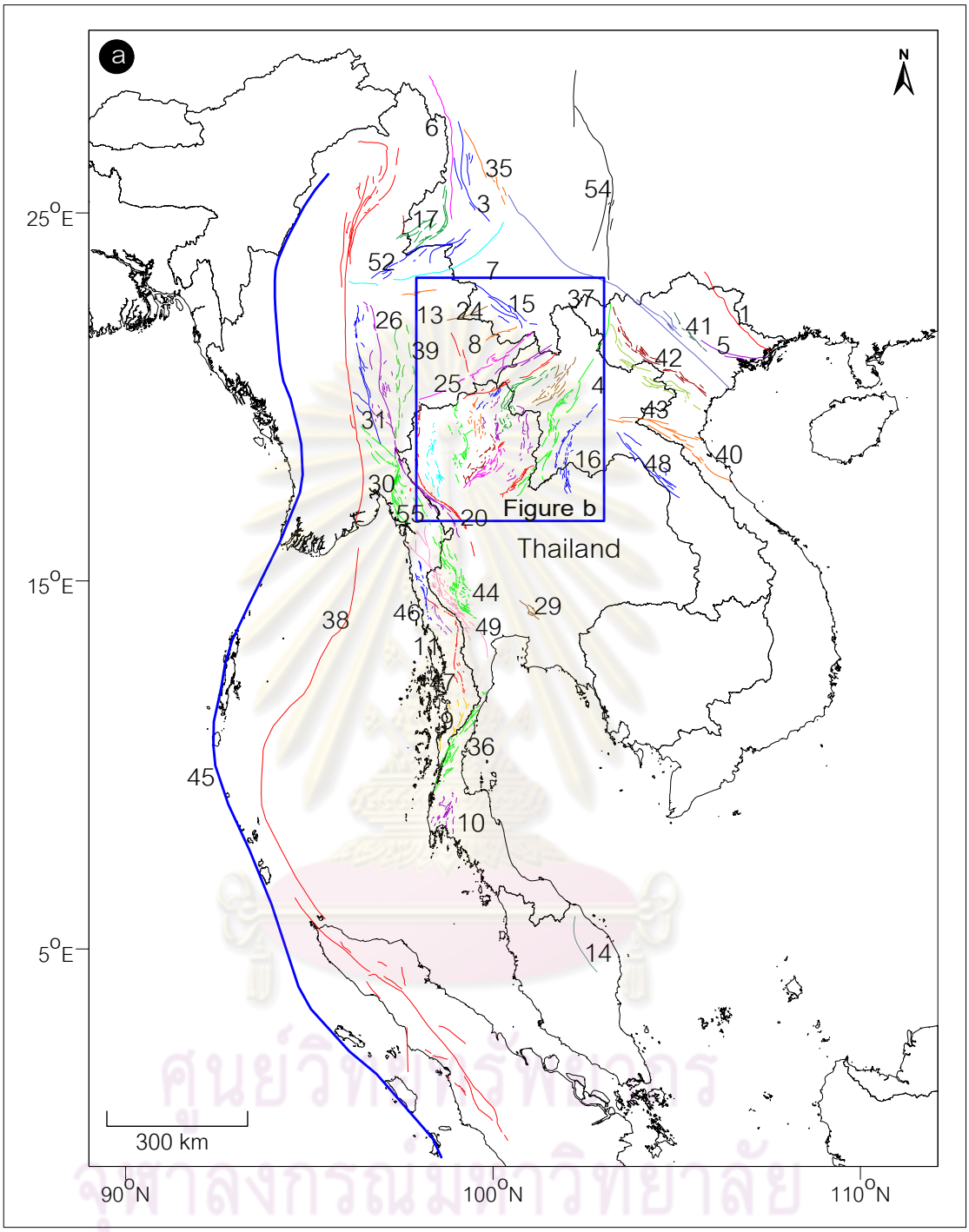

Figure 3. 11. a) Map of the study region showing 55 active faults interpreted from remote sensing data in this study. Box area is for Figure b; b) enlarged map showing the possible active faults in northern Thailand and surrounding areas. In both maps, individual fault zones are distinguished by color and numbered. The numbers mentioned in this map is equivalent to the "*Fault no.*" of Table 4.2.

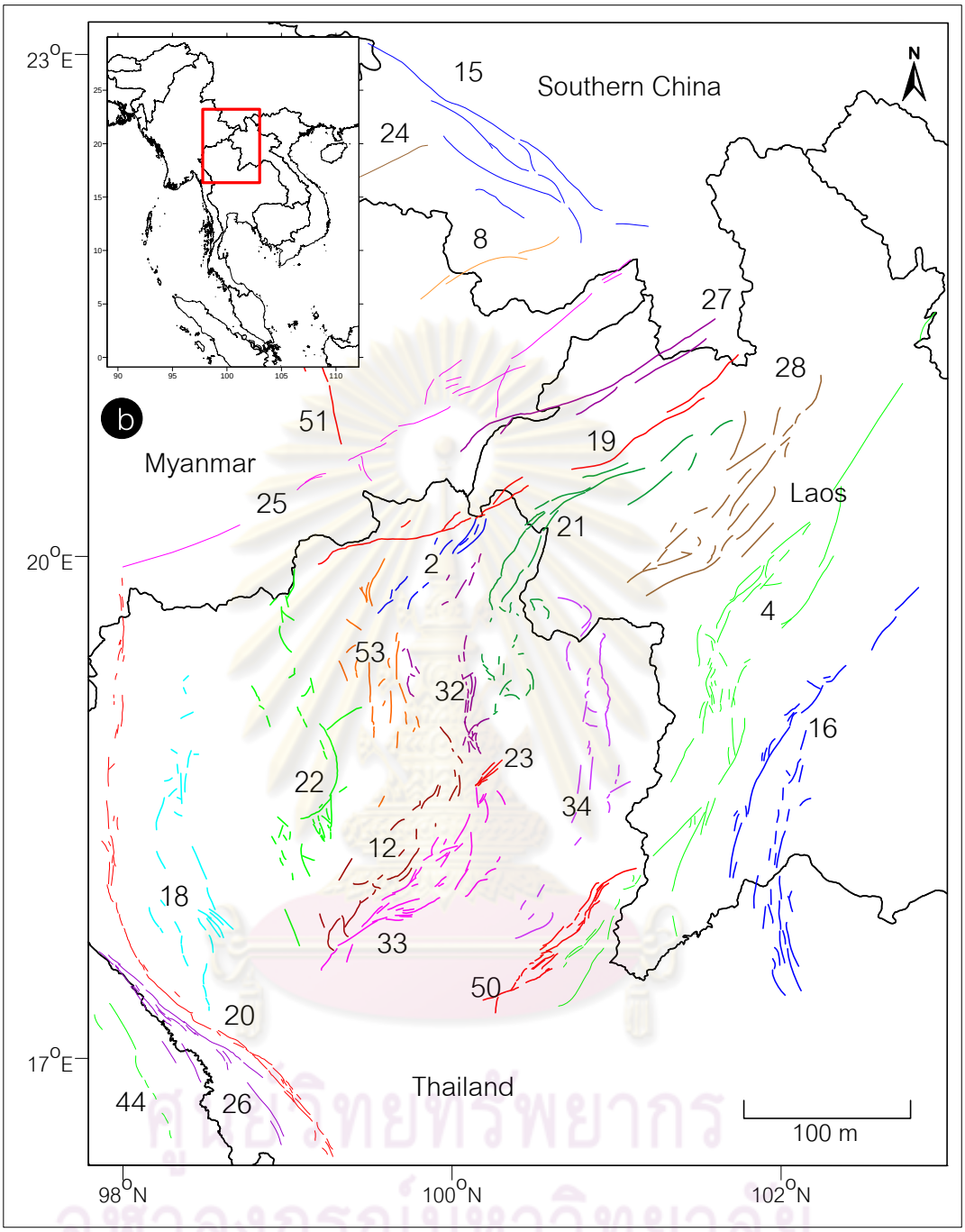

Figure 3. 11. (cont.) a) Map of the study region showing 55 active faults interpreted from remote sensing data in this study. Box area is for Figure b; b) enlarged map showing the possible active faults in northern Thailand and surrounding areas. In both maps, individual fault zones are distinguished by color and numbered. The numbers in this map is equivalent to the "*Fault no.*" of Table 4.2.

3.3 Field Investigation

The site of interest selected for paleo-seismological investigation is in eastern Myanmar. The site locates in the latitudes 97°15'-98°00'E and the longitudes 17°00'-18°15'N along the Thailand-Myanmar border which is the northern branch of Sri Sawat Fault Zone (Figure 3.12). The site can be accessed conveniently by car from Tak province to Mae Sort district, Thailand and then, cross the Myanmar frontier to Myawadi, Hpa-an, Myainggyingu, and Kammamung villages, respectively. Finally, Hutgyi, where the paleo-earthquake is investigated, is accessed easily by taking the long-tailed boat for 1.5 hour along the Thanlwin River from Kammamung (Figure 3.12).

Morphology of the study area is dominated by high-altitude mountains with the intervened, long and narrow alluvial and colluvial plains. There are 4 well-defined northwest-southeast trending faults recognized from the field investigation the IKONOS image interpretation, namely Kyaukpulu, Koshwe-e-we, Yinbaing, and Meseik Faults (F1, F2, F3, and F4 in Figure 3.13a). Among these faults, it is quite likely that the 7-km Kyaukpulu Fault shows more distinct and cryptic evidence of young movement than the others and lies down quite close to the proposed dam site occupied by the Electricity Generating Authority of Thailand (EGAT) (Figures 3.13a and b). Morpho-tectonic evidences, such as triangular facet and offset streams are exposed obviously in this fault (Figure 3.13c). As a result, the paleo-seismology is investigated in detail along the Kyaukpulu Fault according to the McCalpin (1996)'s method as shown in the following;

3.4 Data from Trenching and Trench Logging

In this study, a paleo-seismological trench is excavated perpendicular to the Kyaukpulu Fault (Figure 3.13c) to investigate the earthquake faulting evidences. Trench logging reveals a basement rock unit (unit G) and six unconsolidated sediment layers (units A-F) as described and shown in Figures 3.14 and 3.15. From trench-log stratigraphy, it is quite clear that the trench has relatively much more deformed stratigraphy. On the trench walls, some faults cutting across basement rocks through the overlying sediment units were observed in different locations. However, based on the principle of the cross-cutting relationship in the trench (shown in Figure 3.15) three earthquake events were identified using nature and orientation of faults.

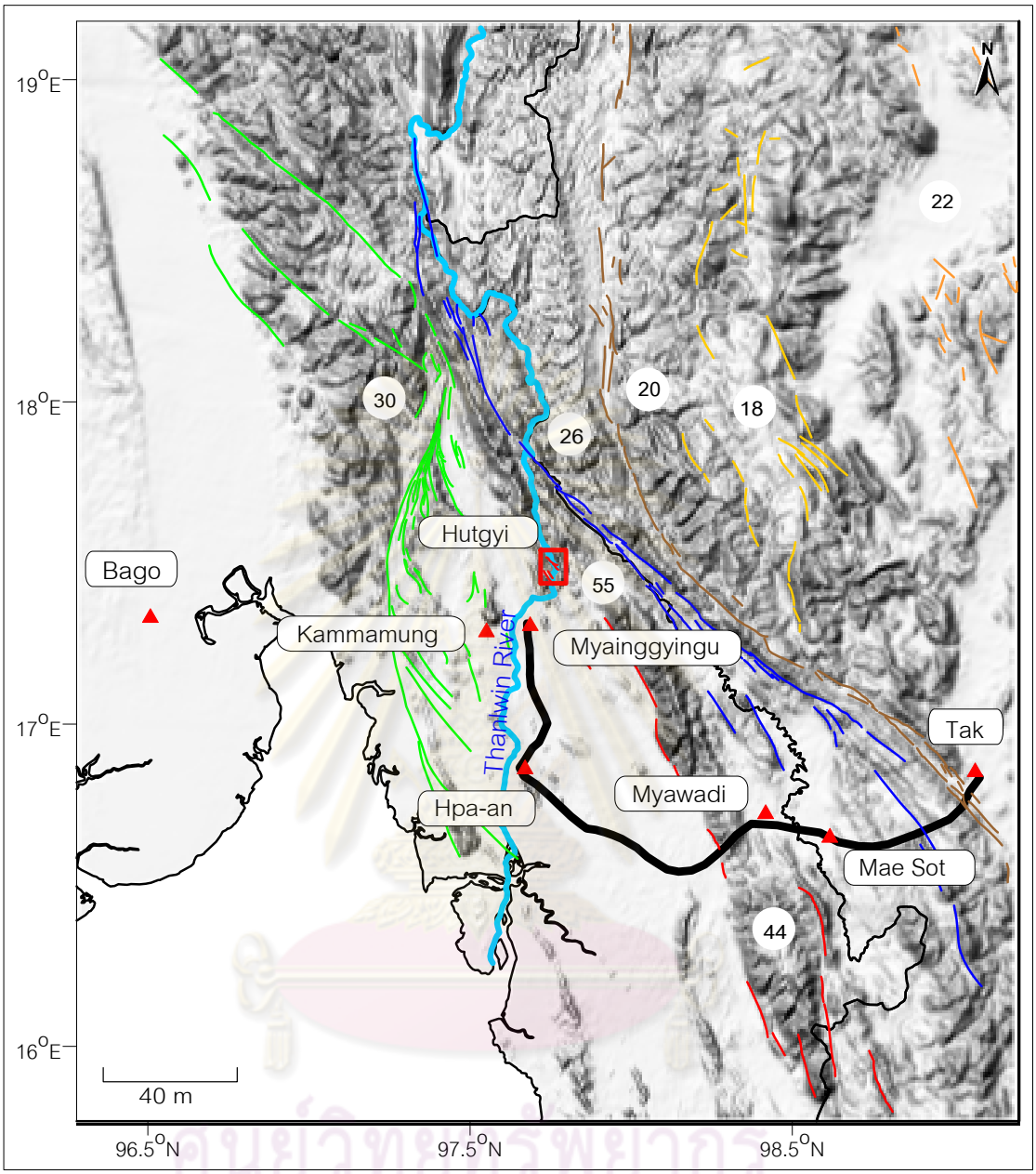

Figure 3.12. DEM map of Thailand-Myanmar border showing fault lines and the location of paleo-seismological investigation (red square). The numbers mentioned in this map is equivalent to the “fault no.” column depicted in Table 4.2. The black line is the traverse to the site.

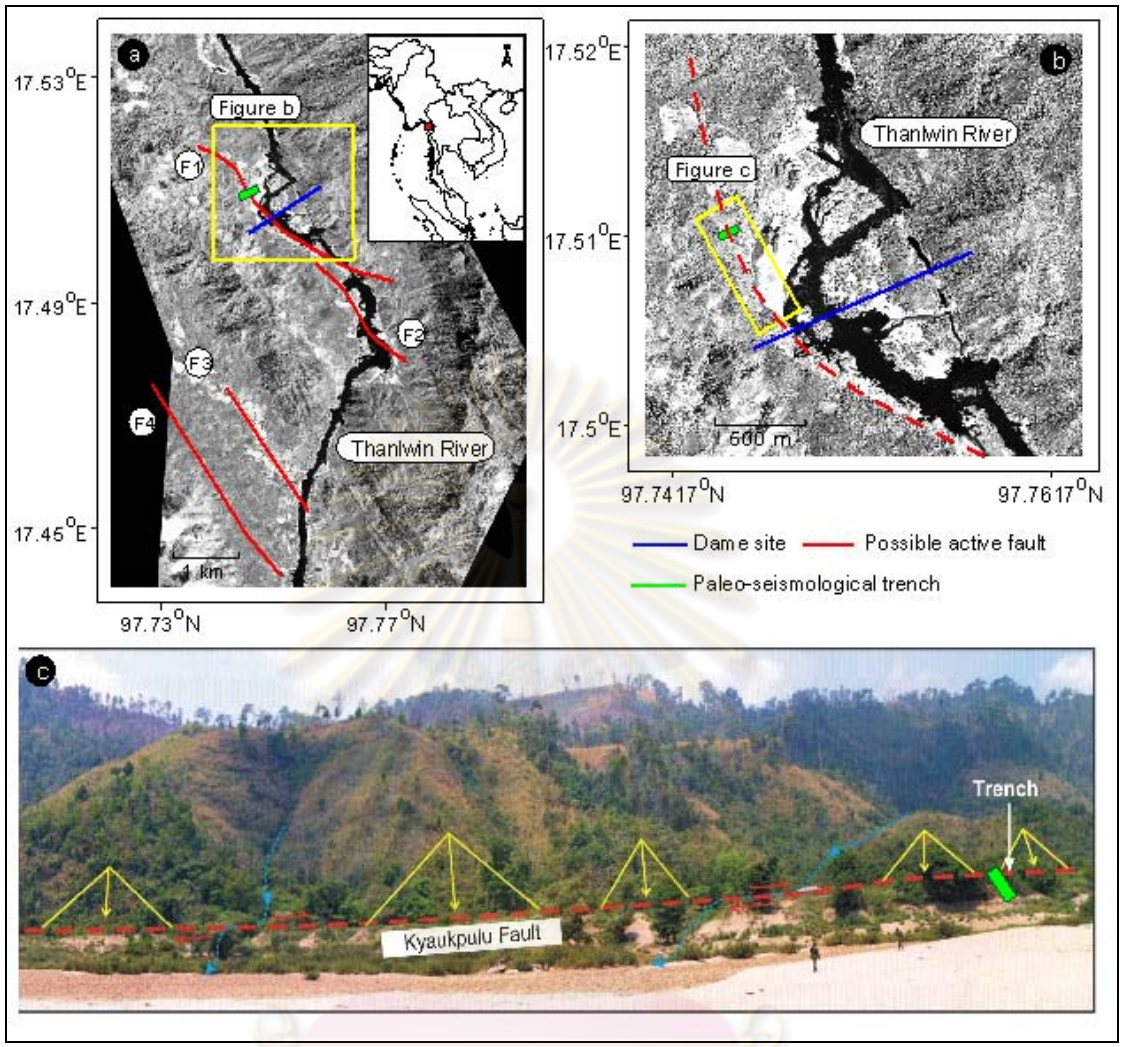

Figure 3.13. a) IKONOS satellite image showing locations of proposed dam sites (blue lines) along the Thanlwin River or Salawin and the interpreted active faults (red lines); b) Close up of IKONOS image showing the location of the Kyaukpulu fault (dash red line) and the location of paleo-seismological trenching (green color); c) View (looking southwest) showing location of the Kyaukpulu Fault some morpho-tectonic features, such as triangular facets (yellow lines) and offset streams (blue lines). One trench was excavated across the fault (green box).

Figure 3.14. Photograph of the south wall exposed in the trench showing stratigraphy and evidence of fractures and faults affected from the paleo-earthquakes. This trench is excavated perpendicularly to the Kyaukpulu Fault as shown in Figure 1.13c.

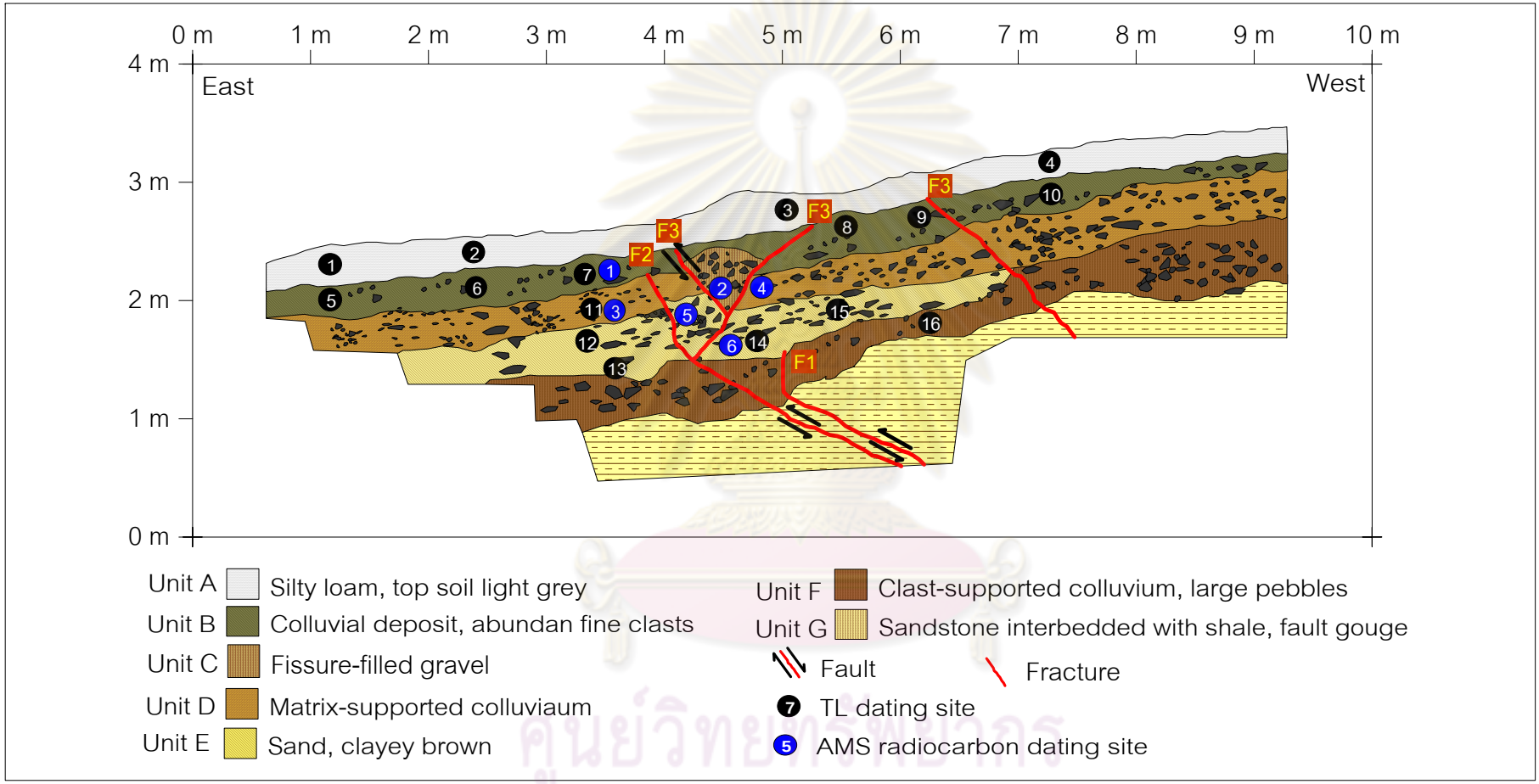

Figure 3.15. Sketch map of interpreted stratigraphy and associated fractures and faults on the south wall of the trench excavated perpendicularly to the Kyaukpulu Fault as shown in Figure 1.13c. The sampling points for TL and radiocarbon dating are shown in the black and white circles, respectively.

- F1 event: the oldest earthquake event postdating the large-pebble colluvium deposit of unit F and predating the clayey sand deposit of unit E.
- F2 event: the second earthquake event postdating the medium-grain colluvium deposit of unit D and predating the colluvium deposit of unit B.
- F3 event: the last earthquake event which postdates the colluvium sediment of unit B and predating the silty loam of unit A.

3.5 Fault Age Dating

As mentioned above, geochronological data is important for paleo-seismological interpretation. In this study, most of the previous geochronological data represented as the rate of fault slip (S) used for SHA are complied as shown in Table 4.2. All the faults mentioned in the table are identical to those present in the map (Figure 3.11). After field trench-log investigation of earthquake faulting events from the associated sediment layers, geochronological investigation was launched. This includes identifying sample location and collecting specific sample materials. In this study, two types of materials; organic fragments and sediment samples are collected for AMS-radiocarbon and TL dating, respectively. Totally, 6 charcoal fragments can be found in the sediment units B, C, and D. For TL dating, the more the finer-grained sediments (down to fine-sand and silt ranges) the better the result is (Charusiri et al., 2005). Sixteen samples of sediments are collected for TL dating. The results of these two scientific dating methods can be then compared and discussed, and this can make the more accuracy in the fault age dating and the more relevance of the results.

3.5.1 AMS-Radiocarbon dating

For AMS-radiocarbon dating, the outer part of the obtained charcoal fragments are stripped and a routine cleaning method is conducted to prevent possible contamination of the organic samples using the method described by the BETA AMS-radiocarbon dating laboratory, Arizona, USA. The treated samples are over 20 gram in dry weight. Thereafter, the charcoal dates are analyzed by the Accelerator Mass Spectrometry Laboratory, University of Arizona, USA, and the dates are summarized in Table 3.1.

Table 3.1. AMS-Radiocarbon dating of charcoals collected from the trench.

Sample no.	$^{13}C/^{12}C$ ratio	AMS-radiocarbon age (BP)
1	-28.8	950±40
2	-28.8	1,140±40
3	-26.8	960±40
4	-27.6	1,010±40
5	-26.8	2,090±40
6	-27.7	2,490±40

3.5.2 Thermoluminescence dating

TL dating is based on quantifying both equivalent dose (ED) which is the radiation dose received by a sediment sample since its last deposition, and the annual dose (AD) or dose rate which it has experienced during the accumulation period. As a result, the $TL\ date$ can evaluated following the simplified equation 3.1.

$$TL\ date = \frac{ED}{AD} \tag{3.1}$$

where ED is measured in Grey unit and AD is determined in mGrey/year

In individual TL dating, the bulk sample of sediment is dried and evaluated the water content (%). Thereafter, dried sample with about 300 gram by weight is sieved through 840 um mesh filters for determining AD. Then, sample with grain size fraction of 74-250 um is extracted from the rest for ED evaluation.

For AD, the concentrations of the radioactive elements (i.e. Uranium (U), Thorium (Th) and Potassium (K)) are determined by gamma-ray spectrometry. Then, the AD can evaluate from the relationships between the contents of radioactive elements and the given AD according to the standard table proposed by Bell (1979) supplementary with the water content determined in before.

For ED, the quartz inclusion technique using methods described by Zimmermann (1971) and Takashima and Watanabe (1985) is applied for sample treatment. The sediment sample is immersed in hydrochloric acid with 35% of content to

remove the carbonate and organic matter, and then by 24% hydrofluoric acid to dissolve feldspar and clay mineral. Ferro-minerals are eliminated by an iso-dynamic magnetic separator in order to take the pure quartz aliquot in final. TL-intensity of individual aliquot of quartz is measured using the high accuracy TL-OSL instrument occupied by Earthquake and Tectonic Geology Research Unit (EATGRU), c/o Department of Geology, Faculty of Science, Chulalongkorn University. The regeneration technique is applied to determine ED according to Pailoplee (2004)'s suggestion. In final, the TL dates and details are summarized in Table 3.2.

Table 3.2. Thermoluminescence dating of sediments collected from trench.

No.	U (ppm)	Th (ppm)	K (%)	WC (%)	AD (mGy/y)	ED (Gy)	TL age (year)
1	1.47	14.33	1.93	33.58	4.12	1.89	460±70
2	2.45	15.86	2.22	32.26	5.04	3.20	640±200
3	2.64	18.08	2.02	32.74	5.25	3.53	570±200
4	2.74	17.73	2.36	30.99	5.59	2.63	470±180
5	2.19	17.81	2.95	23.17	6.24	10.37	1,650±760
6	3.12	20.11	2.72	27.19	6.59	11.99	1,800±680
7	2.92	21.09	2.60	9.73	7.85	17.57	2,240±260
8	3.19	14.95	1.91	37.55	4.80	8.90	1,850±440
9	2.44	17.45	2.46	9.44	6.84	14.34	2,100±270
10	2.83	19.49	2.48	8.74	7.50	18.49	2,060±380
11	1.86	20.39	2.40	23.55	5.98	20.89	3,500±500
12	2.86	17.99	2.68	11.44	7.22	36.78	5,100±750
13	2.78	20.90	2.89	14.37	7.60	49.32	6,500±500
14	2.56	21.93	2.61	14.57	7.38	38.72	5,250±500
15	2.74	20.06	2.40	14.24	7.02	46.99	6,700±600
16	2.73	19.66	2.86	12.98	7.46	65.12	8,700±870

Based on the obtained trench log and geochronological data, the deposition time span of individual sediment units, which constrained by both TL and AMS-radiocarbon dating, are shown in Figure 3.16. For the uppermost unit A dominated by siltly loam, the TL dates ranges from 290-840 B.P. obtained from TL dates. The unit B of fine-grain colluvium is dated at ca. 890-2,500 B.P. by TL dating method whereas AMS radiocarbon dating reveals 830-950 B.P. For the wedge of gravel classified in unit C, the possible date is around 1,040-1,120 B.P. based only on AMS-radiocarbon dating. For unit D, both TL and AMS-radiocarbon date can yield the ages of the medium-grain colluvium at ca. 3,000-4000 B.P. and 890-1,010 B.P., respectively. For the clayey sand of the unit E, TL date is within the range of 4,350-7,300 B.P. meanwhile the AMS-radiocarbon date is much lower (2,020-2,490 B.P.) and unreliable. Finally, the lowermost sediment unit F is 7,830-9,570 B.P. based only on TL dating.

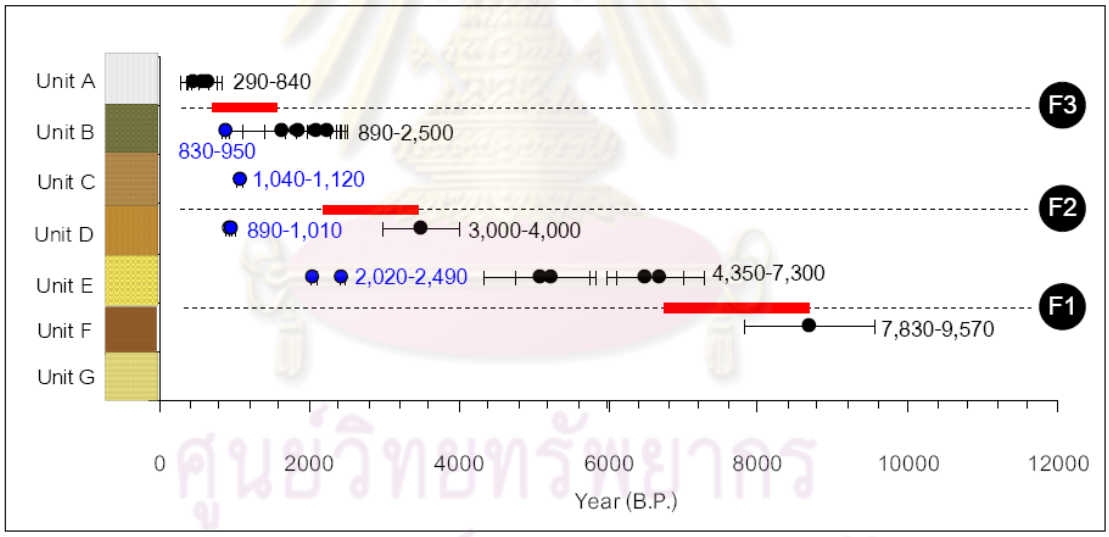

Figure 3.16. Depositional time span of individual sediment unit exposed in the trench. The dates control by TL-dating (black circles and text) and AMR-radiocarbon dating (blue circles and text). The dash lines show the limitation of faulting in sediment units. The red tabs illustrate the time span of fault slip.

As described above, the TL and AMS-radiocarbon dates are different. Although the AMS-radiocarbon dating is widely accepted empirically from the research

communities (Scott et al., 2004), AMS-radiocarbon dates, however, cannot explain effectively as shown by Wang et al. (1996), Rink and Forrest (2005), Phil (2008) and also from the result of this study. For instance, as shown in Figure 3.16, the sediment unit C gives the AMS-radiocarbon date older than the younger unit which is the unit C. These AMS-radiocarbon dates are, therefore, geologically meaningless for this stratigraphy interpretation. Although TL dating data show older and more variable dates when compared with the AMS-radiocarbon dating of the same unit (Figure 3.16), the obtained TL dates are usually agree well with the order of sediment deposition. These imply that TL dating data can show directly the absolute age of sediment deposition whereas the AMS-radiocarbon dating may date the age of charcoal fragments which have the possibility to re-work from the other sites. The dates from AMS-radiocarbon dating, therefore, do not represent the precise deposition time of sedimentation which necessary for this earthquake faulting interpretation. Thus, this study design to interpret time span of sediment deposition including earthquake faulting based on the obtained TL dating results.

3.6 Determination of Paleo-Seismological Parameters

3.6.1 Maximum Credible Earthquakes

To determine the Maximum Credible Earthquakes ($MCEs$), the relationship between moment magnitude (Mw) and fault rupture length at the surface (SRL) proposed by Wells and Coppersmith (1994) are applied (equation 3.2). The SRL used for the Mw calculation is taken from the length of the longest fault segment in each fault zone. Moreover, the rupture area A_f, which also required for SHA, are determined by using the empirical relationship between the obtained Mw from equation 3.2 and A_f (Wells and Coppersmith, 1994) of equation 3.3:

$$Mw = 5.08 + 1.16\log(SRL) \tag{3.2}$$

$$\log(A_f) = -3.49 + 0.91Mw \tag{3.3}$$

where Mw is moment magnitude, SRL is surface rupture length of fault (km), and A_f is rupture area of the fault (km^2).

Based on satellite image interpretation, the morpho-tectonic evidences show that the Kyaukpulu Fault has the SRL of 7 km. As a result, the Kyaukpulu Fault can generate an earthquake with a maximum Mw of around 6.0 and an estimated A_f around 106 km^2. In addition, the other fault zones proposed in Figure 3.11 are also determined SRL, Mw and A_f as summarize in Table 4.2. From 55 proposed fault zones in this SHA, the Sumatra-Andaman Subduction Zone can generate the maximum Mw of around 9.2 whereas the Red River and Sagiang-Sumatra Fault Zones can generated the earthquake around 8.5 Mw which is the maximum level from the inland earthquake fault.

The $MCEs$ of the active faults in Thailand is shown in Table 4.2. It is qeute likely that the $MCEs$ of the active faults in Thailand vary from Mw 5.9 to Mw 7.9 at the Moei-Tongyi Fault Zone. It is possible to infer that this fault zone used to produce the maximum earthquake in Thailand.

3.6.2 Rate of fault slip

Judging from the TL dates (Figure 3.16) as in the case of eastern Myanmar, it is considered that the oldest paleo-earthquake (F1) exposed on the trench occurred during 6,700-8,700 years ago. Then, the second and the youngest events (i.e. F2 and F3) took place during 2,240-3,500 and 640-1,650 years, respectively (see red tabs in Figure 3.16).

Based on elastic rebound concept (Reid, 1910), the slip rate has been defined as the rate of slip of a fault averaged over the time period involving earthquakes. Assuming both that the rate of fault slip is constant over the period of observation and that there is no creep, the slip rate can be estimated (as shown in equation 3.4) using the cumulative offset divided by the total time span of fault displacement in vertical, horizontal or absolute net directions (McCalpin, 1996).

$$S = \frac{D}{T} \tag{3.4}$$

where S is the rate of fault slip (mm/year), D is total fault displacement (m), and T is the time span during the fault is slip totally (year).

Unfortunately for the Kyaukpulu Fault, no clear evidence of vertical movement exposed in the trench. However, the horizontal movement can be estimated from the displacement of stream that offset. From the detailed measurement in the field, the stream is offset around 30 m in the dextral lateral sense of movement along the Kyaukpulu Fault.

If taken into account all faulting events detected in the trench (i.e. F1, F2, and F3), the total time span for fault movement to shift the stream is 8,060 years (cal. 8,700-640 years). As a result, the slip rate of the Kyaukpulu Fault is estimated to be 3.7 mm/year.

Table 4.2 shows the summary of all the available rates of slips from several active faults in Thailand. So, it is summarized that the slip rates for Thai Faults range from 0.1 mm/year (Klong Marui Fault Zone) to 3 mm/year (Mae Chan Fault Zone).

For 55 fault zones within the study area, few studies of slip rates have been reported. For instance, Andaman Subduction Zone (no. 45 in Figure 3.11a) has the slip rate 43 mm/year (Paul et al., 2001). For inland active fault zones, Charusiri (2005) investigated the paleo-seismology along the Ongkalak Fault Zone in central Thailand (no. 29 in Figure 3.11a) and proposed that this fault zone indicated almost 0.2 mm/year of a fault slip. The Ranong Fault Zone (no. 36 in Figure 3.11a) has a slip rate of 1 mm/year, whereas the slip rate of the Klong Marui Fault Zone (no. 10 in Figure 3.11a) is 0.1 mm/year as reported by Wong et al. (2005). The highest slip rate of inland active fault zones is occupied by the Sagiang-Sumatra Fault Zone which is 23 mm/year (Bertrand and Rangin, 2003). Finally, the comprehensive literature search for information about slip rates are summarized in Table 4.2.

CHAPTER IV
SEISMICITY INVESTIGATION

In this Chapter, the earthquake catalogue has been analyzed and catalogued. Several earthquake magnitudes reported in different scales have been converse to the same scale. Then de-clustering has been made to identify only the main-shock earthquake without using the fore-shock and after-shock earthquakes. Then will the use of the most-recent identification of seismic source zone, earthquake potential of individual zones can be determined with more confidence and accuracy.

Although the instrumental earthquake records cover a much shorter time period than paleo-seismological data, the earthquake records they provide are indispensable. Several parameters obtained from seismicity investigation (i.e. earthquake catalogues) are required for determining potentials of earthquake sources in SHA (Kramer, 1996). In this study, seismicity data within the study area are clarified in order to evaluate the earthquake potentials of individual earthquake sources. The methodology analyzing seismicity data is according to Caceres and Kulhanek (2000) as following (see also Chapter 2 in Figure 2.3).

4.1 Earthquake Catalogue Investigation

From earthquake catalogue investigation, some networks of instrumental earthquake recording stations, which recorded the present-day earthquakes covered the study area, have been developed. These include a local network occupied by the Thai Meteorological Department (TMD) and three global networks operated by the Incorporated Research Institutions for Seismology (IRIS), the US National Earthquake Information Center (NEIC), and the Harvard Seismology Centroid–Moment Tensor Project (CMT) (Figure 4.1).

Empirically, any earthquake catalogue is the result of seismological signals recorded on complex, spatially and temporally heterogeneous networks of seismometers, and processed using a variety of software, assumptions and also judgments (Habermann, 1987; Habermann, 1991; Habermann and Creamer, 1994; Zuniga and Wiemer, 1999).

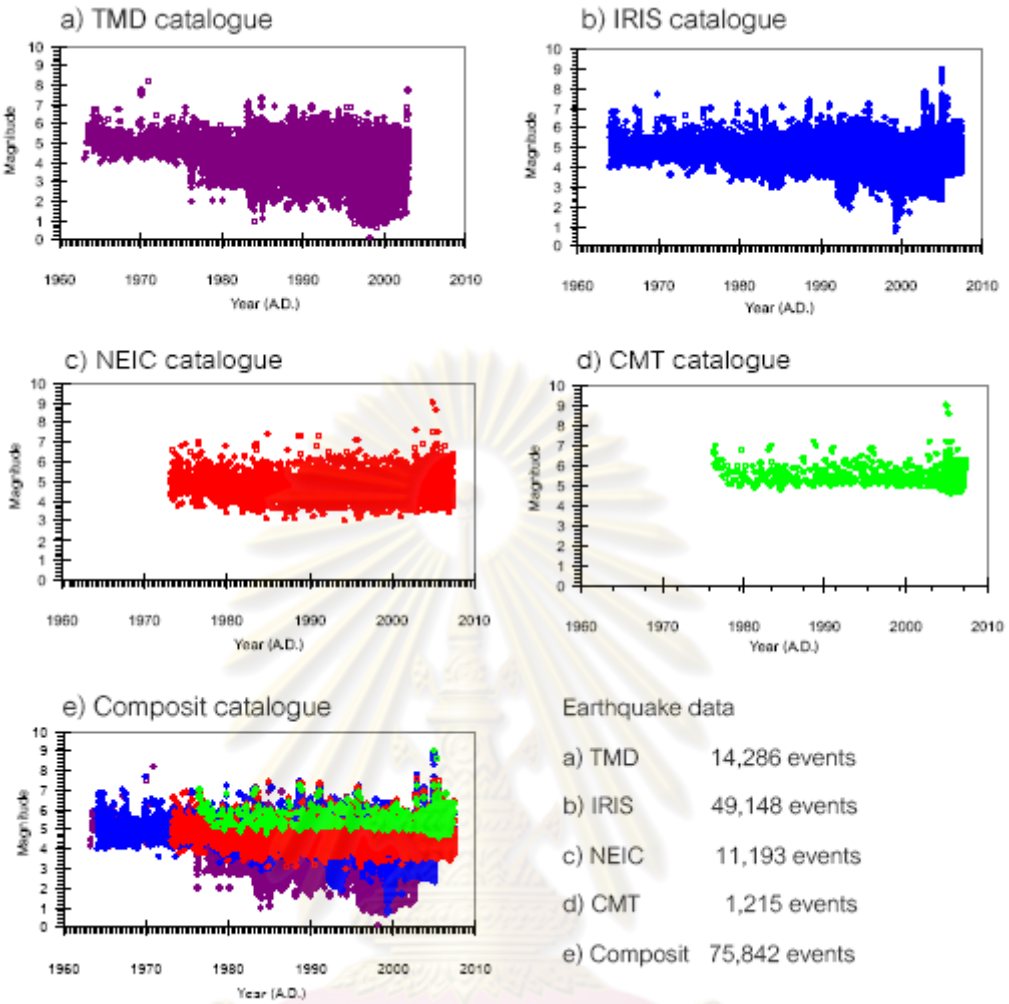

Figure 4.1. Relationship between magnitude and date of earthquakes recorded in individual earthquake catalogues.

The earthquake catalogues contributed by these different networks, therefore, have both advantages and disadvantages themselves in terms of the continuity, recording time span, and limit of the recordable magnitude range including the type of proposed magnitude scales of their records. The far-field global networks (i.e. IRIS, NEIC, and CMT) are recordable continuously with the large- to medium- size earthquakes over a long time span, whereas the local one can record efficiently the smaller shaking events (see also Figure 4.1). In addition, in the magnitude scales, the CMT catalogue records simultaneously the moment magnitude (Mw), surface wave magnitude (Ms), and body wave magnitude (mb) for individual earthquake events whereas the rest catalogues record the earthquakes non-systematically in different

scales. The IRIS and NEIC catalogues record variably the earthquake size in Ms, mb, and Mw in the order of amount, meanwhile the TMD usually records mb, local magnitude (ML), and moment magnitude (Mw), respectively.

In SHA, the longer of earthquake recording time span, the wider detectable of the magnitude range including reliable recording magnitude scale cause the more accurate in the numerical analysis of earthquake source potential (Kramer, 1996). As a result, the critical issue to be addressed before seismicity analysis is to assess the quantity, quality, and consistency of those earthquake data. Consequently, the unified earthquake catalogue for the SHA is need.

4.2 Earthquake Catalogue Combination

To improve the quantity and quality of earthquake data, combination a new earthquake catalogue is prepared. All existing earthquake catalogues (i.e. TMD, IRIS, NEIC, and CMT) are merged in this study. The composite earthquake catalogue contains totally 75,842 earthquake events (Figures 4.1e), ranging in Mw from 2.4 to 9.0. In order to avoid double-counting earthquake events, recordings that refer to earthquakes already listed have to be identified and excluded. According to Suckale and Grünthal (2009), the assumption considered to be identical events is that if the earthquake events of interest describe earthquakes that lie within a time window of 20 s and a space window of 50 km of each other, those earthquake events are assumed to be identical. When the duplets exist, the magnitudes Mw, mb, Ms, and ML are preferred in order, for reason of reliable magnitude scale as described in the next section. If both identical earthquakes record the magnitude in the same scale, then the catalogues (CMT, IRIS, NEIC, and TMD) are selected respectively. After eliminating the identical events, it is found that 31,942 entire earthquakes remain in the final composite earthquake catalogue, all of which in the time period 1963-2007.

4.3 Earthquake Magnitude Conversion

After combining and excluding the duplicate earthquake events, the new merged earthquake data composed of the heterogeneous magnitude scales (including Mw, Ms, mb, and ML) are ready to apply to the next step. It is noted that each scale is derived by a specific assumption and analytical method which have a

valid but different value and unique meaning. The mb analyzed is obtained from the first arrival P-wave from a seismogram and the Ms and ML are from the S-wave and the surface wave, respectively. In SHA, Mw is the reliable magnitude scale used and represents directly the physical properties of an earthquake source (Hanks and Kanamori, 1979), which avoids the "saturation phenomenon" at large seismic moments (Campbell, 1985). Therefore, the conversion of different magnitude scales to only one standard, viz. the Mw scale, is inevitably important for qualitative improvement of the composite earthquake catalogue.

At first, the earthquake data recorded in study area are used to develop relationships between the different magnitude scales and thus converted the remains mb, Ms, and ML to the standard Mw. As earlier described, the CMT catalogue provides simultaneously mb, Ms, and Mw magnitudes for individual earthquake events. These data are carefully used to calibrate the relationship of Mw to both mb and Ms (Figure 4.2). It is notable that the upper limits of the calibrated earthquake magnitudes are 6.8, 7.6, and 6.8 for mb, Ms, and ML, respectively (e.g., Howell, 1981; Ottemoller and Havskov, 2003). Therefore, earthquake events reported with magnitudes larger than mb of 6.8, Ms of 7.6, or ML of 6.8 are decided to be misreported which is seismologically meaningless for this magnitude-scale calibration (see inset of herein Figure 4.2).

Due to the most safety scenario in this study, when the mb and Ms are converted, the largest possible Mw is selected. As a result, the upper-bounded Mw relationships, shown by the solid-line curves in Figure 4.2, are used to convert mb and Ms to Mw. The relationships of Mw to mb and Ms are formulated as shown as equations 4.1 and 4.2. For ML result, the empirical relationship between ML and mb adopted by Palasri (2006) (Equation 4.3) is applied in this study, and then re-convert mb to Mw by using equation 4.1.

$$mb = -0.023Mw^2 + 1.2285Mw - 1.0919 \quad ; mb \leq 6.8 \qquad (4.1)$$

$$Ms = -0.0832Mw^2 + 2.5357Mw - 6.6609 \quad ; Ms \leq 7.6 \qquad (4.2)$$

$$ML = \frac{mb - 1.64}{0.63} \quad ; \; ML \leq 6.8 \qquad (4.3)$$

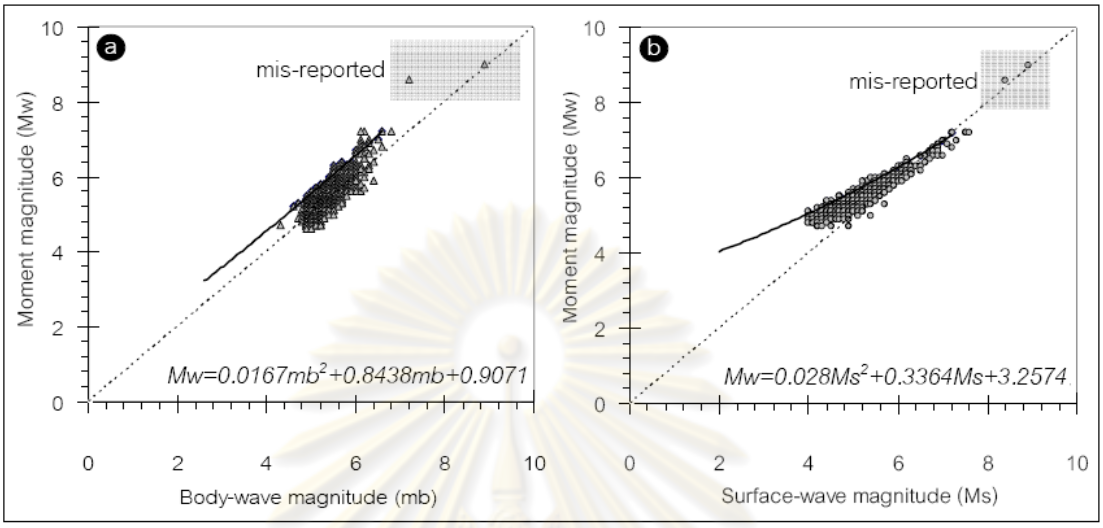

Figure 4.2. Empirical relationships a) between body wave magnitude (mb) and moment magnitude (Mw), and b) between surface wave magnitude (Ms) and moment magnitude (Mw). The earthquake events within the gray squares are those of the misreported magnitudes.

4.4 Earthquake de-clustering

In nature, when any cluster of earthquakes occurs, the earthquake can be classify temporally into 3 types; foreshock, main shock, and aftershock, relatively. In this study, the definitions proposed by Gardner and Knopoff (1974) have been applied. Foreshocks are earthquakes which precede larger earthquakes in the same or nearby location whereas aftershocks are smaller earthquakes which occur in the same general area during the days to years following a larger event or "main shock".

As reported by Cornell (1968), only the main shock, which represent the exact seismic stress released from the tectonic activities, are herein considered. To satisfy this requirement, the earthquake data obtained from the previous procedures need to be de-clustered by filtering main shocks from foreshocks and aftershocks in order to obtain a complete independent earthquake (i.e. only main shock) distribution.

In the earthquake de-clustering, the empirical model proposed by Gardner and Knopoff (1974) are applied in this study similar to Petersen et al. (2004) and Palasri

(2006) who de-clustered the earthquake data in the Sumatra-Andaman subduction zone and Thailand region, respectively. Windowing algorithms for cluster identification make use of a space and time windows around and following each event, whether it is a cluster event or not. Any earthquake occurring within the window is deemed a cluster event. The window is opened wider for stronger predecessor events (above red lines in Figure 4.3).

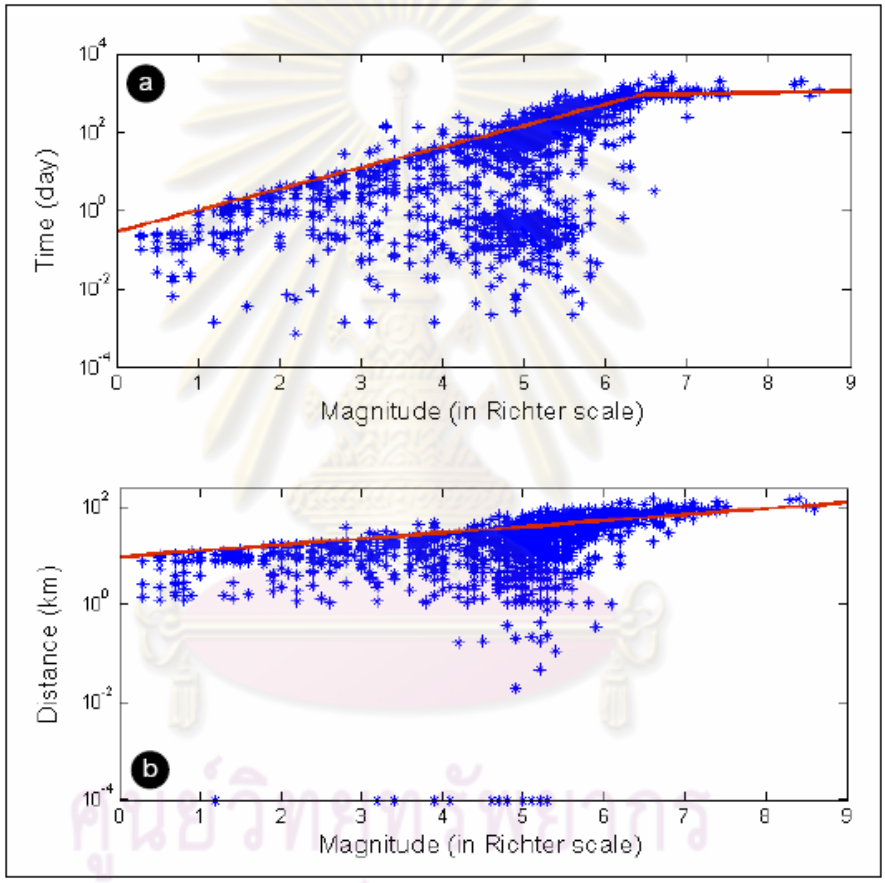

Figure 4.3. Parameters used to de-cluster and remove foreshocks and aftershocks according to the model of Gardner and Knopoff (1974). (a) Time window and (b) space window. The earthquakes (blue stars) is above the red lines of both time and space windows are identified as main-shock events.

From the Gardner and Knopoff algorithm, the results can distinguish 1,615 clusters from 31,942 earthquake events. Of these events, a total of 27,775 events (87%) are classified as foreshocks or aftershocks and therefore are eliminated (Figure 4.3).

Finally, the new earthquake catalogue derived for Thailand and surrounding areas contains 4,164 main shocks. After the completion of the de-clustering, the results are summarized as shown in Figure 4.4. This meaningful catalogue which can be related directly tectonic activities is used to evaluate the earthquake source potential described in the next section.

4.5 Earthquake Source Identification

Generally, SHA requires the accurate geometry and distribution of earthquake sources, and this has been traditionally accomplished through the geographic delineation of the 1) active faults or 2) seismic source zones (Thenhaus and Campbell, 2003). The active faults represent the source which can generate the earthquakes associated with faulting whereas the regional seismic source zones reveal the background earthquakes which are the earthquakes not associated with significant fault rupture. In this SHA, both active fault zones and seismic source zones are considered to be the possible earthquake sources.

4.5.1 Active fault zone

In this study, 55 possible active fault zones as clarified in chapter III are applied. All fault segments within individual fault zones are assumed to be generated by the same tectonic activities illustrated the same earthquake potential.

4.5.2 Seismic source zone

The term-seismic source zone is defined herein as a regional seismically homogenous area, in which every point within the source zone is assumed to have the same probability of being the epicenters of future earthquakes (Algermissen et al., 1982; Thenhaus and Campbell, 2003). An ideal delineation of seismic source zones requires a complete comprehension of geology, tectonics, paleo-seismology, historical and instrumental seismicity, and other neo-tectonic features of the region under study.

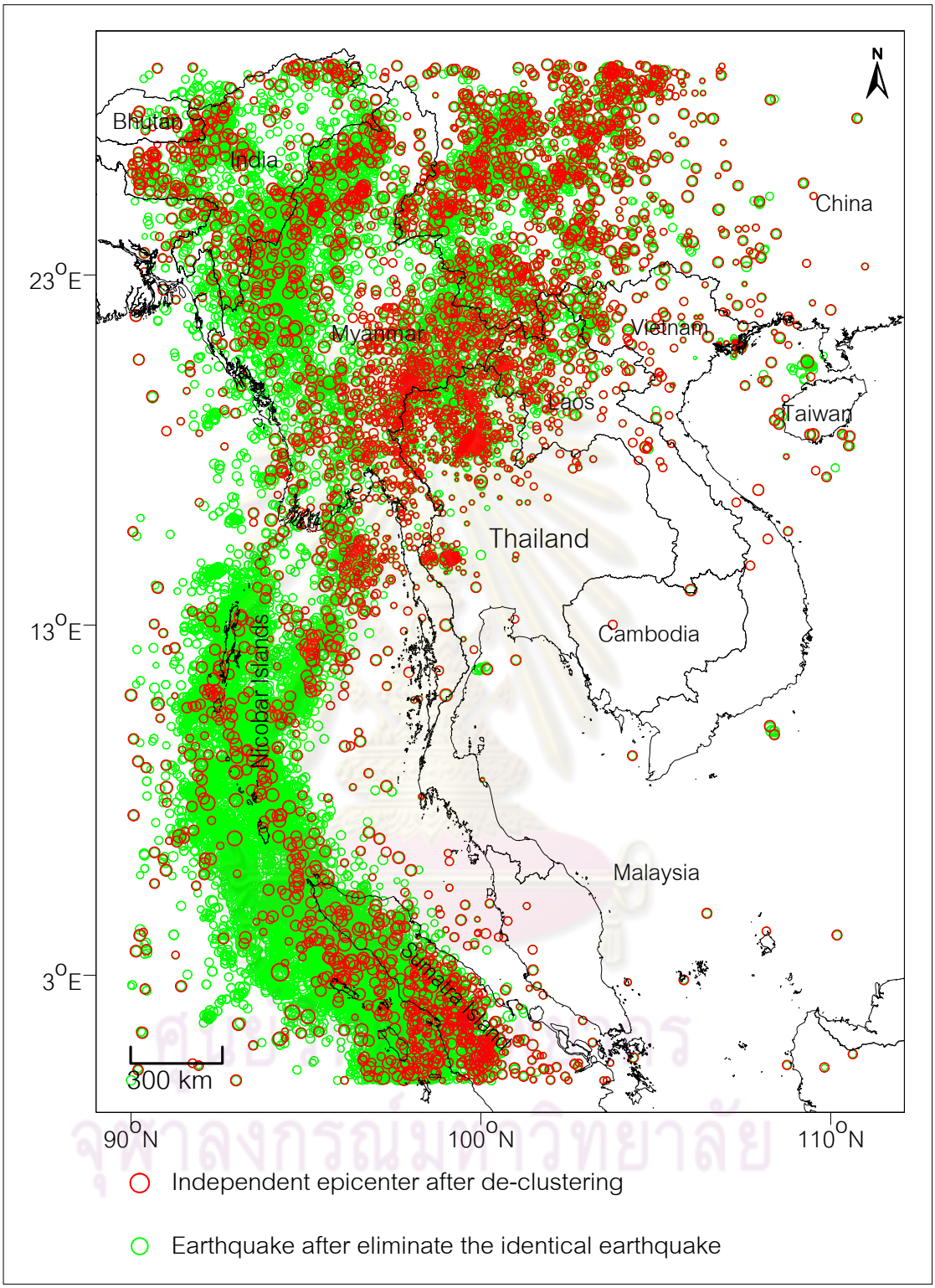

Figure 4.4. Map of SE Asia showing epicentral distributions of earthquakes before and after using foreshock-aftershock de-clustering of Gardner and Knopoff (1974).

Based on literature reviews, there are few published studies of seismic source zones in Thailand and adjacent areas in the past two decades. The pioneer is that of Nutalaya et al. (1985) who proposed 12 seismic source zones (i.e. zones A-L) in the study area consisting of zone A: Arakan Coastal Area, zone B: West-Central Burma Basin, zone C: East-Central Burma Basin, zone D: Bhamo-Paoshan Area, zone E: Burma Eastern Highlands, zone F: Tenassarim Range, zone G: Northern Thailand, zone H: North Indochina, zone I: South Yunnan-Kwangsi, zone J: Andaman Arc, zone K: Andaman Basin, and zone L: Andaman-Sumatra (Figure 1.6a). Although each of the seismic source zones of Nutalaya et al. (1985) had specific geological, geophysical, and seismological characteristics, they did not recognize the seismic source areas which cover southern peninsular Thailand and the Sumatra region.

Thereafter, Charusiri et al. (2005) revised the seismic source zones of Nutalaya et al. (1985) and extended the coverage areas of seismic source to include southern peninsular Thailand and northern Sumatra. Their revision of the seismic zoning was based on the epicentral distribution of earthquakes over the past two decades, present –day to Cenozoic tectonic environments, active faults, regional geomorphology, and plate boundaries. As a result the amount of seismic source zones increased to 21 zones, such as Zone A: Andaman subduction, Zone B: West-Central Myanmar, Zone C: East-Central Myanmar, Zone D: Mae Hong Son – Matabar, and Zone E: Muang Pan–Chiang Rai (see Figure 1.9a). Beside the active fault zones, the most up-to-date seismic source zones of Charusiri et al. (2005) are also considered for this study.

4.6 Earthquake Potential Determination

Principally, SHA requires assessment of earthquake source parameters in order to estimate earthquake potentials in individual earthquake sources. Based on Kramer (1996), the necessary earthquake source parameters capable to analyze from the earthquake catalogue are the maximum earthquake magnitude which can be generated by individual earthquake sources and the earthquake activity along the earthquake sources.

4.6.1 Maximum earthquake magnitude

The maximum earthquake magnitude ($M_{\max}$) is an important parameter in SHA because the highest magnitude earthquakes can contribute most seismic hazard to the analysis. For seismic source zones, the largest present-day earthquake reported within a seismic source zone is used to represent the $M_{\max}$ for seismic hazard analysis for that zone (Table 4.1). For the obtained 55 active fault zones, the length of surface faulting determined by paleo-seismological results are used to estimate maximum earthquake magnitude as described previously in chapter III and summarized in Table 4.2.

4.6.2 Earthquake activity

For this SHA, the earthquake activity of 21 seismic source zones including 55 active fault zones can be quantified using the frequency-magnitude distribution (FMD) of earthquakes. The FMD, known in the east as Ishimoto and Iida (1939) relations and in the west as the Gutenberg and Richter (1942) relations, defines the distribution of earthquakes with respect to magnitude as shown in equation 4.4.

$$\log(n(M)) = a - bM \tag{4.4}$$

For a certain region and time interval, the equation 4.4 describes the number of events, $n(M)$, with the magnitude equal or larger (cumulative distribution) than M, where a and b are positive, real constants. The a-value implies the entire earthquake activity and the ratio of the occurrence of small to large earthquakes in a seismogenic volume is measured by the b-value. For SHA, the constant a- and b-values in equation 4.4 are the key elements in estimating the probability that an earthquake with magnitude M or larger will occur within individual earthquake sources.

For each earthquake source, the optimal values of a and b are estimated to yield the observed FMD by using ZMAP software (Woessner and Wiemer, 2005). The magnitude of completeness (Mc) is defined as the magnitude above which all earthquakes are considered to be fully reported (Figure 4.5). The summarize of the FMD are illustrated clearly in appendix A. Table 4.1 shows a- and b-values for seismic source zones and Table 4.2 for those of the active fault zones. For instance,

Zone N (Andaman basin) revealed the highest values of a and b, which implies the highest earthquake activity. In contrast, there are several seismic source zones (G, L, and Q) where the total number of earthquakes is insufficient to properly evaluate earthquake activities. These seismic quiescent zones are, therefore, excluded from the SHA.

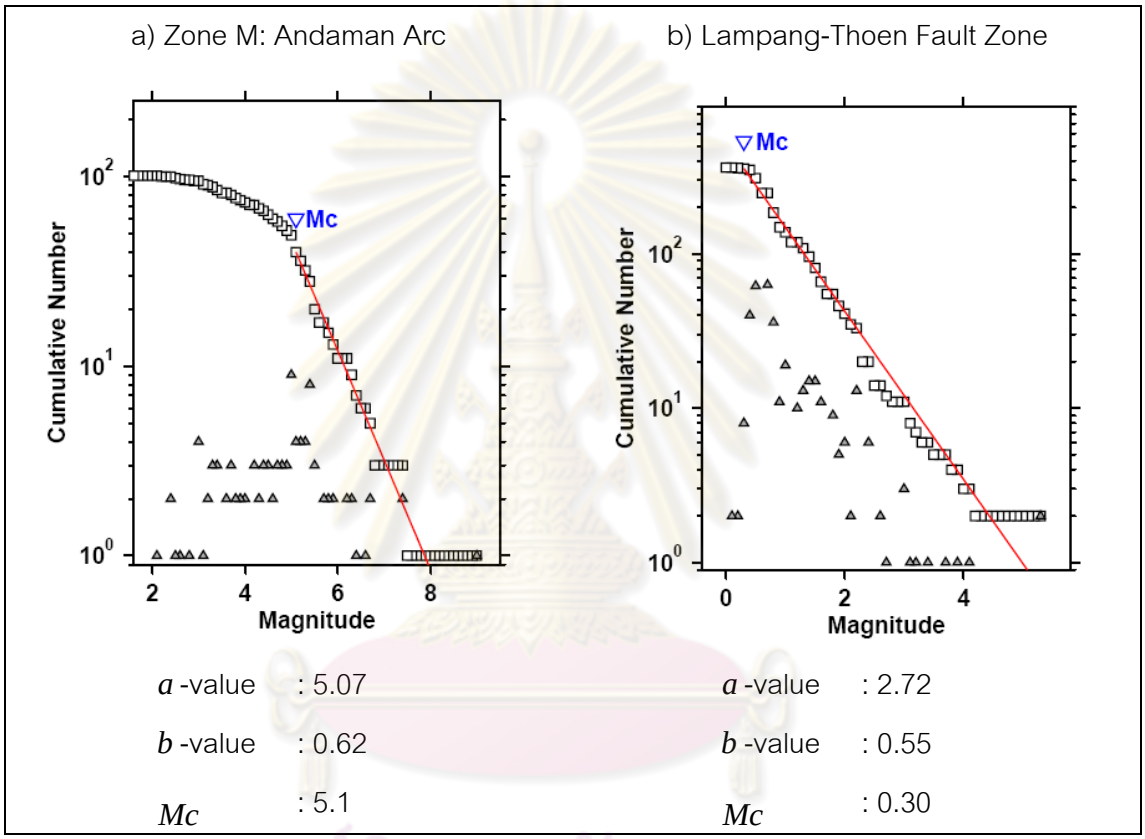

Figure 4.5. Examples of FMD analysis for a) zone M: Andaman Arc, and b) Lampang-Thoen Fault Zone. Each triangle indicates the total number of earthquakes for each magnitude; square represents the cumulative number of earthquakes equal to or larger than each magnitude. The solid red lines are lines of the best fit. Mc is the magnitude of completeness.

Table 4.1. Some important data of earthquake source parameters for 21 seismic source zones defined in this study.

Zone Code	*Zone Name*	*No. of Events*	$Msei_{max}$	*Mc*	*a*	*b*
Zone A	Andaman subduction	101	9.0	5.1	4.55	0.58
Zone B	West-Central Myanmar	61	6.9	3.2	2.73	0.36
Zone C	East-Central Myanmar	87	6.5	3.3	2.72	0.35
Zone D	Mae Hong Son – Matabar	293	6.2	2.2	3.15	0.40
Zone E	Muang Pan – Chiang Rai	140	6.4	2.5	2.79	0.37
Zone F	Chiang Mai – Luang Pra Bang	643	6.6	0.3	2.90	0.32
Zone G	Central Thailand	7	5.0	-	-	-
Zone H	Petchabun – Wang Wiang	26	5.5	2.7	2.75	0.57
Zone I	Khorat Plateau	16	5.8	4.3	3.37	0.64
Zone J	Song Ca	21	5.3	3.4	2.58	0.48
Zone K	Northern Vietnam	17	5.8	3.7	3.05	0.58
Zone L	Eastern Thailand – Cambodia	3	4.6	-	-	-
Zone M	Andaman Arc	131	8.6	5.1	5.07	0.62
Zone N	Andaman Basin	190	6.6	5.4	6.73	0.92
Zone O	Western Thailand	83	6.5	1.6	2.52	0.40
Zone P	Mergui	36	5.7	4.4	3.62	0.60

Table 4.1. (Cont.) Some important data of earthquake source parameters for 21 seismic source zones defined in this study.

Zone Code	*Zone Name*	*No. of Events*	$Msei_{max}$	*Mc*	*a*	*b*
Zone Q	Gulf of Thailand	4	5.4	-	-	-
Zone R	Malaysia – Malacca	33	5.6	3.9	3.44	0.60
Zone S	Aceh – Mentawai	14	6.2	2.4	1.68	0.25
Zone T	Tenasserim	210	8.4	5.2	5.04	0.60
Zone U	Sumatra Island	250	7.4	5.1	5.83	0.78

Remarks: *Zone Code* and *Zone Name* are proposed by Charusiri et al. (2005). *Event* is the number of earthquakes recorded in each seismic source zone. $Msei_{max}$ is the maximum earthquake magnitude recorded instrumentally in each seismic source zone. *Mc* is the magnitude of completeness derived from the *FMD*. Values *a* and *b* are constants of *FMD* representing entire seismicity rate and seismicity potential, respectively.

Table 4.2. Some important data of earthquake source parameters for 55 active fault zones identified in this study.

Fault no.	*Fault Name*	*F*	*SRL*	*S*	Mf_{max}	A_f	*Mc*	*a*	*b*	*Source*
1	Cao Bang - Tien Yen	S	287	-	7.9	8,726	1.5	1.50	0.34	Cuong et al. (2006)
2	Chiang Rai	S	28	-	6.8	552	1.8	2.25	0.42	This study
3	Chong Shan shear zone	S	298	5.00	8.0	9,122	5.2	7.85	1.34	Akciz et al. (2008
4	Dein Bein Fu	S	130	2.00	7.5	3,423	2.8	2.68	0.37	Zuchiewicz et al. (2004)
5	Dong Trieu	S,N	187	-	7.7	5,256	1.5	2.71	0.90	Charusiri et al. (2002)
6	Gaoligong Shan shear zone	S	407	5.00	8.1	13,163	5.2	9.67	1.62	Akciz et al. (2008
7	Hsenwi-Nanting	S	359	1.00	8.0	11,350	5.2	25.80	4.83	Lacassin et al. (1998)
8	Jinghong	S	53	-	7.1	1,187	2.2	2.33	0.40	Lacassin et al. (1998)
9	Kawthuang	-	36	-	6.9	749	2.4	1.68	0.25	This study
10	Klong Marui	S	29	0.10	6.8	576	2.4	1.68	0.25	Wong et al. (2005)
11	Kungyaungale	S	25	4.00	6.7	483	2.4	1.68	0.25	Wong et al. (2005)
12	Lampang-Thoen	S,N	28	0.83	6.8	554	0.3	2.72	0.55	Charusiri et al. (2004)
13	Lashio	S	50	1.00	7.0	1,094	2.2	3.15	0.40	Lacassin et al. (1998)
14	Libir	-	170	-	7.7	4,671	3.9	3.44	0.60	Metcalfe (2000)

Table 4.2. (Cont.) Some important data of earthquake source parameters for 55 active fault zones identified in this study.

Fault no.	*Fault Name*	*F*	*SRL*	*S*	Mf_{max}	A_f	*Mc*	*a*	*b*	*Source*
15	Linchang	S	107	-	7.4	2,695	2.7	2.33	0.29	Lacassin et al. (1998)
16	Loei-Petchabun Suture	S	59	-	7.1	1,328	3.6	3.01	0.62	Lepvrier et al. (2004)
17	Longling-Ruili	S	70	5.00	7.2	1,626	5.2	6.42	1.01	Bai and Meju (2003)
18	Mae Chaem	-	21	-	6.6	398	0.4	1.89	0.32	This study
19	Mae Chan	S	99	3.00	7.4	2,483	2.5	2.64	0.37	Fenton et al. (2003)
20	Mae Hong Sorn-Tak	S	37	-	6.9	766	1.9	2.65	0.38	Charusiri et al. (2004)
21	Mae Ing	S	38	-	6.9	807	2.5	2.56	0.38	Fenton et al. (2003)
22	Mae Tha	S	47	0.80	7.0	1,018	2.2	2.36	0.38	Rhodes et al. (2004)
23	Mae Yom	S	22	0.80	6.6	421	1.0	1.92	0.60	RID (2006)
24	Menglian	S	117	0.50	7.5	3,007	3.0	2.13	0.28	Lacassin et al. (1998)
25	Mengxing	S	75	4.80	7.3	1,792	3.2	2.95	0.40	Lacassin et al. (1998)
26	Moei-Tongyi	S	259	0.73	7.9	7,698	3.0	3.46	0.54	This study
27	Nam Ma	S	177	2.40	7.7	4,920	3.0	3.18	0.58	Morley (2007)
28	Nam Peng	S	51	-	7.1	1,118	3.1	3.08	0.59	Charusiri et al. (1999)

Table 4.2. (Cont.) Some important data of earthquake source parameters for 55 active fault zones identified in this study.

Fault no.	*Fault Name*	*F*	*SRL*	*S*	Mf_{max}	A_f	*Mc*	*a*	*b*	*Source*
29	Ongkalak	S,N	47	0.17	7.0	1,011	1.6	2.52	0.40	Charusiri (2005)
30	Pa Pun	S	143	-	7.6	3,829	2.1	2.58	0.37	Nutalaya et al. (1985)
31	Pan Luang	S	219	-	7.8	6,314	3.2	2.98	0.51	Nutalaya et al. (1985)
32	Pha Yao	S,N	20	0.10	6.6	380	3.2	2.95	0.40	Fenton et al. (2003)
33	Phrae	S	28	0.10	6.8	553	0.3	2.68	0.53	Fenton et al. (2003)
34	Pua	N	29	0.60	6.8	578	1.8	2.44	0.55	Fenton et al. (2003)
35	Qiaohou	-	145	-	7.6	3,885	2.6	2.35	0.25	Lacassin et al. (1998)
36	Ranong	S	46	1.00	7.0	984	2.4	1.68	0.25	Wong et al. (2005)
37	Red River	S	812	4.00	8.5	29,828	5.3	17.60	3.16	Duong and Feigl (1999)
38	Sagiang-Sumatra	S	958	23.00	8.5	36,268	5.5	6.92	0.86	Bertrad and Rangin(2003)
39	Shan	S	66	-	7.2	1,522	2.5	2.93	0.39	This study
40	Song Ca	S	225	-	7.8	6,532	3.4	2.58	0.48	Takemoto et al. (2005)
41	Song Chay	S,N	55	2.00	7.1	1,238	3.7	3.05	0.58	Cuong and Zuchiewichz (2001)

Table 4.2. (Cont.) Some important data of earthquake source parameters for 55 active fault zones identified in this study.

Fault no.	*Fault Name*	*F*	*SRL*	*S*	Mf_{max}	A_f	*Mc*	*a*	*b*	*Source*
42	Song Da	S	46	-	7.0	995	3.7	2.73	0.45	Phoung (1991)
43	Song Ma	S	72	-	7.2	1,685	5.5	6.52	1.06	Phoung (1991)
44	Sri Sawat	S	43	2.00	7.0	922	1.6	2.50	0.40	Songmuang et al., (2007)
45	Andaman subduction	R	3,388	47.00	9.2	161,790	5.3	6.08	0.69	Paul et al. (2001)
46	Tavoy	S	32	-	6.8	656	2.4	2.80	0.79	Wong et al. (2005)
47	Tenasserim	S	50	4.00	7.0	1,089	2.4	1.68	0.25	Wong et al. (2005)
48	Tha Khaek	S	250	-	7.9	7,413	4.0	3.15	0.67	DMR (2006)
49	Three Pagoda	S	141	2.00	7.6	3,760	2.0	2.62	0.51	Fenton et al. (2003)
50	Uttaladith	S	27	0.10	6.7	541	1.6	1.63	0.46	Fenton et al. (2003)
51	Wan Na-awn	-	69	-	7.2	1,609	2.2	2.28	0.35	This study
52	Wanding	S	199	1.90	7.7	5,638	4.9	5.34	0.93	Morley (2007)
53	Wang Nua	-	31	-	6.8	617	0.5	2.27	0.40	This study
54	Xianshuihe	S	505	15.00	8.2	16,993	5.2	6.74	1.05	Eleftheria et al.(2004)
55	Hutgyi	S,R	7	3.7	6.0	106	2.2	1.67	0.34	EGAT (2006)

Remarks: *Fault no.* is the numbers of faults identical to that of the faults shown in Figure 3.11. *Fault Name* are proposed by the previous works as cited in *Source*. F is fault types; S = Strike-Slip Fault, N = Normal Fault, R = Reverse Fault. SRL is surface rupture length of fault (km). $Mfault_{max}$ is the possible maximum earthquake magnitude expected from empirical relationship between SRL and Mw (Well and Coppersmith, 1994) whereas A_f is rupture area (km^2) expected from empirical relationship between Mw and A_f (Well and Coppersmith, 1994). S is slip rate (mm/year). The other parameters are as the same as those mentioned in Table 4.1.

CHAPTER V
STRONG GROUND-MOTION ATTENUATION

When an earthquake is generated from its source, the accumulated strain release in term of ground motion (i.e. ground shaking) will spread out all around from the source. The level of ground motion is absorbed and attenuated when seismic-wave caused ground motion travel through the medium. In practice, the characteristic of ground motion attenuation is specific and different in each region depending on the complexity of geologic and tectonic settings (Douglas, 2001). As a result, beside the determination of location, geometry and potential of earthquake sources (see chapters III and IV), estimation of the attenuated ground motion at a given site from earthquakes of different magnitudes and distances is also considered as one of the critical input to SHA (Kramer, 1996).

These ground motion estimations are usually obtained from equations, called "strong ground-motion attenuation relationship", that express empirically ground motion levels as a function of magnitude (M) and distance from earthquake source to a given site (R) or, in some cases, other variables, such as style of faulting (F) and site condition (S) such as rock site or soft soil sediment (equation 5.1). The standard deviation (ε) is also considered in case of PSHA (Cornell, 1968).

$$ground\ motion = function(M, R, F, S) + \varepsilon \tag{5.1}$$

The *ground motion* generally shows in terms of peak ground acceleration (PGA) or ground shaking intensity (e.g. Modified Mercalli Intensity, MMI). Most commonly used method to obtain this relationship is based on the regression analysis with past strong ground-motion data. Up to the present, a wide variety of empirical ground motion attenuation relationships are available for application in PSHA as summarized in Douglas (2001). Practically, these relationships require a lot of data in order to contribute the reliable relationship (Suckale and Grünthal, 2009). Therefore,

these empirical relationships can develop in only the location where the strong ground-motion recordings are abundant, such as Northwestern America, Philippines and Japan.

The strong ground-motion databases in Thailand and neighborhood areas at present are scantly. As a result, the unique relationships describing the attenuation of ground motion in this region have not been developed yet. Therefore, in this study, focuses are placed on comparing between the existing strong ground-motion data and the strong ground-motion attenuation relationships proposed for the other regions in order to contribute the most appropriate relationship for this SHA.

5.1 Strong ground-motion data

The strong ground-motion data used in this study are compiled from the Thailand Meteorological Department (TMD) seismological station networks. At present, the TMD stations cover almost all over abundantly Thailand region as shown in Figure 5.1. The exact locations and abbreviation description of individual stations are listed in Table 5.1 for (a) analogue and (b) digital seismic stations, respectively. The overall available strong ground-motion data consists of a total of 146 PGA records from 51 earthquake events recorded during A.D. 2003-2007. The earthquake size of events for which data is available varies from 4.1 up to 9.0 Mw (i.e. the 2004 Sumatra-Andaman earthquake's event).

In SHA, the choice of an appropriate strong ground-motion attenuation relationship is governed by the regional tectonic setting of individual sources, whether the earthquake source is in proximity to a subduction zone or inland active fault environment (Kramer, 1996). In this study, both proposed seismic source zones and active fault zones are classified into two categories on the basis of tectonic setting viz. a subduction zone earthquake for the Sumatra–Andaman region (i.e., zones A, B, and M in seismic source zone and fault zone no. 45), and shallow crustal earthquake (i.e. inland active fault zones) for the others. The distribution of the strong ground-motion records, as a result, separated on the basis of tectonic regimes (Figure 5.2); 1) strong ground-motion data from the subduction zone earthquakes and 2) the strong ground-motion data from shallow crustal earthquakes (i.e. inland active fault earthquakes) (see Appendix B). The strong ground-motion database describes;

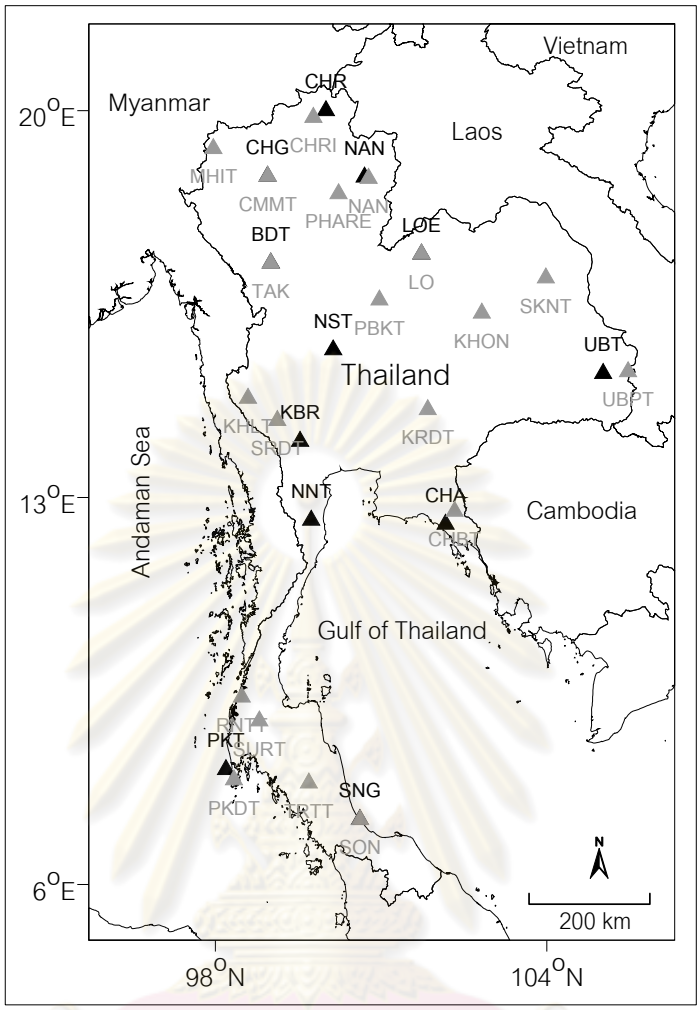

Figure 5.1. Map showing the networks of seismological stations occupied by the Thai Meteorological Department (TMD). The red triangular symbols are digital recording station and the blue ones are analogue recording station.

1) The details of earthquake sources are:

- Number of events (Event);
- Epicenter of earthquakes: longitude (Long) and latitude (Lat);
- Times of the earthquake occurrences: Day, Month, Year; and
- Earthquake sizes in the moment magnitude: Mw.

2) The details of recorded strong ground-motion are:

- Seismic station which record the strong ground-motion data (Station);
- Types of recording instrument (Instrument);

- Digital count which is the peak of the seismic wave amplitude measured in digital count unit (Digital Count). The digital count value depends largely on type of the recording instrument;

- Distance which can be measured from the epicenter to the recording station in km unit (Distance); and

- PGA is peak ground acceleration recorded in the horizontal component in the unit of g (g is the gravitational acceleration, 1g=981gal or cm/s^2) calculated from the equation 5.2.

$$PGA = \frac{(C)(D)}{(G)(Gain)(981)} \tag{5.2}$$

Where: PGA = Peak ground acceleration in horizontal component (g unit)

D = Digital count;

C = Digital count coefficient depending on type of recording instrument

[- SSA-320, 1 digital count = 1.907 x 10^{-6} (volt/count)

- TSA-100, 1 digital count = 2.384 x 10^{-6} (volt/count)];

G = Instrumental constant depending on type of recording instrument

[- SSA-320 = 2.5 (volt/cm/s^2) and

- TSA-100 = 0.0051 (volt/cm/s^2)]; and

$Grain$ Amplification value depending on type of recording instrument

[- SSA-320 = 1 and - TSA-100 = 1].

Table 5.1. List of seismological station operated by the Thai Meteorological Department.

a) Analogue stations

Location	Code	Longitude (ºE)	Latitude (ºN)
Phuket	PKT	98.19	8.08
Chiang Mai	CHG	98.94	18.81
Phumipol Dam	BDT	99.00	17.24
Kanchanaburi	KBR	99.53	14.02
Nong Plub	NNT	99.73	12.59

Location	Code	Longitude (ºE)	Latitude (ºN)
Chiang Rai	CHR	100.00	20.00
Nakhorn Sawan	NST	100.13	15.67
Songkla	SNG	100.62	7.18
Nan	NAN	100.77	18.77
Loei	LOE	101.73	17.41
Chantaburi	CHA	102.17	12.52
Ubonrajchathani	UBT	105.02	15.25

b) Digital stations

Location	Code	Longitude (ºE)	Latitude (ºN)
Mae Sariang	MHMT	97.93	18.18
Mae Hong Sorn2	MHIT	97.96	19.31
Mae Hong Sorn1	MA	97.97	19.27
Bang Wad	PKDT	98.34	7.89
Ranong	RNTT	98.48	9.39
Washiralongkorn Dam	KHLT	98.59	14.80
Rajchaprapha Dam	SURT	98.80	8.96
Chiang Mai	CMAI	98.94	18.81
Nan	NAN	98.94	18.81
Doi Suthep	CMMT	98.95	18.81
Tark	TAK	99.00	17.24
Srinakarin Dam2	SRDT	99.12	14.39
Srinakarin Dam1	KAN	99.12	14.39
Tha Ngiew Dam	TRTT	99.69	7.84
Chiang Rai	CHRI	99.77	19.88
Phrae	PHARE	100.23	18.50
Songkla	SKLT	100.62	7.17
Khao Kho	PBKT	100.97	16.57
Loei	LO	101.73	17.41

Location	Code	Longitude (ºE)	Latitude (ºN)
Lamprapeung Dam	KRDT	101.84	14.59
Kiritharn Dam	CHBT	102.33	12.75
Konkaen	KHON	102.82	16.34
Nampung Dam	SKNT	103.98	16.97
Park Mool Dam	UBPT	105.47	15.28
Songkla	SON	100.62	7.17

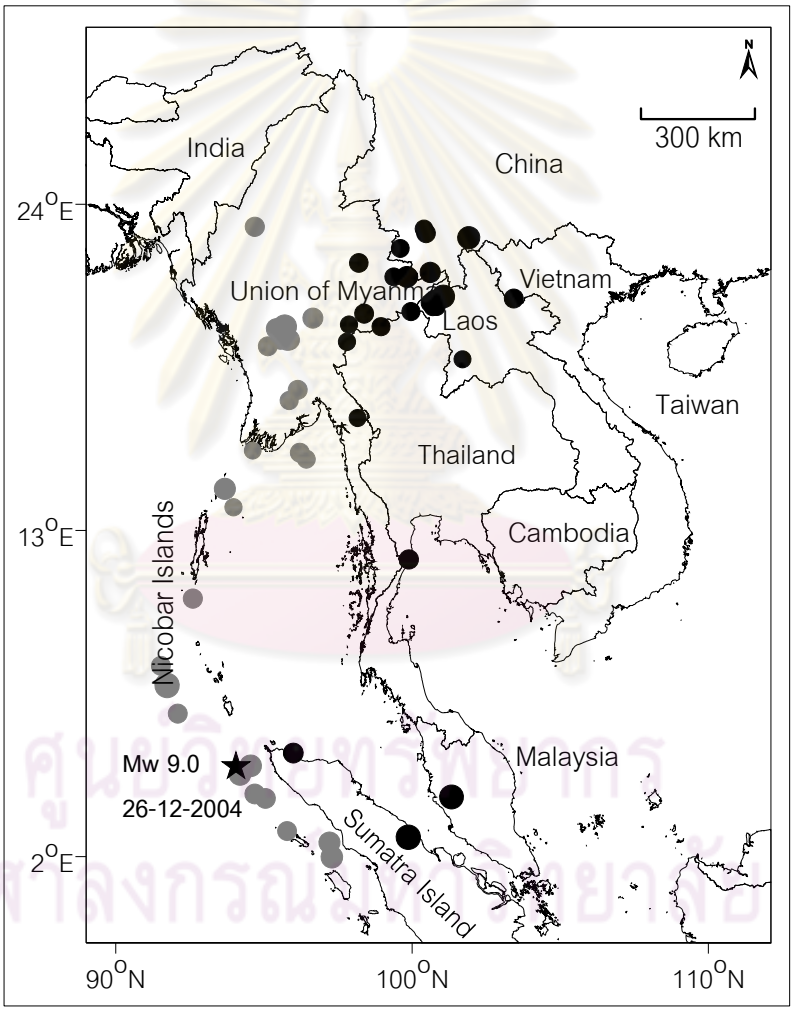

Figure 5.2. Map of Mainland SE Asia showing the epicentral distribution of earthquakes which caused the strong ground-motion recorded in this strong ground-motion database. The grey circles are the earthquake generated by the subduction zone and the black ones are those triggered by inland active fault earthquakes.

In comparison between the candidate strong ground-motion attenuation relationship and the strong ground-motion database, the data can be varied in both magnitude ranges and the source to site distances to represent and reveal exactly of which the candidate strong ground-motion attenuation relationship is the most appropriate for this study. For the strong ground-motion data of the TMD database, in particular for the shallow crustal earthquakes, no near earthquake source ground motion records are available (the shortest source-to-site distance is 272 km and 97 km for the subduction zone and the inland active fault, respectively). However nine strong ground-motion data recorded during 1999-2006 by the Royal Irrigation Department (RID) of Thailand's seismological station (i.e. Khaeng Suer Ten network, Phrae province) are available (see Table B.3 in Appendix B). All data are recorded from the shallow crustal earthquakes which are located closely to the Khaeng Suer Ten network (the shortest source-to-site distance is 19 km). In this study, therefore, the strong ground-motion database from both TMD and RID are combined to solve as much problem of lacking strong ground-motion data recorded at the near earthquake source.

5.2 Subduction Zone Earthquakes

Petersen et al. (2004) collected strong ground-motion data along the Sumatra-Andaman subduction zone which recorded by the Malaysian and Singapore seismological station networks to select the most suitable attenuation relationship for the Sumatra-Andaman subduction zone. They concluded that the strong ground-motion data along this subduction zone is consistent with the attenuation model of Youngs et al. (1997) for the rock site condition (see equation 5.3 and Figure 1.4b), although in the Youngs et al. (1997) model, which is the source-to-site distance (R), was less than 200 km.

$$\ln y_{Youngs}(M,R) = C_1^* + C_2 M + C_3^* \ln\left[R + e^{C_4^* - \frac{C_2}{C_3}M}\right] + C_5 Z_{ss} + C_8 Z_t + C_9 H \tag{5.3}$$

with $C_1^* = C_1 + C_3 C_4 - C_3^* C_4^*$,

$C_3^* = C_3 + C_6 Z_{ss}$, and

$C_4^* = C_4 + C_7 Z_{ss}$.

where y is peak horizontal ground acceleration (cm/s^2), M is moment magnitude (Mw), R is source-to-site distance (km), C_1 = 0.2418, C_2 = 1.414, C_3 = -2.552, C_4 = ln(1.7818), C_8 = 0.3846, and C_9 = 0.00607. Z_{ss} is 0 for a rock site and 1 for a soil site, and H is focal depth (km.). The other coefficients in the equation are not necessary for the rock site condition. The standard deviation of the probability of exceedance (σ) is estimated as σ = 1.45 – 0.1 M .

If the source-to-site distance is equal to or greater than 200 km, the attenuation behavior of Andaman subduction-zone earthquakes is expressed as shown in equation 5.4 (see Petersen et al., 2004).

$$\ln y_{Petersen}(M,R) = \ln y_{Youngs}(M,R) + [-0.0038*(R-200)] \qquad (5.4)$$

Thereafter, very recently Chintanapakdee et al. (2008) compared 55 strong ground-motion data which are categorized into the subduction zone earthquakes with some candidate strong ground-motion attenuation relationship proposed previously by Atkinson and Boore (1997), Crouse (1991), Fukushima and Tanaka (1990), Megawati et al. (2005), and Petersen et al. (2004). They concluded that the Crouse (1991)'s model (equation 5.5) is the most suitable strong ground-motion attenuation relationship for the Sumatra-Andaman subduction zone.

$$\ln y_{crouse}(M,R) = p_1 + p_2 M + p_4 \ln(R + p_5 e^{(p_6 M)}) + p_7 h \qquad (5.5)$$

where y is peak horizontal ground acceleration (cm/s^2), M is moment magnitude (Mw), R is source-to-site distance (km), p_1 = 6.36, p_2 = 1.76, p_4 = -2.73, p_5 = 1.58, p_6 = 0.608, p_7 = 0.00916, focal depths, h, between 0 and 238 km, and σ = 0.773.

In this study, those two candidate strong ground-motion attenuation relationships are re-calibrated to constrain the accuracy of the attenuation characteristic in the Sumatra-Andaman subduction zone. The used strong ground-motion records are provided most up-to-date by the Thai Meteorological Department network (Table B.1 in Appendix B). The strong ground-motion data are separated into the different magnitude

interval; Mw 4-5, 5-6, and 6-7 (Figures 5.3a-c). Unfortunately, the strong ground-motion of the earthquake with Mw more than 7 is lack. There is only one strong ground-motion record according to the 2004 Sumatra-Andaman Subduction Zone is reported (Figures 5.3d). It is recognized that both Crouse (1991) and Petersen et al., (2004)'s models are almost identical. However, Crouse (1991)'s model is more compatible with the compared strong ground-motion data than Petersen et al., (2004)'s. Therefore in this SHA, the strong ground-motion attenuation relationship proposed by Crouse (1991) is selected to represent the attenuation model in the Sumatra-Andaman subduction zone.

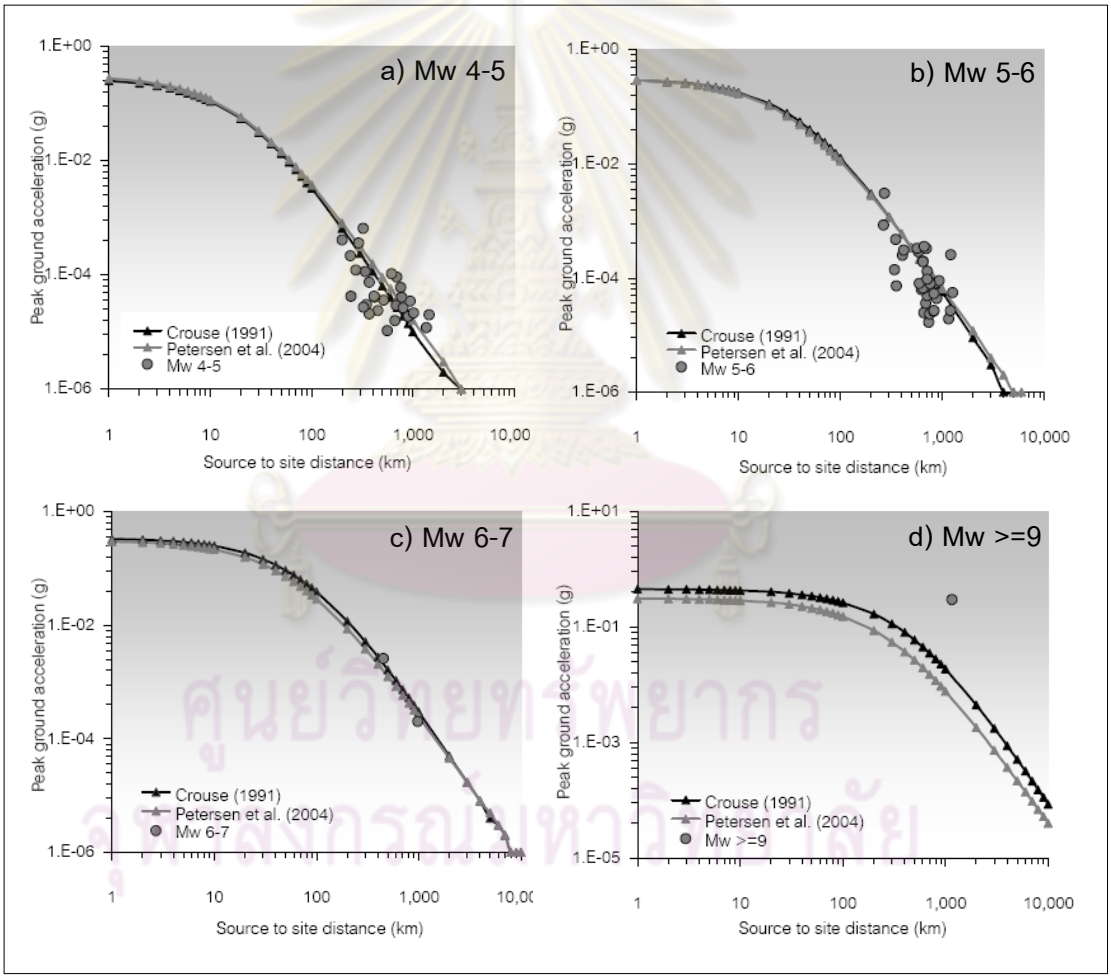

Figure 5.3. Comparison of candidate attenuation models with recorded strong ground-motion data (grey circles) for the Sumatra-Andaman subduction zone.

5.3 Shallow crustal earthquakes

For shallow crustal earthquakes, some strong ground-motion attenuation models were suggested previously for SHA in Thailand and adjacent areas. For instance, Wanitchai and Lisantono (1996) proposed the Esteva and Villaverde (1973)'s model, as shown in equation 5.6, for their SHA in Thailand (see also Figure 1.6b).

$$\ln y_{\text{Esteva and Villaverde}}(M,R) = b_1 e^{(b_2 M)}(R+b_4)^{-b3} \quad (5.6)$$

where y is peak horizontal ground acceleration (cm/s^2), M is moment magnitude (Mw), R is source-to-site distance (km), b_1 =5600, b_2 =0.8, b_3 =2, b_4 =40 and σ =0.64.

Palasri (2006) compared 7 points of strong ground-motion data recorded in Thailand with some candidate strong ground-motion attenuation relationships. He concluded that the Sadigh et al. (1997)'s model is the most fit for Thailand region (Figure 1.9b) whereas Chintanapakdee et al. (2008) proposed the model of Idriss (1993) (equation 5.7).

.

$$\ln y_{Idriss}(M,R) = [\alpha_0 + \exp(\alpha_1 + \alpha_2 M)] + [\beta_0 - \exp(\beta_1 + \beta_2 M)]\ln(R+20) + al \quad (5.7)$$

where y = is peak horizontal ground acceleration (g), M is moment magnitude(Mw);

R = source-to-site distance (km);

a = 0.2

d = source-to-site distance (km);

$\alpha_0, \alpha_1, \alpha_2$ = for $M \leq 6$ = -0.150, 2.261 and -0.083, respectively and
for $M \succ 6$ = -0.050, 3.477 and -0.284, respectively;

$\beta_0, \beta_1, \beta_2$ = for $M \leq 6$ = 0, 1.602 and -0.142, respectively and
for $M \succ 6$ = 0, 2.475 and -0.286, respectively;

F = 0 for strike slip,
0.5 for oblique,
1 for reverse; and

σ = the standard deviation of the probability of exceedance.

From these models proposed previously for SHA in Thailand, the strong-ground motion data obtained in this study are also added up in order to constrain and select the most fit of the attenuation model for the shallow crustal earthquakes that will occur in the study area in the future. The strong ground-motion data are separated into four magnitudes; ranges as the same as for subduction zone earthquakes. Based on the comparison, the strong ground-motion data in all magnitude ranges are compatible with the strong ground-motion attenuation relationship proposed by Idriss (1993) as shown in equation 5.7 whereas the models proposed by Esteva and Villaverde (1973) and Sadigh et al. (1997) are normally over-estimate (see also Figure 5.4). Therefore, the model proposed by Idriss (1993) is finally selected to represent the attenuation model of the shallow crustal earthquake in this SHA.

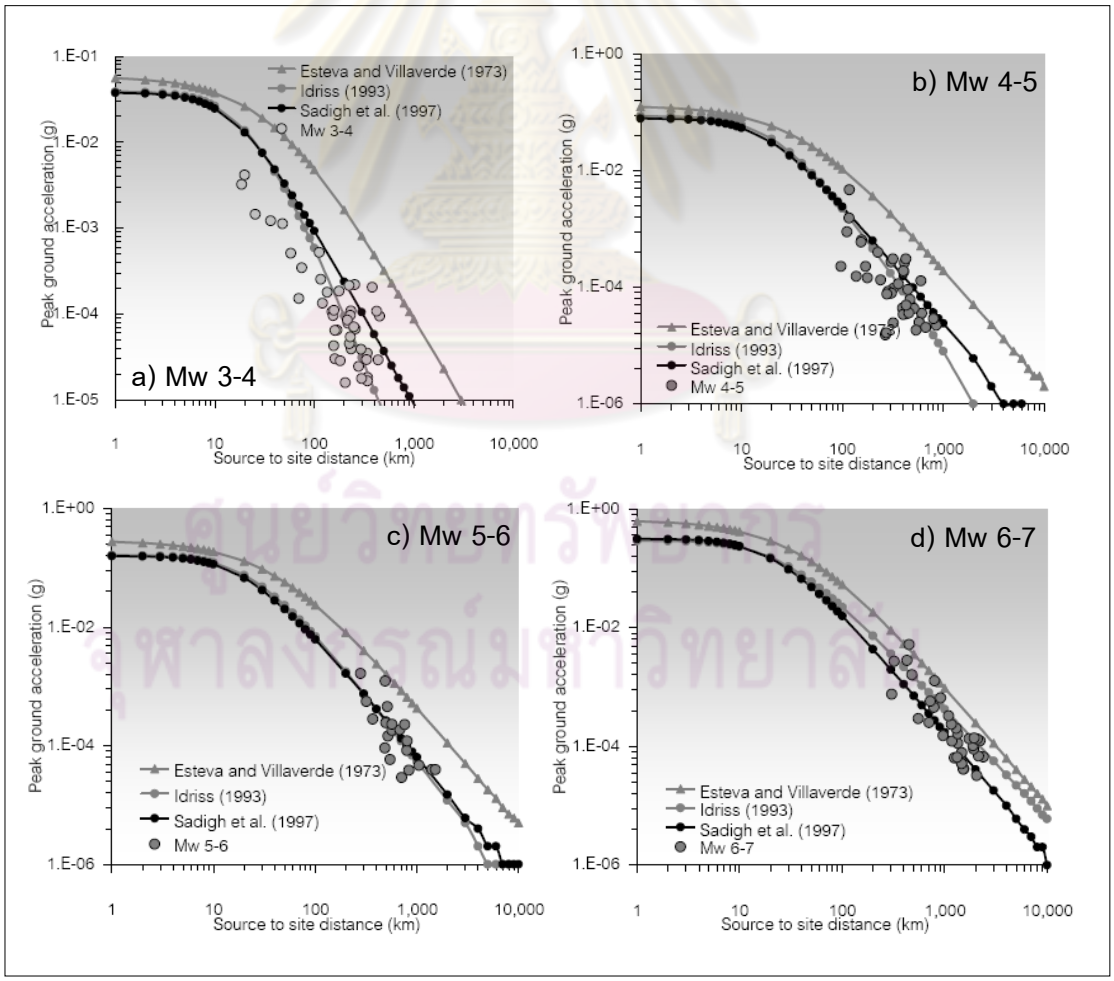

Figure 5.4. Comparison of candidate attenuation models with recorded strong ground-motion data (grey circles) for the shallow crustal earthquake.

5.4 Acceleration-Intensity Relationship

Practically, seismic intensity provides useful information on the regional distribution of earthquake effects and has been used simply to assess seismic hazards (Shabestari and Yamazaki, 2001). The seismic intensity describes qualitatively and classifies severity of the ground motion on the basis of observed effects in the stricken area. Beside the earthquake engineering which required the exact numerical value of ground shaking (e.g. 0.2g), the descriptive presentation of seismic hazard in terms of seismic intensity is more effective than the PGA format in particular for local residence's understanding which have no background of earthquake knowledge.

Up to the present, there are some intensity scales were proposed worldwide. The first intensity scale, the Rossi-Forel scale, was introduced in the late 19th century. Since then numerous intensity scales have been developed and are adopted in different parts of the world, such as the European Macro-seismic Scale (EMS-98) is used in Europe, the Shindo scale is used in Japan, the MSK-64 scale is used in India, Israel, and Russia including the Modified Mercalli Intensity scale (MMI) which has been currently used worldwide. Most of these scales have twelve degrees of intensity, which are roughly equivalent to one another in values but vary in the degree of sophistication employed in their formulation. Among these scales, the most effective and available worldwide MMI scale is adopted to this SHA.

The motivation for this study was provided by the application of PGA-MMI relations to the problem of damage estimations due to strong earthquake ground motion. A function relating PGA to MMI allows one to convert the probabilistic information on PGA, the typical parameter of seismic hazard analyses, to MMI, the parameter most commonly correlated to structural damages. The relationships of PGA to MMI from 12 published models are compared (Fig. 5.5). Cancani (1904) (equation 5.8) are adopted in this study, which, for any data, gave the highest ground-shaking conversion from PGA to MMI. We chose this model to produce the MMI seismic hazard maps because we believe that the possible worst case should be taken into account to allow seismic hazard evaluation of regions lacking sufficient seismicity data, as explained in the equation 5.8.

$$\log(PGA) = 0.33MMI - 1.17 \tag{5.8}$$

Finally, the obtained suitable strong ground-motion attenuation relationships and the selected acceleration-intensity relationship are used supplementary to the SHA in (see the next chapter).

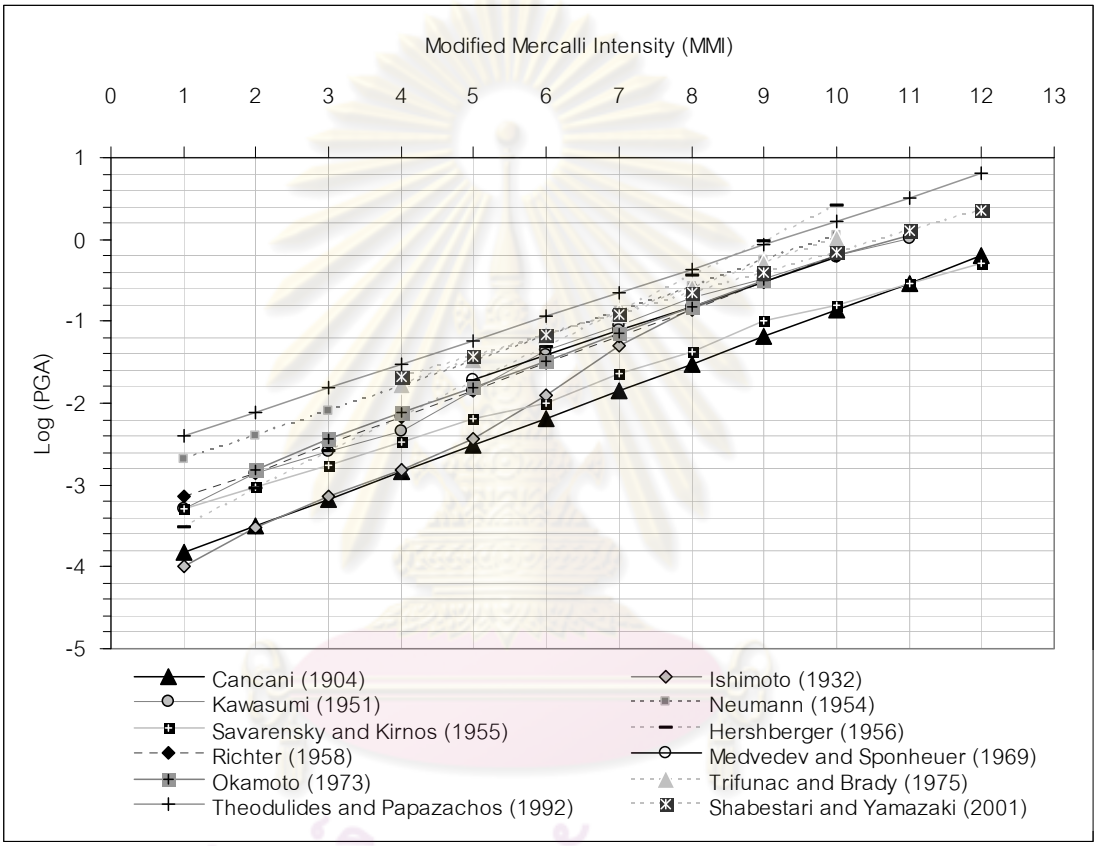

Figure 5.5. Comparison of published relationships between Peak Ground Acceleration (PGA) and Modified Mercalli Intensity (MMI).

CHAPTER VI
SEISMIC HAZARD ANALYSIS

Conceptually, the implementation of SHA involves two key steps: The first step is to model the possible earthquake sources composed of the location, geometry and seismicity parameters characterizing the earthquake potential in the respective sources as described previously in chapters III and IV. The second step is to determine the appropriate strong ground-motion attenuation model for the earthquake-generated ground motion in dependence of magnitudes and the source-to-site distances as described in chapter V.

In this chapter, both DSHA and PSHA approaches mentioned in chapter II are employed in the seismic hazard investigation by integration of various inputs and appropriated models determined in chapters III-V. These two methods (i.e. DSHA and PSHA) have differences, advantages, and disadvantages that often make the use of one advantageous over the other. The detailed analyses for SHA as conducted in this study are clarified in the following. The results, finally, reveal in the series of the seismic hazard maps in Thailand and adjacent areas including;

- For DSHA, the map of possible maximum acceleration which can be reasonably expected to occur anytime (i.e. time-independent map). This map strongly recommended for a critical project where the consequences of failure are intolerable and protection is needed against this worst-case scenario, and
- For PSHA, the series of maps showing the variation of ground shaking which depending on the given considering time period. these maps, usually, can present in two difference type; 1) the map depicts the ground shaking levels (in g unit) having a fixed probability of exceedance (%) and 2) the maps depicts the probability of exceedance (%) having a fixed ground shaking levels (in MMI unit), in a finite-time period of interest (Kramer, 1996). The first ones useful for the engineering works which need the numerical ground shaking levels (i.e. in g unit) to design the earthquake-resistant coefficient in

the infrastructure constructions. In the other hand, the second ones can explain simply to the local people in terms of percent of occurrence in individual descriptive MMI ground shaking intensity.

In computation procedure, MATLAB-scripts employing the SHA algorithm are developed and modified from Palasri (2006). In SHA computation, it is convenient to use a horizontal flat surface grids of rectangular cells, controlled by latitude-longitude coordinate (Lapajne et al., 2003). The centers of grid cells are suitable for representing the multi-points along fault lines (usually a center on a surface fault trace), areal seismic source zone, and the sites of the SHA investigation. As a result, 21 areal seismic source zones and 55 poly-lines of active fault zones obtained in the previous chapters are converted systematically to each individual 0.05° × 0.05° points. The seismic hazard is calculated for 0.25° × 0.25° grid cells located between longitudes 92–106°E and latitudes 0–21°N.

6.1 Deterministic Seismic Hazard Analysis

Krinitzsky (2003) highlights that DSHA uses geological or historical records to identify earthquake sources and to interpret the strongest earthquake each source is capable of producing regardless of time, because that earthquake might happen tomorrow. As we cannot safely predict when an earthquake will happen, the Maximum Credible Earthquakes ($MCEs$) as mentioned in chapter II are what a critical structure should be designed for if the structure is to avoid surprises affect a site.

In this study, DSHA for Thailand and adjacent areas are carried out by considering the past earthquakes, assumed surface rupture lengths of the active fault source and convert the length to the $MCEs$ according to Well and Coppersmith (1994)'s model (see also Table 4.2). The obtained $MCEs$ are assumes to occur within the source at the shortest distances from source to site. Using this situation, the attenuation relations are applied to estimate the PGA. The obtained PGA values indicate the seismic hazard level produce the most severe shaking that possible to occur at a site, without regard to the likelihood of occurrence of that earthquake. If there are more than one earthquake sources considered in the study, all source are calculated the PGA values in individual source. Thereafter when compare the PGA values from all

earthquake sources, the strongest PGA is select to represent the DSHA value at that site.

For instance, when analyze DSHA at Bangkok by considering the obtained 55 active fault zones (Figure 6.1), The $MCEs$ which calculated according to Well and Coppersmith (1994)'s model are shown in Figure 6.1a whereas the Figure 6.1b reveals the shortest source-to-site distance for individual earthquake source. Then, by evaluate deterministically from the strong ground-motion attenuation model according to Idriss (1993), the ground shaking from all earthquake sources shown in Figure 6.2c. From all 55 fault zones, the outstanding high PGA values are according to the Ongkalak (no. 29) and Three Pagoda (no. 49) Fault Zones which indicate 0.087g and 0.12g, respectively. As a result, the DSHA level of Bangkok is selected to be 0.12g.

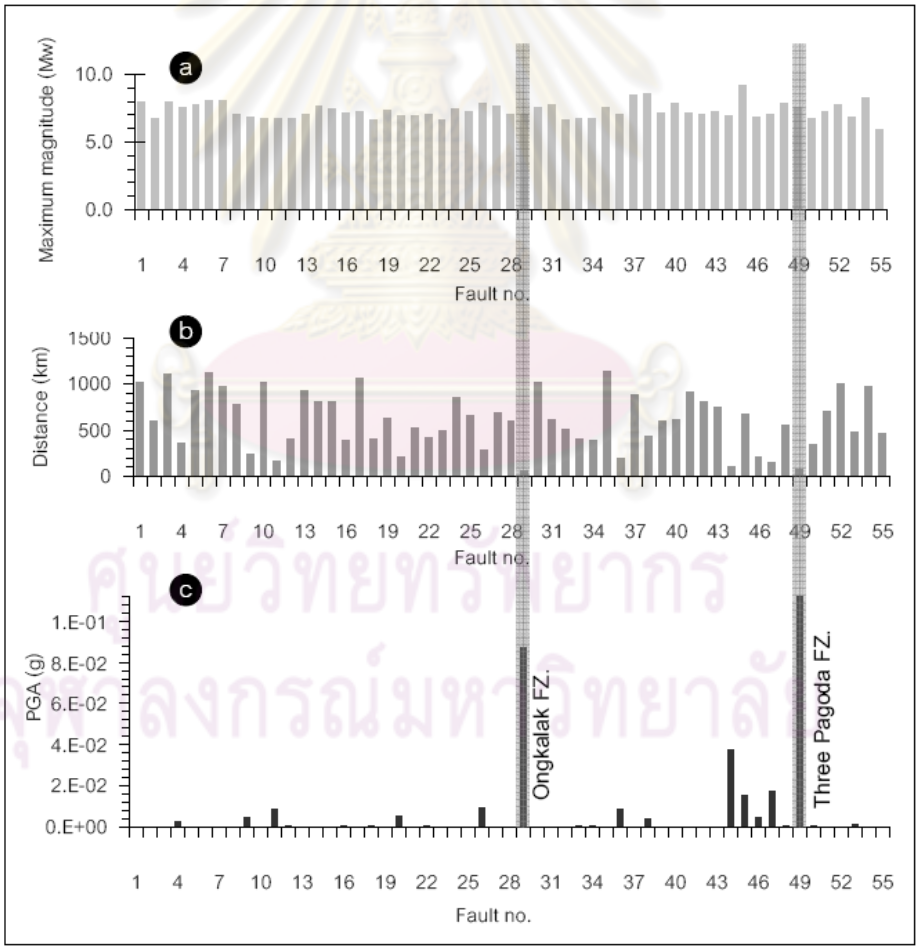

Figure 6.1. Deterministic seismic hazard of Bangkok analyzed from 55 active fault zones. Note that, the fault numbers mentioned in the figure are equivalent to fault numbers indicated in Table 4.2.

6.2 Probabilistic Seismic Hazard Analysis

Mathematically, the PSHA approach estimates the probability λ that a particular ground-shaking level A is equal to or exceeds the ground-shaking level A_0 as shown in equation 6.1 (Cornell, 1968):

$$\lambda(A \geq A_0) = \sum_{i=1}^{Ns} \nu_i \iint f_{Mi}(m) f_{Ri}(r) P[A(m,r) \geq A_0 \mid m,r] dm dr \qquad (6.1)$$

where $f_{Mi}(m)$ is the probability density function of earthquake magnitude (i.e. frequency–magnitude model) that describes the probability of earthquake occurrence having a magnitude in a given range; $f_{Ri}(r)$ is the probability density function for source-to-site distance; $P[A(m,r) \geq A_0 \mid m,r]$ is the probability of exceedance of a threshold value A_0, under the condition that an event of magnitude m occurred at source-to-site distance r. The value of $P[A(m,r) \geq A_0 \mid m,r]$ depends on the strong ground-motion attenuation model used. The coefficient ν_i represents the activity rate, which implies the average rate of earthquake occurrence, for individual fault i from the total of considering faults (Ns).

6.2.1 Probability density function of earthquake magnitude ($f_M(m)$)

In general, the probabilities of earthquake occurrence ($f_{Mi}(m)$) on a given fault follow the Gutenberg–Richter (G–R) relationship (Gutenberg and Richter, 1954; Richter, 1958) as shown in equation 6.2.

$$N(m) = 10^{a-bm} = e^{(\alpha-\beta m)} \qquad (6.2)$$

where $N(m)$ is the number of events that are equal to or larger than a given magnitude m, a and b are constants depending on empirical relationship between m and $N(m)$, $\beta = 2.303b$ and $\alpha = 2.303a$.

However, the G-R relationship usually fails for very large earthquakes due to instrumental or even historical records that are generally too short comparing with the recurrence interval of the large earthquake. Usually, the recurrence interval of large earthquakes can determine from the geological record, for example, from fault slip rates

(Youngs and Coppersmith, 1985). Up to the present, there are 2 models applied world wide to determine the frequency–magnitude relationship of the earthquake source as described below;

Model 1: Exponential magnitude distribution model

Youngs and Coppersmith (1985) proposed the exponential magnitude distribution approach to deal with maximum magnitude ($m_{\max}$) and minimum magnitude ($m_{\min}$) on individual earthquake sources (equation 6.3). The lower threshold $m_{\min}$ can be evaluated from earthquake catalog data. If $m_{\max}$ is known or can be estimated, the cumulative distribution function for the G–R relationship, with upper and lower bounds, can be expressed as an exponential magnitude distribution model ($f_{M\exp}(m)$) as follows (dashed line in Figure 6.2):

$$f_{M\exp}(m) = \begin{cases} 0 & \text{for } m < m_{\min}, \\ \dfrac{\beta e^{-\beta(m-m_{\min})}}{1-e^{-\beta(m_{\max}-m_{\min})}} & \text{for } m_{\min} \le m \le m_{\max}, \\ 0 & \text{for } m > m_{\max}. \end{cases} \quad (6.3)$$

Youngs and Coppersmith (1985) also determined an expression for the activity rate ($\nu_{\exp}$) for the exponential magnitude distribution model as shown in equation 6.4

$$\nu_{\exp} = \frac{\mu A_f S(c-b)[1-e^{-\beta(m_{\max}-m_{\min})}]}{bM_0^{\max}e^{-\beta(m_{\max}-m_{\min})}}, \quad (6.4)$$

where μ is the rigidity or shear modulus (usually taken to be ~3 × 10^2 newtons/m^2), A_f is the rupture area (km^2), S is the slip rate (mm/year) for individual faults, $M_0^{\max}$ is the seismic moment for $m_{\max}$, and c is a constant derived from the relationship between seismic moment (M_0) and magnitude (m) (equation 6.5). The relationship between M_0 and m has not previously been proposed for the Thailand region. In this

study, therefore, we assume that the constants c = 1.5 and d = 16.1, as proposed by Hanks and Kanamori (1979).

$$\log M_0 = cm + d \,. \tag{6.5}$$

Model 2: Characteristic earthquake model

This model is based on the hypothesis that individual faults tend to generate similar-sized or "characteristic" earthquakes and that these characteristic earthquakes occur on a fault not to the exclusion of all other magnitudes, but with a non-exponential frequency distribution (solid line in Figure 6.2) (Youngs and Coppersmith, 1985; Convertito et al., 2006). When the characteristic earthquake model is assumed, it is possible to formulate the corresponding ($f_{Mchar}(m)$) as given by equation 6.6.

$$f_{Mchar}(m) = \begin{cases} 0 & \text{for } m < m_{\min}\,, \\ \dfrac{\beta e^{-\beta(m-m_{\min})}}{1-e^{-\beta(m_{\max}-m_{\min})}}\dfrac{1}{1+c} & \text{for } m_{\min} \le m \le m_{char} = m_{\max} - \Delta m_2\,, \\ \dfrac{\beta e^{-\beta(m_{\max}-m_{\min}-\Delta m_1-\Delta m_2)}}{1-e^{-\beta(m_{\max}-m_{\min}-\Delta m_2)}}\dfrac{1}{1+c} & \text{for } m_{\max} - \Delta m_2 = m_{char} \le m \le m_{\max}\,, \\ 0 & \text{for } m > m_{\max}\,. \end{cases} \tag{6.6}$$

Here, the constant c in equation 6.6 is given by equation 6.7.

$$c = \frac{\beta e^{-\beta(m_{\max}-m_{\min}-\Delta m_1-\Delta m_2)}}{1-e^{-\beta(m_{\max}-m_{\min}-\Delta m_2)}}\Delta m_2\,. \tag{6.7}$$

Parameters β, m, $m_{\min}$, and $m_{\max}$ are the same as in previous equations; Δm_1 and Δm_2 represent two intervals, below and above the magnitude level m_{char}, respectively, which is the characteristic earthquake magnitude (Figure 6.2). Youngs and Coppersmith (1985) proposed values of 1.0 for Δm_1 and 0.5 for Δm_2. Note the unique

characteristic of $f_{Mchar}(m)$, which refers to earthquakes with a magnitude in the range from m_{char} to $m_{\max}$ (the "black plateau" part of the curve of Figure 6.2). Youngs and Coppersmith (1985) also showed that the activity rate (ν_{char}) between m_{char} and $m_{\max}$ is given by equation 6.8. where ν_{NC} (equation 6.9) represents the activity rate for the non-characteristic part ($m_{\min} \leq m \leq m_{char}$) of $f_{Mchar}(m)$ and the constant K is given by equation 6.10.

$$\nu_{char} = \nu_{NC} \frac{\beta \Delta m_2 e^{-\beta(m_{\max} - m_{\min} - \Delta m_1 - \Delta m_2)}}{1 - e^{-\beta(m_{\max} - m_{\min} - \Delta m_2)}}, \tag{6.8}$$

$$\nu_{NC} = \frac{\mu A_f S[1 - e^{-\beta(m_{\max} - m_{\min} - \Delta m_2)}]}{K M_0^{\max} e^{-\beta(m_{\max} - m_{\min} - \Delta m_2)}}. \tag{6.9}$$

$$K = \frac{b 10^{-c\Delta m_2}}{c - b} \frac{b e^{\beta \Delta m_1}(1 - 10^{-c\Delta m_2})}{c}. \tag{6.10}$$

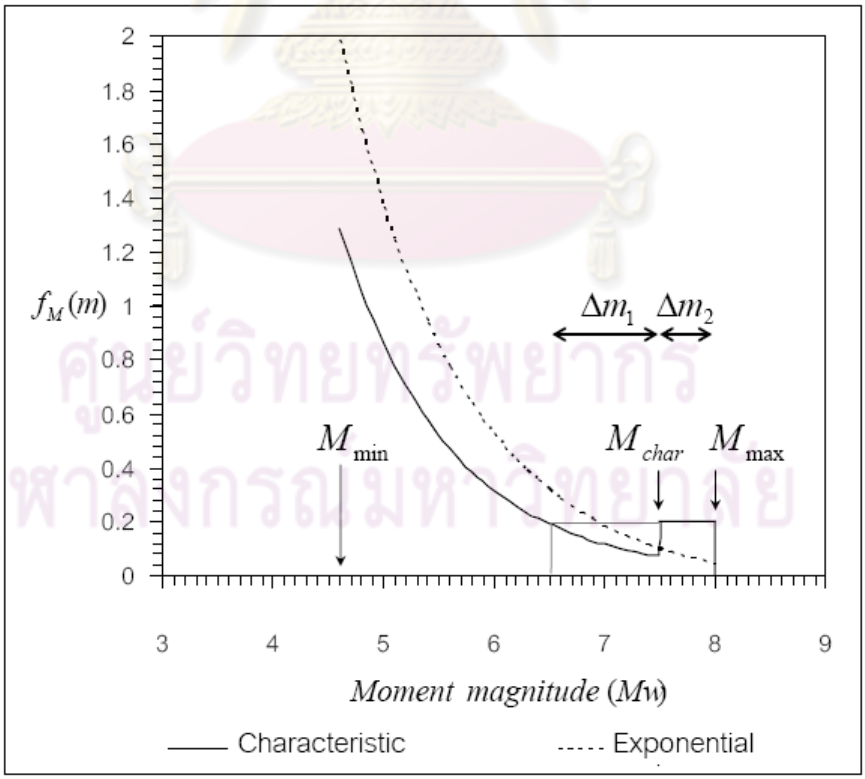

Figure 6.2. Hypothetical recurrence relationship for a fault showing the constraints provided by seismicity data and geologic data (Kramer, 1996)

For instance characteristic earthquake model, Ma Tha Fault zone (no. 22), based on the input parameters in Table 4.2, the probability density function of earthquake magnitude along the Mae Tha Fault Zone are calculated as shown in Figure 6.3. At Mw 4.15, probability of occurrence is 0.24 and decrease exponentially to 0.05 at Mw 5.95. After that, the probabilities of occurrence illustrate the stable characteristic earthquake at 0.04 during the Mw 6.25-7.

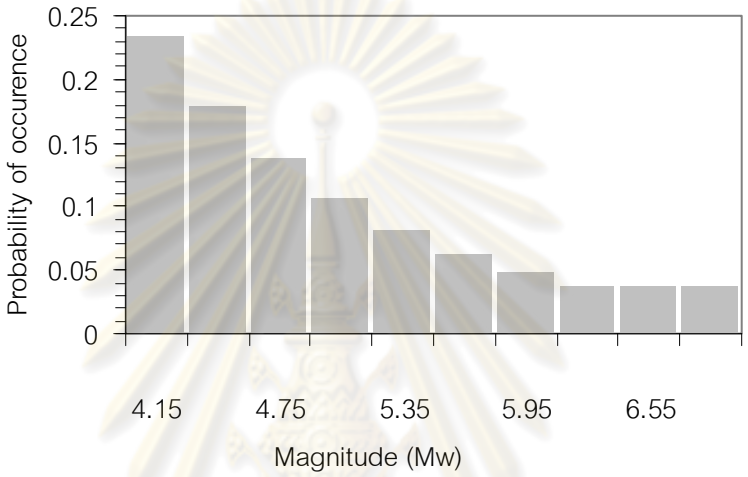

Figure 6.3. Probability density function of earthquake magnitude along the Mae Tha Fault Zone according to characteristic earthquake model.

In the previous research work, Pailoplee et al. (2009) found that comparison of both exponential magnitude distribution and the characteristic earthquake models provide practically similar seismic hazard levels. In addition, it is difficult to determine which of the two frequency–magnitude models is more appropriate for the study area because no evidence of characteristic earthquakes can be clearly identified in the instrumental earthquake records from 1963 to 2007 (see also Figure 7 of Pailoplee et al. (2009)). As a result, this SHA study determine finally the sensitivity of the PSHA results to the weights assigned to the logic-tree branches for both given frequency–magnitude models by weighting in 0.5 probability of occurrence.

6.2.2 Probability distribution of source-to-site distance ($f_R(r)$)

The probability distribution for distance from the site of interest to earthquake rupture on the source is computed. At fist, measure the distances, r, from site to the

earthquake point sources in point by point which assumed that ruptures cannot occur beyond the boundaries of the source zone (or beyond the length of the fault). It was also assumed that ruptures may occur with equal likelihood anywhere in the source zone (or along the fault), as long as they are contained within the source zone (or the fault).

For a given magnitude range, the minimum and maximum of the obtained cluster of distances are selected to be the lower and upper bound of the PSHA considering distances. $f_R(r)$ was approximated by dividing distance range into 50 equal intervals and determining how many of the ruptures fall within each distance interval, normalized by the total number of ruptures (corresponding to that magnitude range) possible for the entire source zone.

For example, Probability distribution of source-to-site distance measured from Chiang Mai province to the Ma Tha Fault zone are calculated and shown in Figure 6.4. The shortest distance is around 22 km whereas the longest possible distance is 109 km. According to Figure 6.4, the distances are abundant during 30-55 km as shown the maximum probability of occurrence 0.065 (i.e. at the distance of 38 km).

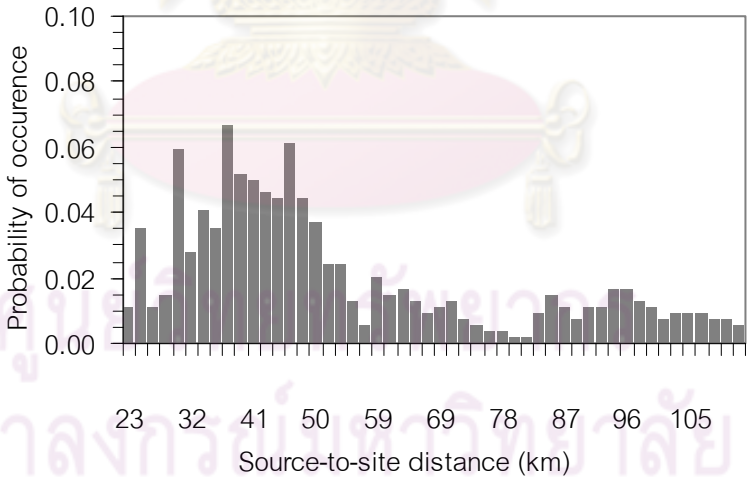

Figure 6.4. Probability distribution of source-to-site distance measured from Chiang Mai province to the Mae Tha Fault Zone.

6.2.3 Probability of exceedance of a threshold value A_0 ($P[A(m,r) \geq A_0 \mid m,r]$)

The threshold value A_0 is the prospected value of the ground shaking (i.e. PGA or MMI) of interest in the PSHA. In this study, 300 cases of A_0 starting with 0.005g and

increase every 0.01g up to 2.995g are considered. The main aim of this section is to determine the probability of exceedance of individual A_0 ($P[A(m,r) \geq A_0 \mid m,r]$) which clarify step by step as following;

- First step, for the individual given Mw (50 cases) and R (10 cases) obtained from section 6.21 and 6.21, PGA are calculated based on the strong ground-motion attenuation models as suggested in chapter V. This obtained PGA is identified to be the mean of possible PGA value ($\overline{PHA}$) which may varies according the uncertainty represented by the standard deviation (σ) of the possible ground shaking in individual given Mw and R.
- Thereafter, from given $\overline{PHA}$ and σ, the probability that a target PGA (A_0) will be exceeded should an earthquake in the given magnitude range occur at the given distance interval, ($P[A(m,r) \geq A_0 \mid m,r]$), can computed from the expression (equation 6.11).

$$P[A(m,r) \geq A_0 \mid m,r] = 1 - \Phi\left(\frac{\log(A_0) - \log \overline{PHA}}{\sigma}\right) \qquad (6.11)$$

Whereas Φ is the probability according to normal distribution.

- Finally, given $f_M(m)$, $f_R(r)$, $P[A(m,r) \geq A_0 \mid m,r]$ and ν, equation (6.1) was employed to calculate the mean annual exceedance rate ($\lambda(A \geq A_0)$) for various target A_0 in each area which analyzed the PSHA.

6.2.4 Hazard curves

After PSHA calculation according to equation 6.1, the exceedance rates ($\lambda(A \geq A_0)$) gives the annual probability that the target accelerations will be exceeded should an earthquake capable of triggering the ground shaking on the site occur in any of the earthquake source zones as shown in terms of the “hazard curves” (Figure 6.5). The hazard curve shows the probability (Y-axis) of exceeding different ground motion values (X-axis) at a site. Seismic hazard curves refer to a specific location within the investigated area. This curve is important for clarifying the (1) probability of occurrence in individual ground shaking of interest or (2) the ground shaking level in any probability of interest.

For instance, the hazard curve which plotted of the PGA against the probability of exceedance at Chiang Mai province considering from the Mae Tha fault zone as shown in Figure 6.5. From the curve, it is notable that;

- Process 1 in Figure 6.5: at Chiang Mai province, the ground shaking that equal or larger than 0.5g occurs around 0.0001 time per year or in another word, 1 time in every 10,000 (cal. 1/0.0001) year return period.
- Process 2 in Figure 6.5: Chiang Mai province, If consider the probability of occurrence at 0.000001, the ground shaking which have probability to occurrence 0.000001 is around 1g.

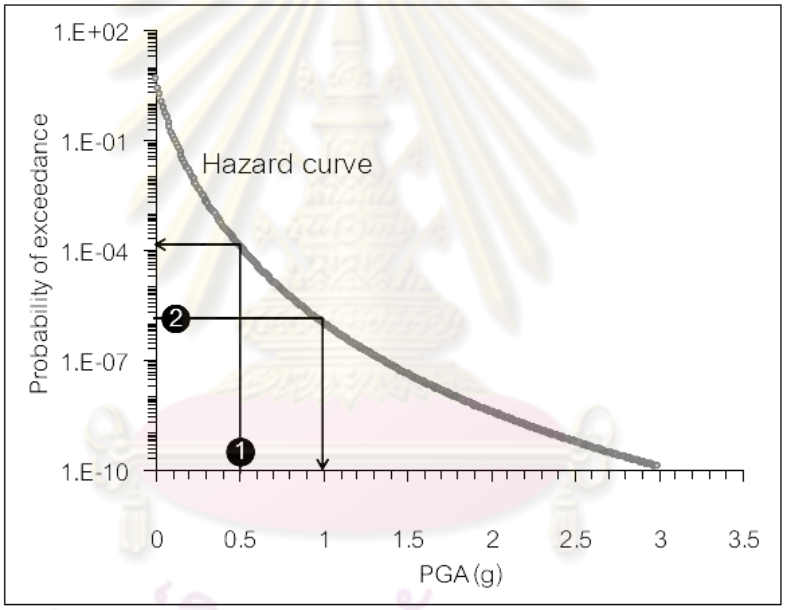

Figure 6.5. The hazard curve of Chiang Mai province considering from the Mae Tha fault zone.

6.3 PSHA Maps

Although the hazard curve as mentioned in the previous section is described efficiently the various probability of occurrence in different ground shaking level at any specific site, the hazard curve, however, cannot present in term of the map. In PSHA mapping, the most useful way of presenting the SHA results are presented in the format of finite time period of interest depending on the life-time of the infrastructure of interest (Cornell, 1968). For example, normal building consider 50-100 year for the building

available whereas the nuclear power plant or dam site may required 1000-10000 years (Cornell, 1968). In the finite time period of interest, Kramer (1996) suggested two representative methods to present the PSHA mapping in specific time period; 1) the ground shaking map described the ground shaking value (i.e. PGA) possible to be exceed in any specific % of interest and 2) the probability map which reveals the % of probability that the ground shaking may exceed the ground shaking level (in MMI scale) of interest. However in individual site, both kind of map are based on the same hazard curve obtained from the PSHA method as described previously. The detailed of individual kind of PSHA maps are described below.

6.3.1 Ground shaking map

Ground shaking map reveals the spatial distribution of ground shaking value (in unit of g) corresponding to a particular probability of exceedance in a given time period. From the obtained hazard curve, the ground shaking level (PGA) can be evaluated from fixed probability of exceedance ($\Pr ob$) in the specific of time span (T) as shown in equation 6.12.

$$\Pr ob\_hazard = -\frac{\ln(1-\Pr ob)}{T} \tag{6.12}$$

For example, in Chiang Mai, the acceleration level that has a 10% probability of exceedance in a 50 year time period would be that;

$$\Pr ob\_hazard = -\frac{\ln(1-\Pr ob)}{T} = -\frac{\ln(1-0.1)}{50} = 0.0021$$

From the seismic hazard curve of Figure 6.5, that the acceleration level that have the probability 0.0021 would be approximately 0.4g. Therefore, the ground shaking of Chiang Mai province corresponding to 10% probability of exceedance in 50 year is 0.4g.

6.3.2 Probability map

The probability map reveals the probabilities of exceedance (%) which may equal or larger than the constant ground shaking interest in a given time period., the probability of exceedance, $\Pr ob$, is associated with the probability of the ground

shaking will be exceed the ground shaking of interest, $\Pr ob\_hazard$, in the return period , T , may be written as shown in equation 6.13.

$$\Pr ob = 1 - e^{(-(\Pr ob\_hazard)(T))} \tag{6.13}$$

For example the at Chiang Mai, the probabilities that ground shaking will be equal to or greater than levels 0.5g for the 50 year time would be that;

$$\Pr ob = 1 - e^{(-(\Pr ob\_hazard)(T))} = 1 - e^{(-(0.0001)(50))} = 0.49 = 49\%$$

Therefore, the probability that Chiang Mai province may be posed by the ground shaking equal to or greater than levels 0.5g for the 50 year time span is around 49%.

6.4 SHA Results

In SHA mapping, totally 2,061 points of 0.25° × 0.25° grid cells located between longitudes 92–106°E and latitudes 0–21°N are contoured. Several hazard maps as described above are presented in this section.

6.4.1 DSHA

The possible maximum acceleration map (Figure 6.6) reveals the ground shaking levels between 0g-0.8g in Thailand and adjacent area. Usually, the high hazard level are posed along the active fault zones supplementary with some background of seismic hazard according to the seismic source zones also recognized in this SHA. The earthquake-prone areas are in central Myanmar, Sumatra, Laos, southern China, northern Vietnam, and northern and western Thailand. In central Thailand, there is a high hazard level in the area close to the Ongkalak Fault Zone. In southern Thailand, there is seismic hazard associated with the Ranong and Klong Marui Fault Zones. For northeastern Thailand, although there has recently been a dramatic decrease in reporting of earthquake ground shaking, the calculated seismic hazard reveals that the far north, close to the Tha Khaek Fault Zone in Laos, may also be subject to damage by seismic activity. In the Nicobar Islands and western Myanmar, close to the Andaman subduction zone, the possible maximum acceleration map shows ground shaking of around 0.6–0.8 g.

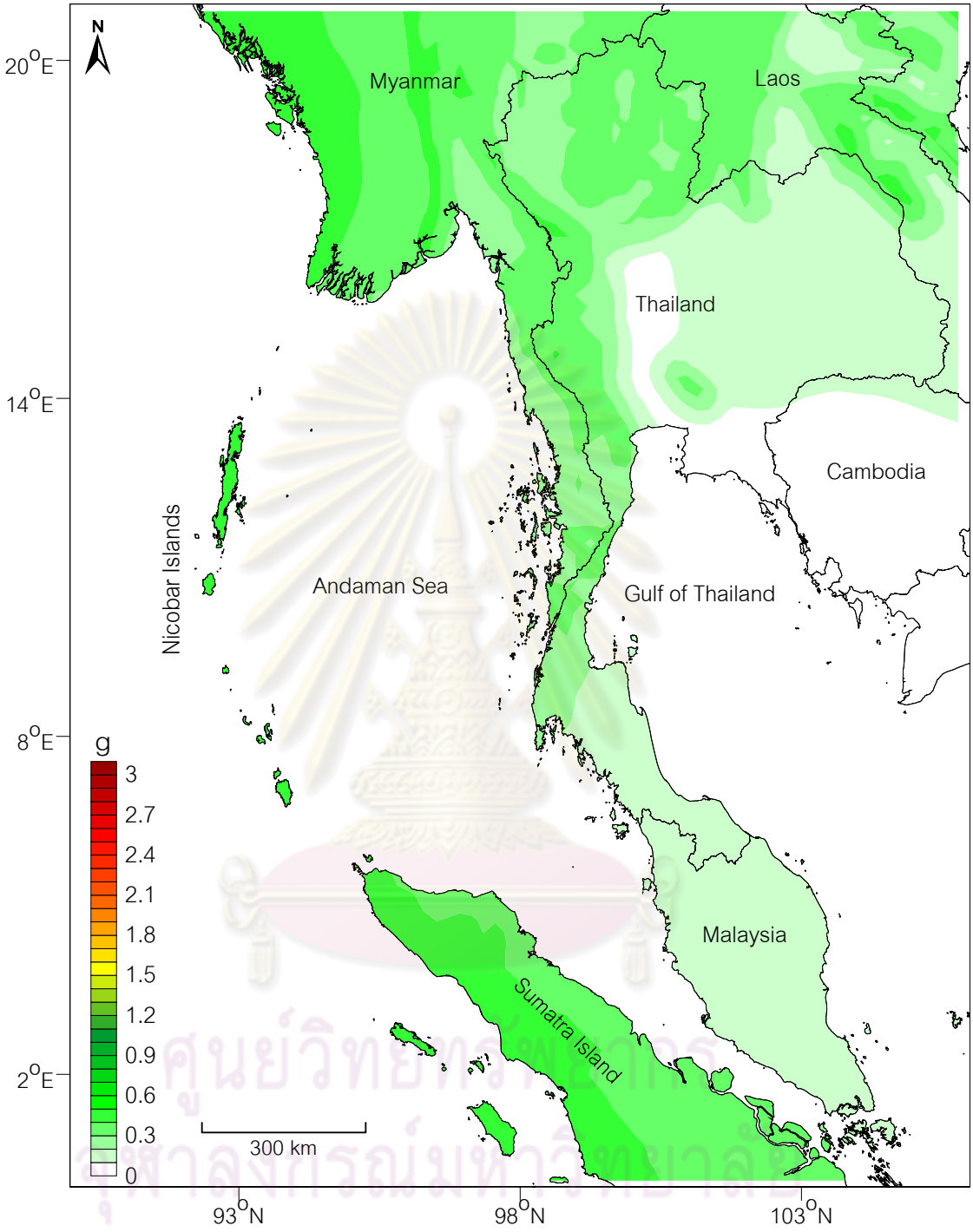

Figure 6.6. Possible maximum acceleration map of Thailand and adjacent areas.

6.4.2 PSHA

Several PSHA maps are presented here. The ground shaking levels are presented in both terms of peak ground acceleration (PGA) of the ground shaking maps and Modified Mercalli Intensity (MMI) of the probability maps as shown below.

For the ground shaking maps, the maps are conducted for 2% and 10% probability of exceedance in 50 and 100 years (Figure 6.7). The spatial distribution of seismic hazard from PSHA is also roughly analogous to that obtained by DSHA, but the hazard level is higher in PSHA than in DSHA.

For instance, taking a 2% probability of exceedance in a 50 period (Figure 6.7a), PGA values indicate high seismic hazard (up to 3g) at the area located along the Sumatra-Andaman Subduction Zone such as western Myanmar and Nicobar Islands. However, the PGA in Thailand shows the lower hazard when compare with those countries of neighboring. The highest level of seismic hazard in Thailand posed in northern and western regions and it decreases gradually toward the east and southeast. The PGA values for 50 year in these areas are around 0.5g and 1g for 10% and 2% probability of exceedance, respectively. In central and eastern Thailand, the ground shaking is quiescence according to this PSHA. However, one outstandingly high hazard area is in the Ongkalak Fault Zone in central Thailand.

In southern Thailand there are two major fault zones, the Ranong and Klong Marui Fault Zones. Judging from the surface rupture length of these fault zones, both of them can generate an earthquake with a maximum magnitude of around 6.8–7. However, the Ranong fault zone has a slip rate of 1 mm/year, whereas the slip rate of the Klong Marui fault zone is 0.1 mm/year (Table 4.2). The Klong Marui Fault Zone, therefore, does not have more significant on seismic hazard comparing with the Ranong Fault Zone.

For the probability maps (Figure 6.8), northern Thailand has the potential to be affected by ground shaking up to MMI level VI for 50 or even 100 years, whereas for western and southern Thailand the levels are IV–V. For the rest of the study area, the possible ground shaking is less than level IV and is zero in some places such as central or eastern Thailand.

a) 2% probability of exceedance in 50 years

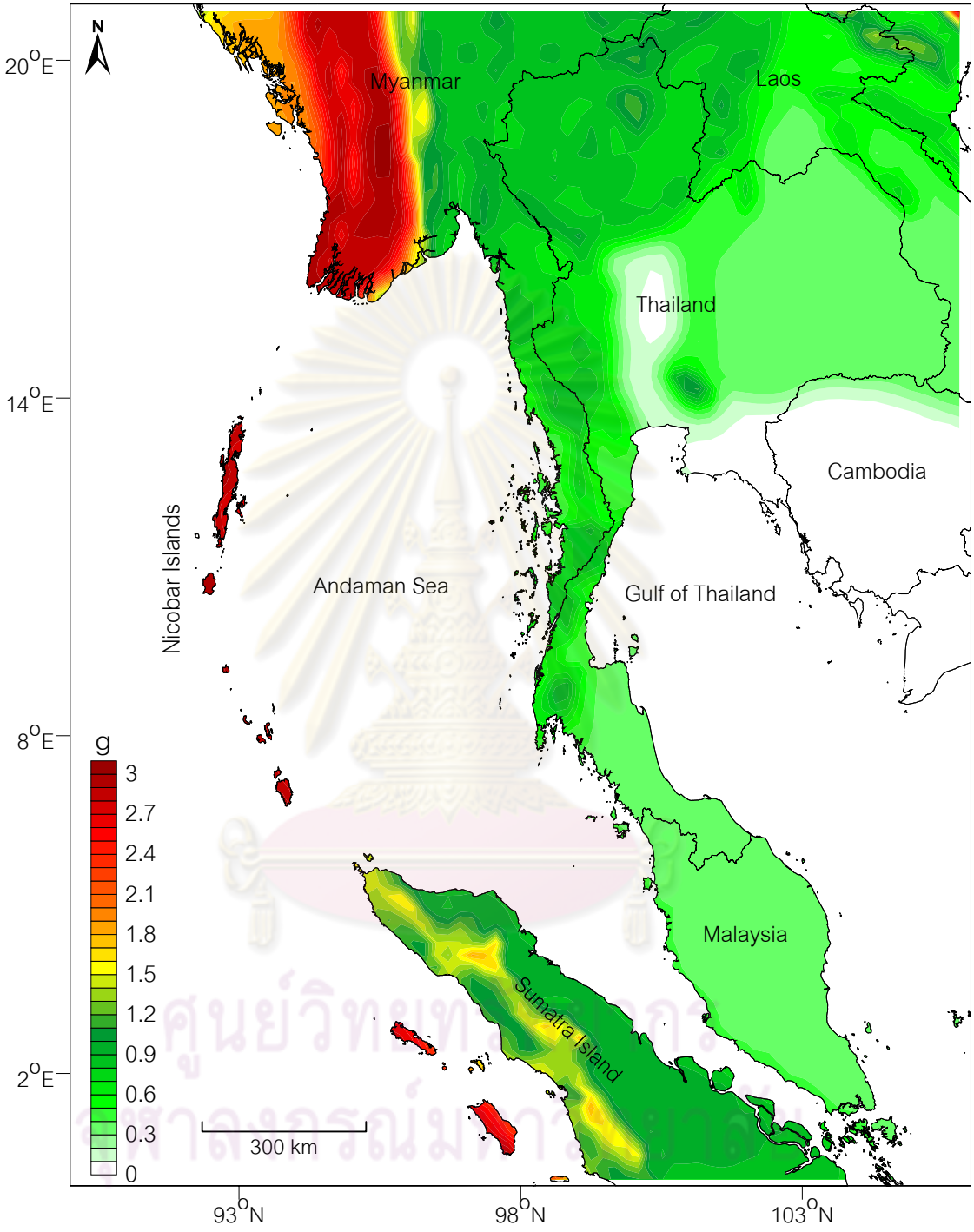

Figure 6.7. Probabilistic seismic hazard maps of Thailand and adjacent areas showing the distribution of Peak Ground Acceleration (PGA) that exceeds in specific % probabilities for return periods of 50, and 100 years.

b) 10% probability of exceedance in 50 years

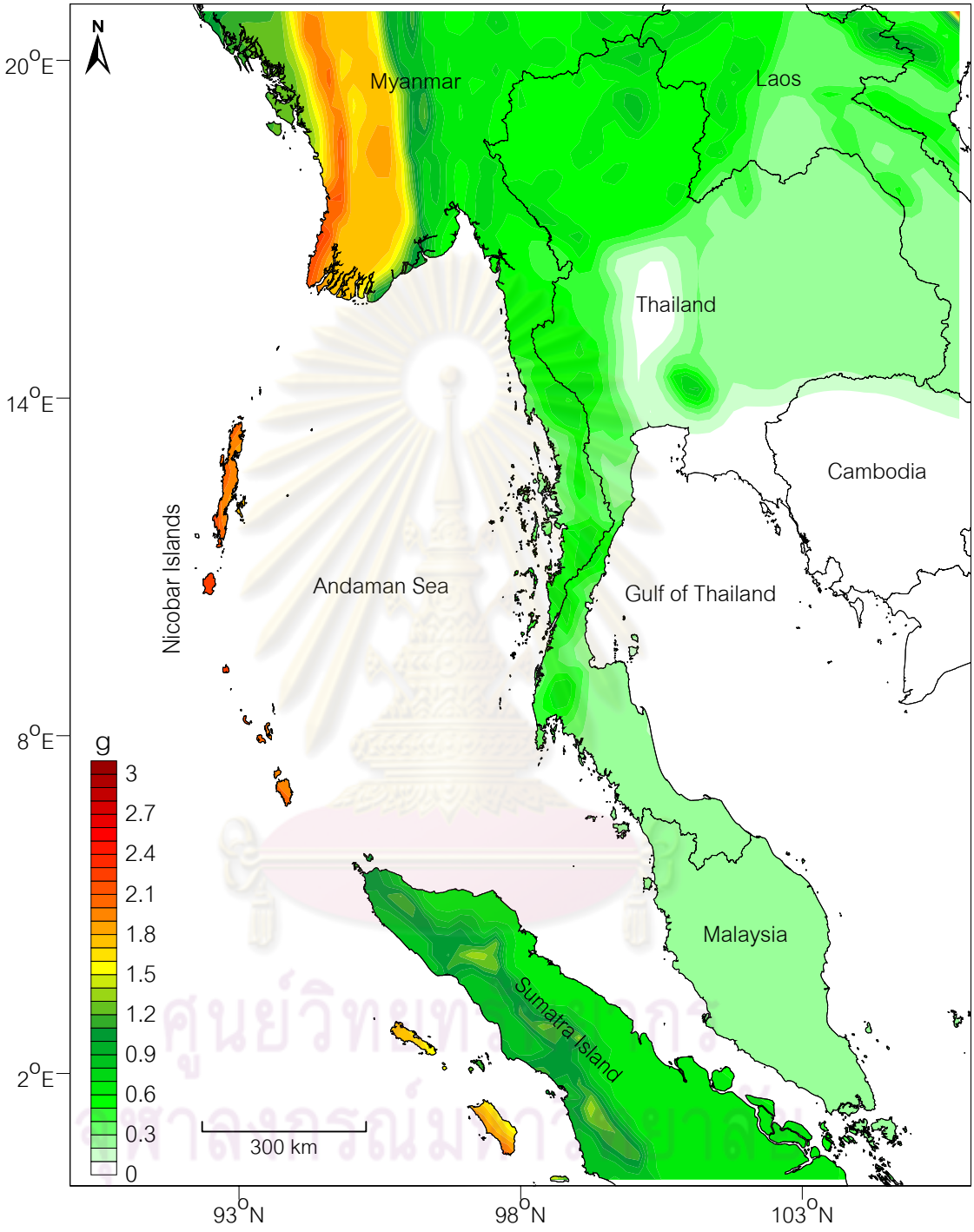

Figure 6.7 (cont.) Probabilistic seismic hazard maps of Thailand and adjacent areas showing the distribution of Peak Ground Acceleration (PGA) that exceeds in specific % probabilities for return periods of 50, and 100 years.

c) 2% probability of exceedance in 100 years

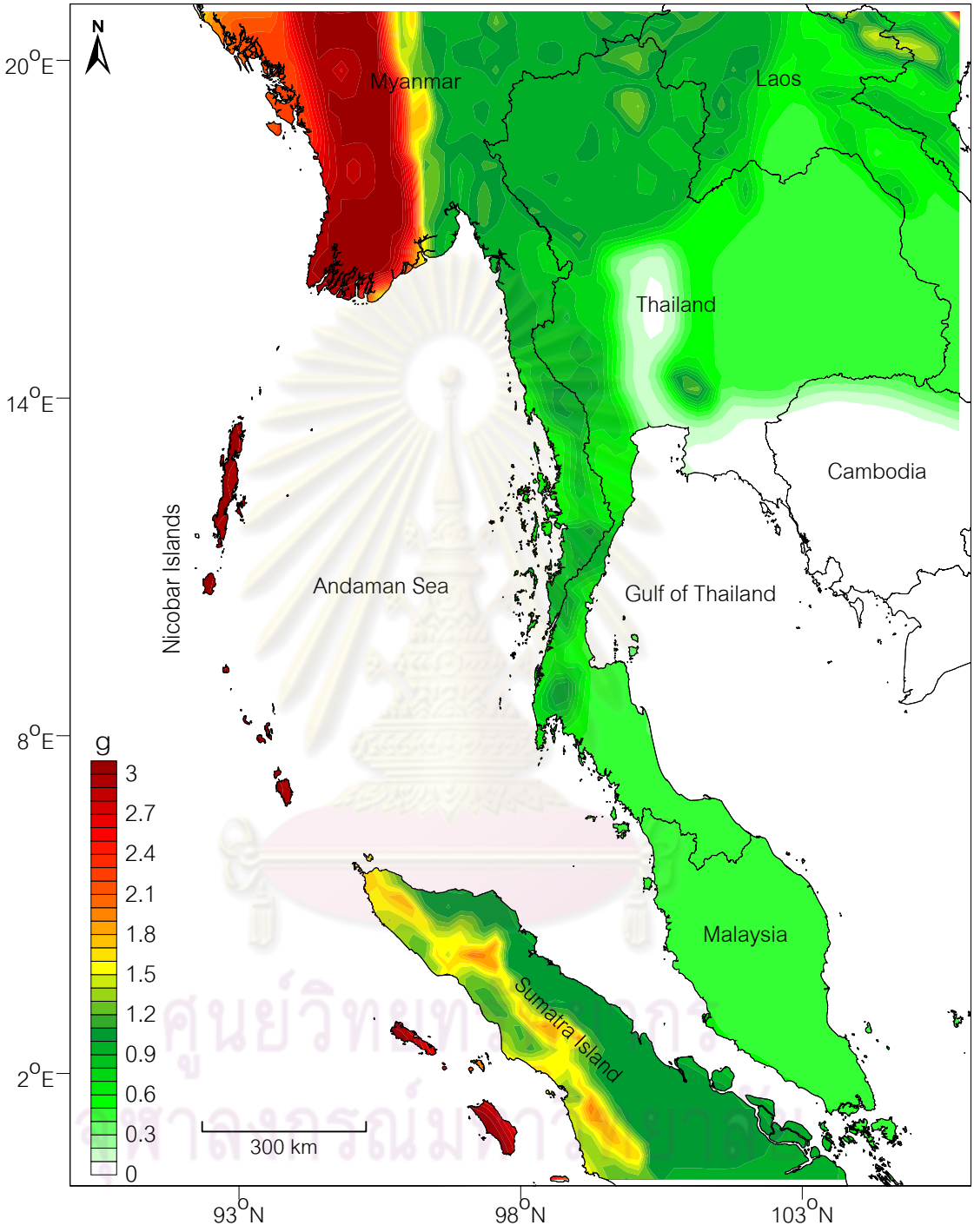

Figure 6.7 (cont.) Probabilistic seismic hazard maps of Thailand and adjacent areas showing the distribution of Peak Ground Acceleration (PGA) that exceeds in specific % probabilities for return periods of 50, and 100 years.

d) 10% probability of exceedance in 100 years

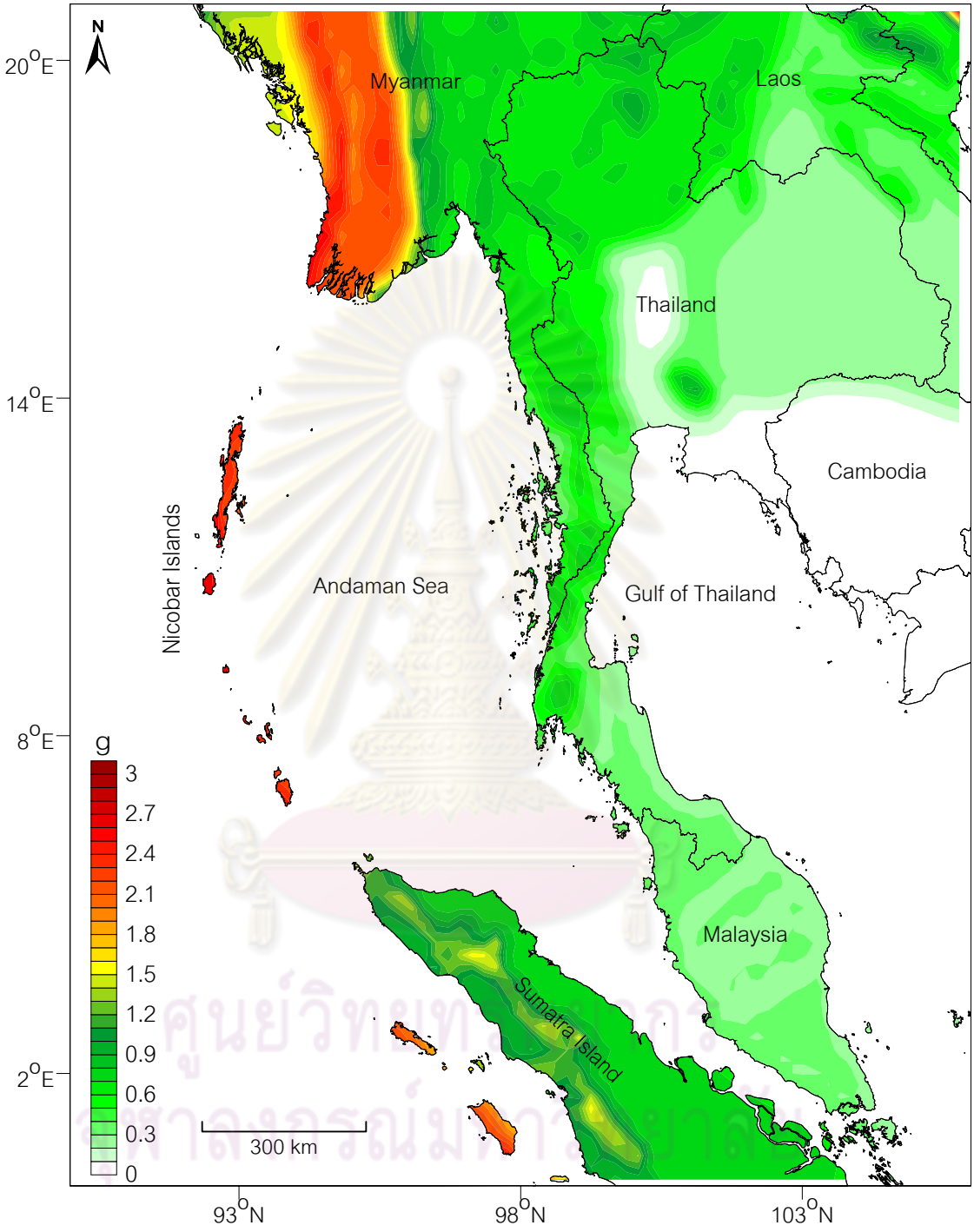

Figure 6.7 (cont.) Probabilistic seismic hazard maps of Thailand and adjacent areas showing the distribution of Peak Ground Acceleration (PGA) that exceeds in specific % probabilities for return periods of 50, and 100 years.

a) % of ground shaking equal or larger than level IV in 50 years

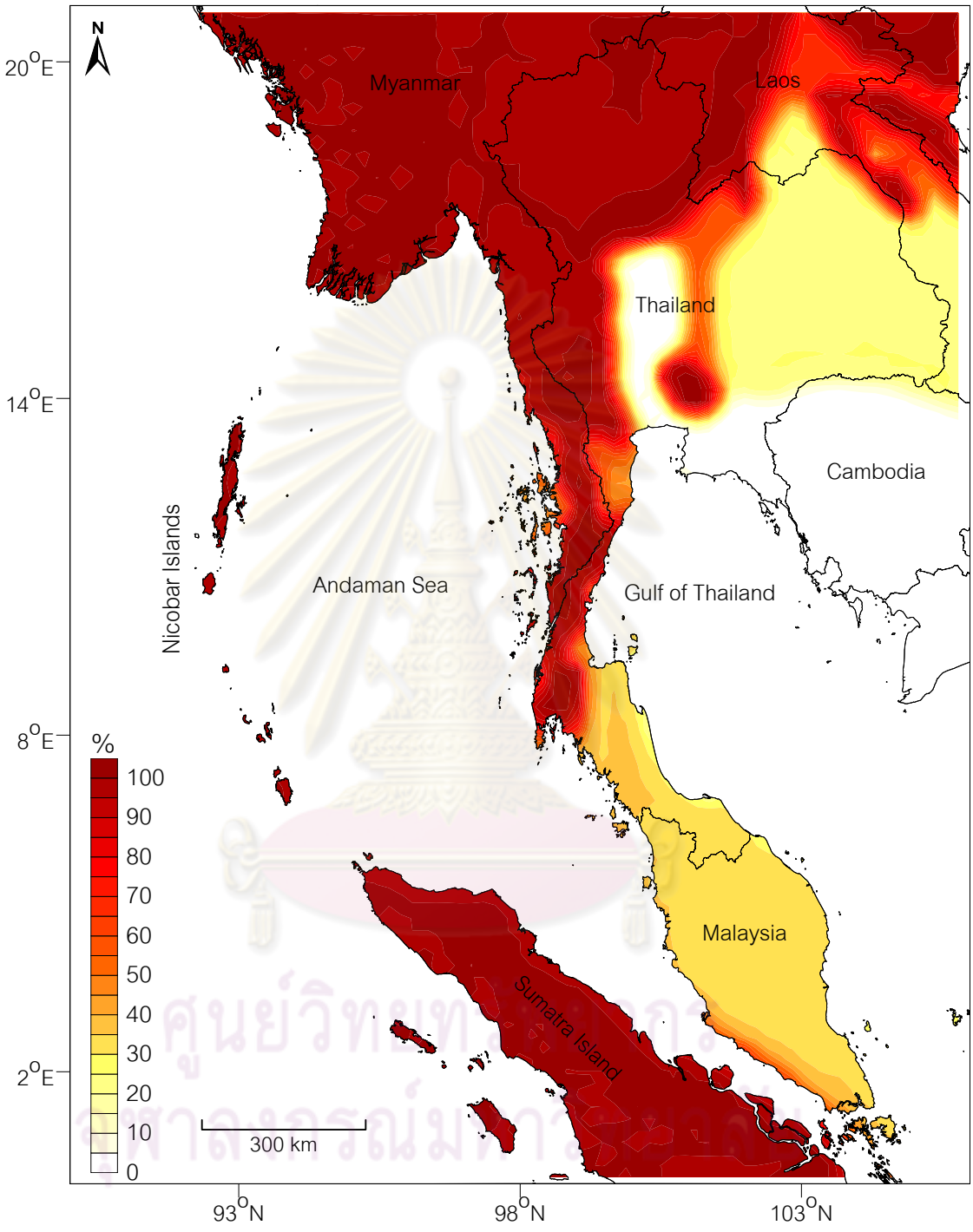

Figure 6.8. Probabilistic seismic hazard maps of Thailand and adjacent areas showing the probabilities (%) that ground shaking will be equal to or greater than levels IV, V, VI, and VII (Modified Mercalli Intensity) for return periods of 50 and 100 years.

b) % of ground shaking equal or larger than level V in 50 years

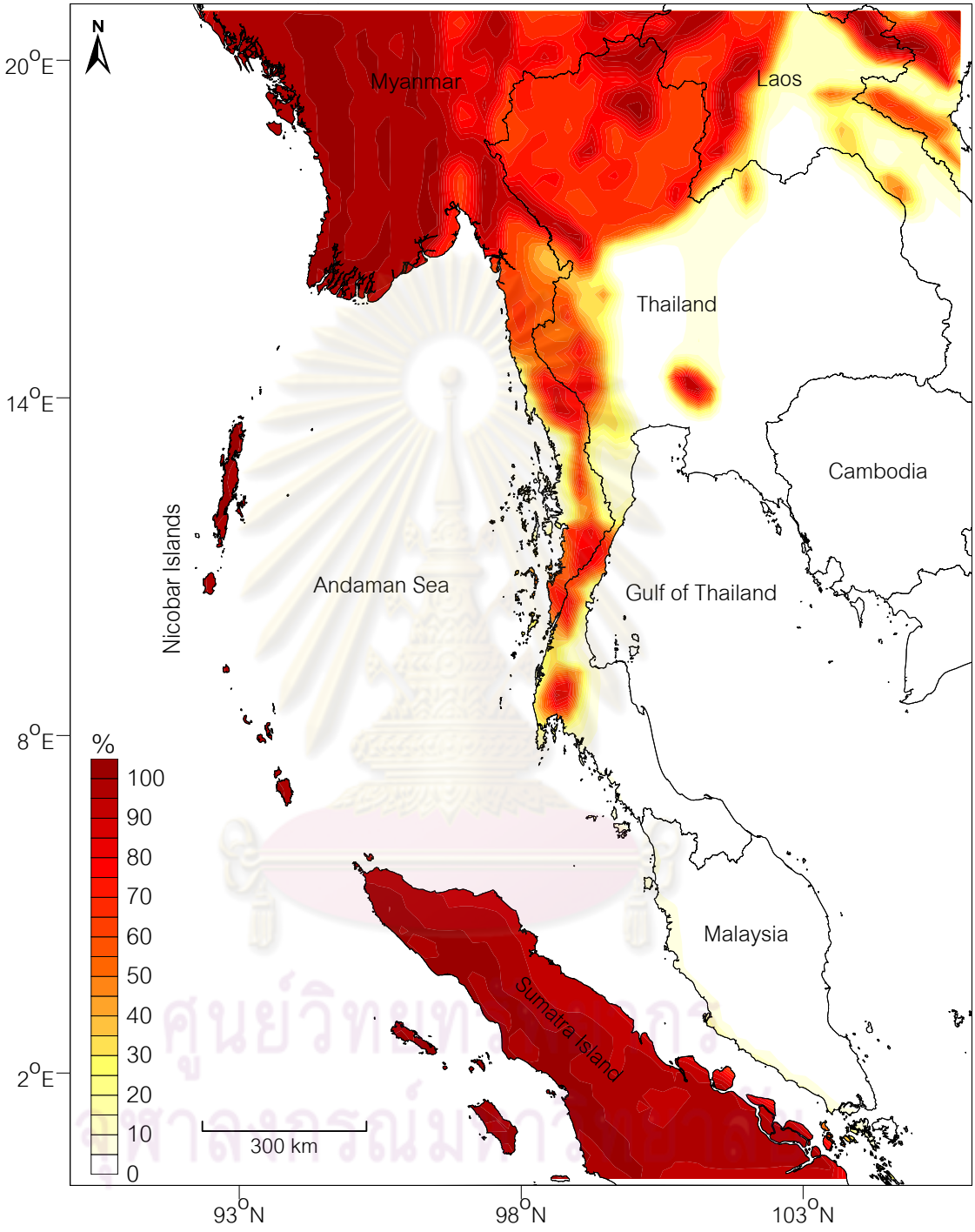

Figure 6.8. (cont.) Probabilistic seismic hazard maps of Thailand and adjacent areas showing the probabilities (%) that ground shaking will be equal to or greater than levels IV, V, VI, and VII (Modified Mercalli Intensity) for return periods of 50 and 100 years.

c) % of ground shaking equal or larger than level VI in 50 years

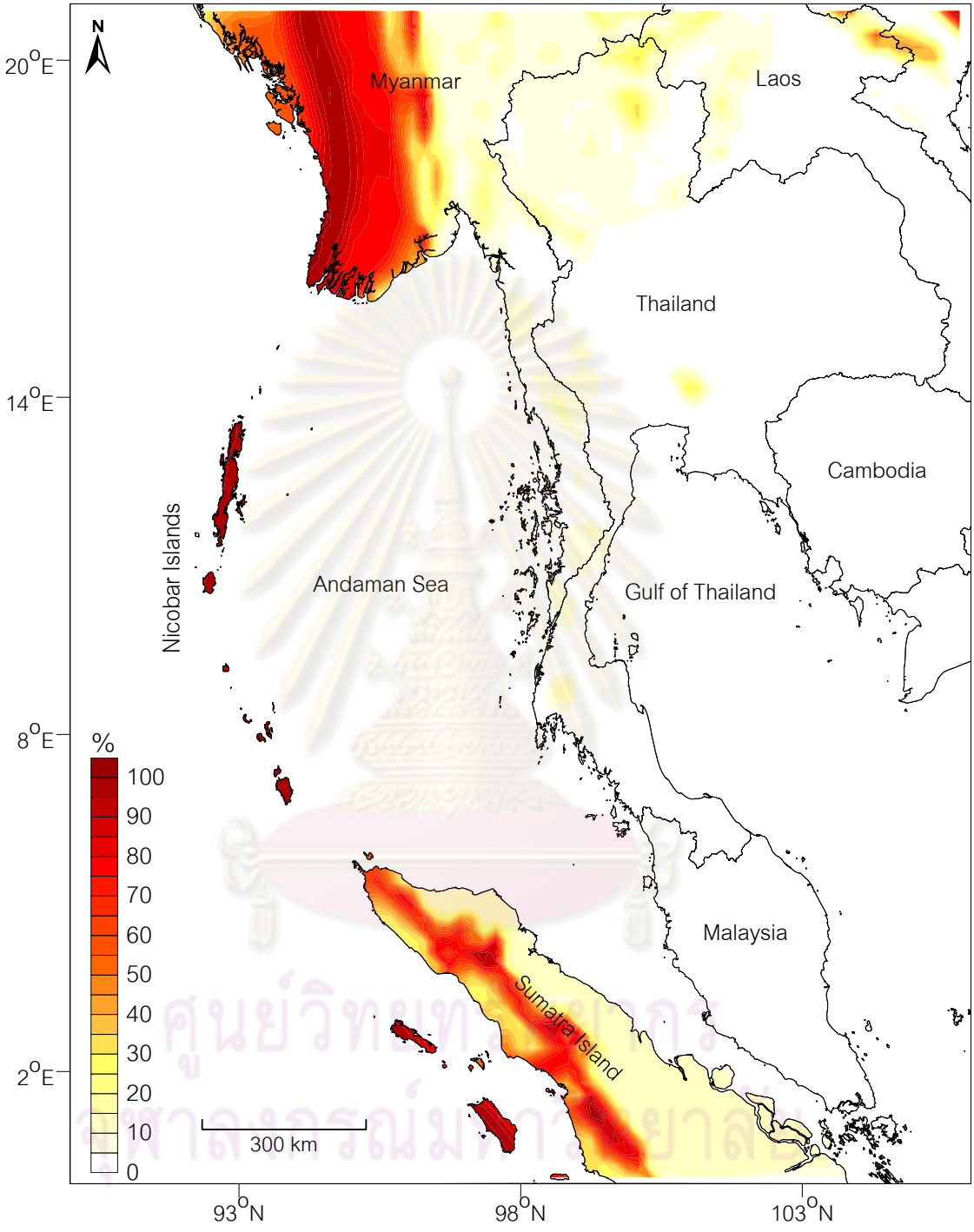

Figure 6.8. (cont.) Probabilistic seismic hazard maps of Thailand and adjacent areas showing the probabilities (%) that ground shaking will be equal to or greater than levels IV, V, VI, and VII (Modified Mercalli Intensity) for return periods of 50 and 100 years.

d) % of ground shaking equal or larger than level VII in 50 years

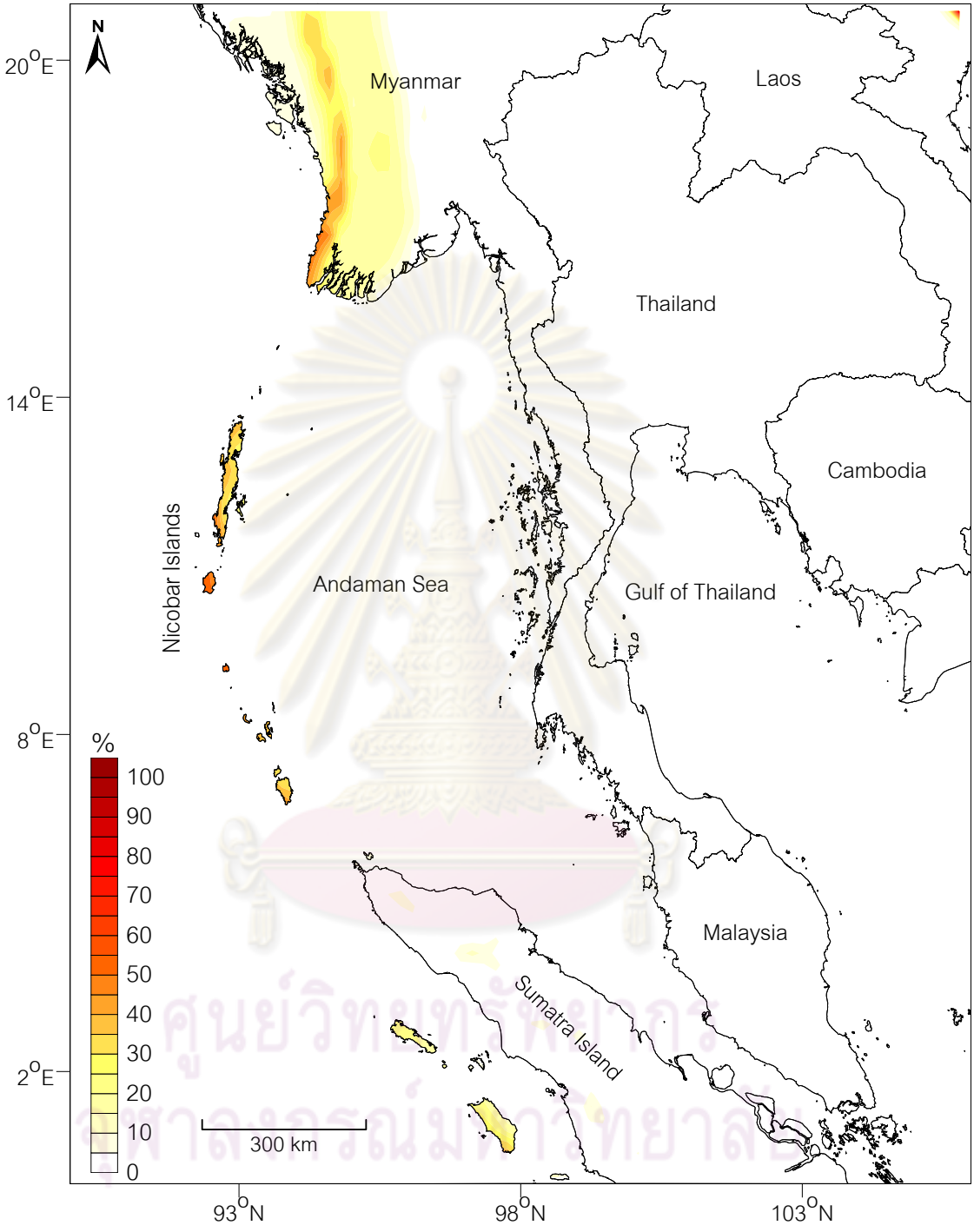

Figure 6.8. (cont.) Probabilistic seismic hazard maps of Thailand and adjacent areas showing the probabilities (%) that ground shaking will be equal to or greater than levels IV, V, VI, and VII (Modified Mercalli Intensity) for return periods of 50 and 100 years.

e) % of ground shaking equal or larger than level IV in 100 years

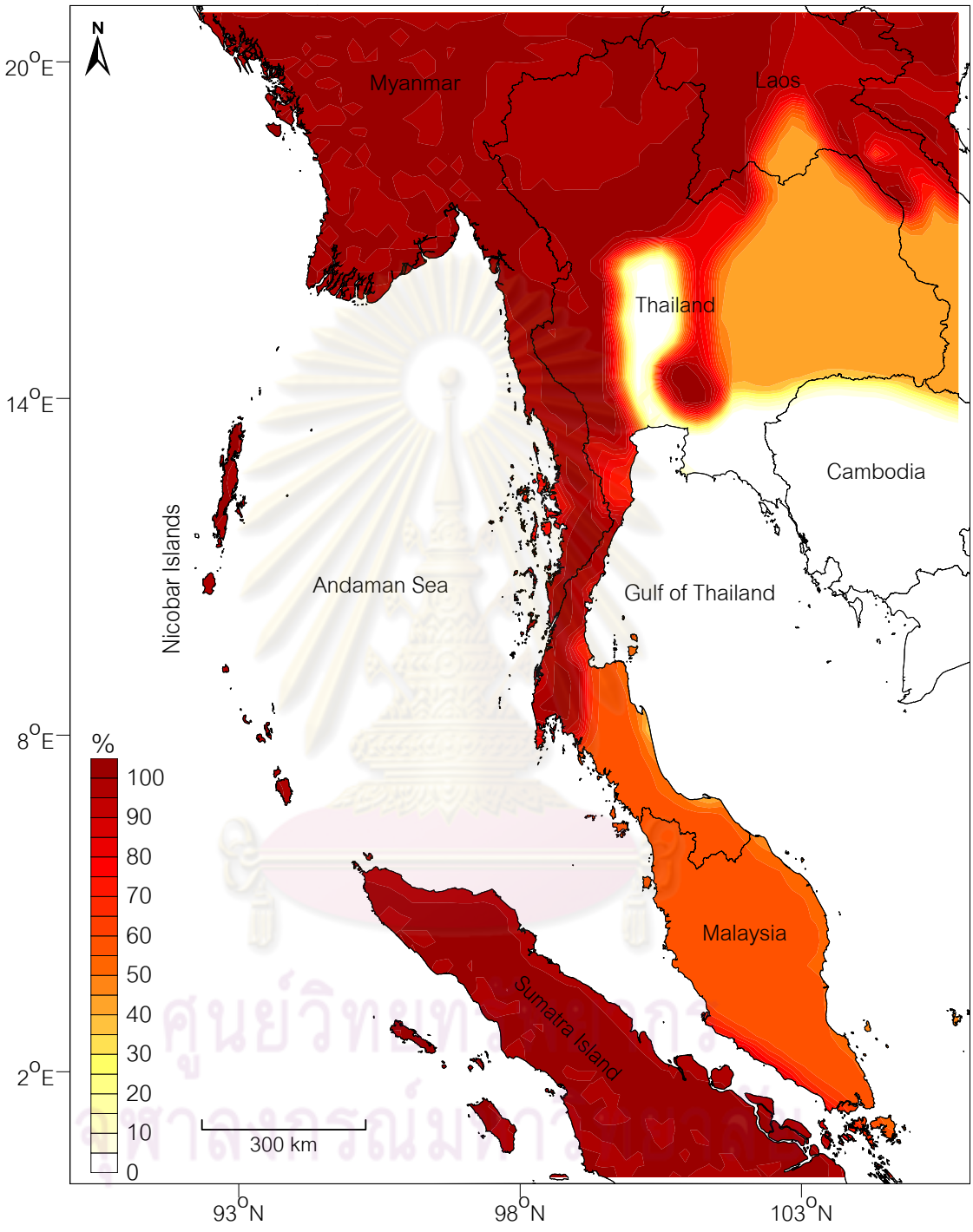

Figure 6.8. (cont.) Probabilistic seismic hazard maps of Thailand and adjacent areas showing the probabilities (%) that ground shaking will be equal to or greater than levels IV, V, VI, and VII (Modified Mercalli Intensity) for return periods of 50 and 100 years.

f) % of ground shaking equal or larger than level V in 100 years

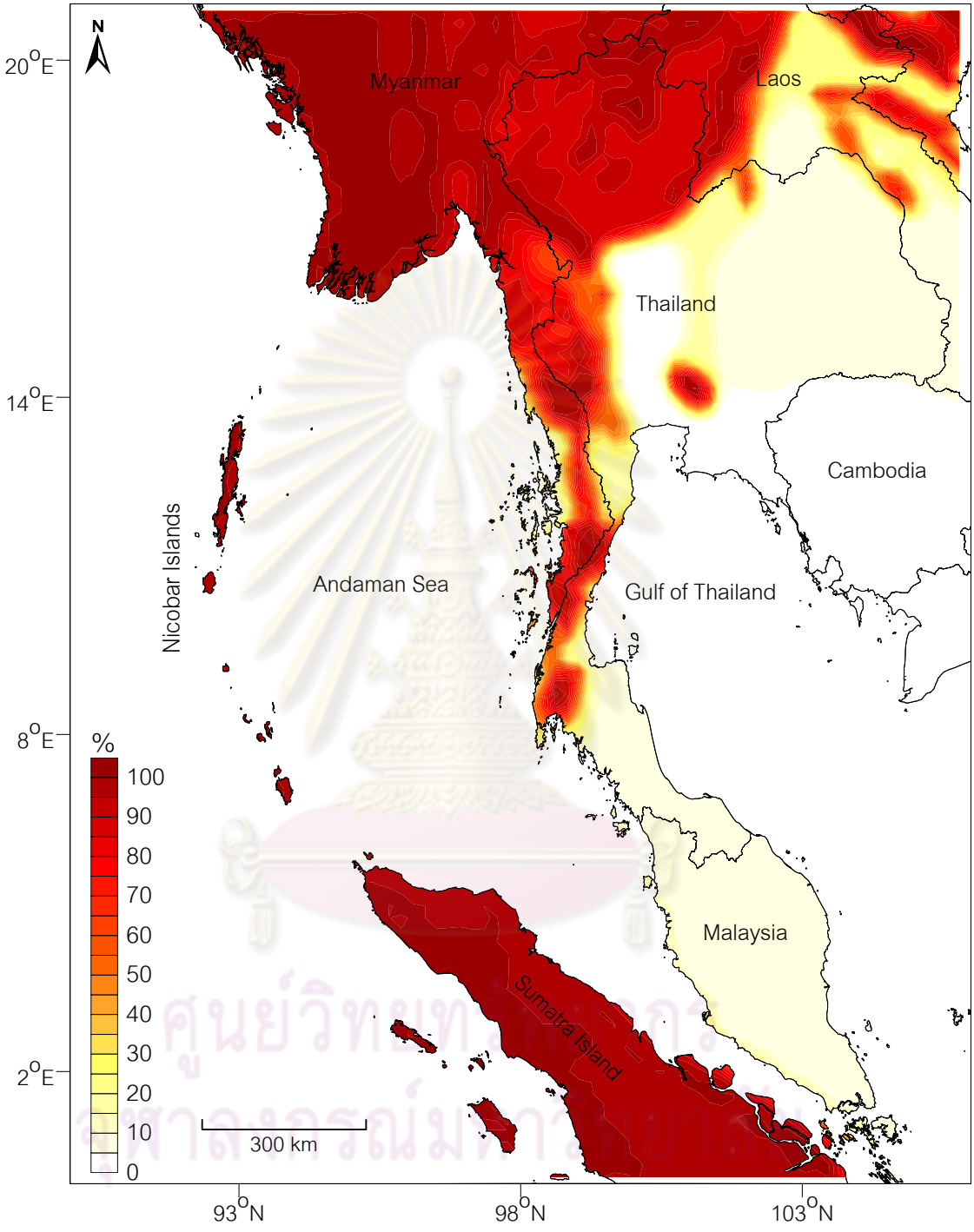

Figure 6.8. (cont.) Probabilistic seismic hazard maps of Thailand and adjacent areas showing the probabilities (%) that ground shaking will be equal to or greater than levels IV, V, VI, and VII (Modified Mercalli Intensity) for return periods of 50 and 100 years.

g) % of ground shaking equal or larger than level VI in 100 years

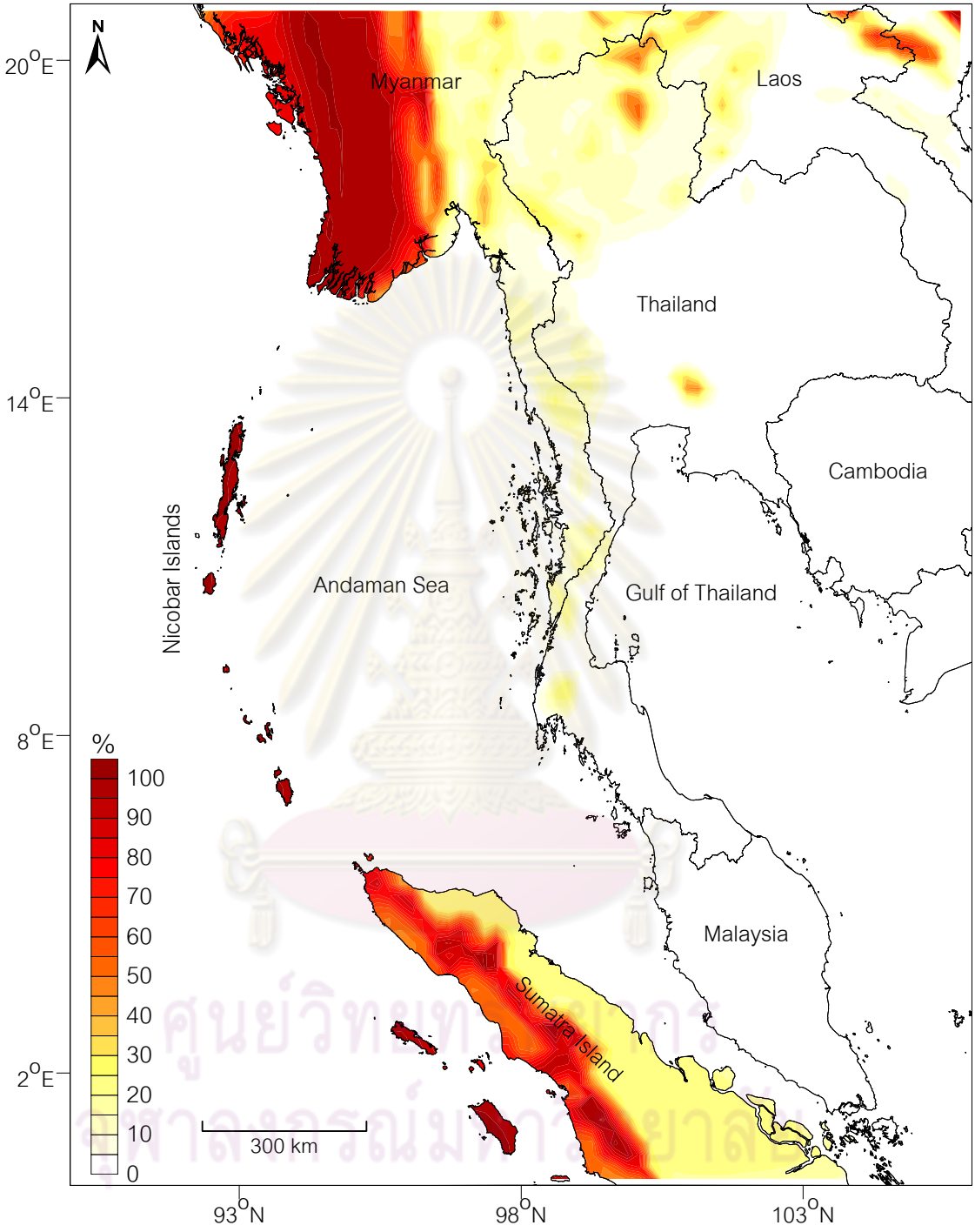

Figure 6.8. (cont.) Probabilistic seismic hazard maps of Thailand and adjacent areas showing the probabilities (%) that ground shaking will be equal to or greater than levels IV, V, VI, and VII (Modified Mercalli Intensity) for return periods of 50 and 100 years.

h) % of ground shaking equal or larger than level VII in 100 years

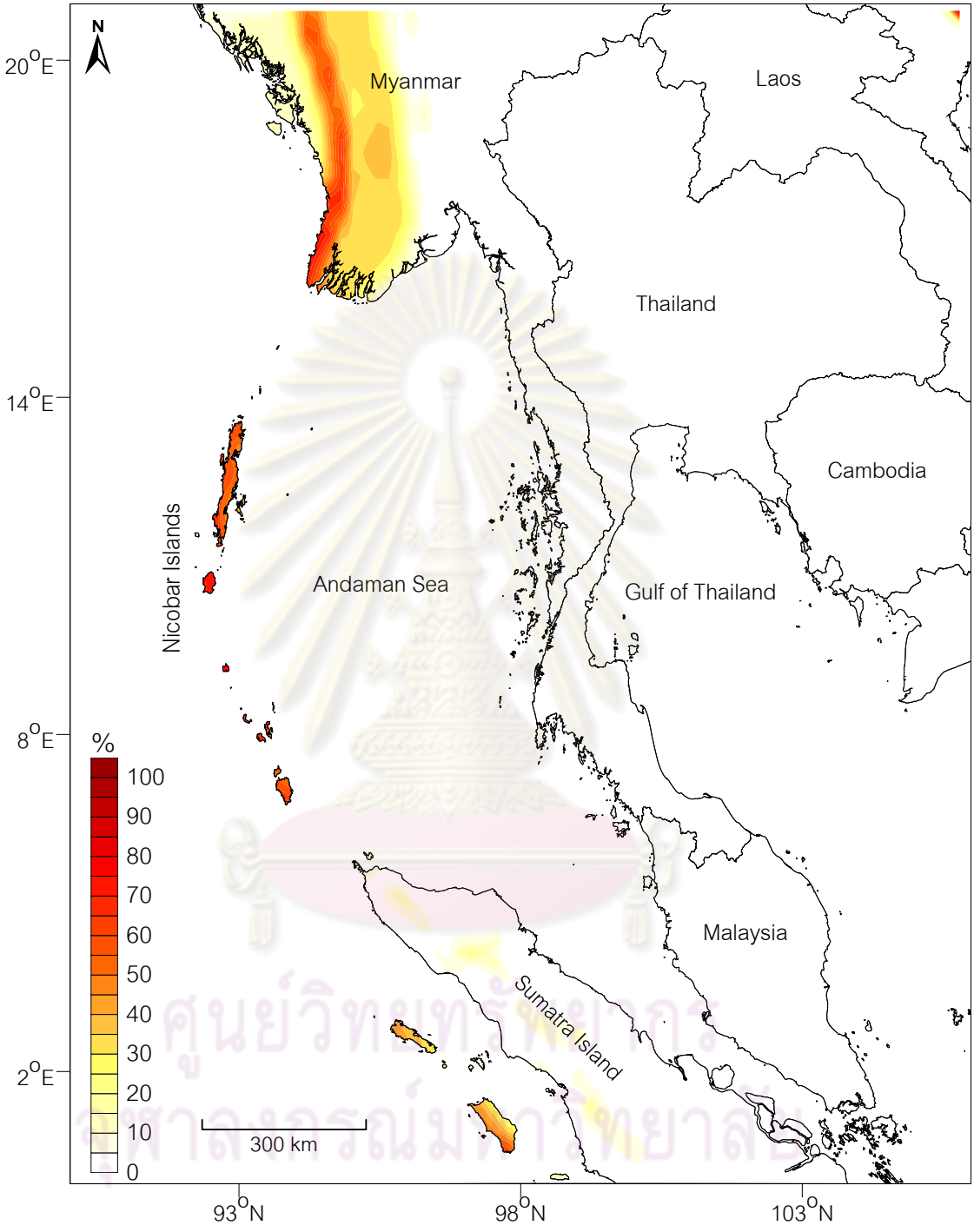

Figure 6.8. (cont.) Probabilistic seismic hazard maps of Thailand and adjacent areas showing the probabilities (%) that ground shaking will be equal to or greater than levels IV, V, VI, and VII (Modified Mercalli Intensity) for return periods of 50 and 100 years.

CHAPTER VII
DISCUSSION

In this study, both maps from DSHA and PSHA are developed for Thailand and adjacent areas using integration of the active faults and seismic source zones. The best-fit strong ground-motion attenuation models are applied to evaluate the SHA in more accurate. Due to the different assumptions and models are applied in this study comparing with the previous works. Beside the DSHA and PSHA results, the earthquake sources and strong ground-motion attenuation models are also discussed in order to clarify the origin of the obtained input parameters and assumptions analyzed with this SHA. It is also noted that some of these discussion topics can be found in Pailoplee et al. (2009a), (2009b), and (2010).

7.1 Earthquake Sources

7.1.1 Active fault

There are some active fault maps and fault zones which are necessary for SHA were proposed previously not only in Thailand but also in foreign countries. However, individual works usually focused in the local fault segments or in specific areas of interest. The overview of fault zones or fault systems in the regional scale is still lacked. As a result, the database of the faults is not complied systematically, yet. For instance, DMR (2006) proposed 15 active fault zones within Thailand territory whereas Nutalaya et al. (1985) interpreted the active faults by focusing mainly in the eastern Myanmar and including some faults in northern and western Thailand. Based on regional investigation of remote sensing in this study, it is clearly indicated that the Moei-Uthai Thani Fault Zone (Saithong et al., 2005) and the Moei Fault Zone (DMR, 2006) are the same fault system with the Tong Gyi Fault Zone of Nutalaya et al. (1985). Therefore, both of them are grouped to be Moei-Tong Gyi Fault Zone (Figure 7.1a) which is meaningful in term of tectonic and SHA interpretation. Moreover in this investigation, some fault zones are proposed newly in the area which is not recognized previously, such as Chiang Rai, Kawthuang, Mae Chaem, Moei-Tongyi, Shan, Wan Na-awn, and Wang Nua Fault Zones (Figure 7.1b-h). Although, these new fault zones have never generated the big

earthquakes in the instrumental records, there are some small to medium-magnitude earthquakes shown in these areas, suggesting that these faults are not dormant from the earthquake. Consequently, these fault zones are also recognized in this SHA results.

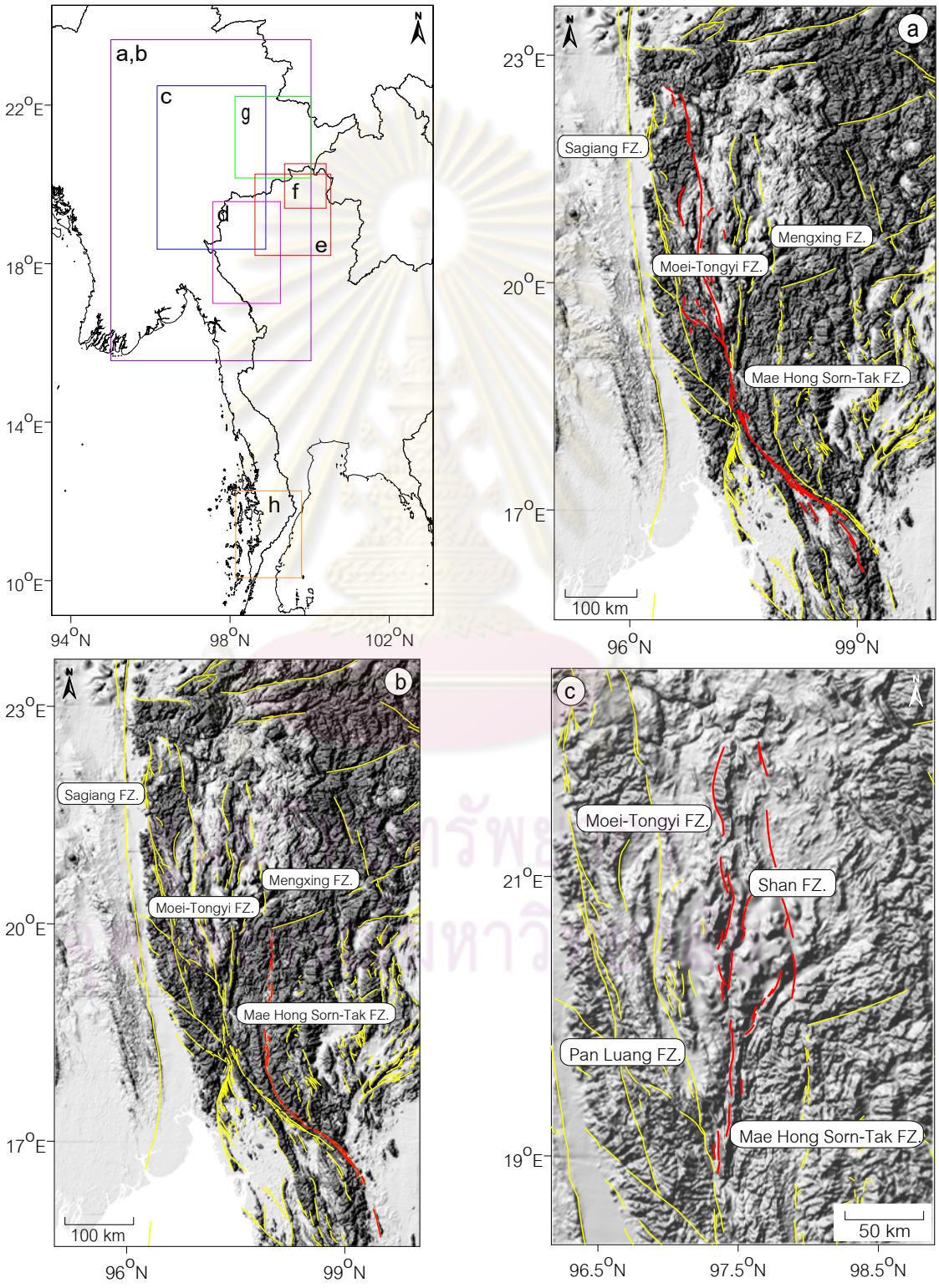

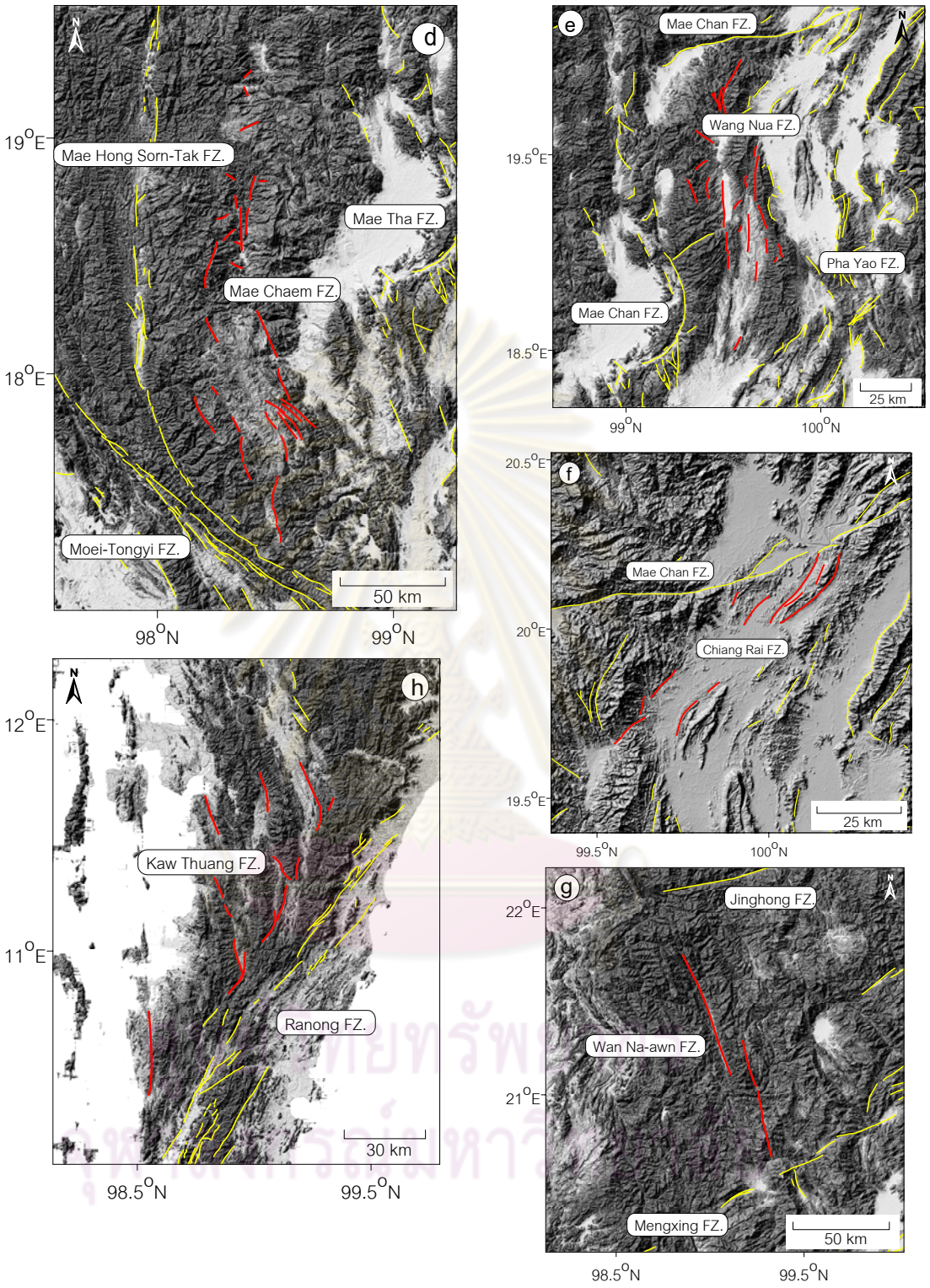

Figure 7.1. DEM maps showing active fault zones proposed in this study. Note that the concerned major fault zone is marked in red. a) Moei-Tongyi, b) Mae Hong Sorn- Tak, c) Shan, d) Mae Cham, e) Wang Nua, f) Chiang Rai, g) Wan Na-awn, and h) Kaw Thuang Fault Zones.

From the paleo-seismological point of view, the Hutgyi area is located in the northern branch of the Sri Sawat Fault Zone is selected (Figure 3.12). This selected site is important because the Sri Sawat Fault Zone interpreted from this study is the longest spray branch from the Sagiang Fault Zone and also its scarcity of earthquake activity within the past century along the northern branch, indicating that it may be a seismic gap capable of producing a large earthquake in the future. Based on trench log investigations and geochronological data, it is estimated that the maximum rate of fault sip is 3.7 mm/year which is higher than 0.67 mm/year of the southern Sri Sawat branch investigated by Songmuang et al. (2007) and Nuttee et al. (2005). This data imply that although the seismic-quiescence Hutgyi area didn't show any present-day seismic activities, the tectonic activities associated earthquake is going-on which should not be neglected in this SHA.

7.1.2 Seismicity

For the seismicity investigation, only one previous work by Palasri (2006) was reported thoroughly allowing the comparison with this seismicity investigation. The earthquake catalogues applied in this study are more update than that used in the previous works in term of recording time span. In addition, this study added 3 global earthquake catalogues integrated with the local TMD catalogue to make more reliable of the earthquake records. Since some catalogues didn't record continuously impractical, this technical problem may lead to the erroneous interpretation of seismicity. The seismicity parameters represented by the earthquake potentials in individual seismic source zones are shown in Figure 7.2. Comparing with Palasri (2006), the estimated maximum magnitudes are almost similar to this study except the seismic source zone G: Central Thailand, zone L: Eastern Thailand – Cambodia, zone Q: Gulf of Thailand, and zone R: Malaysia – Malacca (see also Figure 1.2a) which Palasri (2006) assumed to be the non-seismic prone area which never posed by earthquake (Figure 7.2a).

In the aspect of a values (Figure 7.2b), almost all of the a values obtained from this study is in vicinity of those proposed by Palasri (2006) implies the same entire seismicity rate in this region. However, although the seismic source zones G, L, and Q can evaluate the maximum earthquake magnitude, the seismicity data themselves

cannot analyze statistically the a and b values. This implies that these seismic source zones are the non-seismic prone area. For zone R: Malaysia – Malacca, Palasri (2006) ignored this zone in SHA. However, based on the seismicity investigation in this study, it clearly indicates that zone R has a possibility to generate earthquakes. As a result it is assumed in this SHA.

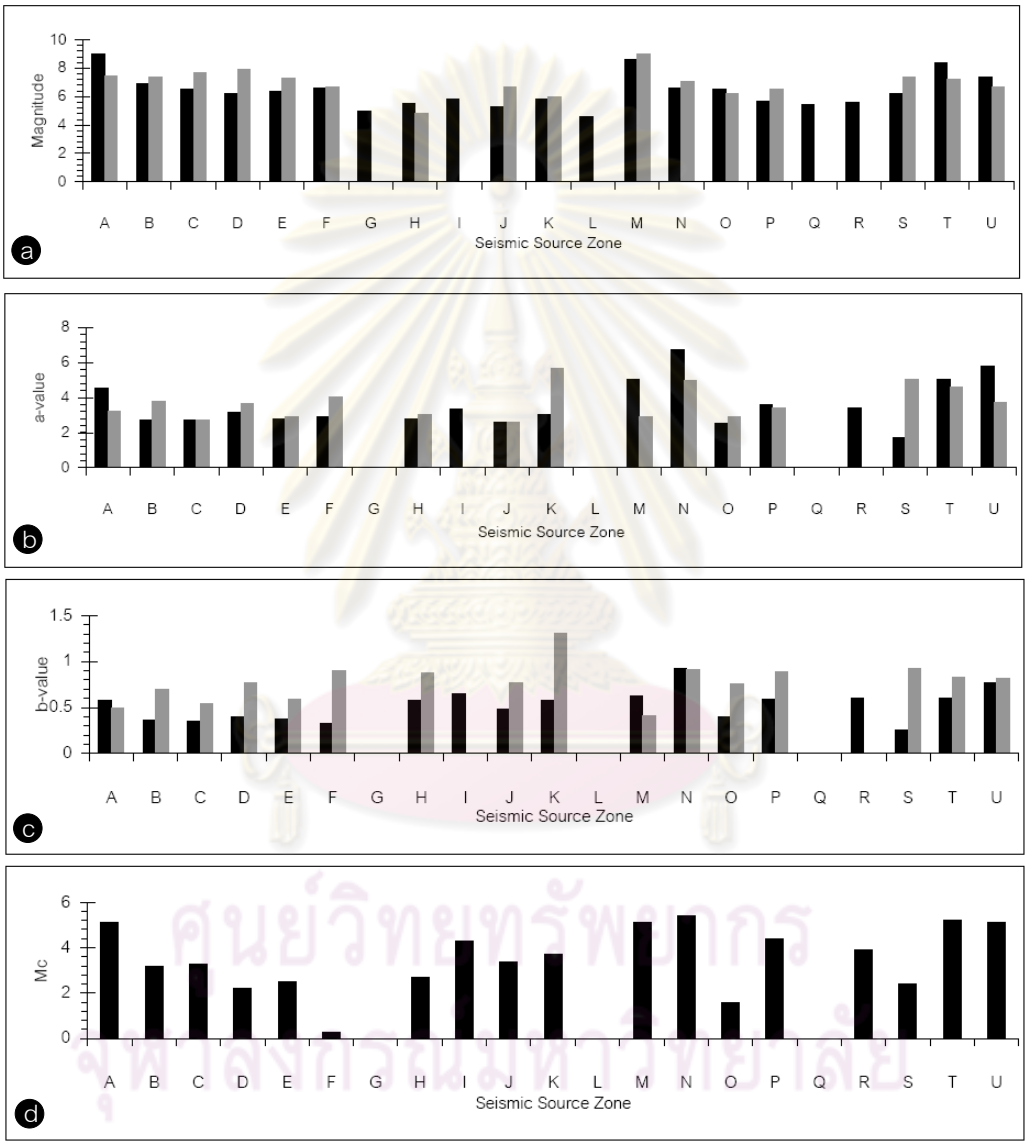

Figure 7.2. Statistical graphs showing a) Maximum earthquake magnitudes proposed in this study (black) and Palasri (2006) (grey); b), c), and d) are a values and, b values, and Magnitude of completeness (Mc), respectively, according to the frequency-magnitude relationship (Gutenberg and Richter, 1942).

Regarding b values (Figure 7.2c), most of b values obtained in this study are lower than those suggested by Palasri (2006). In seismicity investigation, there are some significant explanations for different b values. The decrease (increase) of b is interpreted in the form of stress increase (decrease) before an approaching seismic event (Scholz, 1968; Wyss, 1973). Therefore, based on b it is implied that Thailand region can have the more stress accumulation and become more hazardous earthquake than those proposed by Palasri (2006).

For the magnitude of completeness (M_c)(Figure 7.2d), Palasri (2009) didn't recognize this parameter in the SHA. Although M_c is not required for SHA, the M_c , as defined by the magnitude above which all earthquakes are considered to be fully reported, imply the capability of earthquake recording network (Woessner and Wiemer, 2005). As shown in Figure 7.2d, almost all seismic source zones reveal the M_c lower than magnitude 4.0 which is assumed to be the lower threshold magnitude (i.e. $m_{\min}$) in SHA (Kramer, 1996). Therefore, those seismic source zones can apply efficiently the seismicity parameter with SHA. However, some of them such as zone A, N, and T have the M_c higher than the magnitude 4.0. This implies that these source zones are far away from the seismic record networks and may lack of recording in some earthquake magnitude (in particular the lower magnitude). Therefore in this SHA, the a values are assumed by extrapolation from the larger magnitude associated with the obtained b values.

7.2 Strong Ground-Motion Attenuation

For the strong ground-motion attenuation models, several models were proposed previously for the shallow crustal earthquakes in Thailand and neighborhood countries, for instance, Wanitchai and Lisantono (1996) recommended Esteva and Villaverde (1973)'s model, Palasri (2006) proposed the model of Sadigh et al. (1997), including Kobayashi et al. (2000)'s model suggested by Pailoplee et al. (2009). However, these proposed models are based on the calibration between the some existing foreign models and 7 strong ground-motion records of Mw 5.1 earthquake which occurred on 13th December 2006 at Mae Rim district, Chiang Mai province, Thailand. Since a large number of strong ground-motion records were analyzed and

reported by TMD (2006), these obtained more up-to-dated data leading to more accurate of interpretation and selection of the suitable strong ground-motion attenuation models for this SHA. Figure 7.3 shows the different strong ground-motion attenuation models by Palasri (2006) including Idriss (1993) applied for this SHA. It is notable that if consider only 7 points of strong ground-motion data reported in the past, the most suitable model seem to be Kobayashi et al. (2000). However, if focusing in all existing data at present, the trend of attenuation characteristic is compatible with the Idriss et al. (1993) model as also proposed lately by Chintanapakdee et al. (2008). Therefore, based on the most up-to-date strong ground-motion data proposed recently by TMD (2006), the most reliable strong ground-motion attenuation relationship for Thailand and adjacent areas is the model of Idriss et al. (1993).

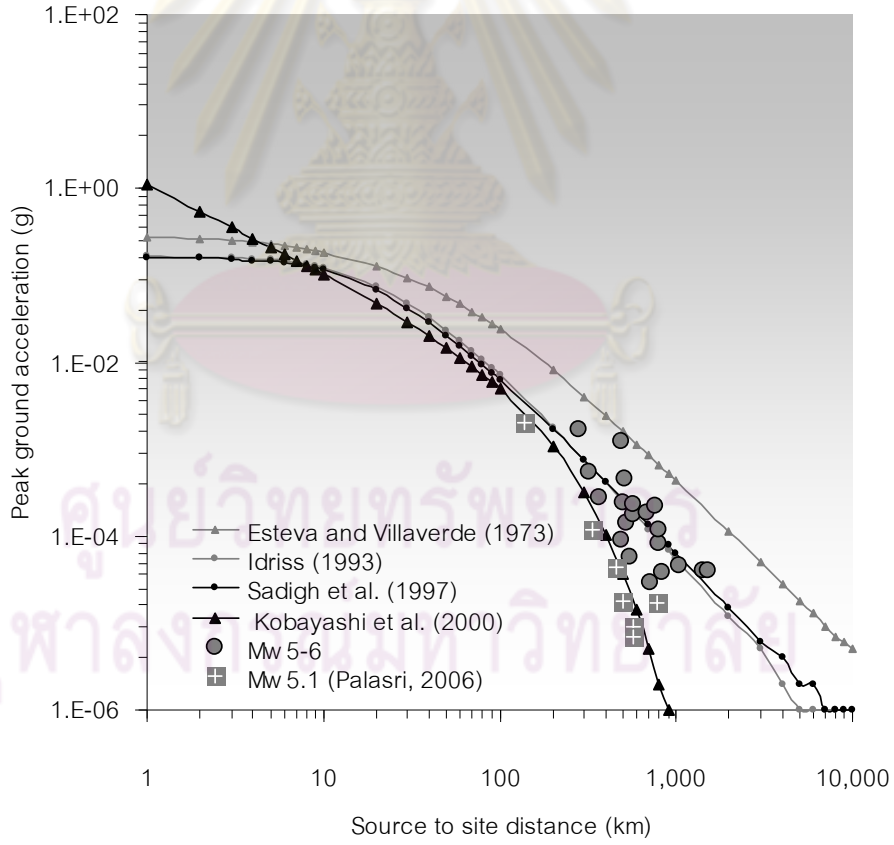

Figure 7.3. Comparison of strong ground-motion attenuation models with the TMD (2006)'s strong ground-motion data (grey circle) and the data of Palasri (2006) (blue squares).

7.3 Seismic Hazard Investigation

Based on maps of DSHA and PSHA shown in Chapter VI, it is notable that the spatial distributions of the seismic hazard levels are directly dependent on both the shape of individual active faults, seismic source zones and the seismic source potentials. The obtained ground motion levels vary between 0.01g-1g in Thailand and up to 3g can be estimated in the neighborhood countries (i.e. western Myanmar, Nicobar Islands, and Sumatra Island where nearby the Sumatra-Andaman Subduction Zone).

7.3.1 DSHA

For the DSHA, Pailoplee et al. (2009) proposed lately the map of DSHA for Thailand and adjacent area (Figure 7.4a). The map analyzed deterministically from the active fault data with the $MCEs$ estimation according to Wells and Coppersmith (1994)'s hypothesis. Strong ground-motion attenuation relationship of Petersen et al. (2004) and Kobayashi et al. (2000) are applied for the subduction zone earthquake and shallow crustal earthquake, respectively. The DSHA levels vary from 0g up to more than 3g. For this study the DSHA, all the earthquake sources are obtained from both the active faults and seismic source zones. Strong ground-motion attenuation relationship of Crouse (1991) and Idriss (1993) are applied for the subduction zone earthquake and shallow crustal earthquake. Comparing with the previous work, the earthquake hazard levels along the Sumatra-Andaman Subduction Zone are almost the same with Pailoplee et al. (2009). This consistency due to the models of Crouse (1991) and Petersen et al. (2004) are similar in the attenuation characteristic as mentioned in section 5.2 (see also Figure 5.3). Regarding the inland earthquake hazard, the results of this study are lower than that proposed by Pailoplee et al. (2009). This difference occurs for individual applied strong ground-motion attenuation models. Although the attenuation characteristic is similarity between Idriss (1993) and Kobayashi et al. (2000) along 10-100 km of the source-to-site distance (Figure 7.3), the ground shaking levels estimated from Kobayashi et al. (2000) are quite higher than that estimated by Idriss (1993) in the distance less than 10 km. As a result, there are the most effect on DSHA. However, comparing with the maximum PGA values recorded in individual TMD seismic record

stations, the possible maximum acceleration map obtained in this study is effective and enough for the earthquake-resistant strategy scenario.

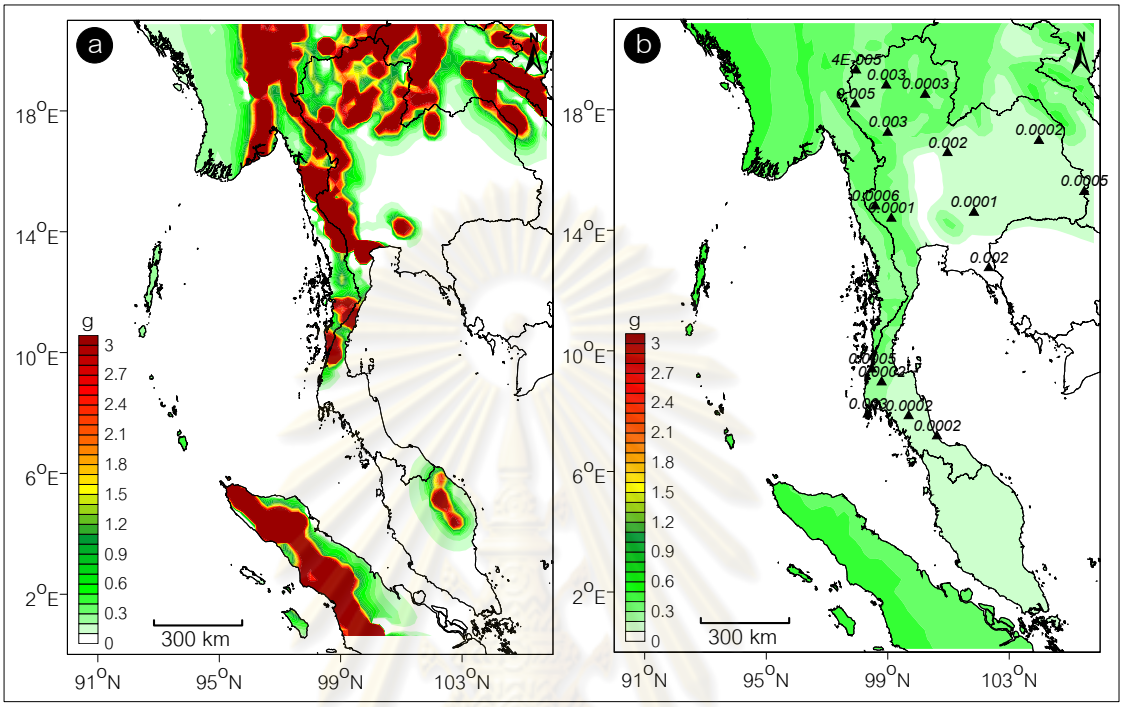

Figure 7.4. Maps showing a) DSHA of Pailoplee et al. (2009) and b) DSHA analyzed in this study. The black triangular are the maximum values of PGA (g unit) in individual seismic record stations recorded by the TMD.

7.3.2 PSHA

Comparing this work with PSHA maps proposed previously, the seismic hazard levels evaluated from this study are higher than their results at site by site. For Myanmar, Giardini et al. (1999) reported the seismic hazard levels with a 10% probability of exceedance in 50 years of Myanmar is around 4 m/sec^2 (0.4g) at western and central Myanmar along the Sagiang Fault Zone and around 1.6 m/sec^2 (0.16g) for the eastern part. Petersen et al. (2007) constrain the PSHA result of 10% probability of exceedance in 50 years proposed by Giardini et al. (1999). They reported that eastern Myanmar is around 0.15g meanwhile 0.7g is posed along the Sagiang Fault Zone. However, it is different when compared with this study. For 10% probability of exceedance in 50 years the hazard levels reveal the 0.3g in the eastern and central Myanmar regions whereas in

western part associated with the Sumatra-Andaman Subduction Zone is up to 1.8g of ground shaking.

Regarding the past big earthquakes, Figure 7.5a shows the location of earthquake (red star) with mb 7.3 occurred at Pyu, central Myanmar on 3 December 1930 and Figure 7.5b for the earthquake of Mw 7.3 at Rangoon, central Myanmar on 4 December 1930. After that, Brown and Leicester (1933) analyzed macro-seismic and reported the iso-seismal map depicted the distribution of the ground shaking intensities (in MMI scale) according to this earthquake. Based on the iso-seismal map, the maximum intensity is about VIII spread decreasingly around its source.

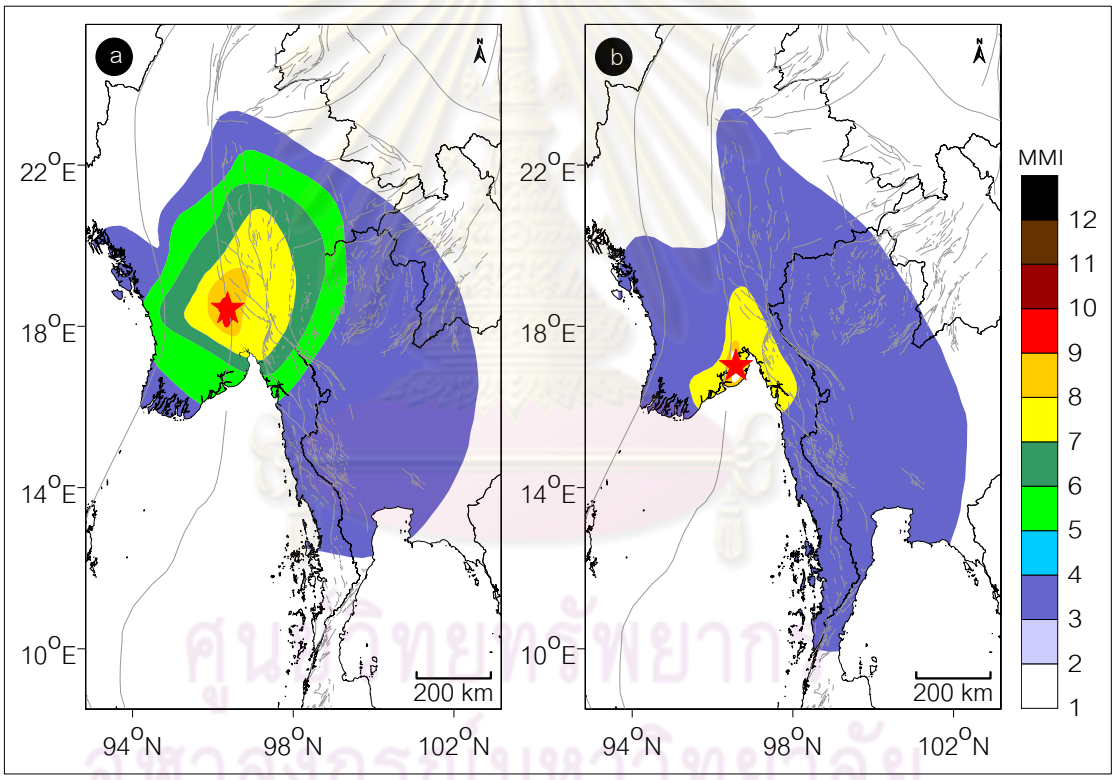

Figure 7.5. Iso-seismal maps showing a) the distribution of ground shaking intensities in MMI scale according to the 7.3-mb earthquake generated at Pyu, central Myanmar on 3 December 1930, and b) for the earthquake of Mw 7.3 at Rangoon, central Myanmar on 4 December 1930 (Brown and Leicester, 1933).

When compared with the probability map which shows the probability of occurrence of intensity levels VI-VII in 50-100 years (see Figure 7.6), it is notable that the PSHA of this study does not show the probability of occurrence in even the ground shaking level VII in 50 and 100 year prediction (Figures 7.6a and b). At the earthquake locations, there is only level VI of this PSHA that is the probability of occurrence around 20% or more.

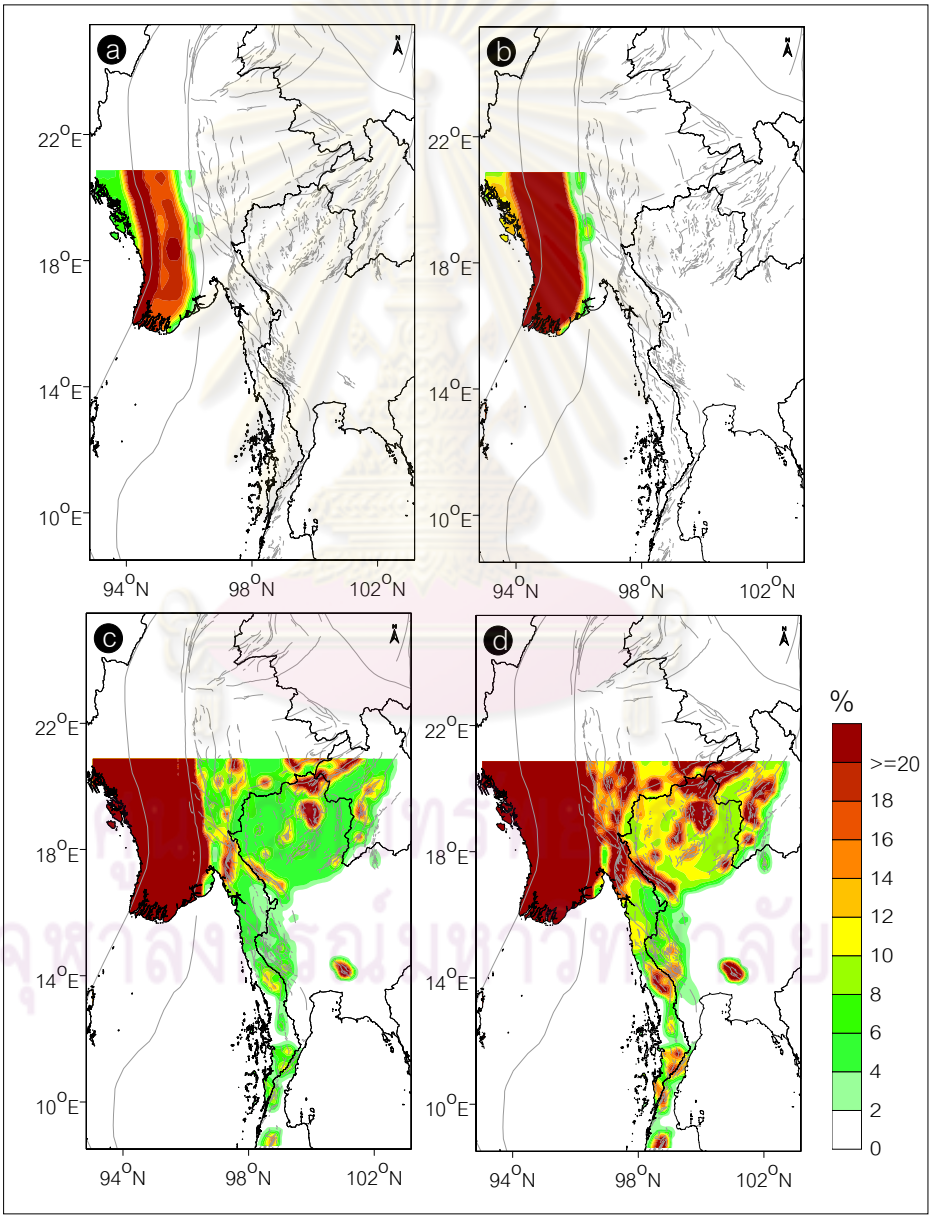

Figure 7.6. a) PSHA map of % of ground shaking ≥ VII in 50 years and b) 100 years.
c) PSHA map of % of ground shaking ≥ VI in 50 years and d) 100 years.

For northern Thailand, the ground shaking levels obtained from this study are between 0.9g-0.5g whereas 0.3g-0.15g and 0.1g-0.05g and are proposed differently by Wanitchai and Lisantono (1996) (Figure 1.7) and Petersen et al. (2007) (Figure 1.12), respectively. However, PSHA in this study seem to be similar to Palasri (2006) who indicated that northern Thailand have 2% probability of exceedance the ground shaking around 0.9g-0.2g in 50 years. Based on the PGA recorded by the TMD during 2003 to 2007 as shown in Tables 5.2 and 5.3, the maximum PGA in individual seismic record station in Thailand regions are shown in Figure 7.7. The figure 7.7 reveals that the maximum PGA which posed to Thailand in the past is between 0.00004g-0.005g which can apply safely the PSHA maps proposed by Wanitchai and Lisantono (1996) and Petersen et al. (2007). However based on the Iso-seismal map of the 4.6-mb earthquake generated at Chiang Mai province on 12 December 2006 reported by the DMR (2006) (Figure 7.8a), the map shows the distribution of ground shaking intensities between II-VI in MMI scale or 0.31g-0.65g when convert from MMI to PGA according to the Cancani (1904)'s model as described in section 5.4. It is implied that the maps of Wanitchai and Lisantono (1996) and Petersen et al. (2007) are under-estimated in this iso-seismal case study and the maps proposed in this study (Figures 7.8b and c) are reported more safe than both of them. If focus in the seismic hazard map proposed by DMR (2005) (Figure 1.8), the ground shaking for northern and western Thailand are proposed between level V-VII (zone 2A) and VII-VIII (zone 2B). The DMR (2005)'s map is also covered the ground shaking reported in this case but seem to be slightly more than.

For Western and Central Thailand, two past earthquake events in Thailand are reported in term of macro-seismological study (i.e. Iso-seismal map) allowing validation the suitability of SHA map in this study. The first event is the earthquake generated at Tak province northern Thailand on 17 February 1975 (Prachaub, 1990) which showing the distribution of the ground shaking between intensities V-VI (Figure 7.9a) and the latter is earthquake event of the Srinakarin Dam, western Thailand on 22 April 1983 (Prachaub, 1990) with IV-VI (Figure 7.9b). Both earthquakes indicate that although the earthquakes are generated from western Thailand, the earthquakes themselves affected not only northern or western Thailand but also in the central part. The PSHA maps

proposed in this study don't report the ground shaking effect in the central Thailand (see Figures 7.9c and d). This may be due to soft soil amplification which is excluded in this study. Therefore, the characteristic of soft soil sediment associated with the ground shaking amplification should be taken into consideration in the further study particularly in the central pain of Thailand.

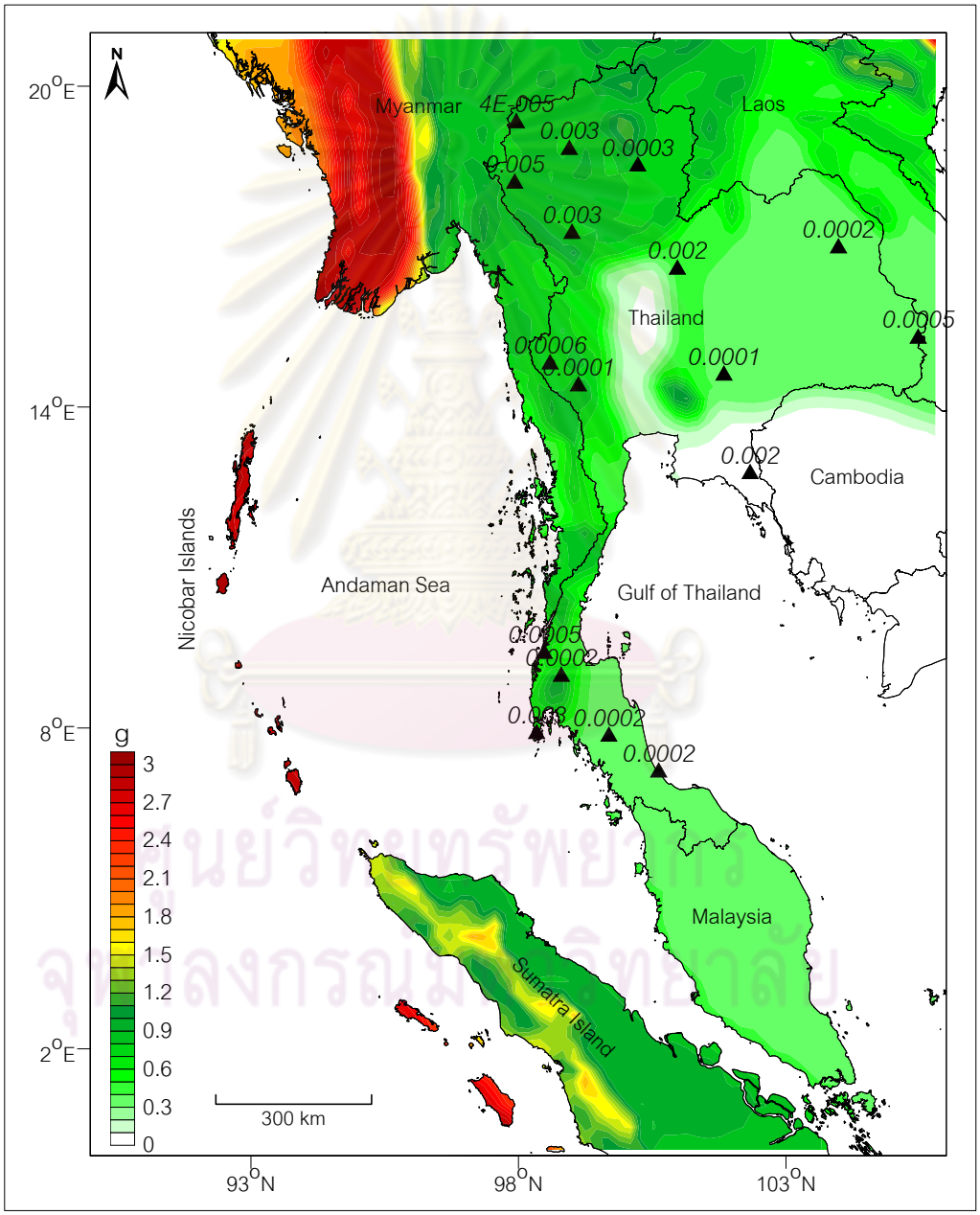

Figure 7.7. PSHA map showing 2% probability of exceedance in 50-year return period and the maximum values of PGA (g unit) in individual seismic record stations occupied by the TMD.

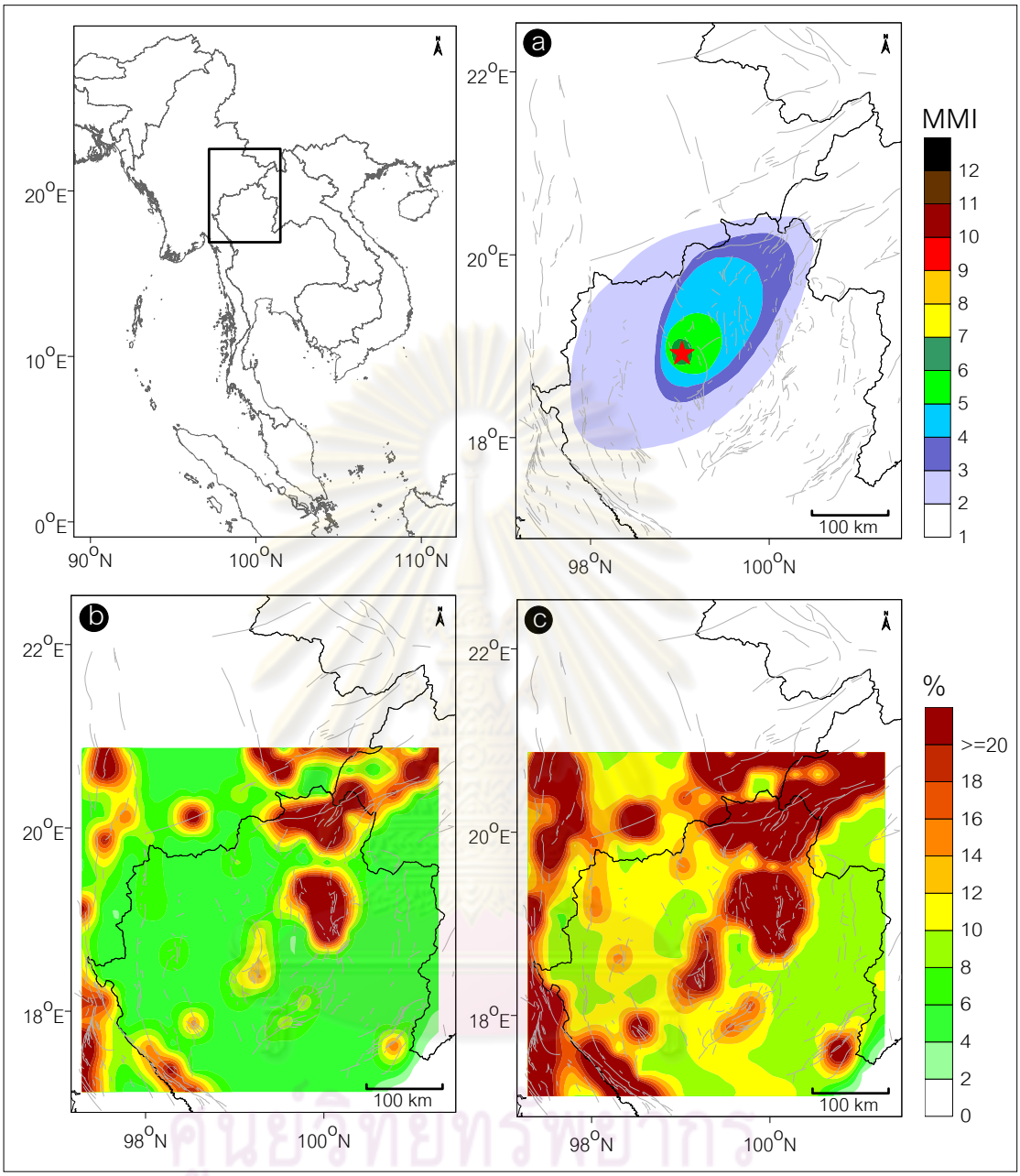

Figure 7.8. Map of northern Thailand and eastern Myanmar a) Iso-seismal map showing the distribution of ground shaking intensities in MMI scale according to the 4.6-*mb* earthquake generated at Chiang Mai province, Thailand on 12 December 2006 (DMR, 2006). b) PSHA map of % of ground shaking ≥ VI in 50 years and c) 100 years, respectively.

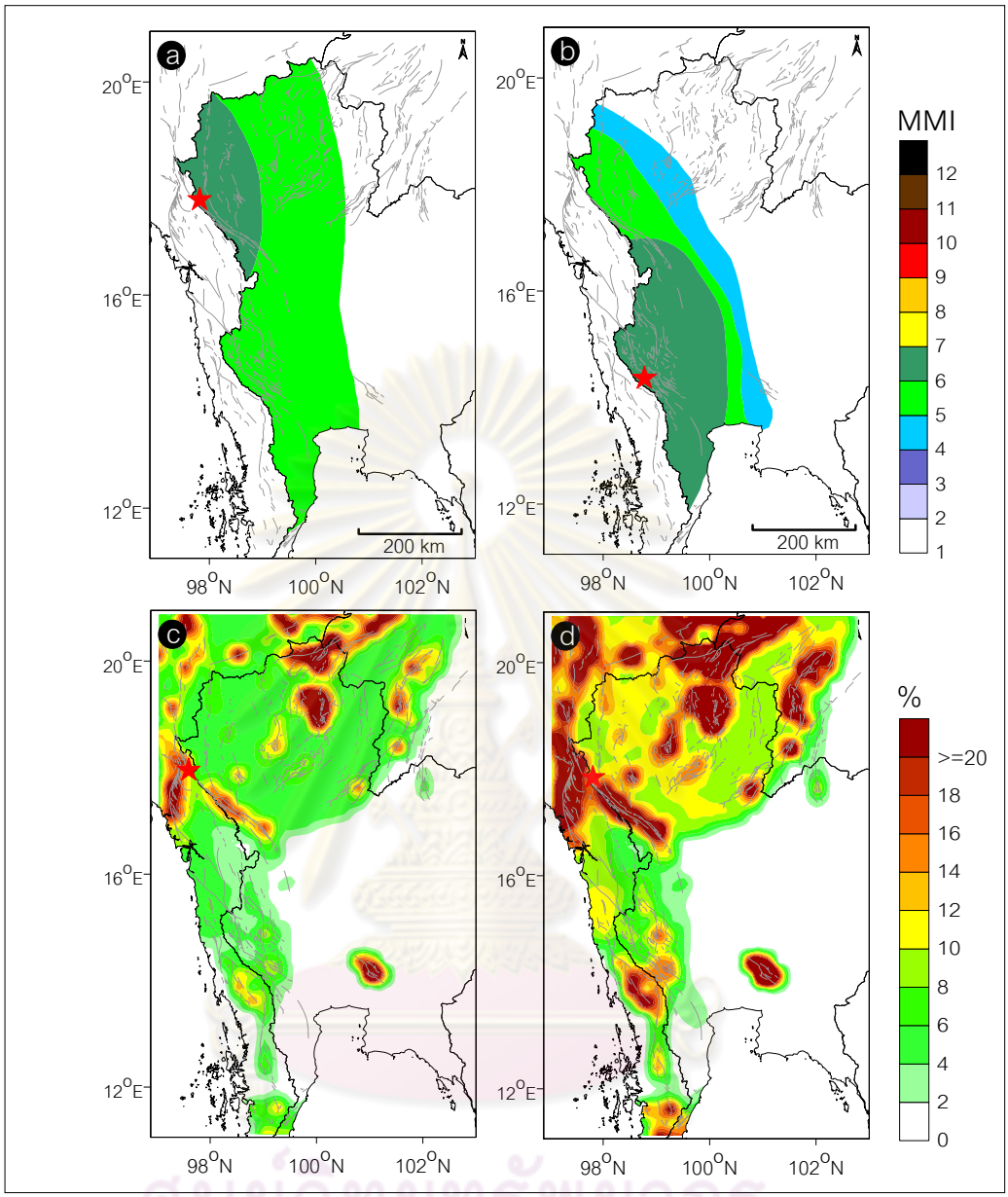

Figure 7.9. Map of northern and western Thailand a) Iso-seismal map showing the distribution of ground shaking intensities in MMI scale according to the 5.6-*mb* earthquake generated at Tak province, northern Thailand on 17 February 1975 (TMD, 1976). b) the distribution of ground shaking intensities according to the 5.9-*mb* earthquake generated at Srinakarin Dam, western Thailand on 22 April 1983 (TMD, 1984). C) PSHA map of % of ground shaking ≥ VI in 50 years and d) 100 years, respectively.

Regarding to southern part, the previous works mentioned that the southern Thailand are low level earthquake-prone area. Petersen et al. (2007) reported the possible PGA around 0.05g-0.1g and DMR (2006) suggested the intensities between V-VII. There is no suggestion about the seismic hazard in southern part reported by Wanitchai and Lisantono (1996), Palasri (2006). For this SHA study, the Ranong and Klong Marui Fault Zone including some seismic-quiescence fault zones in southern Myanmar (e.g. Kungyaungale, Tavoy, and Tenasserim Fault Zone) are recognized. Both DSHA and PSHA reveal that the southern Thailand have a possibility to act by the earthquake causing ground shaking around 0.3g-0.8g particularly along the Ranong and Klong Marui Fault Zones. Since the earthquake at the Gulf of Thailand on 8 October 2006 with the Mw 5.0, RID (2006) investigated and proposed the iso-seismal map as shown in Figure 7.10a. The map showing the ground shaking posed along the southern peninsular of Thailand between II-V levels. This earthquake implies that southern part of Thailand is not entirely safe from the earthquake hazard as Wanitchai and Lisantono (1996) and Palasri (2006) suggestions. However, for this SHA study, it indicates that the southern Thailand has a possibility for the ground shaking level V more than 20% (Figures 7.10b and c) with in the vicinity of the iso-seismal map reported by RID (2006).

According to SHA comparison as discussed above, it reveals that the SHA analyzed in this study usually indicate higher hazard than that proposed previously at site by site. Empirically, these obtained SHA is available for the ground shaking-resistance scenario when compared with the past earthquake. The PGA data recorded by TMD constrain that almost of previous SHA including this SHA study are available. However, based on the iso-seismal maps, the reported ground shaking are usually in vicinity of that proposed by this SHA except some of the large earthquakes in Myanmar and the central plain of Thailand which the soft soil amplification are questionable.

In contrast with central Thailand, this SHA study reveals that northeastern Thailand have a possibility to be posed by the ground shaking higher than the central part. Empirically, northeastern part of Thailand should be peaceful from the earthquake due to there is no clear evidence of earthquake sources or earthquake events are illustrated in this area. However from Table 4.1, seismic source zone I (Khorat Plateau)

reveals totally 16 earthquake events in this zone. This due to the boundary of this source zone extends to the northern part of Vietnam which covering both Song Da and Song Ma active fault zone in Vietnam. As a result, this interpretation of this earthquake source may have some erroneous and need to be redefined in further study.

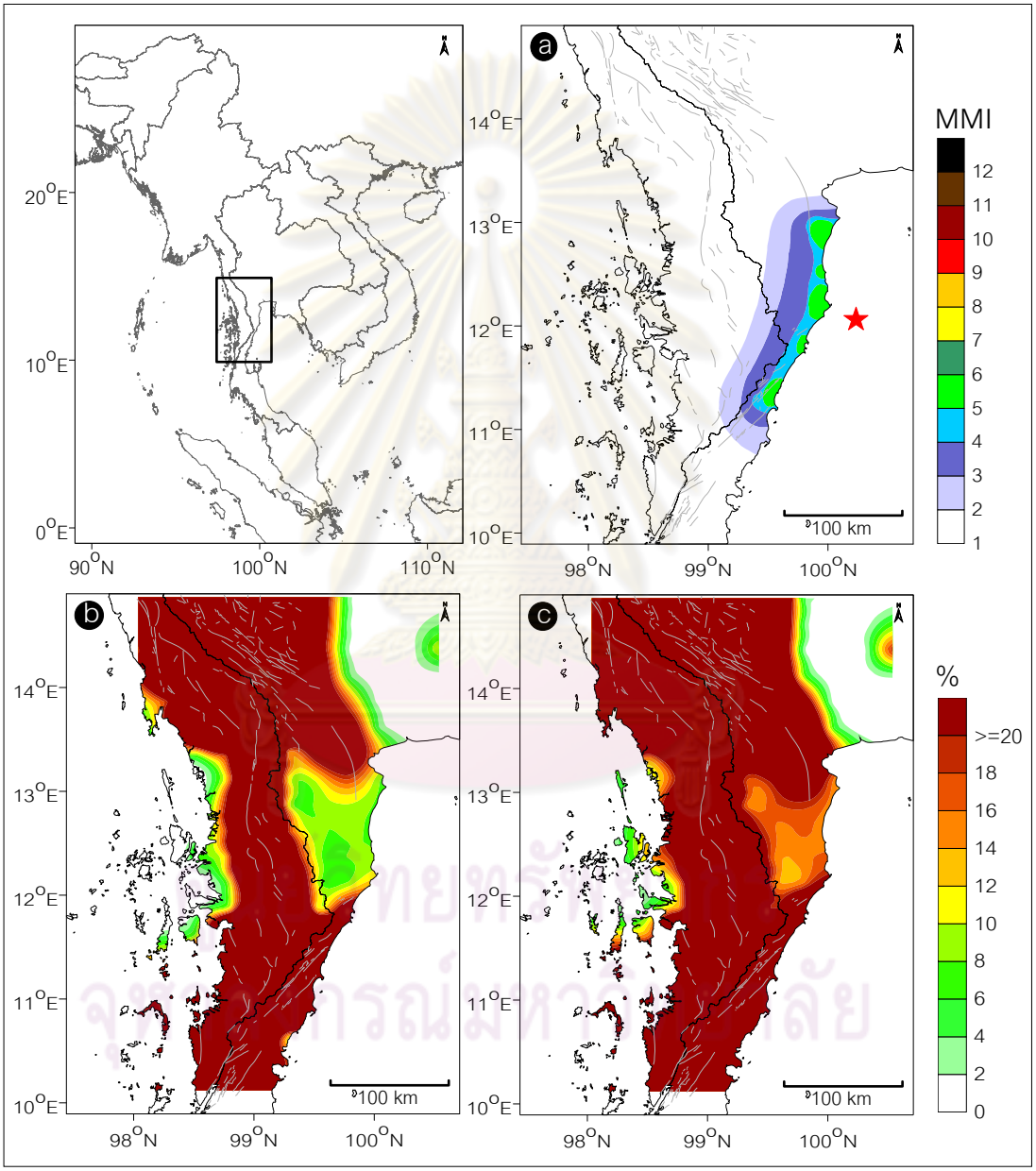

Figure 7.10. Map of western Thailand a) Iso-seismal map showing the distribution of ground shaking intensities in MMI scale according to the 5-Mw earthquake generated at the Gulf of Thailand on 8 October 2006. b) PSHA map of % of ground shaking $\geq$ V in 50 years and c) 100 years, respectively.

CHAPTER VIII
CONCLUSION AND RECOMMENDATION

Seismic Hazard Analysis (SHA) is the research area in seismology which has the strongest impact on society (Orozova and Suhadolc, 1999). The methods of SHA used widely nowadays can be divided into two main scenarios: Deterministic seismic hazard analysis (DSHA) and probabilistic seismic hazard analysis (PSHA). DSHA is based on geology and is attuned to physical reality in nature; PSHA is based on earthquake statistics and theory guided numerical calculations.

Empirically, both approaches have differences, advantages, and disadvantages that often make the use of one advantageous over the other. According to the Krinitzsky (2003)'s suggestion, DSHA is useful for designing critical structures. However, PSHA can be applied for preliminary evaluations or for risk analysis when these are unrelated to design decisions on a critical construction. In this research study both DSHA and PSHA are clarified in order to use the advantages of both approaches. In this chapter, works that have done in the previous chapters are concluded and recommended as following;

8.1 Conclusions

Based on the whole results of this study including literature research, they can conclude that:

1. There are at least 55 earthquake fault zones that have a chance to generate the earthquake which effect to study area (i.e. Thailand and adjacent area).
2. Moei-Uthai Thani Fault Zone (Saithong et al., 2005) and Tong Gyi Fault Zone of Nutalaya et al. (1985) are the identical fault zone.
3. Six fault zones are proposed newly in this study consisting of Chiang Rai, Kawthuang, Mae Chaem, Shan, Wan Na-awn, and Wang Nua Fault Zones.
4. Paleo-seismological investigation of the northern-branch Sri Sawat Fault Zone (Hutgyi area) reveal the slip rate 3.7 mm/year which faster than 0.67 mm/year of the southern branch investigated by Songmuang et al. (2007) and Nuttee et al. (2005). This implies that the tectonic activities associated with earthquake are

different along the fault zone. The more far away from the major strike-slip Sagiang Fault Zone, the more decrease of seismotectonics.

5. For seismicity investigation, the seismic source zones G: Central Thailand, zone L: Eastern Thailand – Cambodia, and zone Q: Gulf of Thailand are defined to be the non-seismic prone area.
6. Almost of b values obtained in this study are lower than those proposed previously, this imply that Thailand region accumulated more stress and more hazardous earthquakes than those previous work suggestion.
7. The high value of magnitude of completeness (M_c) in the seismic source zone implied that zone A: Andaman subduction, zone N: Andaman Basin, and zone T: Tenasserim are the underdeveloped area of the seismic detection network. This problem may effect to the potential of seismicity investigation in accurate.
8. For subduction zone earthquakes the strong ground-motion attenuation model of Crouse (1991) is more compatible with the Sumatra-Andaman Subduction Zone than the Petersen et al. (2004)'s model.
9. For shallow crustal earthquakes the strong ground-motion attenuation model of Idriss (1993) is the best fit when compare with the existing strong ground-motion data recorded in Thailand territory.
10. For SHA, the spatial distributions of the seismic hazard levels are directly dependent on both the shape and potential of individual earthquake source zones.
11. The hazard levels proposed in this study are higher than that proposed previously at site by site.
12. The highest hazard act along the Sumatra-Andaman Subduction Zone with more than 1g.
13. The seismic hazard levels in Thailand are lower than the neighborhood countries such as Myanmar, Sumatra Island, and Sumatra Island of Indonesia.
14. For Thailand, northern, western, and southern Thailand are the earthquake prone area which may be posed by the ground shaking up to 0.8g.

15. The northeastern Thailand releases the seismic hazard at medium level or around 0.4g whereas central and eastern parts are quiescence from the earthquake hazard.
16. Regarding to the probability maps, the maximum intensities that have a possibility to generate is level VII in MMI scale.
17. Comparing with the ground shaking levels reported previously, the SHA of this are effective to withstand the past ground shaking and implied that this SHA is a powerful tool to predict reliably the ground shaking according to the upcoming earthquakes.

8.2 Recommendations

Phenomenally, the earthquake generating process is quite complex depending on various parameters. The ground shaking predicted by SHA, therefore, difficult in practice. Although the most up-to-date SHA presented here is an important step toward an accurate evaluation of seismic hazard potential in Thailand and adjacent areas, this SHA itself is not complete yet which may not predict perfectly the ground shaking generated in the future. More work is needed to refine this SHA. It is emphasized that the extent to which geological information contributes to SHA and that such assessments depend on the quantity and quality of the data collected. To further refine SHA in this region, more detailed active fault data are indispensable. To this end, more observations of strong ground-motion particularly the short source-to-site distance in the region are needed and further seismo-tectonic research should be encouraged to allow the construction of a strong ground-motion attenuation model specific to Thailand and adjacent areas. Furthermore, it is important to note that the strong ground-motion attenuation models considered in this study derive PGA for the rock site condition. In areas covered by thick, soft soils, ground shaking will be much more severe than that indicated by these SHA maps.

REFERENCES

Akciz, S., Burchfiel, B. C., Crowley, J. L., Jiyun, Y., and Liangzhong, C. 2008. Geometry, kinematics and regional significance of the Chong Shan shear zone, east Himalayan syntaxis, Yunnan, China. Geosphere 4(1): pp.292–314.

Algermissen, S.T., Perkins, D.M., Thenhaus, P.C., Hanson, S.L., and Bender, B.L. 1982. Probabilistic estimates of maximum acceleration and velocity in rock in the contiguous United States. United States Geological Survey. Open-File Report: pp.82-1033.

Alvarez, L., Vaccari, F., and Panza, G.F. 1999. Deterministic seismic zoning of eastern Cuba. Pure and Applied Geophysics 156 (3): pp. 469-486.

Alves, E.I. 2006. Earthquake Forecasting Using Neural Networks: Results and Future Work. Nonlinear Dynamics 44: 341–349.

Anderson, J.G., Brune, J.N., Anooshehpoor, R., and Ni, S.D. 2000. New ground motion data and concepts in seismic hazard analysis. Current Science 79: 1278–1289.

Aoudia, A., Vaccari, F., Suhadolc, P., and Meghraoui, M. 2000. Seismogenic potential and earthquake hazard assessment in the Tell Atlas of Algeria. Journal of Seismology 4: pp. 79-98.

Atakan, K., Ojeda, A., Camelbeeck, T., and Meghraoui, M. 2001. Seismic hazard analysis results for the Lower Rhine Graben and the importance of paleoseismic data. Netherlands Journal of Geosciences 80(3-4): pp.305–304.

Bai, D., and Meju, M. A. 2003. Deep structure of the Longling-Ruili fault zone underneath Ruili basin near the Eastern Himalayan syntaxis: insights from magnetotelluric imaging. Tectonophysics 364: pp.135 –146.

Bertrand, G., and Rangin, C. 2003. Tectonics of the western margin of the Shan Plateau (central Myanmar): implications for the India-Indochina oblique convergence since the Oligocene. Journal of Asian Earth Sciences 21: pp.1139-1157.

Bodri, B. 2001. A neural-network model for earthquake occurrence. Journal of Geodynamics 32: pp. 289–310.

Boore, D.M., Joyner, W.B., and Fumal, T.E. 1997. Equations for estimating horizontal response spectra and peak acceleration from western North American earthquakes: A summary of recent work. Seismological Research Letters 68(1): pp. 128–153.

Bott, J., Wong, I., Prachaub, S., Wechbunthung, B., Hinthong, C, and Sarapirome, S. 1997. Contemporary seismicity in northern Thailand and its tectonic implication. In: P. Dheeradilok (Ed. in chief), Proceedings of the International Conference on Stratigraphy and Tectonic Evolution of Southeast Asia and the South Pacific, Department of Mineral Resources, Bangkok, 19-24 August 1997, pp. 453-464.

Brown, J.C., and Leicester, P., 1933. The Pyu earthquake of 3rd and 4th December, 1930 and subsequent Burma earthquakes up to January 1932: Memoirs of the Geological Survey of India 42 (1): pp. 1-140.

Bufe, C.G. 2006. Coulomb Stress Transfer and Tectonic Loading Preceding the 2002 Denali Fault Earthquake. Bulletin of the Seismological Society of America 96(5): pp. 1662–1674.

Caceres, D., and Kulhanek, O. 2000. Seismic Hazard of Honduras. Natural Hazards 22: pp. 49–69.

Campbell K. W. 1985. Strong motion attenuation relations: a tenyear perspective. Earthquake Spectra 1: pp.759-804.

Cancani, A. 1904. Sur l'emploi d'une double echelle seismique des intesites, empiriqueet absolue. G. Beitr. 2: pp. 281–283.

Charusiri, P.2005. Active fault study in Ongkalak Fault Zone, Ongkalak, Nakhon Nayok, Central Thailand. Technical report, Department of Geology, Faculty of Science, Chulalongkorn University, Bangkok, Thailand. 185p. (in Thai with English abstract).

Charusiri, P., Daorerk, V., Archibald, D., Hisada, K., and Ampaiwan, T. 2002. Geotectonic evolution of Thailand: A new synthesis. Journal of the Geological Society of Thailand 1: pp.1-20.

Charusiri, P., Daorerk, V., Choowong, M., Muangnoicharoen, N., Won-in, K., Lumjuan, A., Kosuwan, S., Saithong, P., and Thonnarat, P. 2004. The study on the

investigations of active faults in Changwat Kanchanaburi area, western Thailand. Technical report, Department of Geology, Faculty of Science, Chulalongkorn University, Bangkok, Thailand: 119p. (in Thai with English abstract).

Charusiri, P., Daorerk, V., Wongvanich, T., Nakapadungrat, S., and Imsamut, S. 1999. Geology of the Quadrangle Economic Zone (emphasis on China and Thailand). Technical report, National Research Council of Thailand, Bangkok, Thailand: 189p. (in Thai with English abstract).

Chintanapakdee, C., Naguit, M.E., and Charoenyuth, M. 2008. Suitable attenuation model for Thailand. The 14th World Conference on Earthquake Engineering. October 12-17, 2008, Beijing, China.

Choy, G.L., and Boatwright, J. 2007. The energy radiated by the 26 December 2004 Sumatra-Andaman earthquake estimated from 10-minute P-wave windows. Bulletin of the Seismological Society of America 97(1): pp. S18-S24.

Chuaviroj, S. 1991. Geotectonics of Thailand. Technical report, Geological Survey Division, Department of Mineral Resources, Bangkok, Thailand, p.58. (in Thai)

Cornell, C.A. 1968. Engineering seismic risk analysis. Bulletin of the Seismological Society of America 58: pp. 1583-1606.

Costa, G., Panza, G.F., Suhadolc, P., and Vaccari, F. 1992. Zoning of the Italian region with synthetic seismograms computed with known structural and source information. In Proceeding of 10th World Conference on Earthquake Engineering, Madrid, Spain: 435-438.

Costa, G., Panza, G.F., Suhadolc, P., and Vaccari, F. 1993. Zoning of the Italian territory in terms of expected peak ground acceleration derived from complete synthetic seismograms. Journal of Applied Geophysics 30: 149-160.

Crouse, C. B. 1991. Ground-motion attenuation equations for earthquakes on the Cascadia subduction zones. Earthquake Spectra 7(2): pp. 201–236.

Cuong, N.Q., Swierczewska, A., Wysocka, A., Dong, P.P., and Huyen, V.N. 2006. Activity of the Cao Bang-Tien Yen fault zone (NE Vietnam) – record in associated sedimentary basins. Proceedings of 17th International Sedimentological Congress, Fukuoka, Japan. P-074 (Abstracts).

Cuong, N.Q., and Zuchiewicz, W.A. 2001. Morphotectonic properties of the Lo River Fault near Tam Dao in North Vietnam. Natural Hazards and Earth System Sciences 1: pp.15–22.

Das, S., Gupta, I.D., and Gupta, V.K. 2006. A Probabilistic Seismic Hazard Analysis of Northeast India. Earthquake Spectra 22(1): pp. 1-27.

Department of Mineral Resources. 2006. Active Fault Map of Thailand. Department of Mineral Resources [Online]. Available from: http://www.dmr.go.th [2009, May]

Dewey, J.W., Choy, G., Presgrave, B., Sipkin, S., Tarr, A.C., Benz, H., Earle, P., and Wald, D. 2007. Seismicity associated with the Sumatra–Andaman Islands Earthquake of 26th December 2004. Bulletin of the Seismological Society of America 97(1A): pp. S25–S42.

Douglas, J. 2001. A comprehensive worldwide summary of strong-motion attenuation relationships for peak ground acceleration and spectral ordinates (1969 to 2000). Technical report, Engineering Seismology and Earthquake Engineering (ESEE) 01-1, 144p.

Du, W., and Sykes. L.R. 2001. Changes in Frequency of Moderate-Size Earthquakes and Coulomb Failure Stress before and after the Landers, California, Earthquake of 1992. Bulletin of the Seismological Society of America 91(4): pp. 725–738.

Duong, C.C., and Feigl, K.L. 1999. Geodetic measurement of horizontal strain across the Red River fault near Thac Ba, Vietnam. Journal of Geodesy 73: pp.298-310.

Electricity Generating Authority of Thailand (EGAT). 2006. Active fault and determination of seismic parameters Hutgyi hydropower project. Technical report, Electricity Generating Authority of Thailand, Bangkok, Thailand: 89p.

Eleftheria, P., Xueze, W., Vassilios, K., and Xueshen, J. 2004. Earthquake Triggering along the Xianshuihe fault zone of Western Sichuan, China. Pure and applied geophysics 161(8): pp.1683-1707.

Esteva, L., and Villaverde, R. 1973. Seismic risk, design spectra and structural reliability. Proceeding of 5th World Conference on Earthquake Engineering, Rome, Italy: pp. 2586-2597.

Fenton, C., Charusiri, P., Hinthong, C., Lumjuan, A., and Mangkornkarn, B. 1997. Late Quaternary faulting in northern Thailand. In: P. Dheeradilok (Ed. in chief), Proceedings of the International Conference on Stratigraphy and Tectonic Evolution of Southeast Asia and the South Pacific, Department of Mineral Resources, Bangkok, 19-24 August 1997, pp. 436-452.

Fenton, C.H., Charusiri, P., and Wood, S.H. 2003. Recent paleoseismic investigations in Northern and Western Thailand. Annals of Geophysics 46(5): pp.957-981.

Fu, G., and Sun, W. 2006. Global co-seismic displacements caused by the 2004 Sumatra-Andaman earthquake (Mw 9.1). Earth Planets Space (58): pp. 149–152.

Fukushima, Y., and Tanaka, T. 1990. A new attenuation relation for peak horizontal acceleration of strong earthquake ground motion in Japan. Bulletin of the Seismological Society of America 80(4): pp. 757–783.

Gardner, J.K., and Knopoff, L. 1974. Is the sequence of earthquakes in Southern California, with aftershocks removed, Poissonian?. Bulletin of the Seismological Society of America 64(1): pp.363–367.

Geist, E.L., Titov, V.V., Arcas, D., Pollitz, F.F., and Bilek, S.L. 2007. Implications of the 26th December 2004 Sumatra-Andaman Earthquake on Tsunami forecast and assessment models for great subduction-zone earthquakes. Bulletin of the Seismological Society of America 97(1A): pp. S249–S270.

Giardini, D., Grünthal, G., Shedlock, K.M., and Zhang, P. 1999. The GSHAP global seismic hazard map. Annali di Geofisica 42(6): pp. 1225-1230.

Gurpinar, A. 2005. The importance of paleoseismology in seismic hazard studies for critical facilities. Tectonophysics 408: pp.23– 28.

Gutenberg, B., and Richter, C.F. 1954. Seismicity of the Earth and Associated Phenomena. Princeton University Press, Princeton, New Jersey.

Habermann, R. E. 1987. Man-made changes of Seismicity rates. Bulletin of the Seismological Society of America 77: pp.141-159.

Habermann R. E. 1991. Seismicity rate variations and systematic changes in magnitudes in teleseismic catalogs. Tectonophysics 193: pp.277-289.

Habermann, R. E., and Creamer, F. 1994. Catalog errors and the M8 earthquake prediction algorithm. Bulletin of the Seismological Society of America 84: pp.1551 –1559.

Hanks, T.C., and Kanamori, H. 1979. A moment-magnitude scale. Journal of Geophysical Research 84: pp.2348–2350.

Hanson, J.A., Reasoner, C.L., and Bowman J.R. 2007. High-Frequency Tsunami Signals of the Great Indonesian Earthquakes of 26th December 2004 and 28th March 2005. Bulletin of the Seismological Society of America 97: pp. S232-S248.

Hershberger, J. 1956. A comparison of earthquake accelerations with intensity ratings. Bulletin of the Seismological Society of America 46: pp. 317–320.

Hinthong, C. 1991. Role of Tectonic Setting in Earthquake Events in Thailand. In the proceedings of Asean-EC Workshop on Geology and Geophysics, Jakarta, Indonesia, 7-11 October 1997, pp. 236-242.

Hinthong, C. 1995. The study of active fault in Thailand. In the proceedings of the technical conference on the progression and vision of mineral resources development, Department of Mineral Resources, Bangkok, pp.129-40.

Howell, B.F. 1981. On the saturation of earthquake magnitudes. Bulletin of the Seismological Society of America 71(5): pp.1401–1422.

Idriss, I.M. 1993. Procedures for selecting earthquake ground motions at rock sites. Technical report NIST GCR 93-625, U.S. Department of Commerce, National Institute of Standards and Technology, Gaithersburg, Maryland.

Ishimoto, M. 1932. Echelle d' intensit sismique et acceleration maxima. Bulletin of the Earthquake Research Institute, Tokyo University 10: pp. 614–626.

Ishimoto, M. and Iida, K. 1939. Observations sur les seismes enregistres parle microsismographe construit dernierement. Bulletin of the Earthquake Research Institute, University of Tokyo 17: pp.443-478 (in Japanese with French abstract).

Kawasumi, H. 1951. Measures of earthquake danger and expectancy of maximum intensity throughout Japan as inferred from the seismic activity in historical times. Bulletin of the Earthquake Research Institute, Tokyo University 29: pp. 469–482.

Kirschvink, J.L. 2000. Earthquake Prediction by Animals: Evolution and Sensory Perception. Bulletin of the Seismological Society of America 90(2): pp. 312–323.

Kobayashi, S., T. Takahashi, S. Matsuzaki, M. Mori, Y. Fukushima, J.X. Zhao, and Somerville, P.G. 2000. A spectral attenuation model for Japan using digital strong motion records of JMA87 type, in Proceedings of 12th World Conference on Earthquake Engineering, Auckland, New Zealand, pp. 146-150.

Kramer, S.L. 1996. Geotechnical Earthquake Engineering. Prentice Hall, Inc., Upper Saddle River, New Jersey. 563 p.

Krinitzsky, E.L. 2003. How to combine deterministic and probabilistic methods for assessing earthquake hazards. Engineering Geology 70: pp. 157–163.

Lacassin, R., Replumaz, A., and Leloup, P.H. 1998. Hairpin river loops and strike-slip sense inversion of Southeast Asian strike-slip faults. Geology 26: pp.703–706.

Lapajne, J.K., Motnikar, B.S., and Zupancic, P. 2003. Probabilistic Seismic Hazard Assessment: Methodology for Distributed Seismicity. Bulletin of the Seismological Society of America 93: pp. 2502–2515.

Lepvrier, C., Maluski, H., Tich, V.V., and Leyreloup, A. 2004. The Early Triassic Indosinian orogeny in Vietnam (Truong Son Belt and Kontum Massif); implications for the geodynamic evolution of Indochina. Tectonophysics 393(1-4): pp.87–118.

Martin, S. 2005. Intensity distribution from the 2004 M 9.0 Sumatra-Andaman earthquake. Seismological Research Letters 76: pp. 321–330.

Maryanto, S., and Mulyana, I. 2008. Temporal Change of Fractal Dimension of Explosion Earthquakes and Harmonic Tremors at Semeru Volcano, East Java, Indonesia, using Critical Exponent Method. World Academy of Science, Engineering and Technology 42: pp. 537-541.

McCalpin, J.P. 1996. Paleoseismology. Academic Press: 588 p.

McCue, K. 2004. Australia: historical earthquake studies. Annals of Geophysics 47 (2/3): pp. 387-397.

Medvedev, S.V., and Sponheuer, W. 1969. Scale of seismic intensity. Proceeding of the 5th World Conference Earthquake Engineering, 13–18 January 1969. Santiago, Chile, pp. 135-138.

Megawati, K., Pan, T., and Koketsu, K. 2005. Response Spectral Attenuation Relationships for Sumatran-Subduction Earthquakes and the Seismic Hazard Implications to Singapore and Kuala Lumpur. Soil Dynamics and Earthquake Engineering 25(1): pp. 11-25.

Metcalfe, I. 2000. The Bentong-Raub suture zone. Journal of Asian Earth Sciences 18: pp.691-712.

Morley, C.K. 2007. Variations in Late Cenozoic-Recent strike-slip and oblique-extensional geometries, within Indochina: The influence of pre-existing fabrics. Journal of Structural Geology 29: pp.36-58.

Neumann, F. 1954. Earthquake Intensity and Related Ground Motion. WSU Press, Seattle, Washington.

Nuannin,P., Kulhanek, O., and Persson, L., 2005. Spatial and temporal b value anomalies preceding the devastating off coast of NW Sumatra earthquake of December 26, 2004. Geophysical Research Letters 32: pp L11307-L11311.

Nutalaya, P., Sodsri, S., and Arnold, E.P. 1985. Series on Seismology-Volume II-Thailand. In E.P Arnold (ed.), Technical report, Southeast Asia Association of Seismology and Earthquake Engineering: 402p.

Nuttee, R., Charusiri, P., Takashima, I. and Kosuwan S. 2005. Pakeo-Earthquakes Along the Southern Segment of the Sri Sawat Fault, Kanchanaburi, Western Thailand: Morphotectonic and TL-Dating Evidence. Proceedings of the International Conference on Geology, Geotechnlony and Mineral Resources of Indochina (GEOINDO 2005) 28-30 November 2005, Khon Kaen, Thailand, pp. 542-554.

Okamoto, S. 1973. Introduction to Earthquake Engineering. John Wiley, New York.

Oki, Y., and Hiraga, S. 1988. Groundwater Monitoring for Earthquake Prediction by an Amateur Network in Japan. Pure and Applied Geophysics 126(2-4): pp. 211-240.

Orozova-Stanishkova, I.M., Costa, G., Vaccari, F., and Suhadolc, P. 1996. Estimates of 1 Hz maximum acceleration in Bulgaria for seismic risk reduction purposes. Tectonophysics 258: 263-274.

Orozova, I. M. and Suhadolc, P., 1999. A deterministic-probabilistic approach for seismic hazard assessment. Tectonophysics 312: pp. 191-202.

Ottemoller, L., and Havskov, J. 2003. Moment magnitude determination for local and regional earthquakes based on source spectra. Bulletin of the Seismological Society of America 93(1): pp. 203–214.

Pailoplee, S., Sugiyama, Y., and Charusiri, P. 2009. Deterministic and probabilistic seismic hazard analyses in Thailand and adjacent areas using active fault data. Earth Planets Space 61: pp. 1313–1325.

Palasri, C. 2006. probabilistic seismic hazard map of Thailand, Master's thesis, Department of Civil Engineering, Faculty of Engineering, Chulalongkorn University, Bangkok, Thailand. 143 p.

Panza, G.F., Vaccari, F., and Cazzaro, R. 1999. Deterministic seismic hazard assessment. F. Wenzel et al. (eds.), Vrancea Earthquakes. Tectonic and Risk Mitigation. Kluwer Academic Publishers, The Netherlands: 269-286.

Paul, J., Burgmann, R., Gaur, V.K., Bilham, R., Larson, K.M., Ananda, M.B., Jade, S., Mukal, M., Anupama, T.S., Satyal, G., and Kumar, D. 2001. The motion and active deformation of India, Geophysical Research Letters 28: pp. 647–650.

Petersen, M., Dewey, J., Hartzell, S., Mueller, C., Harmsen, S., Frankel, A.D., and Rukstales, K. 2004. Probabilistic seismic hazard analysis for Sumatra, Indonesia and across the Southern Malaysian Peninsula. Tectonophysics 390: pp. 141–158.

Petersen, M., Harmsen, S., Mueller, C., Haller, K., Dewey, J., Luco, N., Crone, A., Lidke, D., and Rukstales, K. 2007. Southeast Asia Seismic Hazard Maps. Technical report, Department of the Interior U.S. Geological Survey: 65p.

Phil, R.G., 2008. Age discrepancies with the radiocarbon dating of sagebrush (Artemisia Tridentata Nutt.). Radiocarbon 50(3): pp. 347-357.

Phoung, N.H. 1991. Probabilistic assessment of earthquake hazard in Vietnam based on seismotectonic regionalization. Tectonophysics 198: pp.81-93.

Polachan, S., Pradidtan, S., Tongtaow, C., Janmaha, S., Intrawijitr, K., and Sangsuwan, C. 1991. Development of Cenozoic basins in Thailand. Marine and Petroleum Geology 8: pp.84–97.

Prachaub, S. 1990. Seismic data and building code in Thailand. Technical Report, Thai Meteorological Department 550: 34 p. (in Thai).

Radulian, M., Vaccari, F., Mandrescu, N., Panza, G.F. and Moldoveanu, C.L. 1999. Seismic hazard of Romania deterministic approach. Pure and Applied Geophysics. (In press.)

Reid, H.F., 1910. The Mechanics of the Earthquake, The California Earthquake of April 18, 1906. Report of the State Investigation Commission 2, Carnegie Institution of Washington, Washington, D.C.

Richter, C.F. 1958. Elementary Seismology. W.H. Freeman, San Francisco.

Rink, W.J., and Forrest, B. 2005. Dating Evidence for the Accretion History of Beach Ridges on Cape Canaveral and Merritt Island, Florida, USA. Journal of Coastal Research 21(5): pp. 1000–1008.

Rhodes, B.P., Perez, R., Lamjuan, A., and Kosuwan, S. 2004. Kinematics and tectonic implications of the Mae Kuang Fault, northern Thailand. Journal of Asian Earth Sciences 24(1): pp.79-89.

Royal Irrigation Department (RID). 2006. Active fault investigation in Mae Yom fault zone, Kaeng Seur Ten Dam Site, Song district, Phrae Province, Thailand. Technical report, Royal Irrigation Department, Bangkok, Thailand: 175p. (in Thai with English abstract).

Sadigh, K., Chang, C.Y., Egan, J.A., Makdisi, F., and Youngs, R.R. 1997. Attenuation relationships for shallow crustal earthquakes based on California strong motion data. Seismological Research Letters 68(1): pp. 180–189.

Saithong, P., Kosuwan, S., Won-in, K., Takashima, I., Charusiri, P. 2005. Late Quaternary paleoseismic history and surface rupture characteristics of the Moei-Mae Ping fault zone in Tak Area, northwestern Thailand. In proceedings of the International

Conference on Geology, Geotechnology and Mineral Resources of INDOCHINA: November 28–30, 2005, Khon Kaen, Thailand: pp. 511–516.

Savarensky, Y.F., and Kirnos, D.P. 1955. Elements of Seismology and Seismometry, Moscow.

Scholz, C. H. 1968. The frequency-magnitude relation of microfracturing relation to earthquakes. Bulletin of the Seismological Society of America 58: pp.399– 415.

Scott, E.M., Bryant, C., Carmi, I., Cook, G., Gulliksen, S., Harkness, D., Heinemeier, J., McGee, E., Naysmith, P., Possnert, G., van der Plicht, H., and van Strydonck, M. 2004. Precision and accuracy in applied 14C dating: some findings from the Fourth International Radiocarbon Inter-comparison. Journal of Archaeological Science 31 (9): pp. 1209-1213.

Shabestari, K.T., and Yamazaki, F. 2001. A proposal of instrumental seismic intensity scale compatible with MMI evaluated from three-component acceleration records. Earthquake 17(4): pp. 711–723.

Shebalin, P., Keilis-Borok, V., Gabrielov, A., Zaliapin, I., Turcotte, D. 2006. Short-term earthquake prediction by reverse analysis of lithosphere dynamics. Tectonophysics 413; pp. 63–75.

Simons, P. 2008. Earthquake prediction is written in the clouds. Weather eye, the Times: 10 p.

Songmuang, R., Charusiri, P., Choowong, M., Won-In, K., Takashima, I., and Kosuwan, S. 2007. Detecting active faults using remote-sensing technique: A case study in the Sri Sawat Area, western Thailand. Science Asia 33: pp.23-33.

Stirling, M., and Petersen, M. 2006. Comparison of the Historical Record of Earthquake Hazard with Seismic- Hazard Models for New Zealand and the Continental United States. Bulletin of the Seismological Society of America 96(6): pp. 1978-1994.

Suckale, J., and Grünthal, G. 2009. Probabilistic Seismic Hazard Model for Vanuatu. Bulletin of the Seismological Society of America 99(4): pp.2108-2126.

Takemoto, K., Halim, N., Otofuji, Y., Tran, V.T., Le, V.D., and Hada, S. 2005. New paleomagnetic constraints on the extrusion of Indochina: Late Cretaceous

results from the Song Da terrane, northern Vietnam. Earth and Planetary Science Letters 229: pp.273– 285.

Thenhaus, P.C., and Campbell, K.W. 2003. Seismic hazard analysis. In: W.-F. Chen and C. Scawthorn, Editors, Earthquake Engineering Handbook, CRC Press, Boca Raton, FL, USA: pp.8-1–8-50.

Theodulides, N.P., and Papazachos, B.C. 1992. Dependence of strong ground motion on magnitude-distance, site geology and macroseismic intensity for shallow earthquakes in Greece: I, Peak horizontal acceleration, velocity and displacement. Soil Dynamics and Earthquake Engineering 11: pp. 387–402.

Trifunac, M.D., and Brady, A.G. 1975. On The correlation of seismic intensity scales with the peaks of recorded strong ground motion. Bulletin of the Seismological Society of America 65(1): pp. 139-162.

USGS. 2005. Summary of the Sumatra-Andaman Islands Earthquake and Tsunami of 26 December 2004. US. Geological Survey [Online]. Available from : http://www. neic.usgs.gov/neis/ eq_depot /2004neic_slav_summary.html [2009, April].

Wang, Y., Amundson, R., and Trumbore, S. 1996. Radiocarbon Dating of Soil Organic Matter. Quaternary Research 45(3): pp. 282-288.

Wang, Z. 2006. Understanding seismic hazard and risk assessments: An example in the New Madrid seismic zone of the central United States. Proceedings of the 8th U.S. National Conference on Earthquake Engineering. April 18-22, 2006, San Francisco, California, pp. 145-149.

Wanitchai, P., and Lisantono, A. 1996. Probabilistic Seismic Risk Mapping for Thailand. Proceedings of 11th World Conference on Earthquake Engineering, Acapulco, Mexico, pp. 256-259.

Wells, D.L., and Coppersmith, K.J. 1994. Updated empirical relationships among magnitude, rupture length, rupture area, and surface displacement. Bulletin of the Seismological Society of America 84: 974–1002.

Woessner, J., and Wiemer, S. 2005. Assessing the quality of earthquake catalogues: Estimating the magnitude of completeness and its uncertainty. Bulletin of the Seismological Society of America 95: pp.684-698.

Wong, I., Fenton, C., Dober, M., Zachariasen, J., and Terra, F. 2005. Seismic hazard evaluation of the Tha Sae project, Thailand. Technical report, Punya Consultants Co. Ltd., 118 p.

Wyss, M. 1973. Towards a physical understanding of the earthquake frequency distribution. Geophys. J. R. Astron. Soc. 31: pp.341–359.

Wyss, M., and Stefansson, R. 2006. Nucleation Points of Recent Mainshocks in Southern Iceland, Mapped by b-Values. Bulletin of the Seismological Society of America 96(2): pp. 599–608.

Yagi, Y., Kikuchi, M., and Sagiya, T. 2001. Co-seismic slip, post-seismic slip, and aftershocks associated with two large earthquakes in 1996 in Hyuga-nada, Japan. Earth Planets Space 53: pp. 793–803.

Yeats, R.S, Sieh, K.E., and Allen, C.A., 1996. Geology of earthquakes. Oxford University Press, New York: 576 p.

Youngs, R.R., and Coppersmith, K.J. 1985. Implications of fault slip rates and earthquake recurrence models to probabilistic seismic hazard estimates. Bulletin of the Seismological Society of America 75: pp. 939-964.

Youngs, R.R., Chiou, S.J., Silva, W.J., and Humphrey, J.R. 1997. Strong ground motion attenuation relationships for subduction zone earthquakes. Seismological Research Letters 68: pp. 58-73.

Zmazek, B., Vaupoti, J., Ziv-ci, M., Premru, U., and Kobal, I. 2000. Radon Monitoring for Earthquale Prediction in Slovenis. Fizika B (Zagreb) 9(3): pp. 111-118.

Zuchiewicz, W., Cuong, N.Q., Bluszcz, A., and Michalik, M. 2004. Quaternary sediments in the Dien Bien Phu fault zone, NW Vietnam: a record of young tectonic processes in the light of OSL-SAR dating results. Geomorphology 60: pp.269–302.

Zuniga, F. R., and Wiemer, S. 1999. Seismicity patterns: are they always related to natural causes?. Pure and applied geophysics 155: pp.713-726.

APPENDICES

APPENDIX A

FREQUENCY-MAGNITUDE DISTRIBUTION

Figure A.1. Graphs showing the frequency-magnitude distribution for the seismic source zones cited in Table 4.1. Each triangle indicates the total number of earthquakes for each magnitude; square represents the cumulative number of earthquakes equal to or larger than each magnitude. The solid lines are lines of the best fit. Mc is the magnitude of completeness.

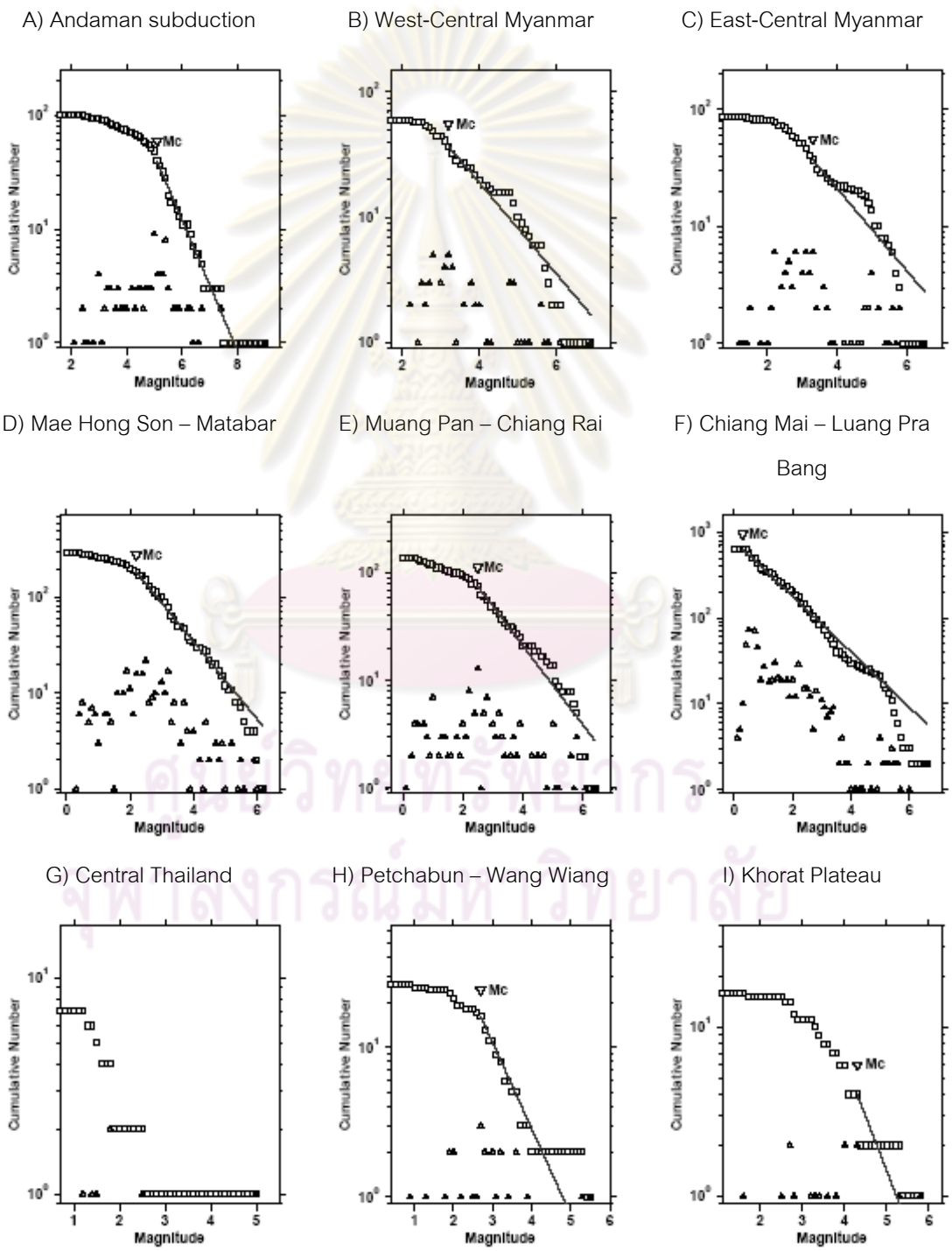

J) Song Ca

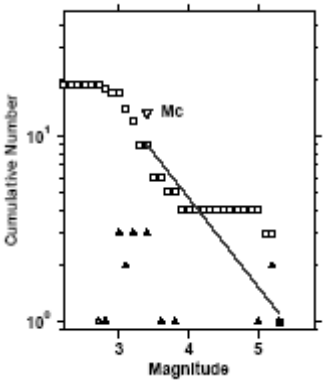

K) Northern Vietnam

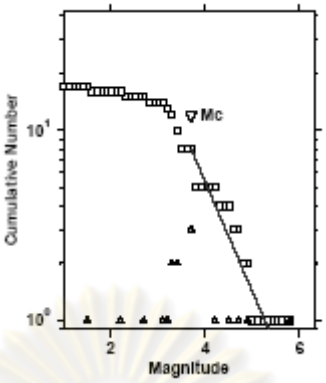

L) Eastern Thailand– Cambodia

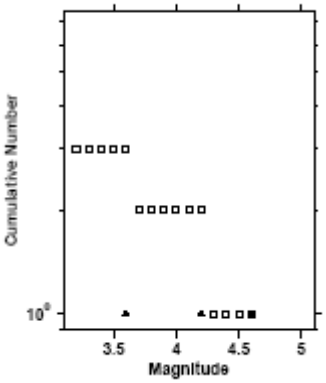

M) Andaman Arc

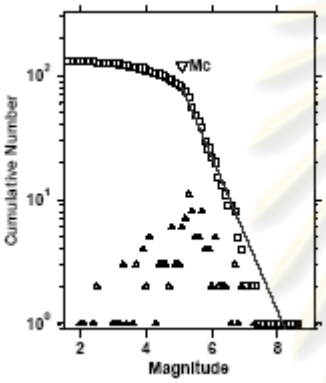

N) Andaman Basin

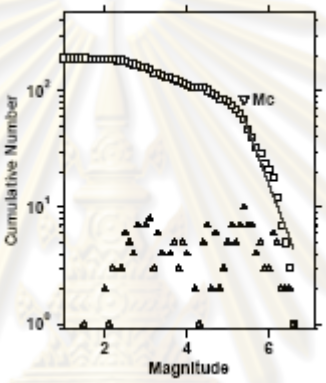

O) Western Thailand

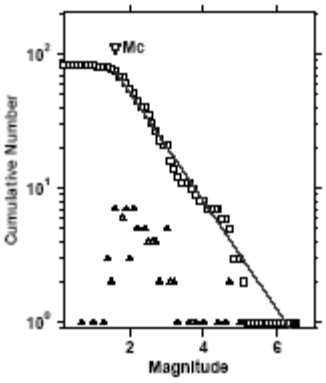

P) Mergui

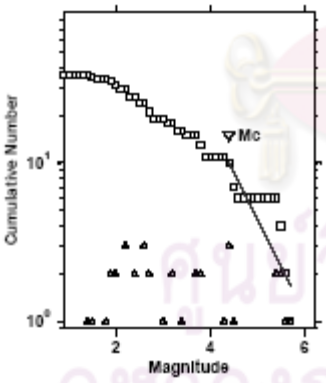

Q) Gulf of Thailand

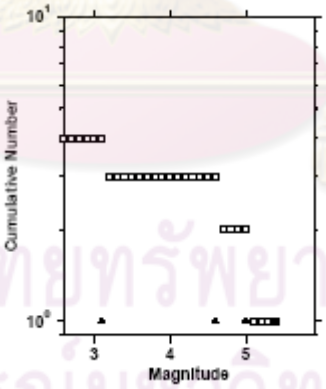

R) Malaysia – Malacca

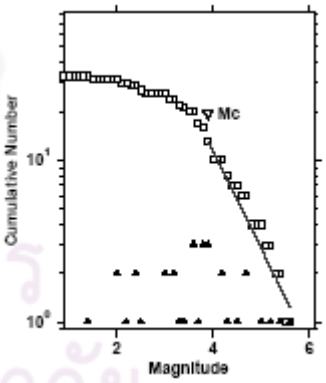

S) Aceh – Mentawai

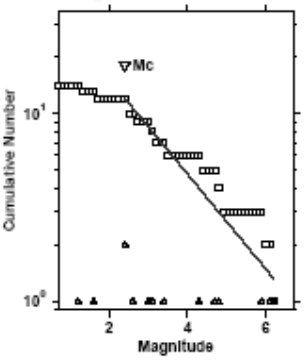

T) Tenasserim

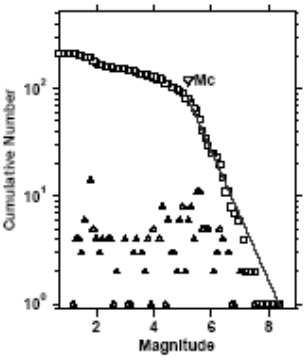

U) Sumatha Island

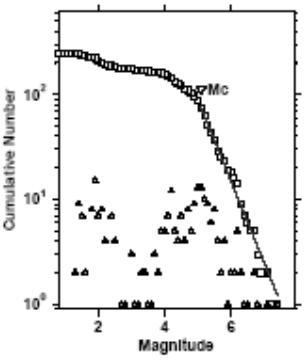

Figure A.2. Graphs showing the frequency-magnitude distribution for the active fault zones cited in Table 4.2. All symbols are identical as described in Figure A.1.

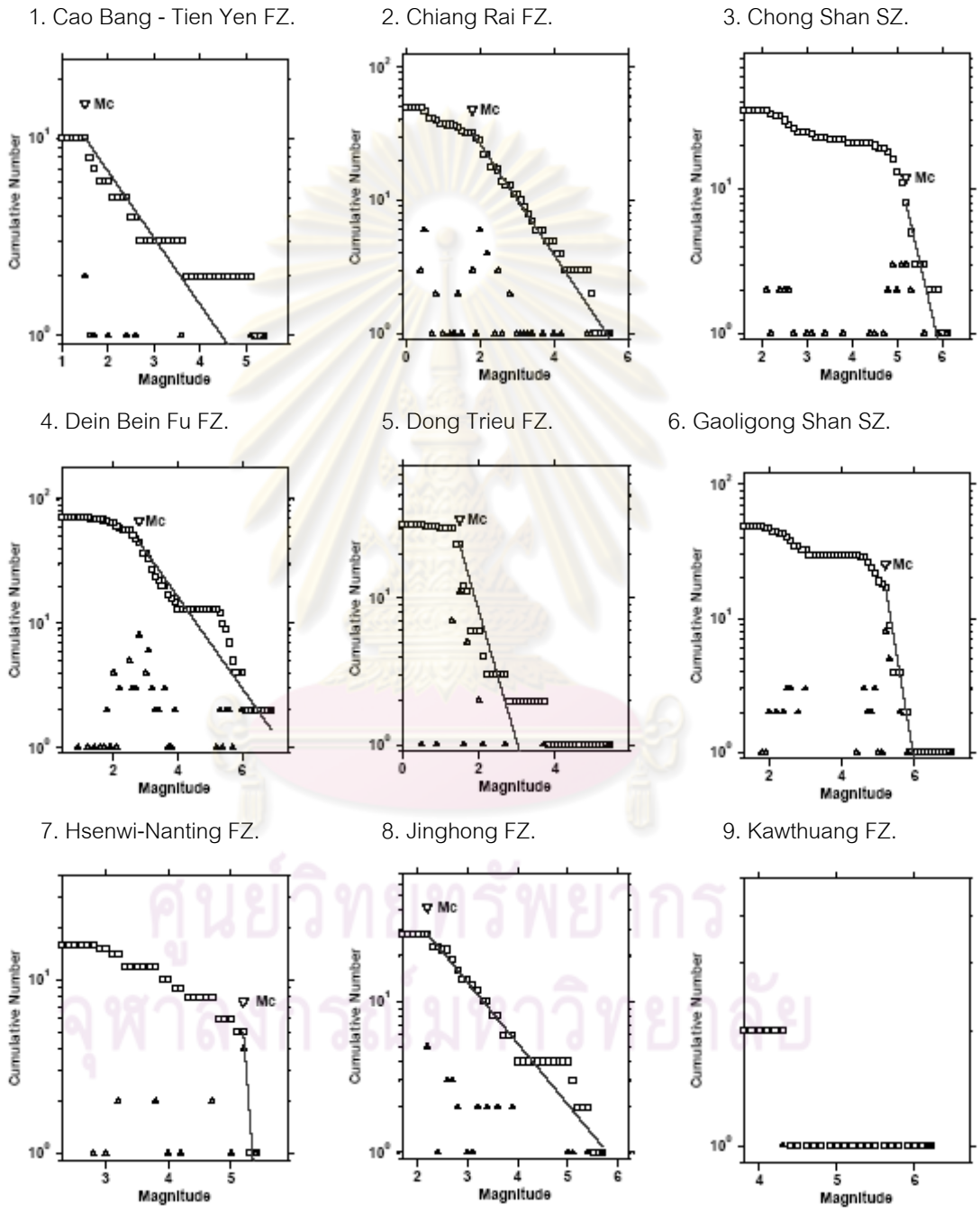

10. Klong Marui FZ.

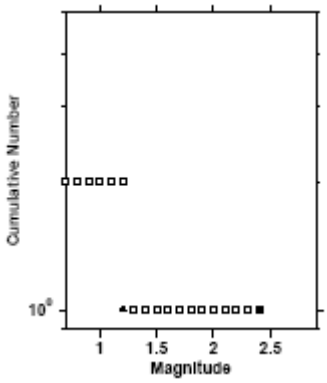

11. Kungyaungale FZ.

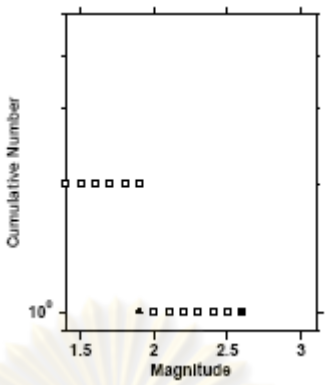

12. Lampang-Thoen FZ.

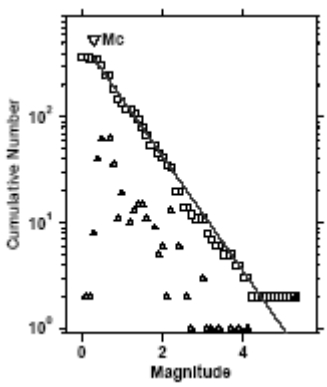

13. Lashio FZ.

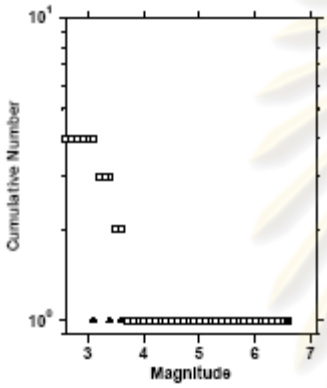

14. Libir FZ.

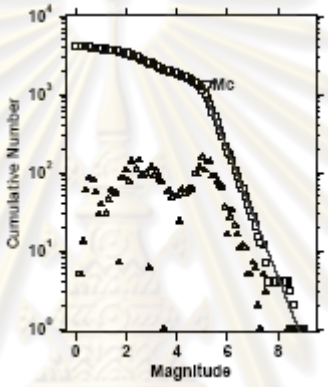

15. Linchang FZ.

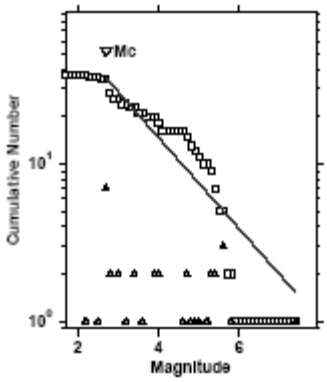

16. Loei-Petchabun FZ.

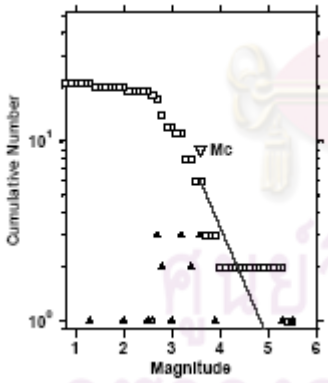

17. Longling-Ruili FZ.

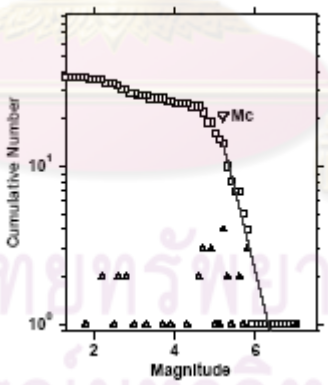

18. Mae Chaem FZ.

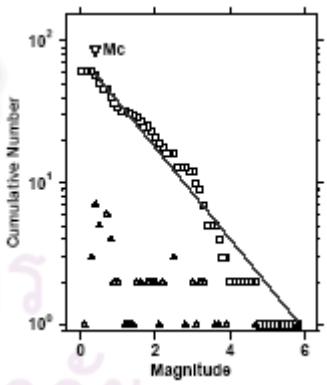

19. Mae Chan FZ.

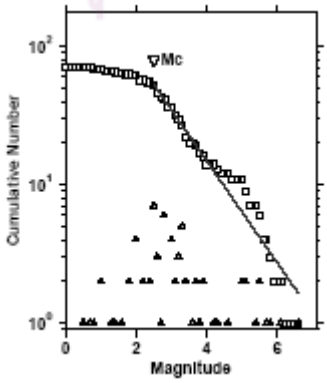

20. Mae Hong Sorn-Tak FZ.

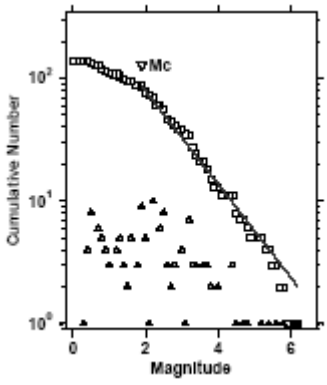

21. Mae Ing FZ.

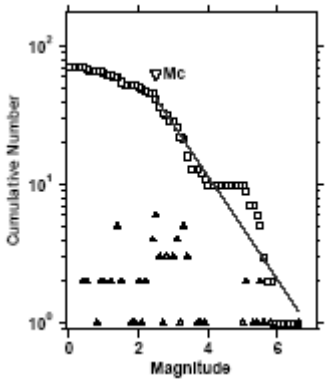

22. Mae Tha FZ.

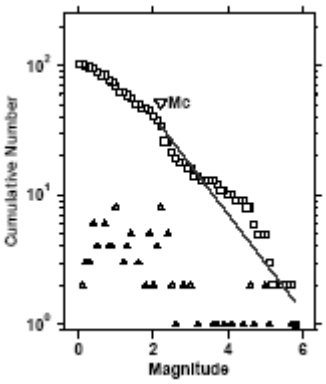

23. Mae Yom FZ.

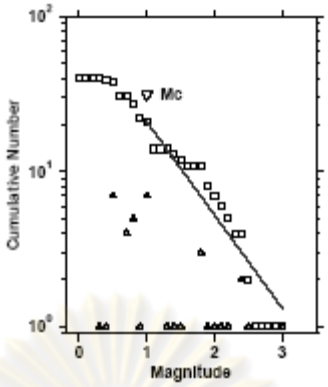

24. Menglian FZ.

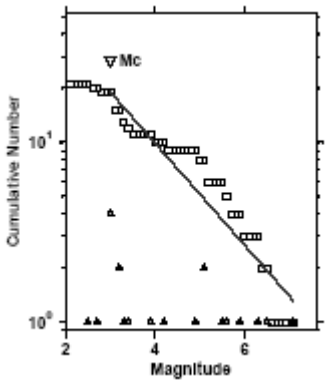

25. Mengxing FZ.

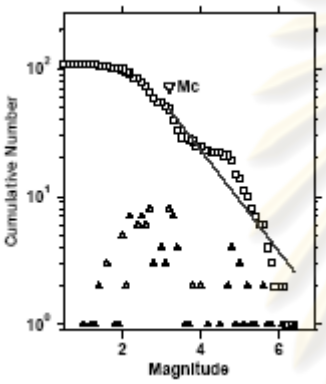

26. Moei-Tongyi FZ.

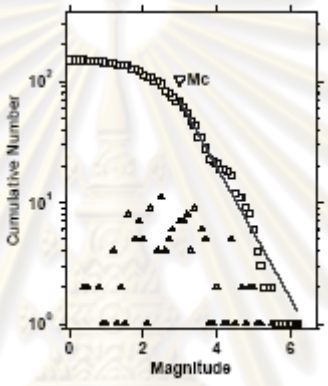

27. Nam Ma FZ.

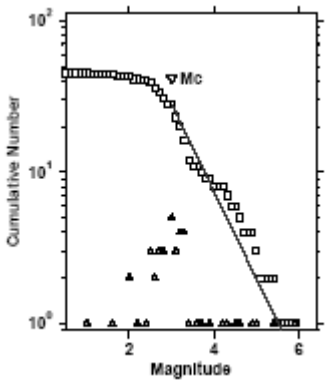

28. Nam Peng FZ.

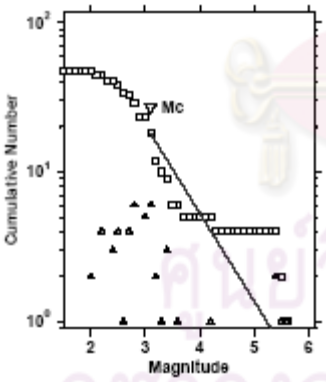

29. Ongkalak FZ.

N/A

30. Pa Pun FZ.

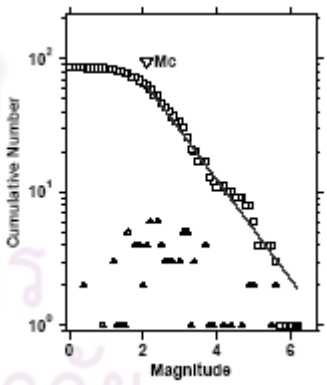

31. Pan Luang FZ.

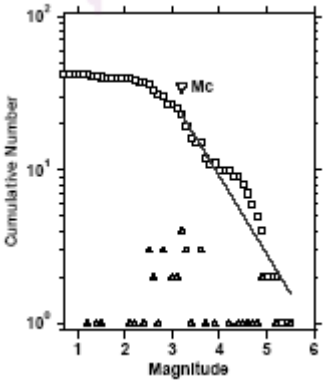

32. Pha Yao FZ.

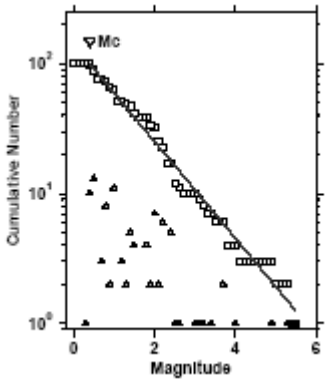

33. Phrae FZ.

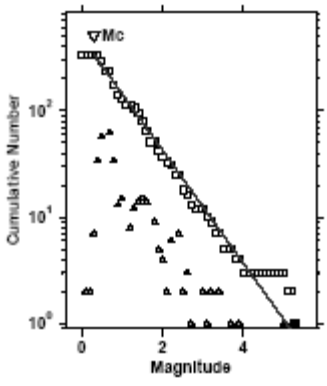

34. Pua FZ.

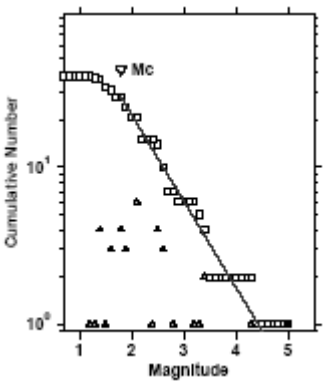

35. Qiaohou FZ.

N/A

36. Ranong FZ.

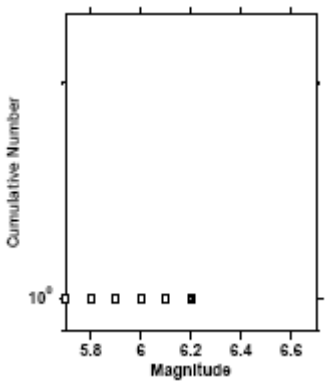

37. Red River FZ.

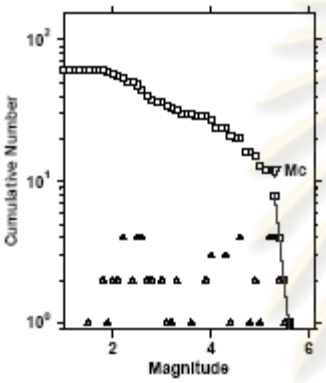

38. Sagiang-Sumatra FZ.

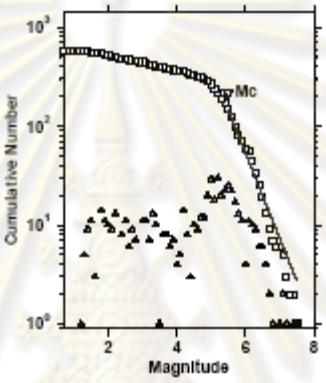

39. Shan FZ.

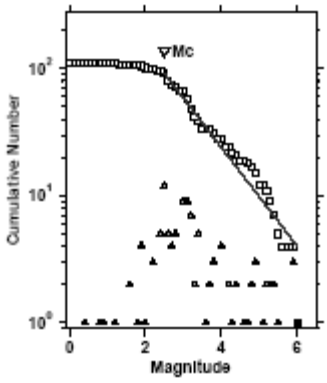

40. Song Ca FZ.

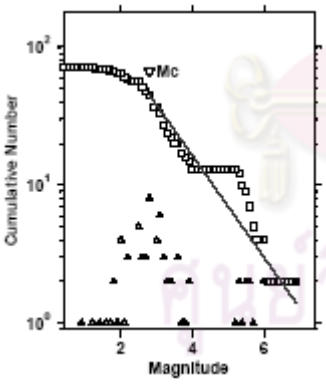

41. Song Chay FZ.

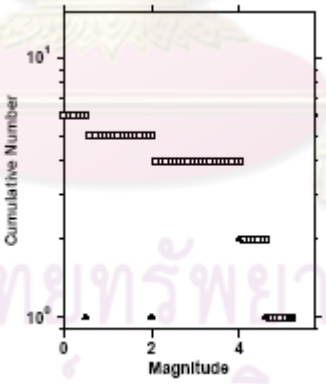

42. Song Da FZ.

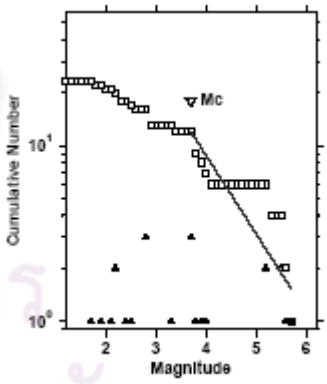

43. Song Ma FZ.

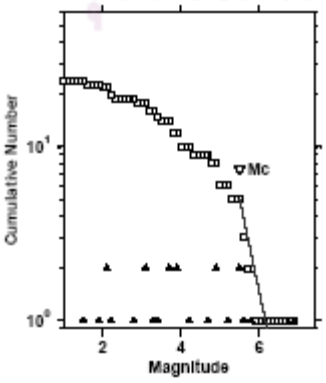

44. Sri Sawath FZ.

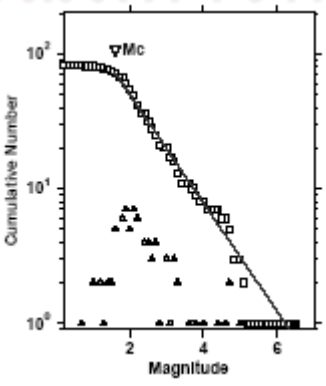

45. Andaman subduction

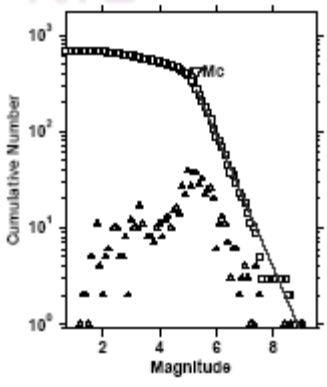

46. Tavoy FZ.

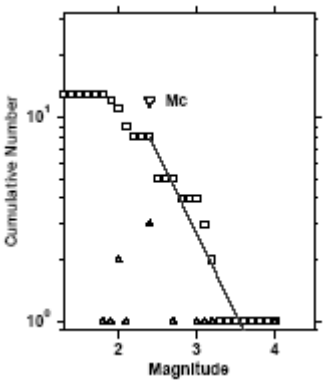

47. Tenasserim FZ.

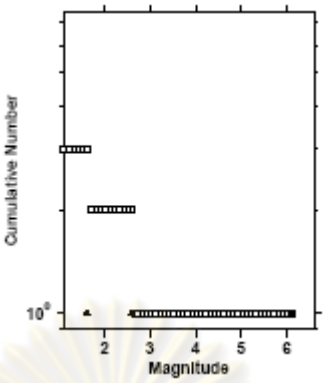

48. Tha Khaek FZ.

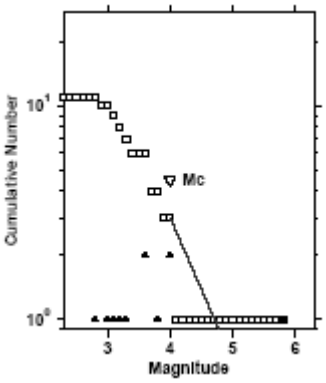

49. Three Pagoda FZ.

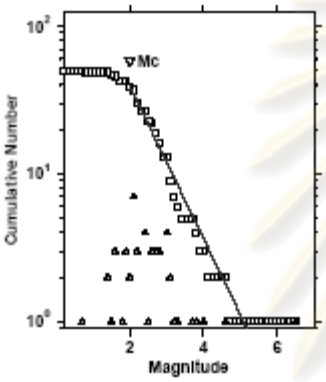

50. Uttaladith FZ.

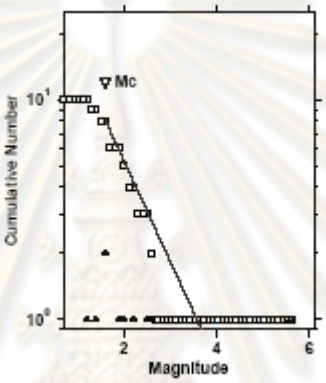

51. Wan Na-awn FZ.

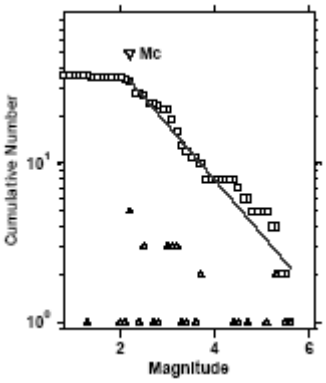

52. Wanding FZ.

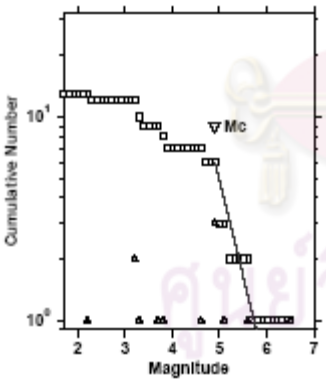

53. Wang Nua FZ.

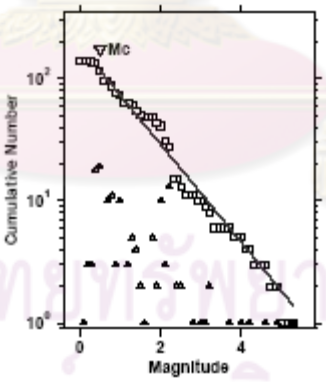

54. Xianshuihe FZ.

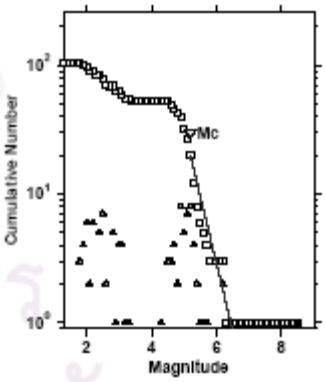

55. Hutgyi FZ.

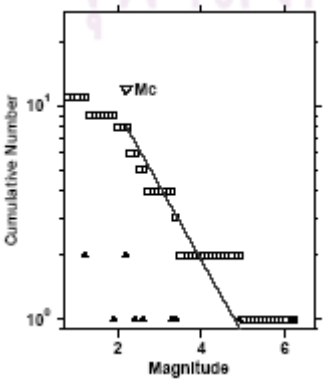

APPENDIX B

STRONG GROUND-MOTION DATA

Table B.1. Strong ground-motion data recorded by the TMD seismological station network. The earthquake epicentral distributions are located in the Sumatra-Andaman Subduction zone.

Event	Long	Lat	Day	Month	Year	Mw	Station	Instrument	Digital Count	Distance (km)	PGA (g)
1	95.704	19.87	21	9	2003	6.6	TAK	SSA0320	2437	453	2.59E-03
2	96.65	20.16	30	10	2003	5.3	TAK	SSA0320	270	407	2.48E-04
2	96.65	20.16	30	10	2003	5.3	PHARE	SSA0320	195	419	3.06E-04
3	95.848	3.226	26	12	2004	9	TAK	SSA0320	2264	1159	2.02E-03
4	91.733	7.771	24	7	2005	7.2	SON	SSA0320	276	985	2.02E-04
5	94.188	4.765	18	11	2006	5.9	RNTT	TSA0100	309	701	3.26E-04
6	91.516	8.431	8	1	2007	6.1	SKLT	TSA0100	41	1016	2.14E-05
6	91.516	8.431	8	1	2007	6.1	SURT	TSA0100	49	807	2.63E-05
6	91.516	8.431	8	1	2007	6.1	TRTT	TSA0100	35	906	1.87E-05
7	95.126	19.21	9	1	2007	4.9	CMMT	TSA0100	49	415	4.22E-05
7	95.126	19.21	9	1	2007	4.9	KHLT	TSA0100	71	617	1.04E-04
7	95.126	19.21	9	1	2007	4.9	MHMT	TSA0100	314	324	6.52E-04
7	95.126	19.21	9	1	2007	4.9	PBKT	TSA0100	147	696	9.17E-05
7	95.126	19.21	9	1	2007	4.9	SRDT	TSA0100	31	687	2.91E-05
8	95.054	3.959	1	3	2007	5.2	CHBT	TSA0100	22	1268	5.50E-05

Table B.1. (cont.) Strong ground-motion data recorded by the TMD seismological station network. The earthquake epicentral distributions are located in the Sumatra-Andaman Subduction zone.

Event	Long	Lat	Day	Month	Year	Mw	Station	Instrument	Digital Count	Distance (km)	PGA (g)
8	95.054	3.959	1	3	2007	5.2	PKDT	TSA0100	295	569	3.30E-04
8	95.054	3.959	1	3	2007	5.2	RNTT	TSA0100	78	714	1.31E-04
8	95.054	3.959	1	3	2007	5.2	SKLT	TSA0100	83	714	4.88E-05
8	95.054	3.959	1	3	2007	5.2	TRTT	TSA0100	88	671	6.71E-05
9	92.599	10.7	1	3	2007	5	PKDT	TSA0100	111	705	9.07E-05
10	97.292	1.979	7	3	2007	5.9	PKDT	TSA0100	219	668	3.56E-04
10	97.292	1.979	7	3	2007	5.9	RNTT	TSA0100	42	834	5.31E-05
11	95.776	2.859	7	4	2007	6.1	KHLT	TSA0100	29	1363	1.19E-05
12	96.209	15.62	26	4	2007	4.9	KHLT	TSA0100	101	275	1.21E-04
12	96.209	15.62	26	4	2007	4.9	MHMT	TSA0100	123	341	1.14E-04
13	94.549	5.059	27	4	2007	5.9	CHBT	TSA0100	211	1215	2.54E-04
13	94.549	5.059	27	4	2007	5.9	PKDT	TSA0100	2195	525	2.98E-03
13	94.549	5.059	27	4	2007	5.9	SKLT	TSA0100	132	713	9.48E-05
13	94.549	5.059	27	4	2007	5.9	TRTT	TSA0100	258	649	1.92E-04
14	94.693	23.24	7	5	2007	5	MHMT	TSA0100	46	660	2.43E-05

Table B.1. (cont.) Strong ground-motion data recorded by the TMD seismological station network. The earthquake epicentral distributions are located in the Sumatra-Andaman Subduction zone.

Event	Long	Lat	Day	Month	Year	Mw	Station	Instrument	Digital Count	Distance (km)	PGA (g)
15	94.693	4.106	18	5	2007	5.2	PKDT	TSA0100	275	583	2.86E-04
15	94.693	4.106	18	5	2007	5.2	SKLT	TSA0100	41	740	1.65E-05
15	94.693	4.106	18	5	2007	5.2	SURT	TSA0100	29	704	3.00E-05
15	94.693	4.106	18	5	2007	5.2	TRTT	TSA0100	90	691	3.58E-05
16	92.094	6.818	25	7	2007	6.1	PBKT	TSA0100	37	1452	1.99E-05
16	92.094	6.818	25	7	2007	6.1	RNTT	TSA0100	165	761	5.98E-05
16	92.094	6.818	25	7	2007	6.1	SKLT	TSA0100	78	945	3.48E-05
16	92.094	6.818	25	7	2007	6.1	SKNT	TSA0100	75	1716	4.31E-05
16	92.094	6.818	25	7	2007	6.1	SURT	TSA0100	93	778	4.07E-05
17	95.776	19.43	30	7	2007	5.6	BKKA	TSA0100	0	831	7.15E-04
17	95.776	19.43	30	7	2007	5.6	CMMT	TSA0100	916	350	4.69E-04
17	95.776	19.43	30	7	2007	5.6	KRDT	TSA0100	121	854	8.10E-05
17	95.776	19.43	30	7	2007	5.6	MHMT	TSA0100	2600	272	3.03E-03
18	95.776	19.43	30	7	2007	5.6	PBKT	TSA0100	235	648	1.95E-04
18	95.776	19.43	30	7	2007	5.6	RNTT	TSA0100	25	1155	1.92E-05

Table B.1. (cont.) Strong ground-motion data recorded by the TMD seismological station network. The earthquake epicentral distributions are located in the Sumatra-Andaman Subduction zone.

Event	Long	Lat	Day	Month	Year	Mw	Station	Instrument	Digital Count	Distance (km)	PGA (g)
18	95.776	19.43	30	7	2007	5.6	SKNT	TSA0100	121	933	8.89E-05
18	95.776	19.43	30	7	2007	5.6	SURT	TSA0100	40	1211	2.66E-05
19	93.675	14.4	25	8	2007	5.7	CMMT	TSA0100	54	757	2.33E-05
19	93.675	14.4	25	8	2007	5.7	MHMT	TSA0100	75	627	6.25E-05
20	93.675	14.4	25	8	2007	5.7	PBKT	TSA0100	36	834	2.66E-05
20	93.675	14.4	25	8	2007	5.7	PKDT	TSA0100	64	885	4.36E-05
20	93.675	14.4	25	8	2007	5.7	RNTT	TSA0100	134	766	7.86E-05
21	93.675	14.4	25	8	2007	5.7	SRDT	TSA0100	162	596	7.94E-05
22	93.675	14.4	25	8	2007	5.7	SURT	TSA0100	64	825	2.59E-05
23	97.206	2.472	22	12	2007	5.7	SKLT	TSA0100	93	646	6.61E-05

Table B.2. Strong ground-motion data recorded by the TMD seismic station network. The earthquake epicentral distributions are located in the main land South East Asia.

Event	Long	Lat	Day	Month	Year	Mw	Station	Instrument	Digital Count	Distance (km)	PGA (g)
1	100.83	20.53	8	9	2007	4.1	MHMT	TSA0100	34	407	3.98E-05
2	100.76	20.82	16	10	2007	4.1	PBKT	TSA0100	38	473	6.18E-05
2	100.76	20.82	16	10	2007	4.1	CMMT	TSA0100	130	296	7.88E-05
3	101.70	18.77	13	4	2006	4.2	NAN	SSA0320	70	97	2.28E-04
4	98.16	16.79	13	4	2007	4.2	CMMT	TSA0100	389	241	1.33E-04
4	98.16	16.79	13	4	2007	4.2	PBKT	TSA0100	94	307	2.73E-04
4	98.16	16.79	13	4	2007	4.2	KHLT	TSA0100	375	226	3.96E-04
4	98.16	16.79	13	4	2007	4.2	MHMT	TSA0100	440	156	6.46E-04
5	100.69	20.53	17	5	2007	4.2	CMMT	TSA0100	28	268	1.52E-05
5	100.69	20.53	17	5	2007	4.2	MHMT	TSA0100	46	397	4.35E-05
6	97.87	19.94	22	3	2004	4.3	TAK	SSA0320	80	324	9.48E-05
6	97.87	19.94	22	3	2004	4.3	CMAI	SSA0320	325	171	2.27E-04
7	97.80	19.36	15	12	2005	4.3	CMAI	SSA0320	255	138	1.53E-04
7	97.80	19.36	15	12	2005	4.3	NAN	SSA0320	141	319	3.05E-04
8	100.40	23.17	4	6	2007	4.4	MHMT	TSA0100	45	616	3.57E-05

Table B.2. (cont.) Strong ground-motion data recorded by the TMD seismic station network. The earthquake epicentral distributions are located in the main land South East Asia.

Event	Long	Lat	Day	Month	Year	Mw	Station	Instrument	Digital Count	Distance (km)	PGA (g)
9	100.69	20.75	7	6	2007	4.4	CMMT	TSA0100	77	286	8.43E-05
9	100.69	20.75	7	6	2007	4.4	MHMT	TSA0100	213	413	2.62E-04
10	99.60	22.51	30	5	2007	4.5	MHMT	TSA0100	35	514	4.29E-05
11	99.38	21.55	23	6	2007	4.5	PBKT	TSA0100	29	580	2.50E-05
11	99.38	21.55	23	6	2007	4.5	CMMT	TSA0100	148	308	7.84E-05
11	99.38	21.55	23	6	2007	4.5	MHMT	TSA0100	171	407	1.84E-04
12	99.89	21.55	9	9	2007	4.5	CMMT	TSA0100	56	321	2.44E-05
12	99.89	21.55	9	9	2007	4.5	MHMT	TSA0100	42	430	3.47E-05
13	99.96	20.38	18	9	2003	4.6	TAK	SSA0320	119	362	1.13E-04
14	98.95	19.87	6	8	2006	4.6	CMAI	SSA0320	4792	118	4.70E-03
15	100.61	20.67	16	5	2007	4.6	CMMT	TSA0100	38	274	1.66E-05
15	100.61	20.67	16	5	2007	4.6	MHMT	TSA0100	38	402	3.40E-05
15	100.61	20.67	16	5	2007	4.6	PBKT	TSA0100	38	458	3.62E-05
16	100.47	23.02	3	6	2007	4.8	MHMT	TSA0100	171	605	1.28E-04
17	98.20	22.02	7	1	2007	4.8	PBKT	TSA0100	26	674	2.04E-05

Table B.2. (cont.) Strong ground-motion data recorded by the TMD seismic station network. The earthquake epicentral distributions are located in the main land South East Asia.

Event	Long	Lat	Day	Month	Year	Mw	Station	Instrument	Digital Count	Distance (km)	PGA (g)
17	98.20	22.02	7	1	2007	4.8	SRDT	TSA0100	28	854	2.23E-05
17	98.20	22.02	7	1	2007	4.8	KHLT	TSA0100	73	804	2.89E-05
17	98.20	22.02	7	1	2007	4.8	MHMT	TSA0100	298	429	3.04E-04
18	98.38	20.31	29	12	2006	4.9	CMAI	SSA0320	178	178	1.45E-04
19	103.43	20.82	2	5	2007	4.9	PBKT	TSA0100	17	541	1.83E-05
19	103.43	20.82	2	5	2007	4.9	SKNT	TSA0100	47	432	4.93E-05
20	100.76	20.60	15	5	2007	4.9	CMMT	TSA0100	161	278	7.60E-05
20	100.76	20.60	15	5	2007	4.9	PBKT	TSA0100	60	448	9.11E-05
20	100.76	20.60	15	5	2007	4.9	MHMT	TSA0100	153	406	1.90E-04
21	99.89	12.02	7	10	2006	5.0	UBPT	TSA0100	45	712	2.90E-05
21	99.89	12.02	7	10	2006	5.0	MHIT	TSA0100	42	838	3.86E-05
21	99.89	12.02	7	10	2006	5.0	PBKT	TSA0100	64	520	1.44E-04
21	99.89	12.02	7	10	2006	5.0	CHBT	TSA0100	654	280	1.66E-03
22	95.99	5.49	28	12	2007	5.2	SRDT	TSA0101	44	1049	4.68E-05
22	95.99	5.49	28	12	2007	5.2	SKLT	TSA0100	117	547	5.82E-05

Table B.2. (cont.) Strong ground-motion data recorded by the TMD seismic station network. The earthquake epicentral distributions are located in the main land South East Asia.

Event	Long	Lat	Day	Month	Year	Mw	Station	Instrument	Digital Count	Distance (km)	PGA (g)
22	95.99	5.49	28	12	2007	5.2	TRTT	TSA0100	140	487	9.15E-05
22	95.99	5.49	28	12	2007	5.2	SURT	TSA0100	368	496	2.45E-04
22	95.99	5.49	28	12	2007	5.2	RNTT	TSA0100	281	514	4.56E-04
23	100.61	21.70	23	6	2007	5.4	KHLT	TSA0100	106	799	8.29E-05
23	100.61	21.70	23	6	2007	5.4	KRDT	TSA0100	167	802	1.19E-04
23	100.61	21.70	23	6	2007	5.4	PBKT	TSA0100	260	571	1.81E-04
23	100.61	21.70	23	6	2007	5.4	CMMT	TSA0100	502	368	2.79E-04
23	100.61	21.70	23	6	2007	5.4	MHMT	TSA0100	1599	488	1.24E-03
24	99.82	21.55	23	6	2007	5.6	SURT	TSA0100	84	1405	3.93E-05
24	99.82	21.55	23	6	2007	5.6	PKDT	TSA0100	43	1528	3.97E-05
24	99.82	21.55	23	6	2007	5.6	SKNT	TSA0100	197	681	1.86E-04
24	99.82	21.55	23	6	2007	5.6	KHLT	TSA0100	273	763	2.26E-04
24	99.82	21.55	23	6	2007	5.6	PBKT	TSA0100	270	568	2.31E-04
24	99.82	21.55	23	6	2007	5.6	CMMT	TSA0100	1321	319	5.58E-04
24	99.82	21.55	23	6	2007	5.6	CMMT	TSA0100	1321	319	2.26E-04

Table B.2. (cont.) Strong ground-motion data recorded by the TMD seismic station network. The earthquake epicentral distributions are located in the main land South East Asia.

Event	Long	Lat	Day	Month	Year	Mw	Station	Instrument	Digital Count	Distance (km)	PGA (g)
25	101.91	22.87	2	6	2007	6.1	RNTT	TSA0100	77	1546	4.16E-05
25	101.91	22.87	2	6	2007	6.1	KHLT	TSA0100	169	969	1.52E-04
25	101.91	22.87	2	6	2007	6.1	PBKT	TSA0100	482	708	2.52E-04
25	101.91	22.87	2	6	2007	6.1	CMMT	TSA0100	884	554	2.92E-04
26	101.05	20.89	16	5	2007	6.3	SKLT	TSA0100	62	1526	4.15E-05
26	101.05	20.89	16	5	2007	6.3	TRTT	TSA0100	114	1459	5.26E-05
26	101.05	20.89	16	5	2007	6.3	PKDT	TSA0100	152	1474	7.77E-05
26	101.05	20.89	16	5	2007	6.3	SURT	TSA0100	149	1349	1.13E-04
26	101.05	20.89	16	5	2007	6.3	UBPT	TSA0100	334	785	4.53E-04
26	101.05	20.89	16	5	2007	6.3	KHLT	TSA0100	971	727	5.73E-04
26	101.05	20.89	16	5	2007	6.3	CHBT	SSA0320	273	915	6.56E-04
26	101.05	20.89	16	5	2007	6.3	BKKA	TSA0100	935	798	1.26E-03
26	101.05	20.89	16	5	2007	6.3	PBKT	TSA0100	1258	480	1.61E-03
26	101.05	20.89	16	5	2007	6.3	CMMT	TSA0100	7992	323	2.69E-03
26	101.05	20.89	16	5	2007	6.3	MHMT	TSA0100	4991	451	5.16E-03

Table B.2. (cont.) Strong ground-motion data recorded by the TMD seismic station network. The earthquake epicentral distributions are located in the main land South East Asia.

Event	Long	Lat	Day	Month	Year	Mw	Station	Instrument	Digital Count	Distance (km)	PGA (g)
27	101.33	4.01	20	9	2007	6.7	SRDT	TSA0101	43	2061	3.22E-05
27	101.33	4.01	20	9	2007	6.7	SURT	TSA0100	78	1469	5.12E-05
27	101.33	4.01	20	9	2007	6.7	SKLT	TSA0100	105	1246	6.39E-05
27	101.33	4.01	20	9	2007	6.7	TRTT	TSA0100	96	1329	6.53E-05
28	99.87	2.65	13	9	2007	6.9	CMMT	TSA0100	109	2389	6.64E-05
28	99.87	2.65	13	9	2007	6.9	PBKT	TSA0100	129	2141	6.88E-05
28	99.87	2.65	13	9	2007	6.9	KRDT	TSA0101	177	1929	8.95E-05
28	99.87	2.65	13	9	2007	6.9	SRDT	TSA0103	246	1897	1.03E-04
28	99.87	2.65	13	9	2007	6.9	PKDT	TSA0100	299	1185	1.22E-04
28	99.87	2.65	13	9	2007	6.9	SKNT	TSA0102	174	2229	1.23E-04
28	99.87	2.65	13	9	2007	6.9	UBPT	TSA0100	236	2088	1.33E-04
28	99.87	2.65	13	9	2007	6.9	CHBT	TSA0100	248	1734	1.34E-04
28	99.87	2.65	13	9	2007	6.9	KHLT	TSA0100	239	1945	1.37E-04
28	99.87	2.65	13	9	2007	6.9	RNTT	TSA0100	298	1348	1.63E-04
28	99.87	2.65	13	9	2007	6.9	SURT	TSA0104	368	1296	2.02E-04

Table B.2. (cont.) Strong ground-motion data recorded by the TMD seismic station network. The earthquake epicentral distributions are located in the main land South East Asia.

Event	Long	Lat	Day	Month	Year	Mw	Station	Instrument	Digital Count	Distance (km)	PGA (g)
28	99.87	2.65	13	9	2007	6.9	TRTT	TSA0100	332	1166	2.35E-04
28	99.87	2.65	13	9	2007	6.9	SKLT	TSA0101	743	1096	3.27E-04

Table B.3 Strong ground-motion data recorded by the RID seismic station network. The earthquake epicentral distributions are located in the main land South East Asia.

Event	Long	Lat	Day	Month	Year	Mw	Distance (km)	PGA (g)
1	100.12	18.79	19	11	1999	3.0	19	3.20E-03
2	100.36	18.58	7	9	2002	3.2	26	1.45E-03
3	100.05	18.95	18	10	2006	3.4	36	1.21E-03
4	19.96	18.93	10	8	1999	3.4	48	1.12E-03
5	99.31	19.15	26	4	2002	4.3	112	8.88E-04
6	99.19	18.97	12	12	2006	4.9	117	1.53E-03
7	100.60	19.90	2	7	2002	5.0	154	5.95E-04
8	98.11	21.41	26	12	2004	6.5	306	7.57E-04
9	95.73	19.90	21	9	2003	6.6	430	2.78E-03

BIOGRAPHY

Mr. Santi Pailoplee was born in Amphoe Muang, Nakornrajsima Province in 1978. He studied in a local elementary school in Burirum province for 6 years during 1985 to 1990. In 1990, his adventure was started. He decided to study and spent his life at King's College for the pre-university education in Nakornprathom Province from 1990 to 1996. Later on, he attended to Department of Physics, Faculty of Science, Chulalongkorn University. He graduated with the bachelor degree of Science (B.SC.) in 2001 with the computer simulation and nuclear physic experience. Then, he studied and graduated a Master degree (Earth Sciences major) in Department of Geology, Chulalongkorn University with a focus on the application of thermoluminescnece (TL) dating for both geological and archaeological materials. His Ph.D.'s thesis mainly involves in paleo-seismic and present-day seismicity field with a special emphasis on the seismic hazard analyses in Thailand.